Department Chemie
Lehrstuhl für Biotechnologie

Analysis of the fibrilization of the yeast prion protein Ure2p

Silvia Cileni Rodrigues Catharino

Vollständiger Abdruck der von der Fakultät für Chemie der Technischen Universität München zur Erlangung des akademischen Grades eines Doktors der Naturwissenschaften (Dr. rer. nat.) genehmigten Dissertation.

Vorsitzender Univ-Prof. Dr.St. J.Glaser

Prüfer der Dissertation

1. Univ-Prof. Dr. J. Buchner
2 Univ-Prof. Dr. M. Rief

Die Dissertation wurde am 28.07.05 bei der Technischen Universität München eingereicht und durch die Fakultät für Chemie am 13.12.05 angenommen.

Zusammenfassung

Das [*URE3*] Prion aus *Saccharomyces cerevisiae* besitzt viele Gemeinsamkeiten mit Säugerprionen und Polyglutamin-assoziierten Erkrankungen. Es dient daher als Modellsystem für die Untersuchung von Amyloidkrankheiten. Verschiedene Studien konnten zeigen, dass die N-terminale Domäne von Ure2p essentiell für die Prionenbildung ist. In [*URE3*]-Zellen liegt Ure2p als Aggregat vor, während es in Wildtyp-Zellen dimer ist. In dieser Arbeit wurden das Wildtyp-Protein sowie dessen N-terminale Domäne gereinigt und hinsichtlich Struktur und Stabilität charakterisiert. Die Polymerisationskinetiken von Wildtyp-Protein und Mutante wurden in Abhängigkeit von den Lösungsmittelbedingungen (Salztyp und -konzentration, pH-Wert, Temperatur, Puffer) untersucht, und die dabei gebildeten Fibrillen näher charakterisiert. Zudem gelang es, Aufschluß über den Mechanismus der Fibrillenbildung zu erhalten, indem lösliche oligomere Spezies (Nuklei) isoliert und hinsichtlich Größe und Struktur charakterisiert wurden. Die Konversion von Ure2p in eine Struktur mit erhöhtem β-Faltblattanteil konnte sowohl für Fibrillisierungsintermediate als auch für reife Fibrillen gezeigt werden. Diese Ergebnisse untermauern die zentrale Rolle der N-terminalen Domäne bzgl. konformationeller Konversion und Fibrillenbildung, während die Struktur der C-terminalen Domäne in dimerem und fibrillärem Ure2p eine ähnliche Struktur einnimmt.

Summary

The [*URE3*] prion of *Saccharomyces cerevisiae* shares many features with mammalian prions and poly-glutamine related disorders and has become a model to study amyloid diseases. Several studies suggest that the N-terminal domain of Ure2p is essential for prion formation. In [*URE3*] cells, Ure2p is found predominantly in an aggregated state, while it is a soluble dimer in wild-type cells. In this thesis, the dimeric wild-type protein and an N-terminal domain mutant were purified and characterized in relation to structure and stability. Polymerization kinetics of wild-type protein and mutant were investigated under varying conditions e.g. salt concentration, salt type, temperature, pH and buffer, and the resulting fibrillar states were characterized. Moreover, the mechanism of fibril formation was studied by isolating soluble oligomeric species (nuclei) and characterizing them with respect to size and structure. The conversion of Ure2p into a structure with a higher content of β-sheets was demonstrated for both fibrilization intermediates and mature fibrils. These results support the crucial role of the N-terminal domain for conformational conversion and fibril formation, while the structure of the C-terminal domain is very similar in dimeric and fibrillar Ure2p.

Publication generated during PhD work

a) Publication related to the thesis work

- Characterization of Oligomeric Species in the Fibrilization Pathway of the Yeast Prion Ure2p; Biological Chemistry; 386(7)633-641
  S. Catharino, J.Buchner and S.Walter
- The yeast transcription factor Gln3p is a unfolded protein,
  A. Schmidt, B.Boesl, **S. Catharino,** S.Walter, *submitted*.
- Dependence of Ure2p fibrilization on solution conditions, *in preparation*
  S.Catharino, M.Ivanova, S.Walter and J.Buchner
- N-terminal domain fibrilzation and structure, in preparation
  S. Catharino, M.Ivanova, S.Walter and J.Buchner

b) Publication not related to the thesis work

- Hierarchical formation of disulfide bonds in the immunoglobulin Fc fragment is assisted by PDI. J. Biol.Chem. 2004, 279, 15059-15075
  F. Vinci, **Silvia Catharino**, S. Frey, J. Buchner, G.Marino, P.Pucci and M.Ruoppolo
- Protein-modified nanocrystalline diamond thin films for biosensor applications. Nat. Mater, 2004, 3, 736-742
  A. Härtl, E.Schmich, J. Garrido, J. Hernando, **S.Catharino**, S.Walter, P. Feulner, A. Kromka, D. Steinmüller and M. Stutzmann.

1 Introduction

1.1 Proteins

Proteins are the most abundant macromolecules present in a living organism, constituting about 50% of the dry mass of a cell. In the cell, proteins perform almost every task. The human body has hundreds of thousands of protein types. These macromolecules are linear combinations of 20 amino acids that are incorporated into the polymer chain. These linear polymers are called polypeptide chains or amino acid sequences, having thousands of atoms and hence millions of possible inter-atomic interactions. The name polypeptide is often used too, to define short segments of a protein. A protein is as a composition of one or more polypeptide chains and can execute a variety of biological functions in a living system. The majority of polypeptides and proteins adopt a tertiary structure, i.e. a tightly folded compact structural complex, after their biosynthesis allowing them to function (Van Holde et al., 1998) e.g. as molecular machines, enzymes, transcription factors and chaperones. There are, however, cases of proteins functioning without folding or switching between folds (Tompa, 2002). A protein fold is a unique structure, called the native state, which generates the selectivity and diversity in their functions. The native state of a protein corresponds to the most stable structure under physiological conditions. This structure allows it to bind to its natural partners, executing its function. A partial or complete change of this fold to a non-native structure affecting its architecture and biological properties is called misfolding (Dobson, 2004b). Folding and unfolding are the ultimate ways of generating and abolishing cellular activities, and unfolding is also a step in protein degradation via the proteasome (Voges et al., 1999) (Fersht and Daggett, 2002) Understanding folding and the occasional misfolding to other structures are among the most important and fundamental questions of modern science and the achievement of this goal can have strong therapeutic impact.

1.2 Protein structure

In acquiring its folding to the native structure, the polypeptide sequence forms regular secondary structures denominated α-helices, β-sheets, loops and turns. In α-helices, hydrogen bonds link amino acid residues which are relatively close to each other (3-4 amino acid residues apart). The residues rotate in a repetitive manner along the helix-axis. On the contrary, the β-sheet structure can involve links between distant fragments of the same peptide chain or even between fragments of different peptide molecules, leading to self-assembly of these molecules. It is formed by hydrogen bonds and the arrangement (parallel or antiparallel) is adjusted according to the most favorable hydrogen bonding. On this way, proteins can display various combinations of parallel and anti-parallel strands, having a mixed β-sheet arrangement. The connections between α-helices and/or β-strands are the loop regions. The loops are in general rather short and more flexible than the α-helices and β-strands. A β-turn is a short tight form of loop, stabilized by hydrogen bonding and is often an easy and volume-efficient way to reverse the direction of the polypeptide chain. To form an anti-parallel β-sheet, a polypeptide chain must take a complete 180 degrees change in direction; therefore β-turns are the common secondary structure elements between anti-parallel sheets. The tertiary structure is the final three-dimensional arrangement of all the secondary structure elements and their side chains. In aqueous solution, the secondary structure is organized in a way that the hydrophobic residues are buried inside the protein and, the polar and charged side groups interacting with the solvent or participating in salt bridges. Two or more subunits can interact to form a multimeric species, generating a quaternary structure (Van Holde et al., 1998).

1.3 Protein folding

Protein folding is defined as the process that results from the search for the most stable native structure from a random coil or partially unfolded conformation. The folding process takes the protein from an unfolded state (U) to the folded, or native, state (N). The spontaneity of the change of the linear

amino acid sequence to a folded structure depends on the information contained within the amino acid sequence (Anfinsen, 1973) and the contributions from the influence of the crowded cellular milieu (van den et al., 2000) (Van Holde et al., 1998). Anfinsen elaborated the principle of reversibility of protein folding with a global minimum in free energy. Levinthal framed a puzzle with two goals: a protein should achieve a energetic global minimum and do it quickly; and argued that it was impossible for a polypeptide chain to find its native state by exploring the entire conformational space - this was called the Levinthal paradox (Dill and Chan, 1997).

1.3.1 Folding from the atomic point of view

Evidences show that protein folding is a stochastic search between many conformations accessible to the polypeptide chain. This stochastic process enables residues that are far apart in the amino-acid sequence to come into close spatial contact generating different secondary structures. The differing energies associated with positioning different residues near or far from each other or from solvent enable some tertiary structures to be more stable than others (Onuchic and Wolynes, 2004). Despite all the possible conformations that a protein assumes, the protein only uses a very limited region of conformational space (Fersht and Daggett, 2002) (Dobson, 2004b). At this point, the representation of protein folding using energy landscapes where the energy decreases with increasing structure formation is suitable (Dill and Chan, 1997). Energy landscapes describe how the free energy changes as a function of a suitable reaction coordinate and can be described as energy surfaces too. These surfaces are funnel-like energy profiles with a rough surface defined by thermodynamic and kinetic properties. This funneled profile dominates the kinetics of folding (Onuchic and Wolynes, 2004)(Figure 1.1). When the folding process starts, the polypeptide chain collapses to a disordered globule reducing the number of conformations accessible and starting a random search for semi-compact conformation (transitional state) which leads to the native state. During this process, there is a loss of entropy that determines the free energy surface (Dinner et al., 2000). The statistical energy landscape approach explains when and why unique behaviors, such as specific folding pathways,

occur in some proteins and more generally explains the distinction between folding processes common to all sequences and those peculiar to individual sequences(Bryngelson et al., 1995; Dinner et al., 2000; Dill and Chan, 1997; Vendruscolo et al., 2003). To enable a protein to fold efficiently, the landscape required has been likened to a funnel because the conformational space accessible to the polypeptide chain is reduced as the native state is approached (Wolynes et al., 1995). Results by hydrogen exchange indicate that protein-folding landscapes are dominated by a small number of discrete, metastable, native-like partially unfolded forms(Englander, 2000).

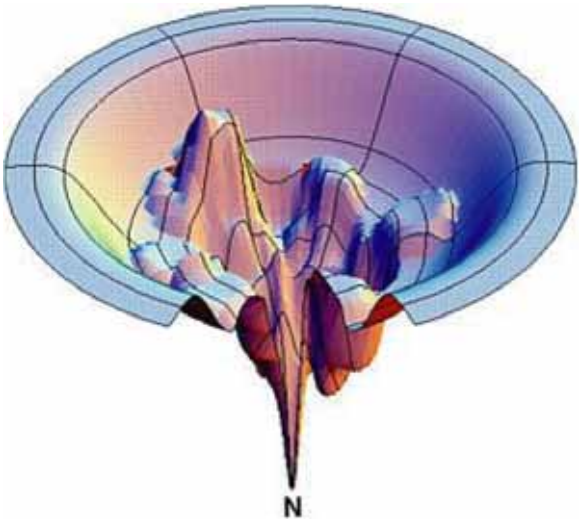

Figure 1-1: schematic energy landscape for protein folding.
The surface 'funnels' the multitude of denatured conformations to the unique native structure (Dill and Chan, 1997).

1.3.2 General principles

A series of hypothesis was suggested for solving the Levinthal paradox and clarify folding mechanisms (Schymkowitz et al., 2002): (i) the nucleation growth model (Wetlaufer, 1973) where there is a nuclei kinetically formed, around which the rest of the structure grows; (ii) the framework model (Ptitsyn and Rashin, 1973), where formation of secondary structure elements followed by the docking of those elements to form tertiary interactions, improved in the (iii) diffusion-collision model (Karplus and Weaver, 1994) where hierarchical secondary structure formation coalesce in multi-microdomain (folding intermediates); (iv) the hydrophobic collapse (Ptitsyn, 1995a) (Shakhnovich et

al., 1996) where a third thermodynamic state of protein molecules - a molten globule - between the native and the unfolded state exists; and (v) the nucleation-condensation model (Daggett and Fersht, 2003) where elements of local structure are formed concomitantly with and stabilized by tertiary interactions. In the hydrophobic collapse model (Ptitsyn, 1995b), at least one intermediate state should be experimentally observed since in this scenario folding is initiated by a rapid initial collapse to a compact state driven by the hydrophobic effect. Many small single-domain proteins (with up to aproximatelly 100 residues) have been found, however, to fold without populating any detectable intermediates species (Jackson, 1998). The "nucleation–condensation"(Fersht, 1995) mechanism can be seen as a combination of the diffusion-collision model and the hydrophobic collapse model (Vendruscolo et al., 2001) (Fersht and Daggett, 2002) (Schymkowitz et al., 2002). According to the "nucleation–condensation" model, a nucleation event is required whereby a small number of amino acids come together to form a critical core that then drives the formation of the final structure (Shakhnovich et al., 1996) (Fersht, 2000) (Fersht and Daggett, 2002). A small set of residue interactions is sufficient to initiate this nucleation process (Figure 1-1). The nucleus is composed predominantly of elements with partly- or well-formed native secondary structure that are stabilized by local and non-local tertiary interactions (Ladurner et al., 1997; Daggett and Fersht, 2003). This process forces the chain to adopt a rudimentary native-like architecture (Fersht, 2000) (Vendruscolo et al., 2001) and the structure then rapidly condenses, defining the overall architecture of the protein fold. This is sustainable because native-like interactions between residues are, on average, more stable than non-native ones (Fersht and Daggett, 2002). If these key interactions are not present, the protein cannot fold into its stable globular structure.(Fersht and Daggett, 2002) For proteins with more than about 100 residues, experiments generally reveal that one or more intermediate is populated during the folding process(Fersht, 2000). A combination of experimental and theoretical results have revealed that large proteins may fold in a modular manner, whereby each of the individual modules fold according to the basic principles that apply to the smaller single-domain substructures (Rumbley et al., 2001) (Vendruscolo et al., 2003). The folding process is not always perfect and can sometimes generate

“wrong” interactions, which can lead to so-called misfolded structures (Dobson, 2001). The interaction between such structures and other proteins may lead to protein aggregation, or as in the case of prions, it can lead to other misfolded proteins.

1.3.3 Folding in the cellular environment

In a cell, proteins are synthesized by the ribosome starting from the N-terminus according to the genetic information encoded in the cellular DNA. Protein folding can be initiated before the synthesis is completed, while a nascent chain is still attached to the ribosome. Some proteins can fold at least partially in such a co-translational manner from a distant domain (Hardesty and Kramer, 2001). Some small proteins need to be synthesized completely and will be folded in the cytoplasm after the release from the ribosome. Others will be transported into and folded in a specific compartment like mitochondria or the endoplasmic reticulum (Hartl and Hayer-Hartl, 2002) (Dobson, 2003). Many details of the folding process will therefore depend on the environment in which folding takes place, such as physicochemical characteristics (charge, secondary-structure propensities and hydrophobicity) in relation to the environment (Baskakov and Bolen, 1998) (Qu et al., 1998), molecular crowding(van den et al., 2000),(Frydman and Hartl, 1996), interactions with other proteins, such as chaperones(Beissinger and Buchner, 1998) (Jaenicke and Seckler, 1997), solute and ligand binding (Jaenicke and Seckler, 1997). Although the fundamental principles of how folding occurs are unlikely to be changed in any significant manner, between the *in vitro* and *in vivo* system, the protein quality control of the cell is essential for *in vivo* folding process. The cell maintains this high specialized system that requires cooperation between proteases, molecular chaperones and regulatory factors to fold and select the proteins. Some chaperones interact with nascent chains as they emerge from the ribosome (Albanese and Frydman, 2002), whereas others chaperones are involved in guiding later stages of the folding process. The supportive role of chaperones is accomplished by inhibiting unproductive interactions and allowing the protein to fold more efficiently in to its native structure (Walter and Buchner, 2002). Specific solutes (called organic osmolytes) can maintain the

structure of proteins in the cell and exert a force to fold proteins that are highly unstable in an aqueous environment (Jaenicke and Seckler, 1997) (Qu et al., 1998; Baskakov and Bolen, 1998) e.g. carbohydrate, lipids and alcohols. A large fraction of proteins will probability not fold or remains misfolded, even after interactions with chaperones or osmolytes. These proteins are eliminated by the quality-control system of the cell (Schubert et al., 2000). Some of this proteins are identified and degraded by proteases even before the completion of their synthesis (Turner and Varshavsky, 2000). Despite this, some misfolded proteins escape all this protective mechanism and form aggregates within cell or in the extracellular space. Usually the cell can deal with misfolding and aggregation. However, when this process becomes unbalanced or the quality control system collapses, a disease can be the consequence (Figure 1-2). These unbalanced conditions can be elevate temperatures, oxidative stress, amino acid mutation, and the tendency of certain proteins to change the conformation due to mutation (Bross and Gregerson, 2003).

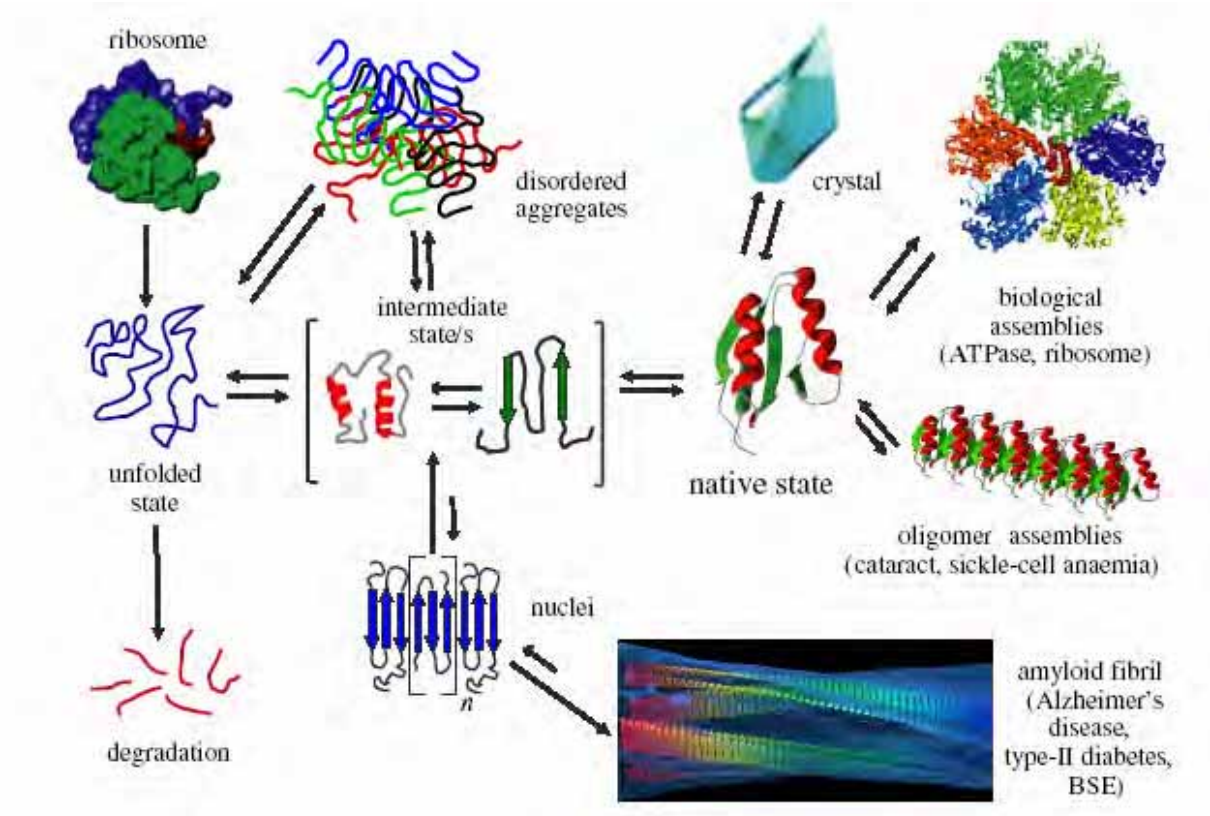

Figure 1-2: Scheme of the possible states accessible to a protein after its biosynthesis.

The folding of a globular protein goes through partially structured intermediates to compact native structures. Different kinds of assemblies can be formed by protein in

the native state, such as three-dimensional crystals and highly complex structures, such as ATPases, ribosomes and hemoglobin. Unfolded and partly folded states can form stable folded aggregates that cannot be destroyed by the normal quality control of the cell, leading to deposition and misfolding diseases. Adapted from ref.(Vendruscolo et al., 2003).

1.4 Natively unfolded proteins

Some proteins can present structurally disordered regions or can even be completely disordered. Proteins that do not have a 3-D structure are called *natively unfolded or intrinsically unfolded proteins (IUP)* and have been observed by numerous NMR studies of proteins (Wright and Dyson, 1999). These proteins do not adopt unique globular structures even under physiological conditions, unless specific partners such as cofactors, other proteins or nucleic acids are present. Most IUPs have regulatory roles in key cellular processes. The open structure provides multiple contact points, and folding occurs upon binding to their target, resulting in reversibility of this high specific binding too. An obvious function for these IUPs would be serve as a hub by binding to a number of partners simultaneously (Tompa, 2002). More then 100 IUPs have been found in vivo among 18 000 proteins in total already known (Dobson, 2004a) (Tompa, 2002). There are two distinctly different mechanisms to force intrinsically unstable-fold proteins to fold: one is to lower the Gibbs energy of the native state by using the binding energy of ligand (Frankel and Kim, 1991) and the other is to make use of the effect of osmolytes on the peptide backbone to raise the free energy of the unfolded state above the level of the native protein (Baskakov and Bolen, 1998).

1.5 Misfolding, aggregation and diseases

Because of the central role of folding in the cell, misfolding can result in malfunction and disease like many forms of cancer and neurodegenerative diseases (Dobson, 2001). A series of neurodegenerative diseases has been reported as result of misfolding and aggregation-like deposits in patients: Alzheimer's (APP protein - Aβ peptide), Parkinson's disease (α-synuclein), Creutzfeldt–Jakob's disease (Prion protein), Huntington diseases (Huntingtin

protein) and some polyglutamine diseases (Atrophin-1)(Ross and Poirier, 2004). These diseases are associated primarily with a single protein or fragment of a protein that forms the core structure of the fibrillar deposits (Sunde and Blake, 1997) (Dobson, 2004a) and in some cases, more then one protein coexists in a plaque but only one is responsible for the appearance of the disease. For these diseases, misfolding leads to an alternative conformation that polymerizes. This is different, for example, for sick cell anemia, where hemoglobulin that polymerizes using its normal folded conformation (Figure 1-2)(Vendruscolo et al., 2003).Three misfolding diseases will be more detailed here: Alzheimer's disease, Huntington's disease and Prion diseases. Yeast prions are here referred to as a model for misfolding diseases.

1.5.1 Misfolding diseases

Alzheimer's disease (AD) is one of the most common neurodegenerative diseases worldwide. Patients are characterized by lesions in the brain that contains amyloid aggregates. These aggregates contain small toxic cleavage products of the amyloid precursor protein, APP. APP is a transmembrane protein and its C-terminal domain can be cleaved by γ-secretase, a large complex of proteins, which cuts at several sites in the transmembrane domain (Figure 1-3A)(Lichtenthaler et al., 2002). Mutation of the cleavage sites in the APP or in one of the proteins that make part of the γ-secretase complex and/or cleavage combination with β–secretase generate increased amount of Aβ peptide. This results in accumulation of the peptide and polymerization to protofibrils (Bossy-Wetzel et al., 2004; Selkoe et al., 1996) (Selkoe and Kopan, 2003).

There are 9 human diseases already identified in relation to the repeat of CAG, the codon for glutamine, where the pathogenic core is based on the homopolymer of glutamine(Ross et al., 1999; Ross et al., 1998). The most well known is Huntington's disease (HD)(Ross and Poirier, 2004). HD is an inherited, neurodegenerative disorder caused by huntingtin protein (htt). Htt is a multidomain protein with a polymorphic glutamine/proline (Q/P)-rich domain at

the N-terminus (Harjes and Wanker, 2003; Ross and Poirier, 2004). Individuals affected by HD have a poly (Q) stretch of 36 or more glutamines. The age of disease onset correlated with the length of the expanded poly (Q) region (Perutz, 1996; Bossy-Wetzel et al., 2004)(Figure 1-3B). Htt can be founded in membranes, cytosol, nuclei, mitochondria and in association with microtubules (Bossy-Wetzel et al., 2004; Harjes and Wanker, 2003) depending of the partner protein. *In vitro*, expanded htt forms fibrillar aggregates with morphological and biophysical properties similar to those formed by Aβ peptide (Scherzinger et al., 1997) and some amorphous aggregates (Masino and Pastore, 2002).

The human transmissible spongiform encephalopathies (TSEs) or prion diseases are a group of rapidly progressive disorders characterized by spongiform (vacuolar) degeneration of brain tissue and variable amyloid plaque formation(Goldfarb and Brown, 1995). TSEs affect humans and animals. Close analogs of human TSE are scrapie in sheep and bovine spongiform encephalopathy ("mad cow disease"). When prion protein (PrP) responsible for these diseases is expressed recombinantly and experiments were done in vitro, this protein form fibrillar species (PrP^{sc}). The cellular human PrP (called PrP^{c}) has a structured globular domain from residues 125 to 228 and an N-terminal flexible and disordered region (Figure 1-3C). PrP is a monomeric extracellular protein involved in signal transduction and control of copper ion concentration (Mouillet-Richard et al., 2000; Burns et al., 2002). The globular domain contains three α-helices comprising residues 144–154, 173–194, and 200–228, and an antiparallel β-sheet consisting of two short strands comprising residues 128–131 and 161–164(Zahn et al., 2000). PrP^{Sc} is derived from PrP^{C} via a posttranslational modification involving a conformational transition of the α-helical structure in PrP^{C} to β-sheet structures in PrP^{Sc}. A series of homologous proteins has been found between mammalian and some other organism (Premzl et al., 2004; Premzl et al., 2003) suggesting a strongly conserved basic function in brain. Yeast and other fungi do not encode for the PrP protein homologues.

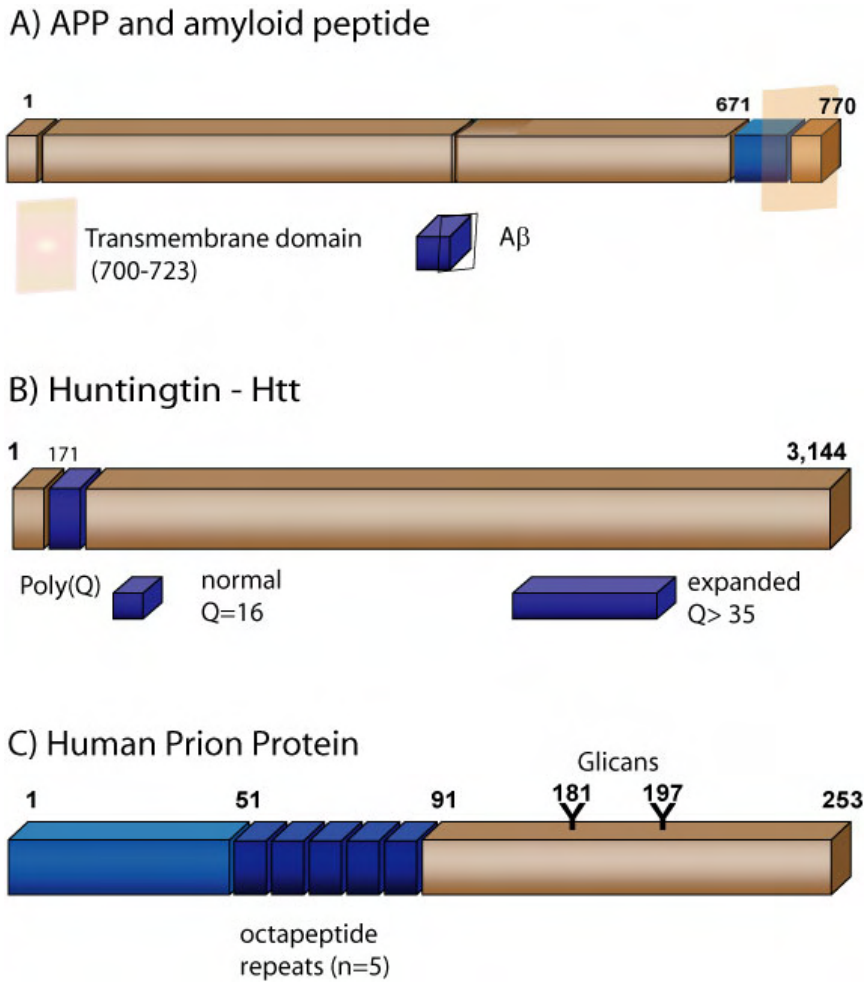

Figure 1-3: Schematic representation of the primary structure of some amyloid-forming proteins.

A) APP, Aβ peptide – $A\beta_{1-40}$ (671-711) and $A\beta_{1-42}$ (671-713); Transmembrane domain (TM) (700-723). B) Huntingtin domain indicating the Poly(Q) position C) Human Prion Protein, PrP. the octapeptide motifs (51–91) that are responsible for Cu binding, the glycosylation position (181, 197) and the proteinase-resistant domain are shown. The first 100 residues are flexible and the C-terminal is folded (James et al., 1997; Xing and Higuchi, 2002).

Yeast and other fungi present a phenotype in which the transmission does not follow Mendelian rules (Lacroute, 1971). The best studied cases are the dominant and heritable [URE3] and [PSI^+]. To explain these phenotypes, Reed Wickner (Wickner, 1994) expanded the prion concept, calling them “yeast prions” (Weissmann, 1994). In [URE3] and [PSI] cells, the agent propagates in the cytoplasm and is transferred to other yeast by cytoplasmic exchange during mating or by cell division and in the absence of nucleic acid(Patino et al., 1996) (Wickner et al., 1999). These phenotypes do not kill cells (Glover et al., 1997) like mammals prions and can be lost when yeast cells are grown in the

presence of millimolar concentrations of the protein denaturant guanidinium chloride (Cox et al., 1988; Eaglestone et al., 2000; Ness et al., 2002).

1.5.2 The 'protein only' hypothesis for prion diseases

Griffith reported that the agent responsible for scrapie was far more radiation-resistant than known viruses or bacteria (Griffith, 1967). This led to the suggestion that the infection agent might be a protein that had the surprising ability to replicate in the body without requiring a nucleic acid for infection (Griffith, 1967; Bolton et al., 1982). This launched the so-called 'protein-only' hypothesis. Proteins are far less sensitive to radiation damage than are DNA and RNA. The purification of PrP and the assignment of a gene that encodes this protein strongly support this hypothesis (Bolton et al., 1982) leading to a Nobel Prize for Stanley Prusiner. PrP can exist in two alternate forms: the cellular protein (termed PrP^{C}) and the pathological isoform (termed PrP^{res} or PrP^{Sc}) (Kocisko et al., 1994; Lansbury, 1994). There is no chemical difference between these two isoforms although the pathological isoform shows some resistance to proteinase (Kaneko et al., 1995). Biochemical characterization demonstrate that this protein can acquire a beta-sheet conformation and can form a structure similar to the described for amyloid (Pan et al., 1993) (Nguyen et al., 1995a). Structural changes are followed by other changes of properties like protease resistance, solubility and ability to form larger-order aggregates. Further biochemical characterization (DeArmond et al., 1985) demonstrated that these aggregates are filaments with twisted appearance. X-ray fiber diffraction showed that this aggregates has a 4.7 Å reflections similar to amyloid (Nguyen et al., 1995b; Goldfarb and Brown, 1995). In contrast to other amyloid diseases, Transmissible Spongiform Encephalopathy (TSE) are considered transmissible, in where the addition of preformed amyloid fibrils to a solution of the same peptide (known as seeding) results in faster polymerization and amyloid formation(Jarrett and Lansbury, Jr., 1993; Goldfarb and Brown, 1995). A crucial facet of the prion hypothesis transmission was shown *in vitro* by Soto and co-workers(Saborio et al., 2001; Castilla et al., 2005), namely the replication of a prion in a cyclical process, in which newly produced PrP^{res} triggered further misfolding to maintain prion propagation

(Edskes and Wickner, 2004). Recently, artificial mammalian prions (a truncated PrP fragment) were polymerized *in vitro* and injected in transgenic mice. Due to extreme conditions used *in vivo*, some researchers have questioned this experiment as a final proof of the hypothesis (Legname et al., 2004). The criteria about infectious has been satisfied in yeast, where some protein behaves much more like the mammalian prion theory. Recombinant yeast prions has propagated *in vitro* some *in vivo* features and displayed some mammalian features too (Zou and Gambetti, 2005).

1.5.3 Yeast prions

For [URE3] and [PSI] prions of *Saccharomyces cerevisiae*, the phenotype can appear without introduction of new DNA but only with the overexpression of the protein. The development of the [PSI+] and [URE3] associated phenotype is thought to be caused by a structural switch in the Sup35p, a translation termination factor (Figure 1-4A), and Ure2p protein, a regulator of nitrogen metabolism, respectively (Figure 1-4B) (Chernoff et al., 1993; Wickner, 1994). Similar to the mammalian prion diseases (Riek et al., 1996), these yeast phenotypes transmit this altered physical state to newly synthesized protein molecules and this way the conformational information is propagated and replicated (Wickner et al., 1995; Tuite, 2000). The protein can exist in two states: a protease sensitive and a protease resistant state. The conformational switch in a single protein leads to the formation of amyloid-like aggregates in cells harboring the respective prion phenotype {Derkatch, 2001 12 /id; Patino, 1996 111 /id; Wickner, 1994 78 /id}.

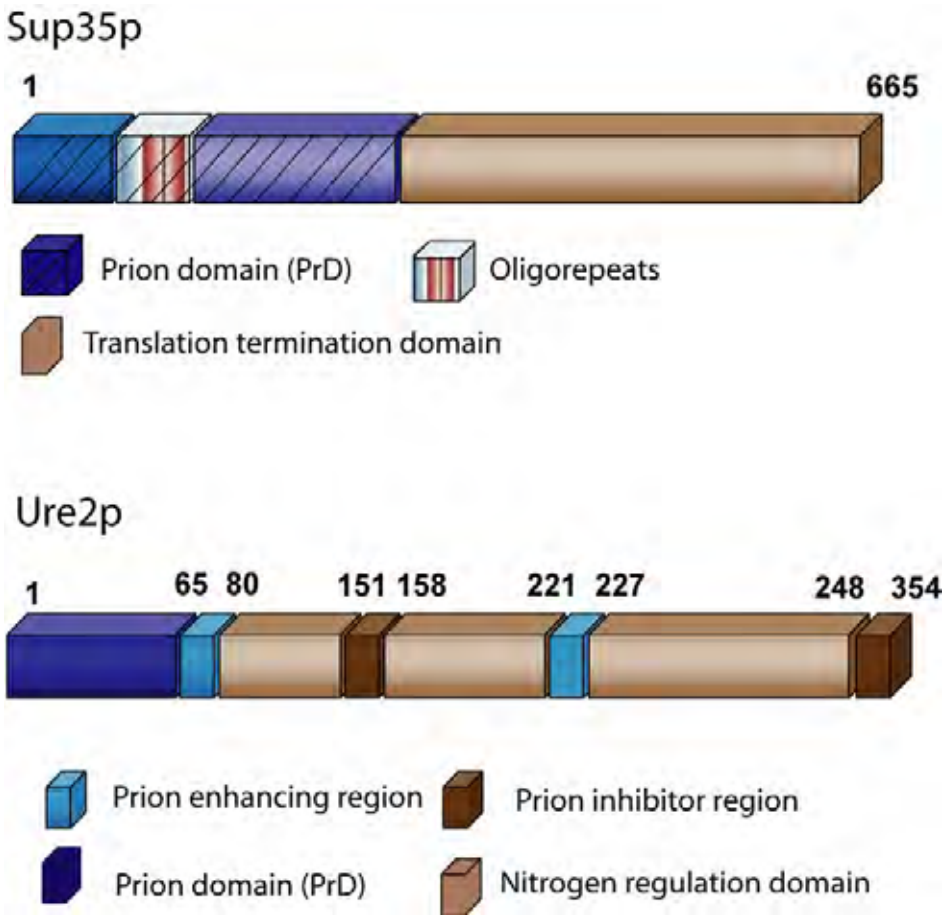

Figure 1-4: Schematic representation of the primary structure of Yeast Sup35p and Ure2p prion.

Yeast prions are composed of prion domain, middle domain and functional domain. A) Sup35; the N-terminal domain (dark blue) with the octarepeats region, the high charged middle domain (light blue) and the C-terminal that has a function of translation termination. B) Ure2p Prion promoting region (dark blue), enhancing (light blue) and inhibiting domain (dark brown) of Ure2p and nitrogen regulation domain (light brown) (Maddelein and Wickner, 1999).

Genetic studies have established that the N-terminal part of the Sup35 protein (Chernoff et al., 1993) and the N-terminal part of the Ure2p (Masison et al., 1997) (Komar et al., 1999) are sufficient for the genesis as well as for the maintenance of [PSI] and [Ure3], respectively. In vitro studies showed that the N-terminal domain of Sup35 can induce fibril formation and self seed solutions (King et al., 1997). The prion forming domain is transferable to another protein and still generate prions in vitro (Schlumpberger et al., 2000; Baxa et al., 2002; Chernoff et al., 1993; Ter Avanesyan et al., 1993). In both cases, the short N-terminal domain, consists of mainly polar, uncharged amino acids that are dispensable for cellular function of the protein (Coschigano and Magasanik, 1991) (Ter Avanesyan et al., 1993). In analogy to the model developed for the

mammalian prion protein PrP, Sup35p and Ure2p are assumed to undergo self-perpetuating changes in their conformation (Uptain and Lindquist, 2002) generating fibrils *in vitro*(Glover et al., 1997). Several other proteins showing prion-like behavior were identified lately in yeast and other fungi. A common structural model has been proposed for yeast prions, where the prion domains stack to form a core fiber of amyloid, which is surrounded by the C-terminal domains. This model has been suggested for Ure2p (Speransky et al., 2001; Taylor et al., 1999; Baxa et al., 2003), Sup35(Glover et al., 1997) and HET(Balguerie et al., 2003; Nazabal et al., 2003).

1.6 Structural and biophysical aspects of Amyloid and prion proteins

1.6.1 The search for common features of amyloid structure

The proteins found in the proteinaceous deposits in a series of amyloid diseases do not show any sequence or structural homology or any other evidence that they form amyloid. The noncrystallinity and insolubility of amyloid fibrils complicate the determination of their structures but same common aspects have already been found and let these diseases be called “protein misfolding diseases”. The change of the conformation in the protein is quite a general concept (Kayed et al., 2003), e.g. from random coil or α-helix to β-sheet conformation in the fibrils. Normal β-sheet-containing proteins avoid such unwanted self-association by preventing their edge strands from making intermolecular interactions. Amyloidogenic proteins do not have this feature and can, thus, make intermolecular interactions (Plakoutsi et al., 2004). The ability of diverse polypeptides to form amyloid fibrils is due to the fact when out of the native state; they can form intermolecular bonds involving the peptide backbone. They are generating stable structures which are difficult to destroy, and thus accumulate in the body. Despite all the variable features of amyloid fibrils, some common macromolecular traits have been found, such as the filamentous structure with a diameter around 10 nm that produces hierarchical

structures with lengths of 0.1–10 μm. The fibrillar structures typical for many of the aggregates have very similar morphologies (long, unbranched and often twisted structures resulting from protofilament association) (Koo et al., 1999). Amyloid fibrils can be stained both *in vitro* and *in vivo* with some dyes like Congo Red and Thioflavin T. The birefringence of bound Congo Red under polarized light was used as a first criteria to define amyloid fibrils. Lately, several studies have been published showing that Congo Red does not only bind to amyloid fibrils but to certain other proteins, too. Thioflavin T has been widely accepted as an alternative dye for amyloid detection (LeVine, III, 1993). In the late 60s, X-ray fiber diffraction analysis has shown the presence of cross-β structure in a number of amyloids(Eanes and Glenner, 1968). This has been confirmed by Sunde (Sunde and Blake, 1997) and Serpell (Serpell, 2000a). This shows that β-strands separated by 4.7 Å are a common feature of the different fibrils. They are running perpendicular to the long axis of the fibrils and β-sheet parallel to this axis (Serpell et al., 2000; Serpell, 2000b) (Figure 1-5A)

1.6.2 Structural models for amyloids and prions

To understand the assembly mechanism of amyloid fibrils, it is necessary to determine the fibril's structure. The insolubility of the fibrils makes structure determination very difficult, but in the past few years a variety of breakthrough contributions have been reported.

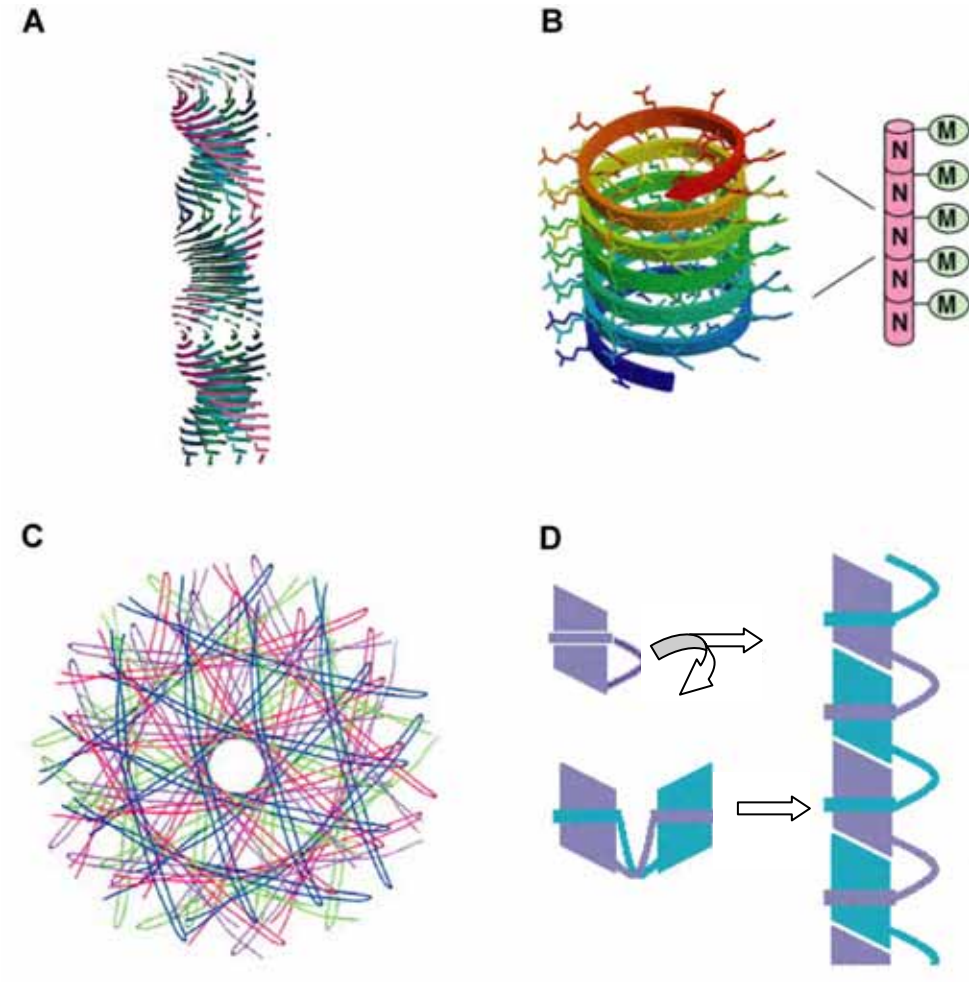

Figure 1-5 : Structural model for amyloids and prions

A) cross-β-structure scheme and helical array of β-sheets parallel to the fiber long axis, with the strands perpendicular to this axis. B) Diagrammatic projection of a helical fiber on a plane normal to the fiber axis. C) Pleated sheet model for Aβ(Li et al., 1999), and D) domain swapping model - PrP fragment can form 3D domain-swapped dimers (equivalent monomers are shown in blue and turquoise for clarity in the dimer) and oligomerize(Knaus et al., 2001; Marianayagam et al., 2004).

1.6.2.1 The cross-β-structure model

The cross-β-structure has been used as a common basic structural feature to define amyloids (Eanes and Glenner, 1968; Sunde and Blake, 1997). According to this model (Figure 1-5A), elementary fibrils are assembled from the stacking of twisted β-sheet perpendicular to the fibril axis. There is some controversy in whether the β-sheets are parallel (Tycko, 2003; Torok et al., 2002) or antiparallel (Serpell, 2000b). The core structures of Aβ, α-synuclein, and polyglutamine proteins appear to involve β-turns and β-strands (Ross and Poirier, 2004; Benzinger et al., 2000), thus the β-strand and β-turn may be a

common feature of amyloids. This model has also been suggested for fibrils of proteins without any connection to diseases, including acylphosphatase (Chiti et al., 1999). Perutz suggested a model based on cross-β–structure for poly (Q) called “Polar zippers” (Perutz et al., 1994; Perutz, 1995)(section 1.7).

1.6.2.2 Complete unfold/misfolding and partial unfold/misfolding

It has been a common believe that fibrillation requires partial unfolding of the native state or partial folding of the unfolded state. Some proteins are unfolded and fold partially to a α-helical intermediate and then into a β-structure, like α-synuclein (Uversky et al., 2001). Examples of globular proteins that can form fibrils after partial unfolding are phosphoglycerate kinase (Damaschun et al., 1999), Aβ(Snyder et al., 1994), PrP (Gasset et al., 1992; Nguyen et al., 1995a), cystatin C(Ekiel and Abrahamson, 1996), and transthyretin(Colon and Kelly, 1992; Colon et al., 1996). Colon and co-workers (Colon and Kelly, 1992) suggested that a presence of a folding intermediate being responsible for amyloid formation. This hypothesis is supported by the work of Dobson on acylphosphatase (Chiti et al., 1999) and lactalbumin (Hamada and Dobson, 2002). These studies show that amyloid formation is strictly related to folding and misfolding of a protein.

1.6.2.3 Polar zipper model

Perutz and co-workers suggested a “polar zipper” model based on experimental data for polyglutamine amyloids (Perutz et al., 1994). In this model, β-sheets are stabilized by a network of hydrogen bonds involving polar residues such as glutamine and asparagine. These “zippers” could pair either intramolecularly (leading to a β-hairpin structure) or intermolecularly (leading to aggregates) (Perutz, 1995). For polyQ, aggregation occurs when the length of the polyQ stretch exceeds a threshold of 37-41 residues (Perutz, 1996). Mammalian and yeast prions have some regions in the N-terminus rich in glutamine and asparagine (Perutz et al., 2002b; Michelitsch and Weissman, 2000; Blondelle et al., 1997).

1.6.2.4 Water filled structure model

Perutz suggested a cylindrical fibril of polar amino acids for Sup35p (Figure 1-5B). These cylindrical β-sheets would have 20 residues per turn, but a single turn would be unstable. This would explain the threshold of 37-40 residues for polyQ diseases. (Perutz et al., 2002a) (Elam et al., 2003) (Sikorski and Atkins, 2005). A similar model was suggest to Sup35 based on x-ray fiber diffraction (Kishimoto et al., 2004).

1.6.2.5 Superpleated β-structure

Steven(Kajava et al., 2004) suggested a planar serpentine arrangement for the N-terminal domain of Ure2p, where the interior of the filament is not stabilized by the packing of apolar side-chains, but by H-bond networks generated by the stacking of Asn side-chains, excluding charged residues. This same model was applied to amylin (Kajava et al., 2005) and is based on another model already suggested for Aβ(Li et al., 1999) (Figure 1-5C) and polyalanine– the pleated sheet model (Blondelle et al., 1997).

1.6.2.6 Domain Swapping

In this model, a protein molecule forms a dimer or an oligomer by exchanging one or multiple structural domains (Schlunegger et al., 1997). Domain swapping was proposed by Eisenberg (Bennett and Eisenberg, 2004; Bennett et al., 1994) as a mechanism of oligomerization (Bennett et al., 1995; Liu et al., 2001; Ogihara et al., 2001). Several groups confirmed this model, and more than 40 proteins are believed to oligomerize via domain swapping (Liu and Eisenberg, 2002; Janowski et al., 2001) (Marianayagam et al., 2004; Liu et al., 2001) (Liu et al., 2002) including human PrP (Knaus et al., 2001) (Figure 1-5D).

1.6.2.7 Anhydrous β-sheet core

Eisenberg identified peptides that fold to a cross β structure with a dehydrated β-sheet core (Balbirnie et al., 2001; Diaz-Avalos et al., 2003). These peptides share the main characteristics of an amyloid, and their β-sheets form a densely

packed structure despite the polar character of the side chains. This was later shown for β-microglobulin (Ivanova et al., 2004), too.

1.6.2.8 β- helical fold

A serie of proteins has already been shown to have a threedimensional structure like parallel β-helices. This folding model forms a bridge between globular and fibrous proteins and permits a folding to form a spiral. This model fits very well for pollar stacks like asparagines ladder and is very good reviewed by Jenkins(Jenkins and Pickersgill, 2001).This model has been suggest for PrP assembly(Wille et al., 2002).

1.6.3 Kinetic and thermodynamic models of amyloid and prion formation

To better understand the kinetic of fibrillation and the cascade of events that lead to fibrils, it is necessary to characterize the early events and pathways leading to fibrils.

1.6.3.1 General observations for amyloid and prion fibrillogenesis

One general idea about amyloid fibrilogenesis is now widely accepted: Fibrillation is a two-step reaction involving an initial lag phase, in which “seeds” are formed, followed by the rapid fibril propagation and aggregation stage(Jarrett and Lansbury, Jr., 1993) (Lomakin et al., 1996). Kinetics has been studied by a number of scientists and the general consensus is that (i) above a critical concentration, peptides micelles are formed leading to oligomerization in solution. These micelles were called nuclei (ii) when specific dyes like Thioflavin T are used to monitor fibril growth, the reaction consists of a lag phase during which the nucleation occurs and an elongation phase, which appears a sigmoidal increase in ThT fluorescence(LeVine, III, 1993). The lag phase disappears when seeds or pre-formed nuclei are added to a saturated solution (Jarrett and Lansbury, Jr., 1993). A number of models have been

developed in order to explain the fibrillation pathway from the kinetic point of view. In the following, some of them will be described briefly.

1.6.3.2 Template-assisted conversion (TA)

Fibrils can act as seeds to start fibrillation by incorporating ‘fresh’ monomers at their ends. In this case, the lag phase is eliminated and the process is commonly known as seeding (Jarrett and Lansbury, Jr., 1993) (Caughey et al., 1995). The conformational conversion of the incorporated protein molecule would be the rate-limiting step. The template model can consider two possibilities: i) that the conformational conversion occurs in solution before binding to the fibril end ii) the binding to the template occurs first and then there is the conformational conversion(Serio et al., 2000). This model has been suggested for human PrP (Prusiner, 1982) (Kocisko et al., 1994; Saborio et al., 2001; Castilla et al., 2005) and for the yeast prion Sup35p(Paushkin et al., 1997; Glover et al., 1997).

1.6.3.3 Nucleation polymerization (NP)

In this model, the rate limiting step is the association to a nucleus, a stable species similar to the nuclei important for crystallization. NP consists of two phases, a nucleation phase and an extension phase. Nucleation is thermodynamically unfavorable and represents the rate-limiting step. This model has been proposed by Eaton (Hofrichter et al., 1974) for sick cell diseases and later suggested by Landsbury (Jarrett and Lansbury, Jr., 1993; Harper and Lansbury, Jr., 1997) and was confirmed by other research groups(Lomakin et al., 1996; Naiki and Nakakuki, 1996). It was also suggested initially to describe fibrillation of Sup35p (Glover et al., 1997) (Paushkin et al., 1997) and polyQ (Chen et al., 2002), but later other models were favored.

1.6.3.4 Nucleation conformation conversion (NCC)

Lindquist proposed the nucleation conformation model, which combines the template assembly model with the nucleation polymerization model, to explain the assembly kinetics of Sup35p (Serio et al., 2000; Scheibel et al., 2004). The main point of this model is that an oligomer may have a distinct stable

conformation that differs from both the monomeric random coil and the aggregated state. This would involve a dual conformational change. Scheibel *et al.* suggested later that this mechanism may involve a separated step of association and conformational change (Scheibel et al., 2004).

1.6.3.5 Other models

A number of model for individual proteins have been suggested, e.g. the common pathogenesis model where soluble oligomers would have a common structure implying a common mechanism of pathogenesis (Torok et al., 2002; Kayed et al., 2003). For certain proteins the folding/misfolding appears to be determined by kinetic rather than thermodynamic factors. In other cases thermodynamics is the essential factor because the free energy barrier can be quite high (Koo et al., 1999). These differences and the existence of all these models argue against a simple model that can explain all amyloids. But one point is clear: fibril formation requires the exposition of the polypeptide sequence responsible for the amyloid fibrillation. In a globular protein, the polypeptide backbone and the hydrophobic side-chains are largely buried within the folded structure. Only when they are exposed, e.g. when the protein is partly unfolded (for example, at low pH) or fragmented (for example, by proteolysis), conversion into amyloid fibrils will be possible (Dobson, 2004b).

1.7 The ure2p protein

Ure2p is a soluble dimeric protein of *S. cerevisiae* consisting of two 40 kDa subunits (Thual et al., 2001; Perrett et al., 1999). It is localized in the cytoplasm, where it interacts with the transcription factor Gln3p. In the presence of good nitrogen sources, such as ammonia, Ure2p binds to Gln3p and prevents its migration to the nucleus (Blinder et al., 1996). When good nitrogen sources are sparse, the Gln3p/Ure2p interaction is weakened by phosphorylation and Gln3p is translocated to the nucleus. There it induces the expression of genes responsible for the utilization of poor nitrogen sources, such as allantoin (Komar et al., 1999). This regulatory principle is called *nitrogen catabolite repression*. In [URE3] cells this regulatory function of Ure2p

is lost, because the levels of soluble Ure2p are strongly decreased due to its aggregation. Therefore, Gln3p is permanently active. In cells carrying the [URE3] phenotype, Ure2p forms large globular or fibrous insoluble aggregates (Edskes et al., 1999; Beck and Hall, 1999; Fernandez-Bellot et al., 2000). Overproduction of Ure2p increases the frequency of [URE3] *de novo* generation by ~100-fold (Masison and Wickner, 1995). Moreover, it was demonstrated that [URE3] propagation depends on an intact *URE2* gene (Masison et al., 1997). Both observations established a tight link between the [URE3] phenotype and the Ure2p protein. On a genetic level, [URE3] cells and wild-type cells are identical. Accordingly, the determinant for the [URE3] phenotype must reside in the Ure2p protein itself. Hence, it was suggested by Wickner that the Ure2p protein is a yeast prion. Later, this notion was supported by a number of experimental findings. It was shown that Ure2p fibrils bind the fluorescent dye Thioflavin T (ThT) and display an increased resistance against proteases (Zhu et al., 2003b; Komar et al., 1997). On a functional level, the Ure2p protein can be dissected in two parts. The C-terminal domain (residues 94-354) is highly homologous to glutathion S-transferases and mediates both nitrogen regulation and dimerization (Figure 1-6) (Umland et al., 2001; Thual et al., 2001). Expression of this fragment in *ure2* knock-out strains restores Ure2p function (Komar et al., 1999; Edskes et al., 1999). These cells, however, cannot acquire [URE3] (Speransky et al., 2001), since the development of the prion phenotype requires the N-terminal domain of Ure2p (residues 1-93) (Masison et al., 1997; Komar et al., 1999). Hence, it is also called the prion domain (PrD) (Figure 1-7).

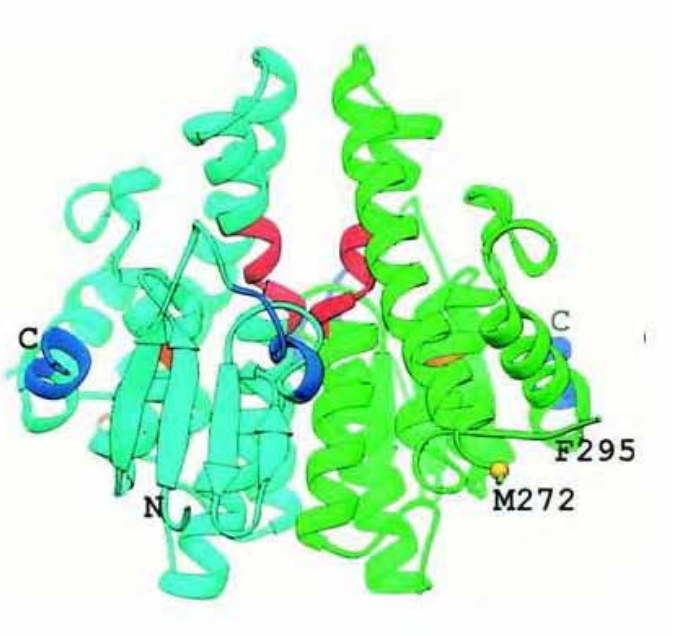

Figure 1-6: Ure2p crystal structure

Monomer A is green and Monomer B is cyan. Prion-inhibiting regions (His-151 to Ser-158 and Val-347 to Glu-354) are indicated in blue, and the prion-promoting region (Ser-221 to Ile-227) is indicated in red. M272 and F295 are residues near the proteolytic clip sites.

The crystal structure has been solved for the C-terminal domain (Umland et al., 2001) (Figure 1-6). Ure2p 95–354 is highly α-helical and is composed of two sub-domains that bind glutathione (Bousset et al., 2002) and have glutathione peroxidase activity (Bai et al., 2004). Comparative studies on full-length Ure2p and the C-terminal domain have shown that the N-terminal region does not contribute to dimerization and folding of Ure2p (Perrett et al., 1999; Thual et al., 2001; Zhu et al., 2003b) and that the C-terminal domain of Ure2p is also unable to propagate [URE3].

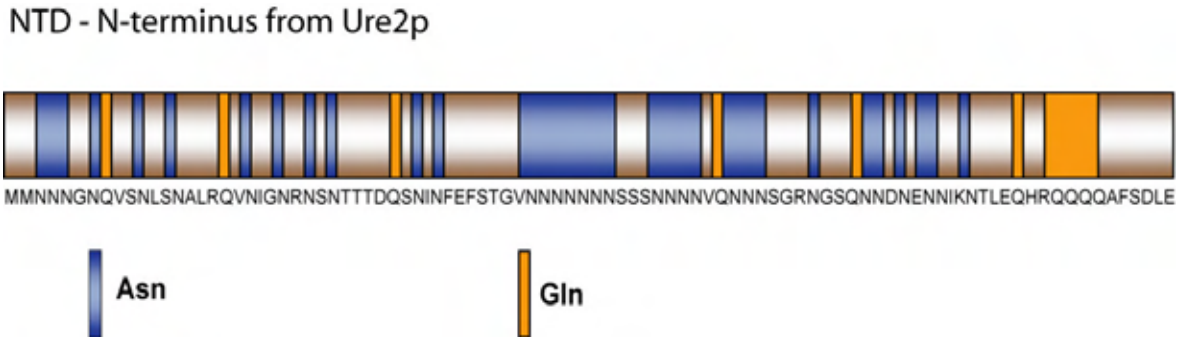

Figure 1-7: The prion forming domain (PFD) or N-terminal domain of Ure2p

N-terminal domain (residues 1-94) of Ure2p consists almost exclusively of polar, uncharged residues such as Asn (~40%, blue) and Gln (~10%, yellow). It is also highly enriched in Ser and Thr.

Unlike the C-terminal domain, the N-terminal domain of Ure2p has been reported to be poorly structured (Thual et al., 2001). In native Ure2p, the N-terminal region is highly protease-sensitive (Perrett et al., 1999) and does not contribute to the stability of the soluble protein (Perrett et al., 1999; Thual et al., 1999; Thual et al., 2001; Zhou et al., 2001). Its inherent tendency to form fibrillar aggregates was demonstrated both *in vitro* (Speransky et al., 2001; Thual et al., 1999) and *in vivo* (Masison and Wickner, 1995). When fused to other protein like barnase and GFP, the N-terminal domain still fibrillates while the fused proteins retain their activity (Baxa et al., 2002). Although residues 1 to 64 are sufficient for prion induction, the fragment from residue 1 to 80 is a more efficient inducer of [URE3]. Deletion of seven residues around position 224 did not affect nitrogen regulation but did eliminate prion induction (Figure 1-4 1-4B) and Figure 1-7). Larger deletions in this area, however, restored prion-inducing ability (Maddelein and Wickner, 1999). Hence, the Q/N-rich N-terminal domain of Ure2p (Figure 1-8) may be essential for the aggregation behavior, but it is not the only determinant. It is not clear whether other regions of Ure2p affect prion formation directly or rather indirectly by changing protein concentration, phosphorylation patterns or interaction with partner proteins. Weismann et al. (Michelitsch and Weissman, 2000) examined more than 30 organisms and showed that the presence of a Q/N rich domains is not a sufficient criterion for a prion protein. From the 100 theoretical yeast prions, only 1 (Rnq1) was shown to aggregate in a prion-like manner (Sondheimer and Lindquist, 2000). In light of this, Baxa et al. (Ross et al., 2004) have constructed five scrambled prion forming domains based on the amino acid composition of the N-terminal domain of Ure2p. The result was that 4 of 5 sequences form prions in vivo and all 5 form prions under native conditions in vitro. This shows that the unusual amino acid composition of the NTD is responsible for the fibrillation. The suggestion was that the high content of serine and the low level of charged amino acids may contribute to the prion formation of Ure2p.

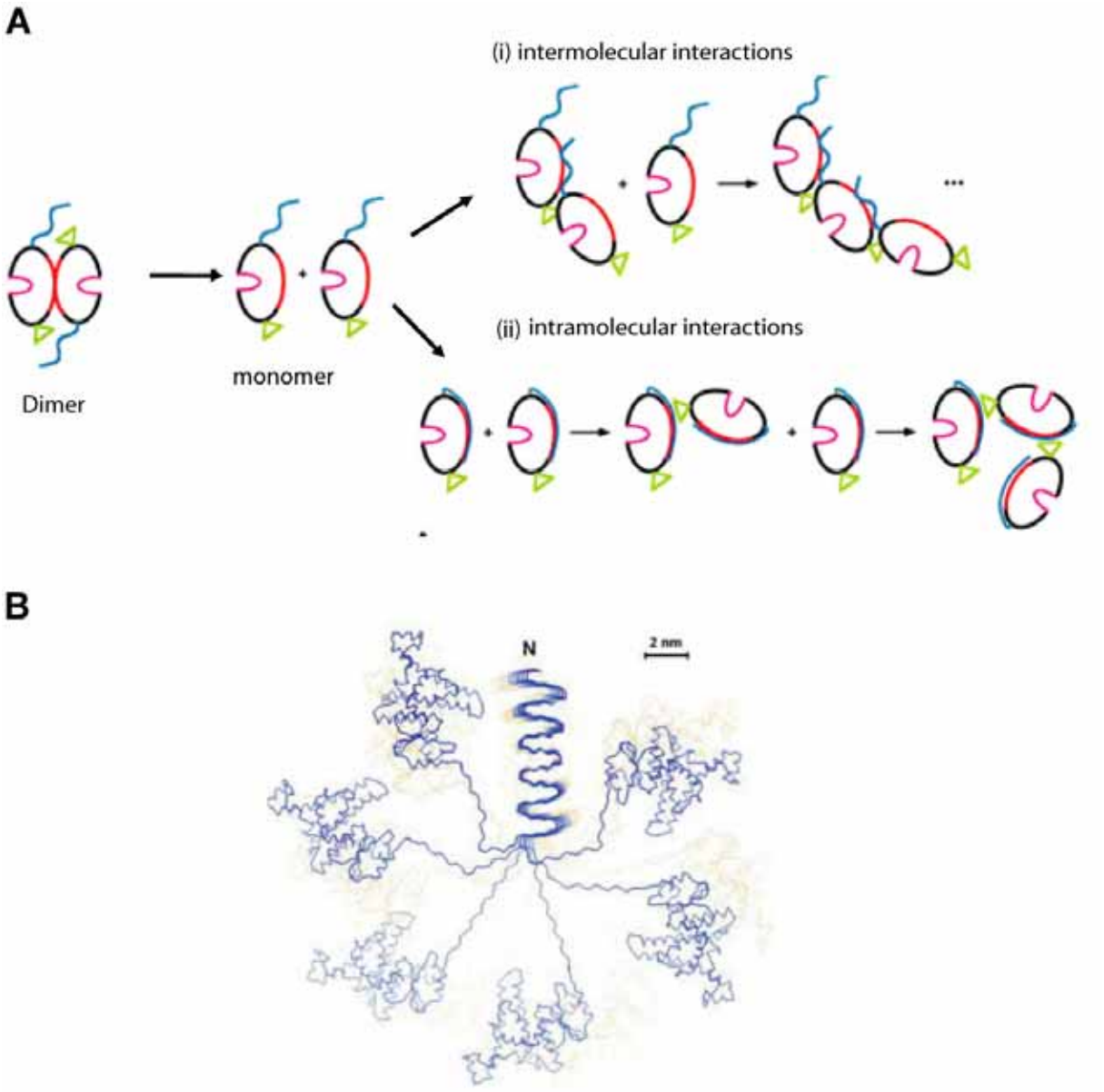

Figure 1-8: Currently published models about ure2p.

A) The model proposed by Melki (Bousset et al., 2002) is based on the observations that a dissociation of the Ure2p dimer occurs prior to assembly into fibrils; (i) the fibrils formed under the conditions lack a cross ß-core and the NTD is interacting with another Ure2p (like in a domain swapping model) and (ii) the observation that Ure2p retains a NTD interacting with the C-terminal domain and with another molecule at the same time. B) According to Steven (Kajava et al., 2004) Ure2p fibrils have a cross ß-structure. The residues of the N-terminal domain are in a planar serpentine arrangement, with a small and potentially variable left-hand twist, stabilized not by packing of apolar side chains but by H-bond networks. This H-bond network is generated by the stacking of Asn side chains. Charged residues are excluded.

Two models have been proposed to account for the assembly of Ure2p into protein fibrils and describe the architecture of the fibrils. The first model suggested Melki (Bousset et al., 2002) (Bousset et al., 2004) assumes that the

assembly of full-length Ure2p into fibrils occurs in the absence of a major conformational change and that Ure2p fibrils rather resemble biopolymers like actin and microtubules (Figure 1-8A). The second model proposed by Wickner (Speransky et al., 2001) (Baxa et al., 2003) (Kajava et al., 2004) (Figure 1-8B and section 1.6.2) hypothesizes that the fibrils are like amyloids, with a cross β-structure, and that the assembly of the protein is driven by a conformational change of the N-terminal domain of the protein (conversion).

2 Problem description

The fibrillation and aggregation of proteins is a complex phenomenon that until today is not really understood at the molecular level. Solving this problem is of high medical importance, as a growing number of severe diseases have been attributed to cellular protein aggregation, including Alzheimer's disease, Chorea-Huntington, and Creutzfeld-Jacob syndrome. Although the proteins responsible for these diseases appear to have little in common besides their tendency to aggregate, there is growing evidence that a similar molecular mechanism is governing pathogenic protein polymerization in vivo. The prion protein Ure2p from S. cerevisiae is a good model system for studying these conformational diseases in vitro, as it i) can be expressed recombinantly in high yields in *E. coli*, ii) is fairly easy to purify, iii) is not toxic or harmful to humans, iv) it readily associates into amyloid fibrils. The aim of this thesis was to acquire knowledge about the fibrillation pathway of Ure2p and compare it with that of other amyloid proteins using Ure2p as a model system for aggregation and self-assembly. These results will hopefully improve our understanding of the principles underlying pathogenic fibrillation and aggregation of proteins.

Specifically, the following issues were addressed in this work:

1. Intermediates of the fibrillation pathway of Ure2p were isolated and characterized. Further, their role and importance for the overall process of fibrillation was determined. This was achieved analyzing early stages of the fibrillation process with AFM, CD spectroscopy, and size-exclusion chromatography.

2. Dimeric and fibrillar Ure2p were extensively characterized on a structural level using optical spectroscopy, TEM, AFM, and X-ray fiber diffraction. Fiber morphology was analyzed to determine the interrelationship of the various fibrillar species. Another important issue was whether Ure2p undergoes a conformational change towards beta-structure upon fibrillation, similar to what has been found for other amyloids.

3. To gain further insight in the role of electrostatic effect on the Ure2p conformation transitions and fibril formation, the dependence of Ure2p fibrillation on salt concentration and effect of cations and anions were investigated. This data can provide important information on the process of fibril formation such as the involvement of electrostatic interactions on the self-assembly. The effect of temperature on self-assembly and conformational behavior was investigated. The rate and effect on fibril formation was assessed using the amyloid-specific fluorescent dye Thioflavin T, TEM and AFM. Ure2p fibrillation was extensively characterized on a structural level using CD spectroscopy and X-ray fiber diffraction.

3 Materials and Methods

3.1 Materials

3.1.1 Chemicals

Acrylamide/ Bis-Acrylamide 19:1, 40 %	Roth, Karlsruhe, Germany
Adenosine-5'-Triphosphate (ATP) Disodium Salt	Roche Diagnostics, Mannheim, Germany
Agarose NEEO, ultra pure grade	Roth, Karlsruhe, Germany
Ammonium Peroxydisulfate (APS)	Serva, Heidelberg, Germany
Ampicillin	Roth, Karlsruhe, Germany
Bacto Agar	Difco Laboratories, Detroit, USA
Bacto Tryptone	Difco Laboratories, Detroit, USA
Bacto Yeast Extract	Difco Laboratories, Detroit, USA
Bromophenol Blue	Serva, Heidelberg, Germany
3-[(*3*-Cholamidopropyl)dimethyl-ammonio]-*1*-propane sulfonate (CHAPS)	Roth, Karlsruhe, Germany
Chloramphenicol	Sigma, St. Louis, USA
Coomassie Brilliant Blue (R-250)	Serva, Heidelberg, Germany
1,4- Dithiothreitol (DTT)	Roth, Karlsruhe, Germany
ECL Plus Western Blotting detection reagents	Amersham Biosciences, Uppsala, Sweden
Ethanol (p.A.)	Riedel de Haen AG, Seelze, Germany
Ethidium Bromide	Sigma, St. Louis, USA
Guanidine Hydrochloride	ICN Biochemicals Inc.,Irvine, USA
N-[*2*-Hydroxyethyl]piperazine-*N*'-*2*-ethanesulphonic acid] (HEPES)	ICN Biochemicals Inc.,Irvine, USA
Kanamycin	Sigma, St. Louis, USA
2- Mercaptoethanol, Ultra Pure Grade	Serva, Heidelberg, Germany

Milk powder	Roth, Karlsruhe, Germany
Polyoxyethylene Sorbitan Monolaurate (Tween 20)	Merck, Darmstadt, Germany
Silver Nitrate	Roth, Karlsruhe, Germany
Sodium Dodecyl Sulfate (SDS)	Roth, Karlsruhe, Germany
N,N,N',N'-Tetramethylethylene-Diamine (TEMED)	Sigma, St. Louis, USA
Thioflavin T	Sigma, St. Louis, USA
[*Tris*-(Hydroxymethyl)-Aminomethane] (Tris)	USB Inc., Cleveland, USA

Additionally used chemicals were obtained from Merck (Darmstadt, Germany) and had a purity grade, if not noted otherwise. For preparation of solutions and buffers quartz bidistilled water was used. All solutions were titrated to the noted pH at the given temperature.

3.1.2 Molecular weight markers, assays and kits

High Pure Plasmid Isolation Kit	Roche Diagnostics, Mannheim, Germany
High Range Molecular Weight Standard (HMW, SDS-PAGE)	BioRad Laboratories, Munich, Germany
Low Range Molecular Weight Standard (LMW, SDS-PAGE)	BioRad Laboratories, Munich, Germany
Roti-Mark prestained	Roth, Karlsruhe, Germany
1 kb DNA-Ladder	PeQlab, Erlangen, Germany
Protein standards for HPLC	Roche, Mannheim, Germany
Bradford Protein Assay reagent	Pierce, Rockford, USA
Maxi-Prep, Plasmid Isolation Kit	Qiagen, Hilde, Germany

3.1.3 Proteins and Antibodies

Proteins	
Bovin Serum Albumine	Roche Mannheim, Germany
Catalase	Sigma, St. Louis, USA
DNaseI	Roche Mannheim, Deutschland
Lysozyme	Sigma, St. Louis, USA
Trypsin	Roche Mannheim, Germany
Antibodies	
FITC-Anti-Rabbit–IgG Conjugate (Goat)	Sigma, St. Louis, USA
Polyclonal Anti-Ure2p (Rabbit)	Dr. J. Pineda Antibody Services, Berlin, Germany
Monoclonal Anti-polyHistidine Clone His-1	Sigma, St. Louis, USA

3.1.4 Consumables

Ultra filtration membranes YM3, YM10, YM30, YM100	Amicon, Witten, Germany
Dialysis tubing Spectra/Por MW 6000-8000 Da	Spectrum, Houston, USA
Immobilon-NC(Nitrocellulose)-membrane	Millipore, Bedford, USA
Immobilon-P(PVDF) membrane	Millipore, Bedford, USA
Syringes 1 ml, 2 ml, 10 ml, 20 ml, 60 ml	Braun, Melsungen, Germany
Reaction cups 0.4 ml, 1.5 ml, 2 ml	Eppendorf, Hamburg, Germany
membranes YM3, YM10, YM30, YM100	Amicon, Witten, Germany
Polyethylene Tubes (15/50 ml)	Greiner Group, Nürtingen, Germany
Polystyrole Petri dishes	Greiner Group, Nürtingen, Germany
Sterile Culture Tubes (17x100 mm)	Elkay Laboratory Products, Hampshire, UK
X-Ray Films X-OMAT AR	Eastman Kodak, Rochester, USA

Filter paper	Whatman, Maidstone, UK
Sterile filters (0.22 μM)	Zefa, Munich, Germany
pH Indicator strips	Roth, Karlsruhe, Germany
Disposable Cuvettes 1.5 ml	Brand, Wertheim, Germany
4-20% Tricin Gradient Gel	Invitrogen, Groningen, Netherlands

Additionally consumables not mentioned were obtained from Firma Zefa (Munich, Germany)

3.1.5 Chromatography equipment and columns

Butyl-Sepharose 4 Fast Flow	Amersham Biosciences, Uppsala, Sweden
DEAE-Sephacel Fast Flow	Amersham Biosciences, Uppsala, Sweden
Hydroxyapatite	BioRad, Munich, Germany
Ni-NTA-Superflow	Qiagen, Hilde, Germany
Resource-Q; Source 15 (FPLC)	Amersham Biosciences, Uppsala, Sweden
HiLoad 16/60 Superdex 200 Prep Grade	Amersham Biosciences, Uppsala, Sweden
HiLoad 26/60 Superdex 200 Prep Grade	Amersham Biosciences, Uppsala, Sweden
HiLoad 16/60 Superdex 75 Prep Grade	Amersham Biosciences, Uppsala, Sweden
Q-Sepharose Fast Flow	Amersham Biosciences, Uppsala, Sweden
Super-Loop 150 ml	Amersham Biosciences, Uppsala, Sweden
ÄKTA Prime:	Amersham Biosciences, Uppsala, Sweden
Peristaltic pump P-1	Amersham Biosciences, Uppsala, Sweden

Fraction collector GradFrac	Amersham Biosciences, Uppsala, Sweden
Recorder REC-1	Amersham Biosciences, Uppsala, Sweden
UV flow through detector UV-1	Amersham Biosciences, Uppsala, Sweden
Sepharose 6	Amersham Biosciences, Uppsala, Sweden
TSK 2000SW	Tosoh GmbH, Stuttgart, Germany
TSK 3000SW	Tosoh GmbH, Stuttgart, Germany
TSK 4000PW	Tosoh GmbH, Stuttgart, Germany
Sephadex 200 HR	Amersham Biosciences, Uppsala, Sweden
Sephadex 200 prep grade	Amersham Biosciences, Uppsala, Sweden
FPLC:	Amersham Biosciences, Uppsala, Sweden
Pump system	Amersham Biosciences, Uppsala, Sweden
UV-VIS Detector	Amersham Biosciences, Uppsala, Sweden
Gradient Unit	Amersham Biosciences, Uppsala, Sweden
HPLC-System:	Jasco, Groß-Umstadt, Germany
PU-1580 HPLC Pump,	Jasco, Groß-Umstadt, Germany
LG-980-02S Gradient Unit	Jasco, Groß-Umstadt, Germany
FP-1520 Fluorescence Detector	Jasco, Groß-Umstadt, Germany
UV-1575 UV-VIS Detector	Jasco, Groß-Umstadt, Germany
Degaser Gastorr 153	Jasco, Groß-Umstadt, Germany

3.1.6 Laboratory equipment

3.1.6.1 Absorbance Spectrophotometer

Ultrospec 3000 UV/Visible	Amersham Biosciences, Uppsala, Sweden
Novaspec II Visible	Amersham Biosciences, Uppsala, Sweden
Cary 30	Varian Germany, Darmstadt, Germany

3.1.6.2 Spectrofluorimeter

SPEX FluoroMax 3	Jobin Yvon, Munich, Germany

3.1.6.3 CD-Spectropolarimeter

J 715 Spectropolarimeter with PTC 343 Peltier Temperature unit	Jasco, Groß-Umstadt, Germany

3.1.6.4 Atomic Force Microscopy

Multimode atomic force microscope	Digital Instruments, Santa Barbara, USA
Nanoscope IV controller	Digital Instruments, Santa Barbara, USA
Type E scanner	Digital Instruments, Santa Barbara, USA
Single-beam silicon cantilever	Veeco, Manheim, Germany
Silicon probes	Veeco, Manheim, Germany

3.1.6.5 Gel Electrophoresis- and Blotting Equipment

Roth RHU10X Gel Electrophoresis Unit	Roth, Karlsruhe, Germany
Mighty Small II Gel Electrophoresis Unit	Amersham Biosciences, Uppsala, Sweden

Biometra Fastblot B44 Apparatus	Biometra, Göttingen, Germany

3.1.6.6 Power Supply

Amersham EPS 3500, 301 and 1001	Amersham Biosciences, Uppsala, Sweden

3.1.6.7 Laboratory Balances

Sartorius Analytical Balance BP 121 S	Sartorius, Göttingen, Germany
Sartorius Top Loading Balance	Sartorius, Göttingen, Germany
Sartorius Semi- Microbalance BL 310	Sartorius, Göttingen, Germany

3.1.6.8 Centrifuges and other equipment

Eppendorf Bench Top Centrifuge 5415	Eppendorf, Hamburg, Germany
Avanti J-25 Beckmann	Beckmann, Palo Alto, USA
J2-HS Beckmann:	Beckmann, Palo Alto, USA
Rotors JA-10, 25.50 and JLA-16.250	Beckmann, Palo Alto, USA

3.1.6.9 Additional laboratory equipment

Varioklav Steam Sterilizer EP-Z	H+P Laboratory Technics, Oberschleißheim, Germany
Ice machine	Ziegra, Isernhagen, Germany
Cell Culture Shaker Certomat S	B. Braun Biotech International, Melsungen, Germany
Magnetic stirrer MR 2000	Heidolph, Kehlheim, Germany
Metalthermoblock TB 1	Biometra, Göttingen, Germany
Thermomixer Compact	Eppendorf, Hamburg, Germany
pH Meter	WTW, Weilheim, Germany
Water bath F6-K	Haake, Karlsruhe, Germany
Rocking Platform Shaker Polymax 1040	Heidolph, Schwabach, Germany
- 80°C Freezer	Sanyo Electric Co. Ltd., Osaka, Japan

Ultrasonic Bath Sonsorex RK 100H	Bandelin, Berlin, Germany
MALDI- TOF Mass Spectrometer Biflex II	Bruker Daltonics, Bremen, Germany
GENios Microplate Reader	Tecan Group Ltd., Männedorf, Switzerland
Vacuum Pump	Vacuumbrand GmbH + Co KG, Wertheim, Germany
Film Developing Unit Optimax TR	MS Laboratory Equipment, Heidelberg, Germany
Pipettes 2.5 µL, 10 µL, 20 µL, 100 µL, 200 µL, 1000 µL	Eppendorf, Hamburg, Germany
Quartz Cuvette	Helma, Pfungstadt, Germany
Transmission-Electron microscope	Phillips, Hamburg, Germany
Scanning-Electron microscope	Jeol, Eching, Deutschland
Sputter	Bal-Tec, Balzers, Lichtenstein
Ultrasound machine Sonifier B-12	Branson, Danbury, USA
Ultrasound bath, Sonsorex RK 100H	Bandelin, Berlin, Germany
Cell opening machine, Basic Z	Constant Systems, Warwick, England
Incubator	New Brunswick Scientific, Nürtingen, Germany

3.2 Computer Software and Web Tools

Microsoft Office 2000	Microsoft (Redmond, USA)
Sigma Plot 2001 for Windows 95/NT	Jandel Scientific, Tallahassee, USA
Microcal Origin 7.0	OriginLab Corporation, (http://www.originlab.com)
ProtParamTool	ExPasy (http://us.expasy.org)
Photo Paint 8.0	Corel Corporation Ltd., Ottawa, Canada
Adobe programs	Adobe Systems Incorporated (http://www.adobe.com)
Borwin	Jasco, Groß-Umstadt, Deutschland
PeptIdent	ExPasy (http://expasy.hcuge.ch/)

CDNN software package	http://www.expasy.org/ (www.bioinformatik.biochemtech.uni-halle.de)
Reference Manager Network Edition	ISI Research Soft (USA)
Image Master 1D	Amersham Biosciences, Uppsala, Sweden
Lab Scan	Amersham Biosciences, Uppsala, Sweden
RasMol 2.7.2.1	RasWin Molecular Graphics, Bellport, USA

3.3 Buffers, Antibiotics and Medium

All buffers, stock solutions and media, if not included here, were performed as described in Sambrook & Russell (Sambrook and Russell, 2001).

Table 3-1: Buffer used for protein methods

Buffer	Recipe
TBS	50 mM Tris/HCl, pH 7.5, 200 mM NaCl
Lysis Buffer 1	50 mM Tris/HCl, 5 mM EDTA, 1 mM DTT pH 8
Ionic Exchange Buffer A	50 mM Tris/HCl, 2 mM EDTA, pH 8
Ionic Exchange Buffer B	50 mM Tris/HCl, 2 mM EDTA, 1 M NaCl, pH 8
SEC-200 Buffer	50 mM Tris/HCl, pH 7.8
Lysis Buffer	50 mM NaPi, 300 mM NaCl, pH 8
Ni-NTA equilibration Buffer	50 mM NaPi pH 7.5, 300 mM NaCl,
Ni-NTA wash	50 mM NaPi pH 7.5, 300 mM NaCl, 20 mM imidazole
Ni-NTA elution	50 mM NaPi pH 7.5, 300 mM NaCl, 300 mM imidazole
SEC-75 buffer	50 mM NaPi pH 7.5, 200 mM NaCl

3.3.1.1 Isopropyl-1-thio-□-D-galactoside (IPTG) stock solution:

IPTG was dissolved in water to the end concentration of 1M, sterile filtered and stored in aliquots at –20°C until used.

3.3.1.2 Antibiotics stock solution

Antibiotics were dissolved, sterile filtered and stored at –20°C, until use. The stock solution was diluted 1:1000 when added to the medium.

Ampicillin, 100 mg/ml in water

Kanamycin, 35 mg/ml in water

Chloramphenicol, 50 mg/ml in ethanol

3.3.1.3 Medium

LB_0:	Bacto Trypton	10 g
	Yeast Extract	5 g
	NaCl	5 g
	H_2O	ad 1 l
	Adjust pH with NaOH at 7,2	
dYT:	Bacto Trypton	16 g
	Yeast Extract	10 g
	NaCl	5 g
	H_2O	ad 1 l
	Adjust pH with NaOH at 7,2	
SB0: Solution 1	Bacto Trypton	20 g
	Yeast Extract	10 g
	NaCl	5 g

	MgSO4·7 H2O	1 g
	NH_4Cl	0.6 g
	NaH_2HPO_4 x H2O	6 g
	$(NH_4)_2SO_4$	2 g
	H_2O	ad 1 l
	Adjust pH with NaOH at 7,2	
Solution 2	KH_2PO_4	13 g
	K_2HPO_4 x 3 H_2O	10 g
Solution 3	Glucose	500 g
	$MgSO_4$ x 7 H_2O	10 g

For SB medium: Solutions 1, 2, and 3 have to be autoclaved separately. It is useful to dissolve the ingredients for 1 in 80 % of the final volume, and the ingredients for 2 in 20 % of the final volume, and then mix solution 1 and 2 before starting the culture. All prepared medium were sterilized by autoclaving for 20 minutes at 2 bars. The autoclaved medium was allowed to cool to 50°C and antibiotics were added, if necessary. 15 g Agar per one liter of medium were added for the preparation of agar plates. Plates were poured and plate edges marked with the appropriate color markers. When the medium has hardened completely, the agar plates were inverted and stored at + 4°C until needed.

3.4 Molecular Biology Methods

To work with micro organism and molecular biology methods, all work was done with sterile solutions. When not described, the work was done at room temperature.

3.4.1 Bacterial strains and plasmids

E.coli is one of the most widely used host for the production of the recombinant proteins (Baneyx, 1999) due to the ability to grow rapidly and at high density at inexpensive substrates.

Table 3-2: Plasmids and Expression Vectors used in *E.coli*

Vector	Marker / Description	Origin/Reference
pET28a	Kan^R, 6xHis C-terminal, lac Operator, T7 Promotor	Novagen, Madison, USA
pET3a	Amp^R, lac Operator, T7 Promotor	Novagen, Madison, USA
pET28a_NT	N-terminal from Ure2p gene in pET28a	A kind gift from Stefan Walter
pET3a_ure2p	Ure2p gene in pET3a plasmid	Cullin et all, (Komar et al., 1998)

Table 3-3: Bacterial Strains information

Strain	Genotype	Origin
E. coli DH10B	F^-*ara*D 139∆(*ara leu*) 7697∆*lac*X74 *gal*U *gal*K *mcr*A ∆(*mrr*$^-$ *hsd*RMS-*mcr*BC) *rps*L *dec*R 380 ∆*lac*Z ∆M15 *end*A1 *nup*G *rec*A1	Jessee, 1986
E. coli XL1 Blue	∆(*mcr*A) 183 ∆ (*mcr*CB-*hsb*SMR- *mrr*) 173 *end*A1 *sup*E44 *thi*-1 *rec*A1 *gyr*A96 *rel*A1 *lac*[F` *pro*AB *lac*I^qZ∆M15 Tn10 (*Tet*^{r})] Su^-	Stratagene, La Jolla, USA
E. coli HB101	*sup*E44 *hsd*S20 ($r_R^-m_R^-$) *rec*A13 *ara*-14 *pro*A2 *lac*Y1 *gal*K2 *rps*L20 *xyl*-5 *mtl*-1	Boyer & Roulland-Dussoix, 1969; Bolivar & Backman, 1979
E. coli BL21 (DE3)	F^-omp T *hsd*S($r_{B-}m_{B-}$) dcm^+ Tet^r	Stratagene, La Jolla, USA

Codon Plus	gal λDE3) endA Hte (argU ileY leuW Cam^r

3.4.2 Long-term storage of bacterial strains

A sterile, disposable polypropylene culture tube containing 5 ml of selective LB medium was inoculated with a freshly grown single bacterial colony and left overnight at 37 °C. The cell suspension was centrifuged and the cell pellets were resuspended in 3 ml selective LB medium containing 55% glycerol. The culture tubes were stored at –20°C until needed. Alternatively, 600 ml of selective LB medium, containing *E. coli* cells freshly growth state, were centrifuged and cell pellets were resuspended in 300 µl glycerol (50%) and stored at –80°C.

3.4.3 Chemically competent E. coli Cells:

10 ml of LB medium were inoculated with a single colony from the LB plate and incubated at 37°C with shaking (200 rpm) overnight. 5 ml of LB medium in a 100 ml of medium was inoculated with the 50 ml overnight culture. The culture was grown in shaking (200rpm) incubator at 37°C until the OD_{600} was between 0.6 – 1.0 (Cuvette path length = 1 cm) means around 10^8 cells per ml of culture (Sambrook and Russell, 2001). The culture was cooled for 60 min on ice, centrifuged for 5 min at 4 °C. The pellet was resuspended in 20 ml Solution A and cooled for 60 min on ice. After a second time of centrifugation, the pellet was resuspended in 2 ml of solution A-glycerin. The solution was separated in aliquots and frozen at -80.

Table 3-4: Buffers for preparation of chemically competent *E. coli* Cells

Solution A:	3 M NaAc (pH 5,5)	13 ml
	1 M $CaCl_2$	100 ml
	2,8 M $MnCl_2$	25 ml

	H_2O	862 ml
	Sterile and filtered	
Solution A - Glycerin:	Glycerin (87%)	69 ml
	Solution A	331 ml

3.4.4 Transformation of the chemically competent bacteria

Transformation of the chemically competent bacteria was done according to the method of Kaderbhai(He et al., 1990).Frozen chemically competent cells were thawed on ice for 5 to 10 min. 1 µl of purified plasmid DNA was mixed in a 1.5 ml Eppendorf tube with 100 µl aliquot of competent *E. coli*. The tube was incubated on ice for 30 min. Cells were heat pulsed at 42°C for 1 min. then cooled on ice for 2-3 min. To this tube, 0.9 ml of pre-warmed LB medium was added and cells were incubated at 37°C for 1 hr with shaking at 300 rpm. Cells were plated on a LB agar plates containing the appropriate antibiotic to select transformants and then incubated at 37°C overnight. Alternatively, 500 µl LB solution containing fresh transformants were added to 5 ml LB with appropriate antibiotic and then incubated at 37°C overnight(Hanahan, 1983).

3.4.5 Plasmid Recovery from E.coli

3 ml antibiotic-containing LB medium was inoculated with a single colony and incubated over night at 37°C under shaking. Plasmids were isolated from cell pellets using High Pure Plasmid Isolation Kit purchased from Roche Diagnostics (Mannheim, Germany), following the manufacture's instructions. This kit was used to prepare purified plasmid DNA in small quantities (5-10 µg), known as mini preparations, using the alkaline method that generates highly purified plasmid DNA from *E. coli*, free of RNA contamination(Sambrook and Russell, 2001). The purified plasmid DNA from *E. coli* was suitable for transformation. Purified plasmids were evaluated by restriction digestion and analytical agarose gel electrophoresis.

3.4.6 Agarose Gel Electrophoresis of DNA

Electrophoresis through agarose was used to separate, identify and purify DNA fragments.

Basic Principles: As small differences in ionic strength or pH create fronts in the gel that greatly affect the mobility of DNA fragments. Using fluorescent dye Ethidium bromide in the DNA sample it is possible to localize DNA on the gel. Ethidium bromide contains a tricyclic planar group that intercalates between the stacked bases of DNA, displaying an increased fluorescent yield compared to that of the dye in free solution. This happens because DNA absorbs UV radiation at 254 nm and transmitted to the dye. Radiation at 302 nm and 366 nm is absorbed by the bound dye itself. In both cases, energy is re-emitted at 590 nm in the red-orange region of the visible spectrum.

Method: Solutions of agarose were prepared in electrophoresis buffer (1x TAE) at a concentration of 1%. This concentration of agarose was used to separate DNAs in a size range from 250 bp to 12 kb. The agarose slurry was heated in a microwave oven and cooled to <60°C before casting the gel. Ethidium bromide was added to a final concentration of 0.4 µg/ml. An appropriate comb was used for forming the sample pockets in the gel, while the agarose solution cool down Electrophoresis buffer was added to cover the gel to a depth of approximately 1 mm. Samples of DNA were mixed with approximately 0.1 volumes of 10x gel loading buffer and loaded to the pockets. Electrophoresis was performed using a constant electric current of 120 mA. The molecular size of the separated DNA fragments was determined using a 1 kb DNA-Ladder.

Table 3-5: Buffers for preparation of Agarose Electrophoresis

Buffer	Recipe
TAE Buffer 50x	2 M Tris/Acetic Acid, 50 mM EDTA pH 8.0 adjusted with Acetic Acid glacial
DNA Gel Loading Buffer 10x	50% (v/v) Glycerol, 10 mM EDTA pH 8.0, 0.2% (w/v) Bromophenol Blue, 0.2% (w/v) Xylene Cyanol
Ethidiumbromid-	0,04% (w/v) Ethidiumbromid

Solution	
1% Agarose solution	1 g Agarose, 100 ml of TAE Buffer 1x, 1 µl of 0.04% (w/v) Ethidium Bromide solution

3.4.7 DNA concentration

The amount of DNA was traced with absorption measurement at 260 nm, assuming that 50 µg/ml double stranded DNA would give a readout of an OD_{260} = 1.

3.4.8 Expression kinetics of target protein in bacterial cultures

A colony of *E. coli* cells with recombinant plasmid was inoculated overnight in 5 ml of LB culture containing the appropriate antibiotics.1 ml from this pre-culture was added to 100 ml of fresh selective medium. When OD_{600} has reached 0.7-1.0 then a sample called “before induction – BI” was taken. 1mM IPTG was added and another sample was taken called “after induction”. Samples were taken every hour and measured at OD_{600}. Following this protocol, test expressions were performed under different conditions (temperature, medium and expression time) to identify the optimal condition where protein expression levels and their solubility’s were reasonably high (Makrides, 1996). After measuring the OD, cells were pelleted and resolubilized in Laemmli Buffer. To very OD value = 0.3, 50 µl of 1 volume of Laemmli Buffer was added. The solution was boiled at 95°C for 5 minutes. Identical sample volumes were applied to SDS-PAGE.

3.5 Electrophoretical methods

3.5.1 SDS polyacrylamide gel-electrophoresis (SDS-PAGE)

SDS-PAGE allows the separation of protein based on mass under denaturing and reducing conditions (Laemmli, 1970). This method was used to analyze the mass of the proteins and the effectiveness of protein purification scheme.

Basic Principles: Polyacrylamide gels are composed of chains of polymerized acrylamide that are cross-linked by a bifunctional agent such as *N,N'*-methylene-*bis*-acrylamide. The gel acts like a molecular sieve where molecules of various size and charge can be separated. The effective range of separation of SDS polyacrylamide gels depends on the concentration of polyacrylamide used to cast the gel (see table). Using this method, the denatured polypeptides bind SDS and become negatively charged. Since the amount of SDS bound is almost always proportional to the molecular weight of the polypeptide and is independent of its sequence, SDS-polypeptide complexes migrate through polyacrylamide gels in accordance with the size of the polypeptide. At saturation, approximately 1.4 grams of detergent are bound per 1 gram of polypeptide. By using markers of known molecular weight, it is possible to estimate the molecular weight of the polypeptide chain.

Method: In this work, SDS polyacrylamide gel electrophoresis was carried out with a discontinuous buffer system in which the buffer in the reservoirs is of a pH and ionic strength different from that of the buffer used to cast the gel (ORNSTEIN, 1964), (DAVIS, 1964). During this work, 12.5% and 15 % polyacrylamide SDS gels were used. The anionic detergent SDS was used in combination with the reducing agent *2*- Mercaptoethanol to dissociate the proteins by heat treatment before they are loaded onto the gel (Laemmli, 1970). 5x concentrated Laemmli sample buffer was added to the protein samples and incubated for 4 min at 95°C prior to loading of the gels. Stacking gels were prepared using 5% polyacrylamide. The accurate composition is listed in Table 4. To the loading of purified protein, the samples were prepared in the volume of 5x Laemmli buffer. SDS polyacrylamide gel electrophoresis was carried out in a vertical electrophoresis apparatus using a constant electric current of 25 mA/gel in 1 X SDS running buffer.

Table 3-6: Marker size (kDa)

LMW	97.4	66.2	45	31	21.5	14.4	-
HMW	200	116	97.4	66,2	45	-	-
Rainbow	220	97	66	45	30	21	14

Table 3-7: Buffers for preparation of SDS-PAGE gels

Buffer	Recipe
2x Stacking buffer	0,25 M Tris/HCl,0,4 % (w/v) SDS pH 6,8
4x Separation buffer	1,5 M Tris/HCl, 0,8 % (w/v) SDS, pH 8,8
APS-Solution	10 % (w/v) APS in H_2O
TEMED-Solution	98 % (w/v) TEMED in H2O
SDS Running Buffer 10x	0.25 M Tris/HCl, 2 M Glycine, 1% SDS pH 8.8
Laemmli Gel Loading Buffer 5x	10% (w/v)SDS, 50% (w/v) Glycerol, 300 mM Tris, 0.05% (w/v) Bromophenol Blue, 5% (v/v) *2*- Mercaptoethanol.
Tricin Running Buffer	0,1 M Tris/HCl, 0,1 M Tricin0,1 % (w/v) SDS pH 8,3
Tricin Loading buffer	0,45 M Tris/HCl, 12% (v/v) Glycerin4 % (w/v) SDS, 0,0025 % (w/v) Coomassie Blue R250

Table 3-8: Preparation of SDS-PAGE gels. Gel solution pro Gel (Gelsize: 10 x 8 x 0,075 cm)

	SG	SG	SG	CG
	10 %	12.5 %	15 %	3 %
40 % AA	2.5 ml	3.125 ml	3.75 ml	0.625 ml
4x SB	2.5 ml	2.5 ml	2.5 ml	-
2x CG	-	-	-	2.5 ml
10 % SDS	0.2 ml	0.2 ml	0.2 ml	0.1 ml
H2O	4.8 ml	4.175 ml	3.55 ml	1.775 ml
Σ	10 ml	10 ml	10 ml	5 ml
10% APS	65 µl	65 µl	65 µl	65 µl
TEMED	3.3 µl	3.3 µl	3.3 µl	3.3 µl

3.5.2 Staining SDS Polyacrylamide Gels with Coomassie Blue

Basic Principles: Coomassie Brilliant Blue is an aminotriarylmethane dye that forms strong (but non covalent) complexes with proteins. This happens most probably by a combination of *van der Waals* forces and electrostatic interactions with NH_3^+ groups (Sambrook and Russell, 2001). The dye is used

to stain proteins after electrophoresis through polyacrylamide gels. The uptake of dye is approximately proportional to the amount of protein, following the *Beer-Lambert* law.

Method: The staining method given below is a modification of the staining procedure originally described by Fairbanks *et al.* (Fairbanks et al., 1971) with slight alterations to incubation times. Proteins were separated by SDS-Page. The gel was incubated in Fairbanks A and placed on a slowly rotating platform for 10 minutes at room temperature. The stain was removed and saved for future use. Next, the gel was destained by soaking it first in Fairbanks B, afterwards in Fairbanks C and finally in Fairbanks D (10 minutes per each destaining step). Solution B and C were also saved for further use, whereas Solution D was discarded. After de-staining, the gel was stored in bidistilled water. To make a permanent record, the stained gel was either scanned or dried.

Table 3-9: SDS-Page buffers for staining Gels with Coomassie Blue

Buffer	Recipe
Fairbanks A	25% (v/v) Isopropanol, 10% (v/v) Acetic Acid, glacial, 0.05% Coomassie Blue R
Fairbanks B	10% (v/v) Isopropanol, 10% Acetic Acid, glacial, 0.002% Coomassie Blue R
Fairbanks C	10% Acetic Acid, glacial, 0.002% Coomassie Blue R,
Fairbanks D	10% Acetic Acid, glacial

3.5.3 Staining protein gels with silver salts

Basic Principles: The silver staining method used in this work was adapted from Heukeshoven (Heukeshoven and Dernick, 1988) and is based on the binding of Silver to the protein (Switzer, III et al., 1979). This type of staining is 100-1000-fold more sensitive than staining with Coomassie Brilliant Blue and is capable of detecting as little as 0.1-1.0 ng of polypeptide in a single band.

Method: The proteins were separated by SDS-PAGE and fixed by incubating the gel for 20 minutes at room temperature with gentle shaking in Fixing Solution 1. The first solution was discarded and added Fixing Solution 2. The gel was incubated for 30 minutes at room temperature with gentle shaking. Fixing Solution 2 was discarded and approximately 10 gel volumes of bidistilled water were added. The gel was incubated for 5 minutes at room temperature with gentle shaking. The described washing step was repeated 3 times. The last of the H_2O washes was discarded, and Staining Solution was added. The gel was incubated for 30 minutes at room temperature with gentle shaking. The Staining Solution was discarded and both sides of the gel were washed with bidistilled water. Next, Developing Solution was added and the gel incubated at room temperature with gentle agitation until protein bands became visible. Incubation was continued to obtain the desired contrast. The reaction was stopped by washing the gel in Stopping Solution. Finally, the gel was washed several times with bidistilled water. To make a permanent record, the stained gel was either scanned or dried.

Table 3-10: Solutions for staining Gels with silver

Buffer	Recipe
Fixing Solution 1	30% (v/v) Ethanol, 10% (v/v) Acetic Acid, glacial,
Fixing Solution 2	2 ml 25% (v/v) Glutaraldehyde, 0.1 g sodium thiosulfate, up to 100 ml with 0.4 M Sodium Acetate, 0.5% Acetic Acid, glacial, 30% (v/v) Ethanol
Staining Solution	6 mM Silver Nitrate, 25 µl 37% (w/v) Formaldehyde up to 100 ml H_2O, bidistilled
Developing Solution	7.5 g Sodium Carbonate, 120 µl 37% (w/v) Formaldehyde, up to 300 ml with H_2O, bidistilled
Stopping Solution	50 mM EDTA pH 7.5

3.5.4 Western blotting

Basic Principles: This method of protein detection was applied to confirm immunological identity of the expressed proteins and to determine presence of any degradation products or isoforms of the purified proteins (Towbin et al., 1979) ;(Burnette, 1981) (Gershoni and Palade, 1983) (Sambrook and Russell, 2001)The membrane is incubated with a first antibody directed against the protein and with a secondary antibody that is directed against the first one. This secondary antibody has an enzyme which covalent linked. A color reaction carried out by an enzyme indicates the position of the protein.

Method: Proteins were separated by SDS-PAGE as described previously using a Rainbow marker as a MW standard. The gel containing the separated protein bands was deposited over a nitrocellulose membrane and assembled in a sandwich form with 6 x Wathman papers. The membrane was placed on the side of the gel facing the anode. Proteins were electrophoretically transferred from the gel using a Blot system for 1.5 h by 72 mA per Gel using Transfer buffer(Towbin et al., 1979). Transferred proteins were then visualized by pre-staining in 0.2% (w/v) Ponceau Red in trichloroacetic acid. The nitrocellulose membrane was incubated for 30 min in blocking reagent. Milk powder is added to suppress non-specific adsorption of antibodies to unreacted binding sites of the membrane. The membrane was washed 3 times with blocking reagent. This step is followed by incubation for 90 min with the rabbit anti-Ure2p antiserum (1000 dilution). For protein detection the primary antibody was diluted in PBS-T Buffer. The membrane was washed 3 times for 10 minutes with 1X PBS-T Buffer on a rotary shaker and incubated for 60 minutes with the anti-rabbit IgG Conjugate antiserum (1000 dilution). After incubation, the antibody was removed and stored at –20°C for future use. Afterwards the membrane was washed for 10 min in PBS-T on a rotary shaker. This washing step was repeated twice. The membrane was washed again with TBS Buffer for approximately 10 minutes. The ECL Plus Western Blotting Detection System was used to visualize the secondary antibody according to the manufacturer's protocol.

Table 3-11: Solutions for Western blot protocol

Buffer	Recipe
Blocking Reagent	PBS + 0.05 % Tween20 + 5 % milk powder
Transfer buffer	8 mM Tris, 39 mM Glycine, 0.037 % SDS, 20 % MeOH
10x PBS	40 mM KH_2PO_4, 160 mM Na_2HPO_4 x $2H_2O$, 1.15 M NaCl pH 7.4
Stripping Buffer	2% SDS, 62.5 mM Tris, 100 mM *2*-Mercaptoethanol pH 6.7

3.6 Protein purification methods

Proteins have a great diversity of molecular and chromatographic characteristics like charge, hydrophobicity, affinity, solubility, stability and molecular weight. Considering the relative characteristics of the target molecule in relation to the other in solution, it is possible to design a strategy and separate it with a desirable purity. The identification of a protein requires a combination of binding assays (Immunoassays), chemical assays (dye binding), physical assays typical spectrophotometry (UV absorbance, etc) and separation assays (electrophoresis and chromatography) (Doonan, 1996a). Purification parameters for each column were chosen based on the extent of purity of protein to be fractionated and the isoelectric point of the protein to be purified from other contaminant proteins using a FPLC system.

3.6.1 Ion exchange chromatography

Basic Principles: Ion exchange chromatography separates proteins according to their net charge. The separation of molecules is based in ionic attraction between molecules of opposite electric charge. An ion exchange packing material (stationary phase) is used in the column and a mobile phase with counter ions of opposite charge. The most common counter ions are small salt

and buffer molecules. Protein can bind and be separated based on the number of positive and negative charges accessible on their surface. The protein binding occurs when the salt concentration of mobile phase is small to the point that the proteins at solution start to serve as counter-ion for the charged group of the stationary phase. Elution takes place when the ionic strength of the mobile phase is increased. At this point, the salt molecules displace the bounded protein back on to the mobile phase and at the same time, the charged groups of the protein are neutralized by the cations and anions in the mobile phase.

3.6.2 Ammonium sulphate fractionation

Basic Principles: Salt-induced precipitation is an extensively used method as an initial step to purify proteins because of its selectivity and low cost. A variety of salts can be used for fractionation but Ammonium Sulphate has the advantage of high solubility in water and is innocuous to proteins (Doonan, 1996b). The precipitation happens because there is an increase in the dielectric constant that promotes protein aggregation by charge interaction. A trial experiment was carried out in order to determine the optimal concentration of ammonium sulphate for the separation of Ure2p from the contaminants. Fractions containing Ure2p in the pellet were identified using SDS-PAGE. The optimal concentration determined was 30% with the advantage of at this concentration of ammonium sulphate only a small number of contaminants are co-precipitated with Ure2p.

3.6.3 Size exclusion chromatography

Basic Principles: Size exclusion chromatography separates molecules according to their size and shape. Proteins which are larger than the pore size cannot enter the pores and elute as the first peak. Proteins which can enter the pores have an average residence time depending on size and shape. Separations of molecules in Gel filtration is determined by the specific mobile phase used and the hydrodynamic volume of the molecule. On this group are the Superdex 75 pg, Superdex 200 pg and Sephacryl 300 pg.

3.6.4 Affinity chromatography (Ni-NTA)

Basic Principles: Affinity Chromatography is based on the specific and reversible adsorption of a molecule to an individual matrix-bound partner. It was used Immobilized Metal Ion Affinity Chromatography (IMAC), an established technique for purifying protein (Quiagen, 1998). In this case a metal chelating substance has been attached to a matrix. A multivalent transition metal ion (Cu^{2+}, Ni^{2+}, Zn^{2+}, Fe^{2+}) is bound to this group in a way that there are still free coordination sites for an interaction with basic groups of proteins. His residues of the protein bind specifically to these free sites. The exposition of the His is required for the adsorption of the protein (Porath et al., 1975). It was used Nickel bounded to a stationary phase of nitrilotriacetic acid derivate due to a high specificity for proteins containing adjacent His residues. For elution and separation of proteins, an imidazole gradient is used which competes for binding sites with the His residues of the bound proteins.

3.6.5 Analytical gel filtration (SEC – HPLC)

Basic Principles: Analytical gel filtration is a combination of chromatographic separation with spectroscopic techniques. To convert the chromatographic separation to an analytical scale, it is necessary to improve resolution, sensitivity and speed. At this point, HPLC offers some advantages in relation to normal FPLC, like the possibility of identification of protein using fluorescence spectroscopy and the reduction of volume and sample dilution.

Method: SEC-HPLC was performed using different columns and buffer systems. The chosen mobile phase for native conditions was 50 mM Tris/HCl, 150 mM NaCl, pH 7.5. The flow rate was 0.5 ml/min. Columns were calibrated by passing through a set of proteins of known molecular weight. Proteins used as molecular mass standards were: Thyroglobulin (670 kDa), Ferritin (440 kDa), Catalase (232 kDa), Aldolase (160 kDa), Bovine Serum Albumin (66 kDa), and Ovalbumin (44 kDa). Proteins were detected by fluorescence (λ_{ex} = 280 nm, λ_{em} = 334 nm) and absorbance (λ = 280 nm). A Superdex 200 HR 10/30 column was used to analyze the quaternary structure of native protein. A

TSK SW 3000 column was used to analyze the intermediate species in the Ure2p fibrillation pathway under native conditions. To analyze the size distribution of Ure2p intermediates under denaturing conditions, experiments were performed using a Superose 6 HR 10/30 column with 50 mM Tris/HCl, 150 mM NaCl, 5 M GdmCl, and pH 7.5 as mobile phase. Proteins were detected by fluorescence (λ_{ex} = 280 nm, λ_{em} = 354 nm).

3.6.6 Recombinant Ure2p purification

5 ml of medium with antibiotics were inoculated with a fresh single bacterial colony and incubated overnight at 37°C with vigorous shaking (200 rpm). Pre-warmed 50 ml of medium in 250 ml flask was inoculated with 0.5 ml of the overnight culture, supplemented with appropriate antibiotics, and incubated at 37°C with shaking (200 rpm). Pre-warmed 200 ml of medium in 1 L flask was inoculated with 20 ml of the overnight culture until the OD_{600} reached the 0.7 value. The cells were added to pre-warm 2 L of medium in 5 L flask with appropriate antibiotics. Cells were grown at 37°C in SB medium containing 100 mg/l ampicillin, and Ure2p production was induced by addition of 5 mM isopropyl-1-thio-β-D-galactoside (IPTG) at an $OD_{600\,nm}$ of ~1. After 10 h, cells were harvested by centrifugation. Pellets were resuspended in Lysis Buffer (5 ml/g wet cells) containing protease inhibitors (Complete EDTA-free). During cell lysis in a BasicZ cell disruptor at 1.8 kbar, add 3 mM $MgCl_2$ and 10 µg/ml DNase I (30 min, 25 °C). The soluble fraction was separated from debris by centrifugation (48,000xg, 1 h, 4°C). The supernatant was applied to a home made column containing Q-Sepharose material, which had been equilibrated with buffer A. After sample injection, the column was washed with Buffer B for 2 column volumes. Flow rate was 2 ml/min. The fraction size of collected eluting protein was about 8 ml. The elution was done by a linear gradient from 0 to 0.5 M NaCl in buffer B with total volume of 20 times the column. The absorbance of the fractions was determined at 280 nm. Fractions containing Ure2p were identified using SDS-PAGE and were pooled together. The protein solution was subjected to precipitation in the 30% (w/v) saturation of ammonium sulphate. Ammonium was added to the protein solution in small

quantities, in slow steps at 4°C. After the addition was complete, the solution was left stirring for 1 hour to ensure equilibrium. The protein precipitate was recovered by centrifugation at about 20000 g and 4 °C for 60 minutes. To ensure the complete precipitation of Ure2p, sample of the pellet and supernatant were analyzed by SDS-PAGE. The final pellet was dissolved in a minimal volume of SEC buffer and submitted to centrifugation again to remove any insoluble aggregates. The protein suspension was injected in a 16/60 cm Superdex 200 gel filtration column equilibrated with SEC buffer C. The flow rate was 0.5 ml/min and the fraction size was about 2 ml. The absorbance of the fractions was visualized at 280 nm. Fractions containing Ure2p were pooled, flash frozen in liquid N_2 and stored at -80°C. All steps were carried out at 4°C as quickly as possible to avoid aggregation of Ure2p. The identity of purified Ure2p was confirmed by mass spectrometry and N-terminal sequencing. The yield of purified protein was typically 15 mg per litter of culture with a final $OD_{595\ nm}$ of 2.3. Before use, thawed samples were centrifuged to remove aggregates.

3.6.7 Recombinant of Ure2p N-terminal domain purification

Cells were grown at 37°C in SB medium containing Kanamycin, and NT-Ure2p production was induced by addition of 1 mM IPTG at an $OD_{595\ nm}$ of ~1. After 12 h, cells were harvested by centrifugation. Pellets were resuspended in Lysis Buffer 2 (5 ml/g wet cells) containing protease inhibitors (Complete EDTA-free). During cell lysis in a BasicZ cell disruptor at 1.8 kbar, it was added 3 mM $MgCl_2$ and 10 µg/ml DNase I (30 min, 25 °C). The soluble fraction was separated from debris by centrifugation (48,000xg, 1 h, 4°C). Cellular lysates of *E. coli* cultures were applied to a previously equilibrated Ni-NTA column with buffer A. Protein bound to the resin was washed with Ni-NTA wash buffer B and then eluted with Ni-NTA elution buffer. The flow rate used was 1 ml/min and the fraction size was about 2 ml. Due to high concentration of imidazole, it was not possible to identify the protein using absorbance. Contaminant proteins that were co-purified along with the recombinant NT-ure2 were separated using gel filtration chromatography. Superdex™75 prepgrade columns (Pharmacia) were used for purifying proteins during this study. The flow rate was 0.5 ml/min and the fraction size was about 2 ml.

3.6.8 N-terminal amino acid sequence analysis

The N-terminal sequence of proteins purified during this work was checked using Edman degradation method, with the aid of an automated –protein sequencer.

3.6.9 Handling and storing of the proteins

All the operations involving the proteins were performed on ice or at +4^{o} C, as not indicated otherwise. A stress was laid on speed of processes, decrease of time consumption and number of purification steps due to fast fibril formation of the protein. NaN_3 was added to prevent bacterial and fungal growth in solutions kept for prolonged time at 4^{o}C. Purified protein was stored at -80^{o}C until further analysis.

3.6.10 Concentration, exchange of buffers and filtration

Concentration, exchange of buffers, filtration and elimination of seeds and aggregates from protein solutions were done using a Millipore centrifugal filter device to in a fixed-angle rotor at 4500 g.

3.7 Spectroscopic methods

3.7.1 Protein concentration determination using optical spectroscopy

Basic Principles: Proteins absorb light and emit radiation in the UV range of the spectrum. The absorbance is caused by peptide groups, by aromatic amino acids and to some extent by disulfide bonds. During absorption light energy is used to promote electrons from the ground state to an excited state. Electrons that participate in delocalized aromatic systems frequently absorb in the near UV or visible region of the electromagnetic spectrum (Van Holde et al., 1998).

Absorbance measurements are most commonly used to determine the concentration of proteins in solution. The absorbance (A) is related to the intensity of the light before (I_0) and after (I) passage through the protein solution by Equation 1 and the absorbance depends linearly on concentration, according to the *Beer-Lambert* relationship (Equation 2):

Equation 1:

$$A = -\log_{10}(I/I_0)$$

Equation 2:

$$A = \varepsilon \cdot c \cdot l$$

I = intensity of transmitted light

I_0 = intensity of incident light

c = concentration of absorbing material [mol/l]

l = optical path length [cm]

ε = molar absorption coefficient [M^{-1} cm^{-1}]

Apart from small contributions of the peptide bonds, which absorb strongly below 230 nm, the absorbance of proteins between 230 and 300 nm depends on Tyr, Trp, Phe and Cys residues. The molar absorbance of Phe (λ_{max} = 257 nm) is smaller by an order of magnitude than that of Tyr and Trp, and it is virtually zero at > 270 nm. This means that above 275 nm absorbance depends only on the aromatic side chains of Tyr, Trp and Cys residues (Wetlaufer, 1973). Disulfide bonds display a weak absorbance band around 250 nm, but the absorption is not significant around 280 nm (Bailey et al., 1968). Therefore, the spectrum of a protein at 280 nm is dominated by the contributions of Tyr and Trp residues. The shape and intensity of a particular protein spectrum depends on the actual number of these two aromatic residues in the molecule. Since the aromatic amino acids do not absorb above 310 nm, solutions containing only protein should not show absorbance at higher wavelengths. The absorbance spectra of the aromatic amino acids depend on their molecular environment, which can produce a broadening of bands, shifts in wavelength,

and overall changes in intensity(Brandts and Kaplan, 1973). In general, the shift in wavelength dominates, and a blue shift of the spectrum is observed when the polarity of the solvent increases. For example, the maximum of the absorbance of the phenol chromophore is blue-shifted by around 3 nm when the solvent is changed from CCl_4 to H_2O. Differences in the absorbance spectra between the native and the unfolded states of a protein are generally small, but they can be determined with good accuracy. They are linear with protein concentration and are extremely useful for monitoring conformational changes of a protein.

Method: For the calculation of the protein concentration it is necessary to determine the respective extinction coefficient ($\varepsilon_{280\ nm,\ 0.1\%,\ 1\ cm}$). These values are quite reliable for proteins containing Trp residues and less reliable for protein that do not. This is done based on the method of Wetlaufer (Wetlaufer, 1973) and Gill (Gill and von Hippel, 1989) where the extinction coefficient of Trp, Tyr and Cys is multiplied by the number of each amino acid.

Prediction of the extinction coefficient of the protein (Pace et al., 1995)

Equation 3

$$\varepsilon_{280\ nm,\ 0.1\%,\ 1\ cm} = (A_{trp}.\ \varepsilon_{M,trp} + B_{tyr}.\ \varepsilon_{M,tyr} + Ccys.\ \varepsilon_{M,cys})/\ Mw$$

where:

$\varepsilon_{M,Trp}$ = Molar Extinction coefficient of Trp (5500 $cm^{-1}l^{-1}$)

$\varepsilon_{M,Tyr}$ = Molar Extinction coefficient of Tyr (1490 $cm^{-1}l^{-1}$)

$\varepsilon_{M,Cys}$ = Molar Extinction coefficient of Cys (125 $cm^{-1}l^{-1}$)

Atrp, Btyr, Ccys = Number of each Amino acid

MW = Molecular weight of the protein [$g.mol^{-1}$]

The theoretical extinction coefficient of Ure2p calculated according to Gill at al. (Gill and von Hippel, 1989) and Pace et al. (Pace et al., 1995) is in agreement with the extinction coefficients determined with the ProtParam tool at the Expasy server(Apweiler et al., 2004; Gasteiger et al., 2003). Ure2p was diluted into a stock solution of 6.6 M GdmCl in 20 mM Na-Phosphate pH 7.5, and the absorbance measured. In the next step, ure2p was measured using 20 mM Na-Phosphate pH 7.5, as native buffer.

Equation 4

$$\varepsilon_{280nm}^{native} = \varepsilon_{280nm}^{denatured} \cdot \frac{A_{280nm}^{native}}{A_{280nm}^{denatured}}$$

Ure2p concentrations were determined applying the Lambert-Beer equation and using an extinction coefficient of $A_{280\ nm}^{0.1\%,\ 1\,cm}$ = 1.19. Molar concentrations given in the text refer to the monomer. To eliminate the presence of aggregates in solution that scatter the light, a correction of the absorbance was carried out. A graph was plot as *log (Abs)* vs. *log (λ)*. A linear regression was done in the baseline area between *log (400 nm)* and *log (320 nm)*. This baseline was subtracted from the observed *log (Abs)* values. The corrected spectrum was then transformed (*log (Abs)* $\rightarrow$*Abs)* and plotted the resulting values against $\tilde{\lambda}$

In case, the protein does not have aromatic amino acids, it is possible to use the

Equation 5:

$$\varepsilon_{205} = 27.0 + 120 \times \left(\frac{\mathrm{A}_{280}}{\mathrm{A}_{205}} \right) \text{ in (ml/mg*cm)}$$

Being necessary to repeat the measurement in different concentration and conditions to get an average value (Scopes, 1974).

3.7.2 Protein concentration determination using Bradford method

The concentrations of proteins in solution were also estimated using the method by Bradford (Bradford, 1976) with the assistance of the Pierce Bradford Protein Assay reagent.

Basic Principles: Coomassie Blue R, under acidic conditions, forms a micro precipitate with many (but not all) proteins. In the process the light absorbance moves from a maximum in the red region to the blue region, i.e., the pigment turns blue in the presence of protein.

Method: A series of dilutions of samples of BSA in buffer at different concentrations was prepared keeping the final volume at 100 µl. The buffer used was the same as for the protein of interest. The reagent working solution was prepared by 1:5 dilution of Pierce-reagent stock solution in TBS buffer or water. The BSA samples were mixed with 900 µl of working solution. After thoroughly mixing the sample, the OD_{595} was measured. A standard curve was generated. As a reference similar mixture was prepared with 100 µl of water instead of protein solution. OD_{595} was subsequently converted into the protein concentration on the basis of a BSA standard curve. A second calibration curve was done using Ure2p as standard protein.

3.7.3 Fluorescence spectroscopy

Basic Principles: Fluorescence is the emission of light after light absorbance (photon). By absorbing light of a specific wavelength, an electron from the molecule can switch to an excited state (S_1) for a few nanoseconds. Fluorescence emission is observed, when electrons return from the first excited state back to the ground state. In the excited state, some energy is always lost by non-radioactive processes (such as vibrational transitions). Accordingly emitted light has a higher wavelength than the excitation wavelength (*Stokes shift*) (Van Holde et al., 1998) (Schmid, 1989). This behavior can be recorded as an emission spectrum. The shape of the emission spectrum is characteristic for each molecule and depends on its surrounding in the excited state. Fluorescence is widely used to investigate conformational changes of proteins because the process is too fast to allow any change in the conformation of the protein. Therefore, the conformation of the protein can be considered “frozen”. Intrinsic and extrinsic fluorophores can be used.

Intrinsic fluorophores are aromatic amino acids like Trp, Tyr and Phe which emit light between 280 and 350 nm. Changes in protein conformation, such as unfolding, which is induced by temperature and denaturants like GdmCl and urea, very often lead to changes in the fluorescence emission. In proteins that contain all three aromatic amino acids fluorescence is usually dominated by the contribution of the Trp residues. The fluorescence intensity of Trp is around 10

times higher than of Tyr. Phe fluorescence is not observed in native proteins because its sensitivity is very low (Schmid, 1989). The maximum of the Tyr fluorescence is usually around 303 nm. The maximum of Trp is in the range of 320 and 350 nm.

The emission of Trp extremely depends on the polarity of the protein environment. This means that Trp emission spectrum changes depending on the protein folding and environment. In proteins that contain Trp residues and are soluble in hydrophilic solvent, both shifts in wavelength and changes in intensity are observed upon unfolding. The emission maximum of Trp is usually shifted from approximately 333 nm in the native state to 350 nm in the unfolded state. A wavelength of 350 nm corresponds to the fluorescence maximum in aqueous solution. On the other hand, in a hydrophobic environment, such as the interior of a folded protein, Trp emission occurs at smaller wavelengths. The same effect is obtained when a protein is dissolved in a hydrophobic solvent. The fluorescence of the exposed aromatic amino acids of a protein depends on the solvent conditions and the emission maximum of Trp occurs at smaller wavelengths of approximately 320 nm. Looking at environmental effects, such as temperature, the fluorescence intensity generally decreases with increasing temperature. To a first approximation, Tyr emission decreases $\geq$ 1% per degree increase in temperature. The dependence on temperature of the fluorescence of Trp is even more pronounced. Due to this relation of temperature and fluorescence, the thermal denaturation is qualitatively determined but not quantitatively using fluorescence. The best method for using denaturation following the intrinsic fluorophores is chemical denaturation. Denaturants like GdmCl and urea exert also a significant influence on the fluorescence of Tyr and Trp residues. For proteins that contain both Tyr and Trp residues, the emission of the unfolded protein can be represented by an appropriate mixture of the two aromatic amino acids. The dependence of the emission of this mixture on denaturant concentration is often very useful to determine the baseline equivalent to the unfolded protein for the quantitative analysis of unfolding transition curves(Schmid, 1989). On this studies, it was used GdmCl. The mechanism of binding of the guanidinium group to the protein is done preferentially using hydrogen bonds and on this way to the water solubilizing apolar groups. The protein has a preferential interaction with

GdmCl ion then from the Urea ion. Once that the concentration of the GdmCl ion increases, the denatured state is favorable due to the greater surface of the protein to interact with the denaturant.

Method: The intrinsic fluorescence of a protein was measured in a Fluoromax-3 spectrofluorimeter with a thermostatically controlled cell holder at 20°C, using 1 cm quartz cuvettes. Emission spectra were recorded in the range of 290–440 nm with an excitation wavelength of 280 nm. The spectral bandwidths were 3 nm for excitation and 5 nm for emission, respectively. To obtain spectra for the denatured protein, samples were incubated overnight in buffer containing denaturant solution.

Extrinsic chromophores bind through covalent or non-covalent interactions to specific parts of a protein. This binding depends on the protein folding, so the shape and/or intensity of the emission spectrum can help to recognize the protein structure. Some extrinsic Fluorophores can bind to hydrophobic surfaces (e.g. ANS) and to β-sheets (e.g. Congo Red and Thioflavine T).

3.7.4 ANS-Fluorescence spectroscopy

Basic Principles: The 1-Anilino-8-naphthalene sulfonate (ANS) is a water-soluble non-planar anionic compound. It binds to hydrophobic (nonpolar) surfaces of proteins through its nonpolar anilino-naphthalene group. An ionic binding between positively charged amino acid side chains and the sulfonate group of the ANS also plays an important role. To have a fluorescence, ANS must be binding in this two modes (getting a planar configuration) at the same time when an increase in ANS fluorescence intensity can be observed (Matulis et al., 1999). The fluorescence can only happen when the compound is in a planar mode because in a non-planar this transitions are forbidden (Buchner and Kiefhaber, 2004).

Method: Different measurements with changes in parameters and wavelengths were done to get the optimal excitation and emission wavelengths. For fibrillation studies, the maximum fluorescence intensity was reached with an excitation wavelength of 365 nm, the emission spectra was measured from 400 to 600 nm and the concentration of dye was 20 μM as a standard (or 20 fold in

excess). For unfolding studies, Excitation was at 395 nm and the emission spectra measured from 420 to 650 nm (maximum change in emission on unfolding is at 480 nm). Final concentration was 200 μM (or 40 fold protein concentration).

3.7.5 Thioflavin T Fluorescence Binding Assay

Basic Principles: Thioflavin T (ThT) selectively stains amyloid structures under the appropriate conditions due to its binding to β-sheet structure common to amyloids(LeVine, III, 1993; LeVine, III, 1997). ThT emission is stimulated by excitation at 385 nm (excitation bandpass 3 nm, emission bandpass 8 nm) when it is free in solution and by excitation at 444 nm when binding to oligomeric species and fibril. The fluorescence of the dye is not affected by high salt concentration. Because of this behavior, ThT can be used to measure amyloid fibril formation. The mechanism of ThT binding is not yet known, but β-sheets are supposed to play an important role.

Method development: The fluorescence is measured by rapidly mixing the protein solution with the ThT stock solution. Two kinds of assay were tested: a) online assay where Ure2p is diluted to a ThT solution in the cuvette and measurements were done undisturbed for the necessary time and a time point assay, where samples were taken and ThT was added in the moment of the measurement. Before each experiment, a series of steps were taken, for example: a) Screening of the effect of the buffer from protein solution on the ThT fluorescence versus a normal ThT buffer, b) measurement of a fibril solution and a non fibril containing solution to check the best band pass to each new experiment.

Experiments: To monitor Ure2p fibrillation, aliquots were removed periodically from the samples and mixed with a ThT stock solution. ThT fluorescence was measured at 20°C in 50 mM Tris/HCl pH 8.0 using an excitation wavelength of 442 nm and an emission wavelength of 482 nm. Each data point taken represents the average of three scans measured for one sample. One data point in the graph represents the average of 5 different samples measured at the same time. Values were corrected for background fluorescence of free ThT.

3.7.6 Circular Dichroism Spectroscopy

Basic Principles: Circular dichroism (CD) spectroscopy measures differences in the absorption of left-handed polarized light versus right-handed polarized light which arise due to structural asymmetry. Secondary structure can be determined by CD spectroscopy in the "far-UV" spectral region (190-250 nm). The CD spectrum of a protein in the "near-UV" spectral region (250-350 nm) can be sensitive to certain aspects of tertiary structure. At these wavelengths the chromophores are the aromatic amino acids and disulfide bonds. The amide chromophore of the peptide bond in proteins dominates their CD spectra below 250 nm (Van Holde et al., 1998). In an α-helical protein, a negative band near 222 nm is observed due to the strong hydrogen environment of this conformation. A second transition is spitted in to a negative band near 208 nm and a positive band near 192 nm. The CD spectra of a β-sheet structure displays a negative band near 216 nm and a positive band between 195 and 200 nm (Pelton and McLean, 2000).

The molar ellipticity $[\Theta]$, and the residue ellipticity $[\Theta]_{MRW}$, are calculated from the measured Θ (in degrees) using the follow equation:

Equation 6

$$\Theta_{MRW} = \frac{\Theta \cdot 100 \cdot MRW}{c \cdot d} = \frac{\Theta \cdot 100 \cdot M}{c \cdot d \cdot N_A}$$

Θ_{MRW} in degrees x cm^2 x $dmol^{-1}$

Θ is the measured ellipticity in degrees,

MRW is Mean residue weight

c is the protein concentration (mg/ml)

d is the path length in cm.

M_r Protein molecular weight (g/mol)

N_A Number of amino acid per protein

The factor 100 comes from the conversion of the molar concentration to the dmol/cm^3 (Schmid, 1998).

Method: Far-UV CD measurements (Table 3-12) were carried out in 50 mM Na_2HPO_4/NaH_2PO_4 pH 7.5, 200 mM NaCl using a protein concentration of 5 µM. Spectra were recorded at 20°C in a Jasco J-715 spectropolarimeter equipped with a PTC 343 Peltier unit. The averaged signal was corrected for the buffer signal. Spectra were analyzed using the CDNN software package (www.bioinformatik.biochemtech.uni-halle.de)(Boehm, 1997) that uses model polypeptides and globular proteins of known crystal structure.

Table 3-12: Experimental parameter used for CD measurements

Parameters	Far-UV	Near-UV
Start wavelength	250 nm	350 nm
End wavelength	190 nm	250 nm
Resolution	0.2 nm	0.2 nm
Scanning rate	20 nm/min	20 nm/min
Response	1.0 s	1.0 s
Accumulation	16	10
Quartz Cell path length	0.1 cm	0.5 cm

In the presence of GdmCl it is not feasible to record a full-CD spectrum for the denatured protein because absorption by GdmCl precludes the measurements below 210 nm.

3.8 Microscopy

Microscopy (SEM and TEM) yields the following information: size, shape and the arrangement of the particles showing their relationship to each other. High resolution images of biological materials can be obtained using high energy electron techniques like SEM and TEM. Other types of microscopy are the Scanning Probe microscopes. All SPM are based on the measurement of an interaction between the sample surface and a probe located very close to it

making them powerful complements to other analytical techniques. This instrument generates images by “feeling” rather then “looking” at specimens. Using this technique it is possible to distinguish aromatic rings from aliphatic chains or carbon atoms in graphite (Ikai, 1996).

3.8.1 Scanning Electron Microscopy

Basic Principles: The surface of the sample is scanned by an electron beam in a series of parallel lines. The interaction of the electron with the surface induces a radiation that is counted by the detector and displayed. The three-dimensional topographic image is constructed using secondary electrons by the interaction with the beam. Usually samples are coated with gold to improve the image due to the conductivity of the gold. The resolution can range between 100 nm to 1 mm (Buchner and Kiefhaber, 2004).

Method: Samples of ure2p fibrils were fixed in a surface and dried. The coating with gold is done by vacuum evaporation from a tungsten filament.

3.8.2 Transmission Electron Microscopy

Basic Principles: Negative staining of biological samples: Salts containing heavy metal atoms can surround and permeate small biological molecules and dry forming amorphous glass. When illuminated by an electron beam inside of a TEM, much less of the transmitted electron beam will pass directly through the stained region than through the region containing the biological sample. This selective scattering of the electron beam is responsible for the image production. The visualized image is a two dimensional image but has enough information to generate a three dimensional image from images reconstruction. TEM images can reveal the external outline and the cavities in biological particles (Buchner and Kiefhaber, 2004).

Method: 10 µl aliquots of a sample containing fibrillated Ure2p (10 µM) were applied on to a carbon-coated grid. After 1 min, samples were washed with water and incubated with 10 µl of 2% (w/v) uranyl acetate for 1 min. Samples

were air-dried and examined at a nominal magnification of ×100,000 using a Philips CM12 electron microscope operating at 120 kV.

3.8.3 Atomic Force Microscopy

Basic Principles: AFM provide high-resolution, three-dimensional surface structure of biological species. In AFM, the measurement is done using the attractive and repulsive forces between atoms of the thin tip that scans its and the atoms of the surface. AFM is performed by scanning the surface of the sample with a sharp tip on the end of a flexible cantilever, following parallel lines, while maintaining a small, constant force. The tips typically have an end radius of 5 nm to 10 nm, although this can vary depending on the tip type. The sample is assembled on a piezoelectric support enabling the scanning through the displacement of the sample on the *xy* plane. The scanning motion is conducted by a piezoelectric tube scanner that scans the tip in a raster pattern with respect to the sample. The tip-sample interaction is monitored by focusing a laser beam on the end of the tip, and the reflection of the laser beam is focused on a photodiode. As the tip moves in response to the sample topography during scanning (for the movement on the *z*-axis), there is a variation of the angle of the reflected laser beam producing changes in the intensity in the photodiode. This minimal twisting of the cantilever reflects the interaction of the tip with the sample (Santos and Castanho, 2004). The values are registered by the computer and used for the reconstitution of a pseudo-three-dimensional picture of the sample (Figure 3-1). The two most commonly used modes of operation are contact mode AFM and Tapping Mode™AFM, which are conducted in air and liquid environments(Santos and Castanho, 2004). In this study Contact and Tapping Mode AFM were conducted in Air. The Tapping mode consists of oscillating the cantilever at its resonance frequency (typically ~300 kHz) and scanning across the surface with constant amplitude. The advantage of Tapping Mode is that it typically operates with a lower vertical force than that possible with contact mode, leads to higher resolution images and eliminates the lateral shear forces that can damage soft samples.(Santos and Castanho, 2004)

Method: 30 µl aliquots (0.1-5 µM Ure2p) were placed on mica, left for 5 min, and then washed 3 times with 50 µl of distilled water to remove salt and unbound protein. Samples were air-dried overnight and mounted on the microscope scanner head. Images were acquired in tapping mode on a multimode AFM using type E scanner. All images were obtained in air using single-beam silicon cantilever probes (Veeco, Germany). AFM images were obtained at imaging speeds of 0.5-1.0 Hz recording 512 lines per image. The resonance frequency was ~300 kHz.

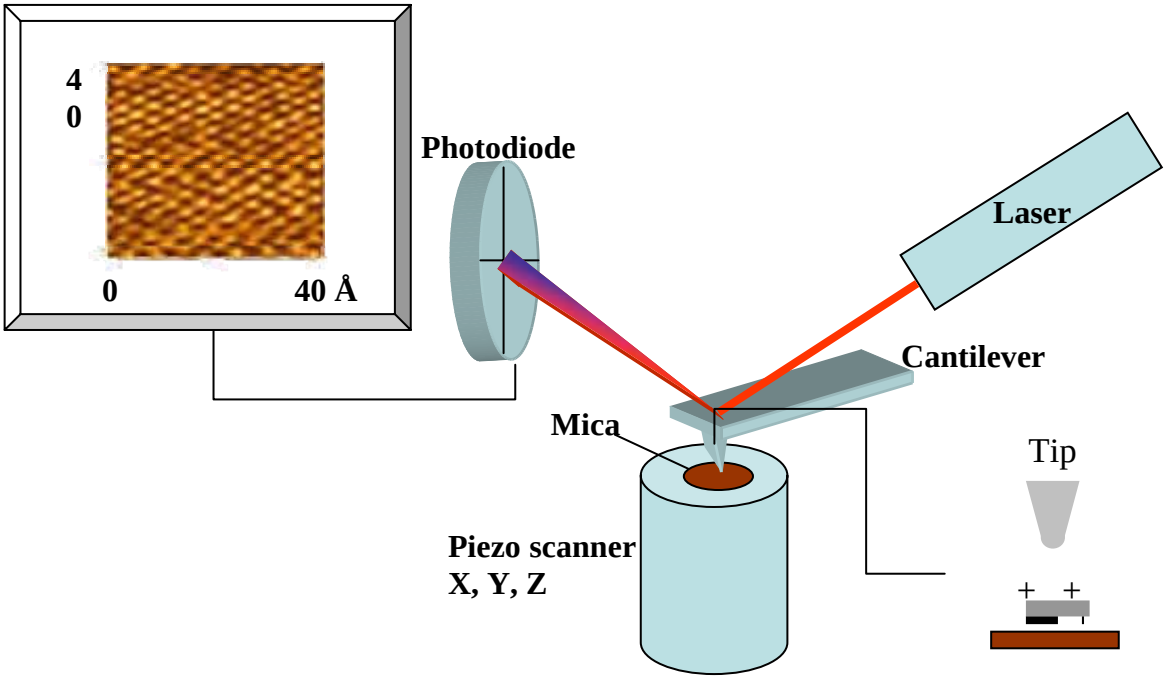

Figure 3-1: Scheme from the AFM measurements and nanoscope assembly (Woolley et al., 2000)

A) Showing an image of mica mineral, dimensions of the image 40 Å. B) scheme of the tip over the sample. The positively charges amino acids from protein may interacts with the negatively charged surface of mica and counter-ions of the buffer can help to stabilize the adsorption

Tapping mode and contact mode images using the same tip, and taken of the same sample showed no height differences. However biological samples are more sensitive to damage caused by multiple scanning in contact-mode. The imaging of the sample in air can provide detailed information about the different fibril types, average height, approximate diameter and periodicity.

3.9 X-ray fiber diffraction

Basic Principles: In the early 1930, the first x-ray fiber pictures of wool gave was taken. The name was done by cross β-sheet due to the fact the chain run cross the fiber axis. Cylindrical fibrous proteins don't crystallize but form ordered structures that spread reflections in a disk, showing a symmetrical diffraction pattern. On the fiber diffraction the diagram, the direction parallel to the fiber axis is known as the meridian and the perpendicular direction is the equator. Fiber are crystalline along the fiber axis and this produces strong sharp reflections on the meridian (Buchner and Kiefhaber, 2004). Amyloid fibrils commonly show a cross-β pattern. In well oriented fibril samples (Figure 3-2) the reflections appear as arcs, rather than rings, and have distinguishing positions: the 4.7Å reflection lies on the meridian and the 8- to 11-Å reflection lies on the equator. The 4.7Å reflection arises from the inter-strand spacing between β-strands in a β-sheet, in the direction of hydrogen bonding, and the 8- to 11-Å reflection corresponds to the intersheet spacing. In β-sheets, the side chains extend alternatively on either side of the main chain which makes them around 10 Å thick. A single sheet gives a weak set of signal and two sheets with 10 Å would give a broad, weak reflection of 10 Å spacing. The addition of more sheets would make the reflection sharper and stronger.

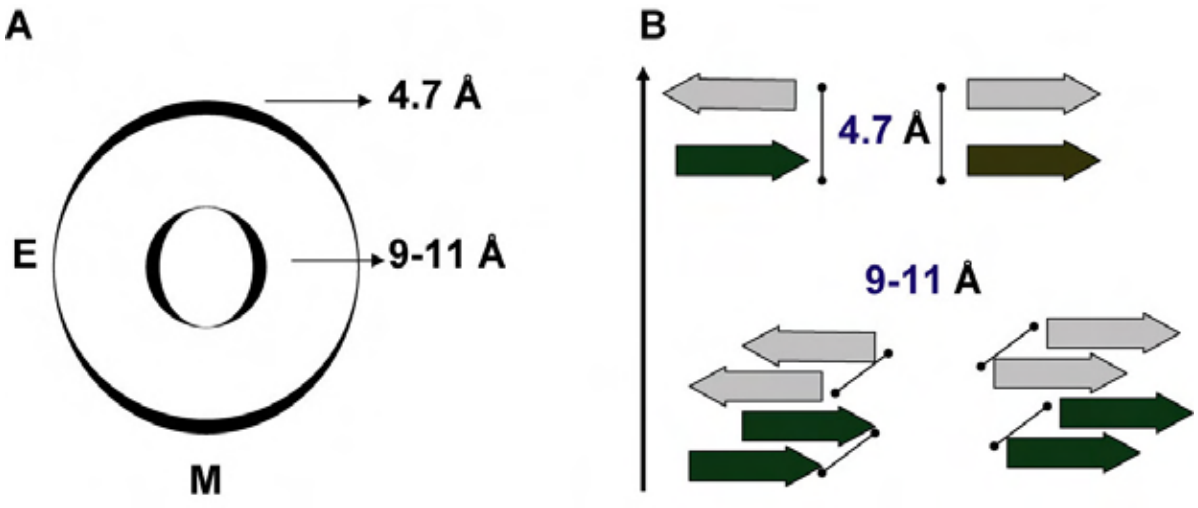

Figure 3-2 Scheme of the cross spacing from X-ray fiber diffraction of amyloid fibrils.

A) Scheme of the measured diffraction, showing meridional (M) and equatorial (E) reflections. B) 4.7 Å reflections correspond to the hydrogen bond between β-strand

and the 9-11 diffraction correspond to the intersheet distance. The arrow indicates the fibril axis direction and the meridional direction (Serpell, 2000b).

Method: A highly concentrated solution of fibrils (300 μL) were centrifugated with about 20000 x g for 5 min, and the pellet was resuspended in 20 mM Tris pH 7.5. For preparation of dried fibers, about 20 μL of this viscous solution (about 10–20 mg/ml) was placed at a 1 mm gap between the ends of two glass rods with a diameter of 3 mm (hang drop method), and allowed to dry over several hours at room temperature. For preparation of oriented liquid crystalline solutions of the fibrils, the highly concentrated solution containing fibrils was drawn into a glass capillary with a diameter of about 1.5 mm, and the fibers were oriented by a magnetic field of 2 T. The data collection was done using a CCD camera.

3.10 Fibril and protein methods

The experiments were done taking in consideration an international standard defined for biochemical experiments (Maxwell et al., 2005).

3.10.1 Chemical unfolding transition

Table 3-13: Buffers used for chemical unfolding transition

Buffer	***Recipe***
TBS	50 mM Tris/HCl, pH 7.5 200 mM NaCl
TBS GdmCl	50 mM Tris/HCl, pH 7.5 200 mM NaCl 7.3 M GdmCl
NaP	50 mM Na_2HPO_4/NaH_2PO_4 pH 7.5, 200 mM NaCl
NaP-GdmCl	50 mM Na_2HPO_4/NaH_2PO_4 pH 7.5, 200 mM NaCl, 7.3 M GdmCl

3.10.1.1 Using Fluorescence spectroscopy

Fluorescence spectroscopy is often used to study the conformational changes of proteins (3.7.3). The wavelength corresponding to the highest signal change is determined by subtracting the native and unfolded spectra. The maximal

difference between the native state and the unfolded state means a wavelength were the emission is highest and the best to follow the unfolding transition.

Method: Samples were added to buffer containing different concentrations of GdmCl and allowed to equilibrate overnight at 20 °C, before taking measurements. Measurements were done according to section 3.7.3. A control experiment was done using the buffer which the protein was solubilized.

3.10.1.2 Unfolding Transition using CD spectroscopy

Method: Samples were added to buffer containing different concentrations of GdmCl and allowed to equilibrate overnight at 20 °C, before taking measurements. Data were recorded, and the buffer signal was subtracted. Samples were monitored using a 0.1 cm cuvette. Measurements were done according to section 3.7.6.

3.10.2 Thermal denaturation of protein

The measured ellipticity is not dependent on temperature and this makes CD spectroscopy a good method for measurement of thermal stability of protein.

Method: Samples were equilibrated for 10 min at 20 °C, before starting measurements. Samples were monitored using a 0.2 cm cuvette. Measurements were done according to section 3.7.6. The temperature ramp was done between 20 and 100 °C with a heating of 30 °C/h. A spectra was recorded every 10 °C. The ellipticity was followed at 208, 218, 222 and 230 nm. The concentration was 0.2 mg/ml. The control experiment was done using the buffer in which the protein was solubilized. The buffer used was NaP due to the small pH change with temperature.

3.10.3 Standard growth of fibril

Table 3-14: Buffers used for fibril growth.

Buffer	Recipe
Buffer A	25 mM sodium acetate pH 5
Buffer B	50 mM Tris/HCl, pH 7.5

3.10.3.1 Fibrillation pathway analysis

In all experiments, the protein was then passed through a 0.2 mm cut off filter for further experiments to ensure homogeneity in the solution. Samples measured by HPLC were found to contain dimeric species and very low concentrations of oligomeric species. To ensure dimeric species, solutions were passed through a Millipore membrane of cut off around 100 kDa. The concentration was measured and adjusted with buffer for desired final conditions. Solutions were used immediately due to fast fibril formation. A series of parameters were studied such as agitation, temperature, concentration, pH, shaking, seeding, buffer, time, and ionic strength. Samples were incubated for days and fibril formation was monitored using ThT fluorescence and another spectroscopic method in addition. To confirm the presence or absence of fibrils in each experiment, samples were also examined by negative stain EM or AFM. Here, samples were withdrawn from the assay, placed onto an EM grid or mica and imaged as described in sections 3.8.1 and 3.8.3.

3.10.3.2 Screening between soluble and insoluble species

Protein solubility is governed by many factors including pH, surface hydrophobicity, surface-charge distribution, size, salt type, and salt concentration. The separation here was done by size and the objective was to get longer fibrils and aggregates separated from small and very soluble species.

Method: To do a screening between soluble and insoluble species in solution during aggregation, the polymerized solution was subjected to centrifugation at 16000x g during 15 minutes at 4 °C. The supernatant was removed from the cup the pellet was vigorously resuspended in buffer. Soluble means species between dimer and protofilaments and insoluble means fibrils and aggregates. The same procedure was used to distinguish between soluble Ure2p and amorphous aggregates. Samples were analyzed by TEM and AFM sections 3.8.1 and 3.8.3.

3.10.4 Measurement of fibrils

All fibril dimensions were calculated from height images. Height measurements of fibrils were carried out using the periodic low point and performed manually using the software provided with the Nanoscope instrument. Axial periodicities were the result of measured peak-to-peak distances.

3.10.5 Molecular Volume of protein

To determine the molecular mass of oligomeric Ure2p species by AFM (3.8.3), a calibration curve was recorded using p23 (26.5 kDa), ovalbumin (44 kDa), bovine serum albumin (66 kDa), aldolase (160 kDa), catalase (232 kDa), and thyroglobulin (670 kDa) in 50 mM Tris/HCl pH 7.5. The diameter of the protein particles on mica was measured at half maximal height to avoid overestimation generated by tip contact. An average of 6 molecules was measured for each type of protein (height h and radius r). From these parameters, the molecular volume V_m of the protein particles was calculated using the procedure described by Schneider *et al.*, which treats proteins as segments of a sphere(Schneider et al., 1998; Valle et al., 2002).

Equation 7

$$V_m = (h/6)(3r^2 + h^2)$$

V_m was found to be in good agreement with the theoretical volume V_c calculated from the molecular mass M_0.

Equation 8

$$V_c = (M_0 / N_0)(V_1 + dV_2)$$

In this equation, N_0 is Avogadro's number, V_1 and V_2 are the partial specific volume of the protein (0.74 $cm^3\ g^{-1}$) and of water (1 $cm^3\ g^{-1}$), respectively and *d* is the extent of protein hydration (0.4 mol H_2O/mol protein) (Schneider et al., 1998).

3.10.6 Seed preparations

For seeded growth, fibrils of Ure2p were formed under the desired conditions. The fibrils were then collected by centrifugation for ten minutes, and the supernatant was removed. The pellet was re-suspended in 500 μL buffer and the solution was sonicated 6 times for 5 s, meanwhile left on ice. The concentration of the solution was measured and the quality of fibrils was analyzed by AFM. 1 to 5 % (w/w) of this suspension was added to solution of dimeric Ure2p.

3.11 Mathematical Methods in protein

3.11.1 General considerations and definitions

The free energy of Gibbs, ΔG, is of great importance to decide the directions of the process.

Equation 9

$$\Delta G = \Delta H + T\Delta S$$

Equation 10

$$\Delta G = -RT \ln([U]/[F]) = -RT \ln K$$

Where R is the gas constant and T, the absolute temperature, K is the equilibrium constant. The protein can be summarized by the entropy (ΔS) and the enthalpy of the native (F) and unfolded state (U)(Van Holde et al., 1998). The contributions of the entropy (ΔS) can be described as: In the denatured

state, the polypeptide has a high configurationally freedom and upon folding to the native state, this freedom is lost, thus folding must happens under a gain of energy upon interactions. The contributions of the enthalpy (ΔH) can be described as: The native state is stabilized by a large number of interactions and this interactions energy constitute the favorable enthalpic term of protein stability.

3.11.2 Solvent-induced unfolding transitions

The change of intrinsic fluorescence intensity of Ure2p was monitored at 327 nm. The fluorescence values were plotted versus concentrations of GdmCl. The effect of the environmental conditions on the stability of the protein was determined by fitting the unfolding curves to chosen equations.

$\Delta G_U(H_2O)$ is the free energy of unfolding in the absence of denaturant.

m is the coefficient of linear dependence between the free energy of unfolding and GdmCl concentration. The m value for a protein is related to the amino acid composition and varies directly with the change in solvent exposed surface between the unfolded and folded states. Since accurate m-values are intrinsically hard to obtain from equilibrium data most interpretations are based on the transition midpoints. $[GdmCl]_{1/2}$ is the midpoint of the transition, the concentration of denaturant at which equal proportions of folded and unfolded protein are present and K =1.

3.11.2.1 2 state equation

The two state transition assumes that a protein can exist only in 2 conformations, N (native) and U (unfolded) (section 1.3.2)

$$N \Leftrightarrow U$$

where N, represents the native state and U, the unfolded state. In the two state unfolding, the curves can be divided in three regions: a) the pre-transition region, related to the signal of the folded protein, Y_N; b) the transition region, where unfolds occur, and c) the post-transition region, related to the signal of the unfolded protein, Y_U.

Equation 11

$$Y_N = Y_N^0 + m_N[GdmCl]$$

Equation 12

$$Y_U = Y_U^0 + m_U[GdmCl]$$

These are the equations for the pre- and post-transition base lines and Y_N and Y_U are obtained by extrapolation from the pre and post- transitional baseline. m_N and m_U are the slopes related to each state.

Equation 13

$$Y = \frac{Y_N - (Y_N - Y_U)}{1 + \exp(-(\Delta G + m[GdmCl])/RT)}$$

Equation 14

$$f_n = \frac{y - y_u}{y_n - y_u}$$

Equation 15

$$f_u = \frac{y_n - y}{y_n - y_u}$$

Equation 16

$$f_n + f_u = 1$$

where f_N and f_U represents the fraction of the protein present in the folded and unfolded conformation, respectively.

3.11.2.2 <u>3 state equation</u>

In the analysis, the presence of a intermediate species, I were included

$$N \Leftrightarrow I \Leftrightarrow U$$

In the three state unfolding, the curves can be divided in 4 regions: a) the pre-transition region, related to the folded protein, Y_N; b)the N→I transition region, where the unfolds start to occur, c)the I→U transition region after intermediate species, and d) the post-transition region, related to the completely unfolded protein. This transition region present a mid-point defined as:

Equation 17

$$\Delta G_a(H_2O) = m_a[GdmCl]_{1/2\ a}$$

Equation 18

$$\Delta G_b(H_2O) = m_b\left[GdmCl\right]_{1/2\ b}$$

Equation 19

$\Delta G_U(H_2O)=\Delta G_a(H_2O)+\Delta G_b(H_2O)$,

where ΔG_U is for the whole transition.

The baselines may be defined:

Equation 20

$$Y_N = Y_N^0 + m_N\left[GdmCl\right]$$

Equation 21

$$Y_I = Y_I^0 + m_I\left[GdmCl\right]$$

Equation 22

$$Y_U = Y_U^0 + m_U\left[GdmCl\right]$$

Using the below equation, the baseline slope is subtracted from the data and data are normalized.

Equation 23

$$Y = \frac{Y_N - \left(Y_N - Y_I\right)}{1+\exp\left(-\left(\Delta G_a + m_{ax}\left[GdmCl\right]\right)/RT\right)} - \frac{Y_I - Y_U}{1+\exp\left(-\left(\Delta G_b + m_{bx}\left[GdmCl\right]\right)/RT\right)}$$

Equation 24

$$f_n + f_i + f_u = 1$$

To compare different curves, the normalized curve by fitting was plotted.

3.11.3 Fitting of thermal unfolding transition

The thermal unfolding of a protein can be explained in a simplified way:

Equation 25

$$\Delta G_{den} = \Delta H_{den} + T\Delta S_{den}$$

The breaking of the favorable interactions will require an input of energy, so ΔH is positive, looking for the equation above, ΔS is positive this means a low temperature the $\Delta G > 0$, at high temperature, the $\Delta G < 0$. This imply that a low

temperatures the native state is favorable and if reach a high enough temperatures the denatured state will be favorable.

The data were fitted to a two-state equation, under the assumption that the enthalpy of unfolding is linear with temperature (Walter et al., 1995). The two-state transition analysis using the van't Hoff equation in these cases was carried out only to determine the approximate values of thermodynamic parameters.

t = temperature in degrees Celsius.

Equation 26

T = 273.15 +*t*;

Equation 27

$$\Delta G_D(T) = RT \ln K(T)$$

Gibbs- Helmholtz equation

Equation 28

$$\Delta G_D(T) = \Delta H_m(1 - \frac{T}{T_m}) - \Delta C_p\left[T_m - T + T\ln(T/T_m)\right]$$

Tm is the midpoint of thermal unfolding, △H is the van't Hoff enthalpy at Tm, and △Cp is the change in heat capacity upon unfolding. DG (T) is the free energy change for folding at any temperature.

Equation 29

$$Y_N = Y_N^0 + m_N[T]$$

Equation 30

$$Y_U = Y_U^0 + m_U[T]$$

The pre and pos-transitional baselines are assumed to depend linearly of the temperature. M_n and m_u are the slopes of the pre and pos transitional baseline.

The follow equation is derived from Gibbs-Helmholtz equation above.

Equation 31

$$Y(T) = Y_N^0 + m_N.T - \frac{Y_N^0 + m_N.T - Y_U^0 - m_U.T}{1 + \exp\left\{-\frac{\Delta G_D(T)}{RT}\right\}}$$

3.11.4 Fitting of ThT fibrillation kinetics

For comparison of different effects of incubation conditions on fibrillation kinetics, the ThT fluorescence measurements were plotted as a function of time and fitted by a sigmoidal curve as described by Fink(Nielsen et al., 2001) and Perret (Zhu et al., 2003b):

Equation 32

$$Y = y_i + m_i x + \frac{y_f + m_f x}{1 + e^{-[(x - x_0)/t]}}$$

where *Y* is the fluorescence intensity, subscripts *i* and *f* denote initial (*t*=0) and final (*t*=infinity), *m* is the slope, *x* is time, and x_o is the time to 50% of maximal fluorescence.

Thus, the apparent rate constant, k_{app} or the elongation rate is calculated by:

Equation 33

$$K_{app} = \frac{1}{\tau}$$

The nucleation rate is given by:

Equation 34

$$K_N = \frac{1}{x_0 - 2\tau}$$

where $x_0 - 2\tau$ is the lag time and τ is the width of the sigmoidal

These data can be obtained based on the Boltzmann equation offered by Origin software.

3.11.5 Routine for Fitting of transitions

A nonlinear least-square analysis of at least 50 iterations was done using Marquardt-Levenberg routine provided with the Origin^{TM} software. The iterations were done until the fractional change in χ^2 value was within the tolerance limit set to 5 x 10^{-2}. All the parameters were floated freely.

4 Purification, structural characterization and stability of native Ure2p

4.1 Physical - chemical parameters of Ure2 sequence

Ure2p contains 354 amino acids with a theoretical molecular mass of 40.3 kDa and a theoretical pI of 6.0. The extinction coefficient is 1.198 M^{-1} cm^{-1} at 280 nm (section 2.5.1). The normalized hydrophobicity of sequence was plotted according to Eisenberg (Eisenberg et al., 1984) (http://www.expasy.org/tools/protparam.html).

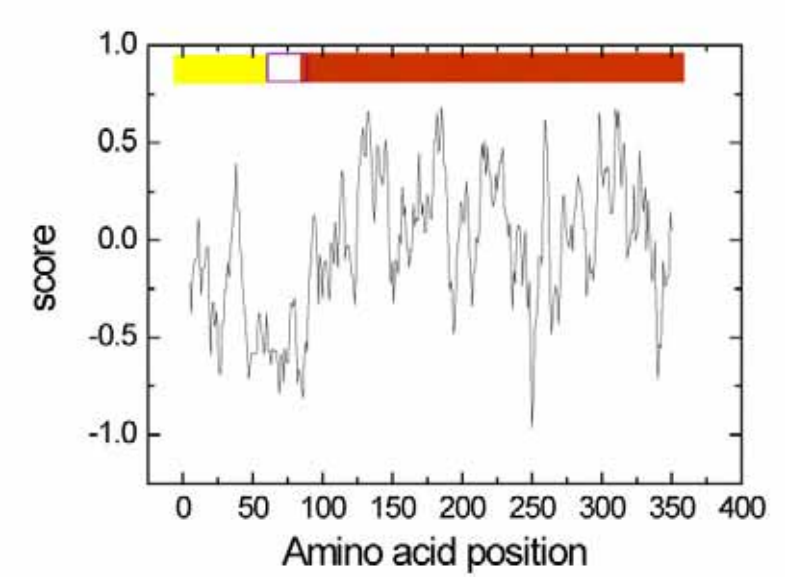

Figure 4-1: Hydrophobicity profile of Ure2p according to the Eisenberg consensus scale.

Positive and negative values indicate hydrophobicity and hydrophilicity, respectively. Red means the folded C-terminal domain and in yellow/white, the partially folded N-terminal. The yellow color assign the prion forming domain, 1-63 and white, the link region, 64-100 amino acid.

Analyzing Figure 4-1 it is possible to hypothesize that the C-terminal domain (in red) has a folded conformation due to the alternation of hydrophobic and hydrophilic regions (alternating high and low score region). This is in agreement with the published crystal structure from the C-terminal domain (Umland et al., 2001). The N-terminal domain presents an uncommon region with high polarity

between amino acids 43 to 100 (low score region). As suggested by Wickner and co-workers (Maddelein and Wickner, 1999), the N-terminal domain is composed of a high polar prion forming domain (yellow region) and a charged link region (white region).

4.2 Three-dimensional structure analysis of Ure2p

The structure of the C-terminal domain was visualized by Deep View software. The intrinsic fluorescent probes are highlighted to analyze possibilities of characterization using intrinsic fluorescence as characterization.

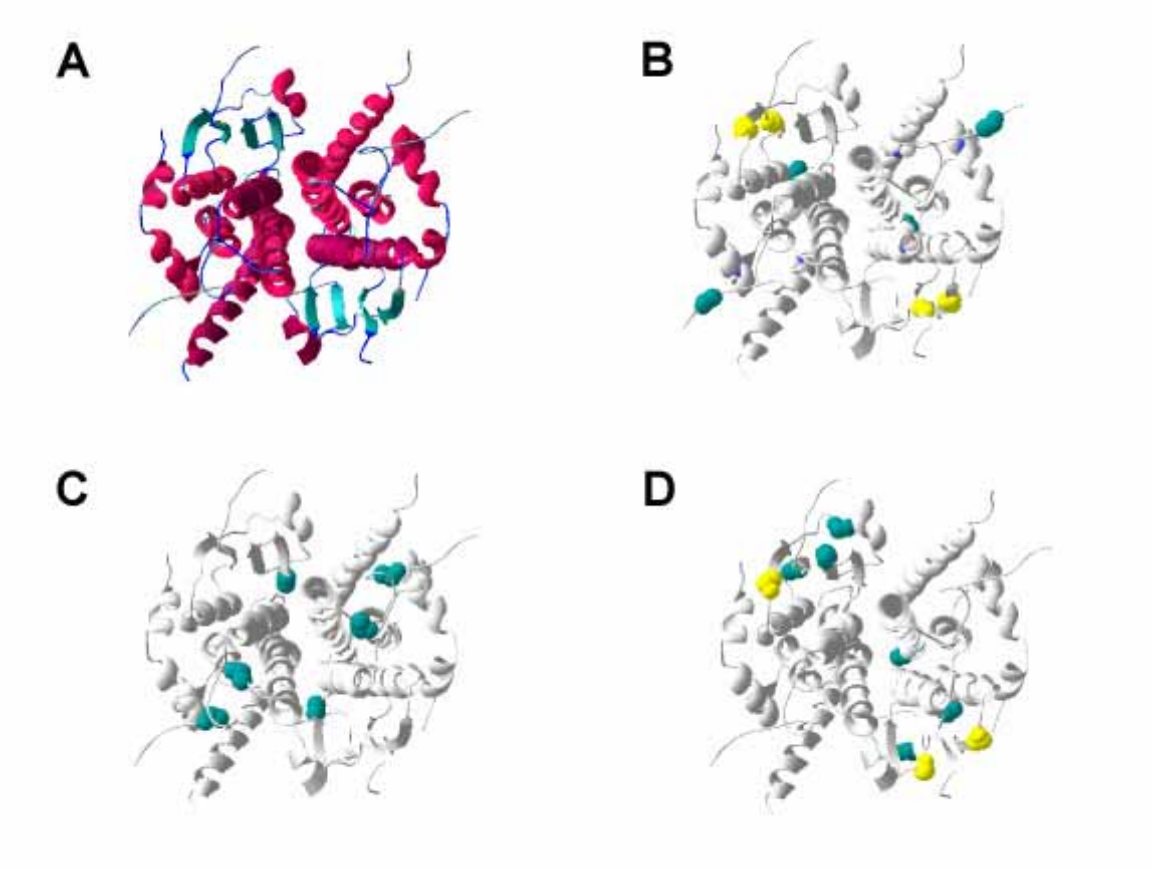

Figure 4-2: Three dimensional structure analysis using the crystal structure.
3-D structure of Ure2p drawn with 'Deep View/ PDB viewer' and localization of fluorescent intrinsic probes (trp, thr) and His. A) Crystal structure of C-terminal domain of Ure2p (Umland et al., 2001), B) Localization of tyr residues in the structure. C) Localization of trp residues in the structure, D) Localization of His residues. Amino acids are colored according to the secondary structure in which they were localized: yellow (β-sheet), blue (α-helices) and green (loop or unstructured region).

The Ure2p C-terminal region is rich in α-helices (50%) and β-sheet (20-30%) according to the crystal structure (Figure 1-6) (Umland et al., 2001), and has 6 Trp and 10 Tyr (Figure 4-2A, B and C). Cys, Met and His are potential quenchers of Trp fluorescence when located in the vicinity of it (section 2.5.3). Ure2p does not contain Cys in the amino acid sequence and Met is present only in the N-terminal domain. Tyr are exposed to solvent (Figure 4-2B) and Trp are buried in the structure (Figure 4-2C). There is only Tyr candidate for quenching Trp, the Tyr-335 that is close to Trp 337, despite that both are not facing each other. All His residues in the C-terminal domain are far away from Trp and are excluded as potential quenchers of Trp (Figure 4-2D). With this it is possible to conclude that there is basically no quenching of Trp by any other amino acid present in the C-terminal domain of Ure2p.

4.3 Purification of recombinant Ure2p

Ure2 was overexpressed in *E. coli* in order to ensure sufficient yield of protein to carry out extensive biophysical measurements. For protein expression, the *E. coli* strain BL21(DE3) was transformed with plasmid pET2a-Ure2 (gift from C. Cullin, Bordeaux France). The level of expression was higher at 37°C then at lower temperatures under high aeration conditions. The expression and purification was easily monitored by SDS-PAGE using 12.5% acrylamide gels (Figure 4-3). 10 hours after IPTG addition, the expression reached a maximum (Figure 4-3A and section 2.4.5). The protein was purified in soluble form, under non-denaturing conditions to homogeneity (around 95% purity). For a successful purification adding DTT or β-mercaptoethanol in the purification buffer is required. These agents may help to reduce some *E. coli* protein present in the lysate or avoid aggregation of some *E. coli* protein. The practical result of the presence of DTT is to avoid the co-elution of these proteins with Ure2p. 2 successive chromatographic steps were necessary for purification (Figure 4-3 and described at section 2.3).

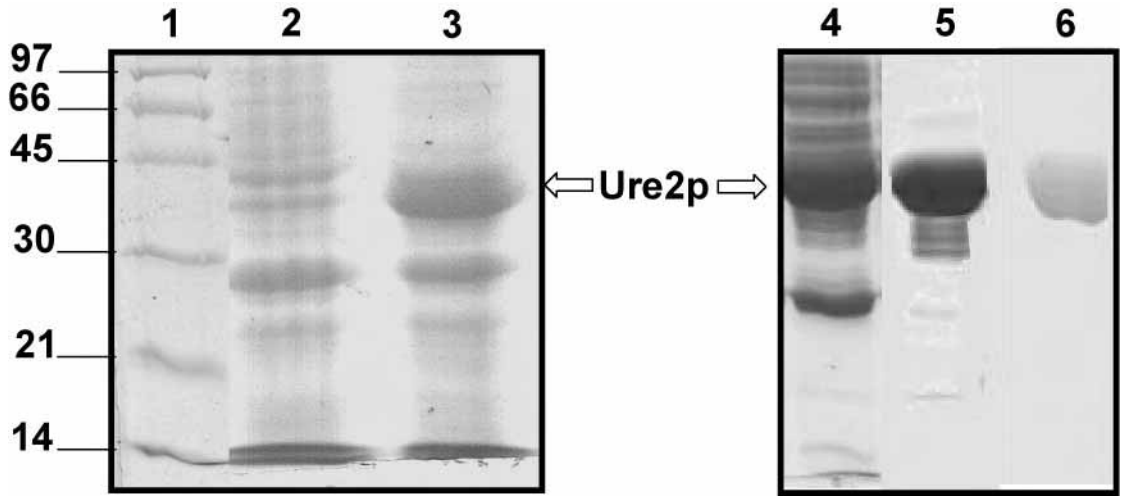

Figure 4-3 : Coomassie-stained SDS-PAGE (12.5%).
1) LMW marker in kDa 2) and 3) Bacterial extracts from Ure2p expression kinetics. 2) Before induction. 3) After 10.5 hours of induction 4, 5, 6) Analysis of the purification, 4) Fraction after ion exchange chromatography containing Ure2p, 5) Fraction after 30%Ammonium Sulphate precipitation and 6) peak of the gel filtration column elution and as a single band in the gel around 40 kDa.

On SDS-PAGE, full-length Ure2 appear to be around 40 kDa in the denaturating gel. The speed of the purification becomes extremely important as increasing the protein concentration. Concentrations of protein higher then 150 μM require a stabilizing agent (section 3). An additional purification step using a Hydroxyapatite column can be performed when the protein is not pure enough after gel filtration. The purified protein was subjected to automated Edmann degradation (N-terminal domain sequencing) showing that was the correct protein.

4.4 Light scattering correction for concentration determination

In order to determine protein concentration accurately, samples were measured using UV-vis spectroscopy with 0.1 cm cuvettes. The high absorption at wavelengths higher then 320 nm is indicative of the existence of large aggregates that scatter light in the solution (Figure 4-4 - dotted curve). The value of absorbance was corrected to eliminate contributions of the scattering of particles in solution (section 2.5.1).

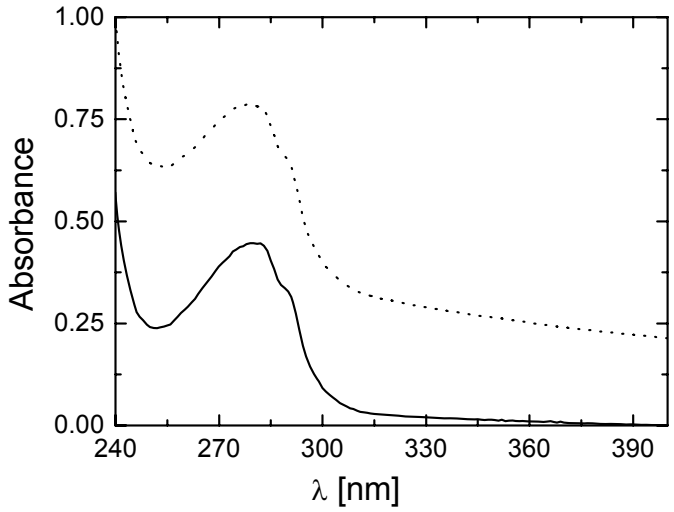

Figure 4-4: Light scattering correction for concentration determination.
Determination of Ure2p concentration in solution at 20˚C, with possible presence of some aggregates; (…) measured values and (-) values corrected for light scattering of the aggregated particles. Buffer was subtracted from data.

In Figure 4-4, the absorbance caused by aromatic amino acids present in the Ure2p sequence (Tyr, Trp and Phe) is shown. The protein concentration was determined using a molar extinction coefficient at 280 nm of 1198 M^{-1} cm^{-1}. The aggregates were not removed by centrifugation in this experiment. Values of 6.54 mg/ml were measured for samples composed of protein and aggregates. The corrected values of 3.62 mg/ml (91 μM) were measured for soluble protein. This figure shows the necessity to control the existence of aggregates and eliminate the scattering signal for measurements of Ure2p concentration.

4.5 Ure2p secondary structure

The folded state of a protein is sensitive to a wide variety of parameters, including pH, buffer and concentration. For biophysical experiments, it is important to know at which conditions the proteins are fully native, stable and folded. A series of conditions was explored using unfolding transitions as a method for determining the stability of the protein. In order to control the folding of the protein and the sensitivity to pH the CD spectra of Ure2p was measured in different conditions. To analyze the stability of Ure2p with change of pH,

values near physiological and non-physiological region were tested. A secondary structure analysis was done for determination of the of the secondary structure analysis. The observed optical activity was expressed as the mean residue molar ellipticity $[\theta]_{MRW}$ (degree cm^2 $dmol^{-1}$) (section 2.5.7). GdmCl was used as a denaturant because the protein does not unfold completely at 8 M urea showing that Urea is an insufficient denaturing agent for this protein (Perrett et al., 1999).

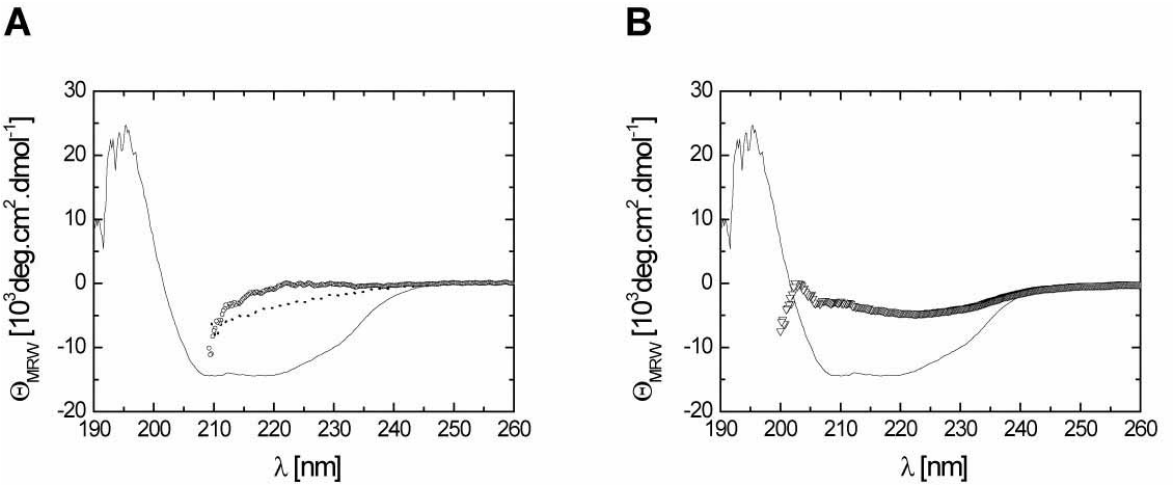

Figure 4-5: Secondary structure of Ure2p.
Far-UV spectra of the recombinant Ure2p. A) native Ure2p(-), Ure2p in 3M (--) and 6M GdmCl (o). B) Ure2p at pH 7.5 (-) and pH 5.0(∇). An average spectrum of 10 measurements for each sample was done. Buffer NaP/Tris 0.2 M NaCl pH 7.5 (or 5.0 when was the case) were subtracted from measured native data and buffer containing respective GdmCl concentrations were subtracted from GdmCl graphs. The temperature was 20 ˚C.

In the native state, Ure2p shows two peaks of negative ellipticity at 208 nm and 222 nm consistent with a high α-helical content (Figure 4-5 A). At 3 M GdmCl, Ure2p still shows some secondary structure, which is completely disrupted at 6 M GdmCl as the protein completely unfolds. At this point, there is no significant ellipticity at >220 nm indicating that the unfolded polypeptides assume a random coil conformation. The secondary content of the recombinant protein was obtained by deconvolution of the data using CDNN software. The analysis shows that the purified protein is correctly folded. According with the CDNN predictions, about 44% of amino acids of the recombinant Ure2 are folded into α-helices and about 26% are β-strands. This results are in agreement with published data using CD spectroscopy (Thual et al., 2001) and are consistent with the structure determined by X-ray crystallography of the C-terminal domain

(Umland et al., 2001) when considering the N-terminal domains as unfolded. Figure 3-5B shows the effect of decreasing the pH under the pI value, leading to a change of secondary structure and consequent amorphous aggregation formation showing that Ure2p is not stable under this condition Ure2p presents no visible change of secondary structure under the near physiological pH 7.2 until 8.4 (results not shown). Considering this, Ure2p is stable at near physiological and physiological pH and shows that near physiological pH are more suitable to work with this protein.

4.6 Tertiary structure of Ure2p

To obtain information about the protein tertiary structure, fluorescence spectroscopy (section 2.5.2) and Near-UV-CD spectroscopy were used to analyze the environment of the aromatic amino acids (section 2.5.7). The fluorescence of Trp and - to a lesser extent - Tyr residues is sensitive to changes in their solvent accessibility and in the hydrophobicity of their respective environment, and thus constitutes a probe for changes in the tertiary structure of a protein (Schmid, 1989).The presence of Trp and Tyr distributed throughout the C-terminal region (Figure 4-2) permits to monitor structural changes in the folding using intrinsic fluorescence with excitation at 280 or at 295 nm (section 2.5.2).

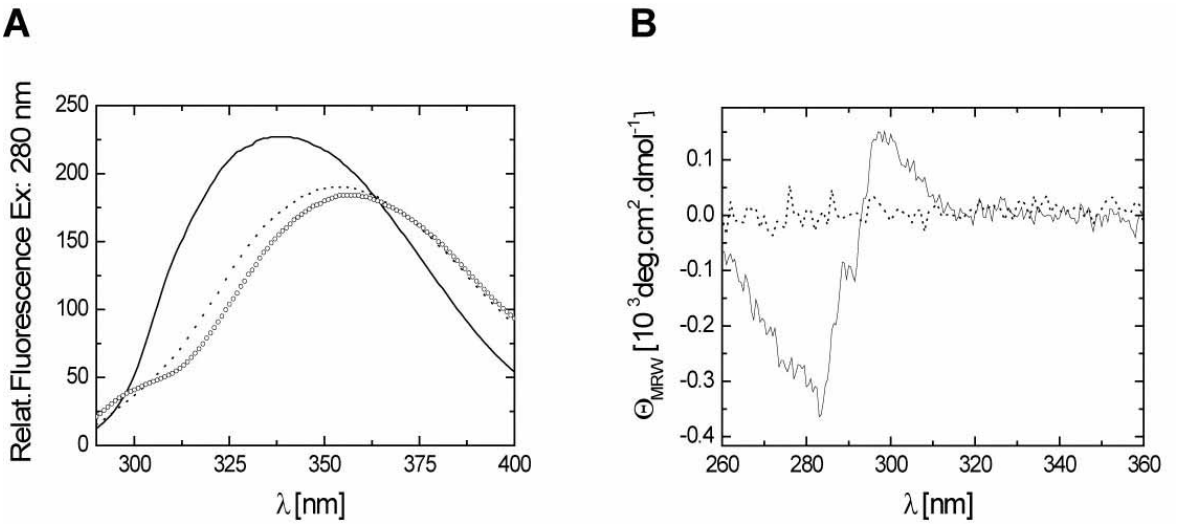

Figure 4-6: Tertiary structure of Ure2p

A) Fluorescence spectra of recombinant Ure2p in 0 M (-), 3.0 M (--) and 6 M GdmCl (o). Denaturation-induced fluorescence λ_{max} changes as a function of [GdmCl].

Excitation was done at 280 nm. Cuvette: 1 cm. B) near-UV CD spectra of the recombinant native dimeric Ure2p (full line) and denatured Ure2p in 6 M GdmCl (dotted line), cuvette: 0.5 cm. Buffer NaP/Tris/Cl 0.2 M NaCl pH 7.5, Ure2p concentration: 5μM. T= 20 ˚C.

The fluorescence spectra of folded Ure2p show the emission maximum of the Trp at 337 nm (Figure 4-6A). At intermediate GdmCl concentration (3 M, for example), Ure2p has a fluorescence spectrum intermediate between the folded and denatured spectra. This could mean that at this concentration a partially structured folding intermediate is present, or that there is equilibrium of folded and unfolded protein. Fluorescence spectra of Ure2p under 3M and 6M GdmCl indicate exposure of the buried Trp and Tyr to solvent during unfolding with the change of the λ_{max}. When excited at 280 nm or 295 nm, there is a red shift of the emission maximum, from 337 to 354 nm, accompanied by a decrease of the emission intensity. This decrease in intensity and the red-shifts is consistent with the exposure of the Tyr and Trp to denaturant. When excited only at 295 nm, the emission maximum of the Trp is still at 337 nm and this indicates that it is partially buried. The agreement at both excitation that the native Ure2p present a λ_{max} of 337 nm suggests an insignificant contribution of Tyr residues to the bulk emission of the native protein (in agreement with Figure 4-2B. showing that major part of the tyr are exposed to the solvent). Due to this result it is possible to monitor the unfolding transition using intrinsic fluorescence. Figure 4-6B shows the near-UV CD spectrum of the folded and unfolded Ure2p. Folded Ure2p exhibits a strong negative CD signal at 283 nm and a weaker negative band at 290 nm and a weaker positive band between 297-305 nm. This suggests that aromatic amino acid residues (Phe, Tyr, Trp) are immobilized in asymmetric environment in the folded state. The unfolded protein does not show a signal in these regions, meaning that the native tertiary structure is entirely lost upon GdmCl. According to Figure 4-4, the absorbance around 280 nm is dominated by the Trp. This means that the immobilized aromatic amino acid is Trp because Tyr and Phe have a low near UV-CD signal in this region. These results are in agreement with CD measurements done by Perret and co-workers (Perrett et al., 1999).

4.7 Quaternary structure of Ure2p

Using SEC it is possible to determine the oligomeric state of a protein in solution. Recombinant Ure2p was analyzed by SEC using different column matrices, buffers, temperatures and pH (section 2.5.6).

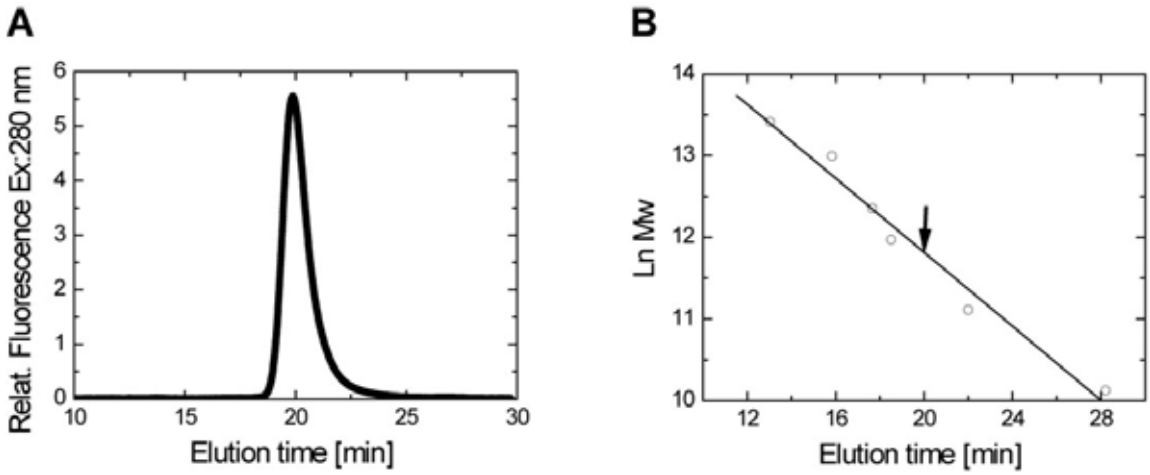

Figure 4-7: SEC-HPLC elution profile of recombinant Ure2p
Elution using a TosoHaas TSK SW 3000 column, buffer 50 mM Tris, 200 mM NaCl, pH 7.5, 20°C, Fluorescence curve, excitation : 280 nm and emission at 334 nm, T= 20 ˚C. A) Ure2p elution. Concentration: 0.1 μM B) standard globular protein, thyroglobulin (670 kDa), ferritin (440 kDa), catalase (232 kDa), aldolase (158 kDa), BSA (67 kDa) and chymotrypsin (25 kDa). The arrow indicates the position of Ure2p.

Ure2p elutes as a single peak in the TosoHaas TSK column (Figure 4-7A). According to the fitting and the elution profile of the standard proteins (Figure 4-7B), Ure2p elutes between the molecular weight markers aldolase (158 kDa) and BSA (67 kDa). The retention time of Ure2 was equivalent to that of a globular protein of approximately 120 kDa. No other peaks were observed under the conditions described in section 2.5.6. This would correspond to a dimeric or trimeric protein. Experiments done on a Superose 6 and Sephadex-200 column using different buffers showed that Ure2p behaves like a 130 kDa protein (a trimer/tetramer) (data not shown).This unexpected behavior of Ure2p do not relate to globular protein and may represent a dimeric species. This behavior may be due the unfolded N-terminus. It is known that unfolded proteins shown an increasing in the hydrodynamic radius of almost two times

the own molecular weight due to the hydration of the polypeptide chain (Garcia, 2001). Ure2p runs stable as a dimeric species in buffer like Hepes, NaP and Tris over a broad range of concentrations (data not shown). Temperature does not lead to the appearance of different species but aggregates that can stack to the column pre-filter making it difficult to analyses Ure2p at high temperature. Ure2p was described to be dimeric in different publications (Perrett et al., 1999; Thual et al., 1999; Thual et al., 2001). It is common for some protein to adopt dimeric structure because this minimize the thermodynamics unfavorable solvent exposition from some hydrophobic chain in the surface (Jones and Thornton, 1995). In the GST class, the dimeric structure is important for the function and stability (Hornby et al., 2000). Experiments done at low concentration shows a monomeric protein present in relation 20% from the total (results not shown).

4.8 Solvent stability of dimeric Ure2p

Trifluoroethanol (TFE) is an alcohol based co-solvent that weakens the hydrophobic interaction that stabilize the compact native structures of proteins while stabilize secondary structure in partially folded peptides. The destabilizing of the native structure is done by penetrating into the protein core making a preferential solvation of hydrophobic groups of the protein (Del Vecchio et al., 2003). It was analyzed the behavior of Ure2p in presence of an organic solvent.

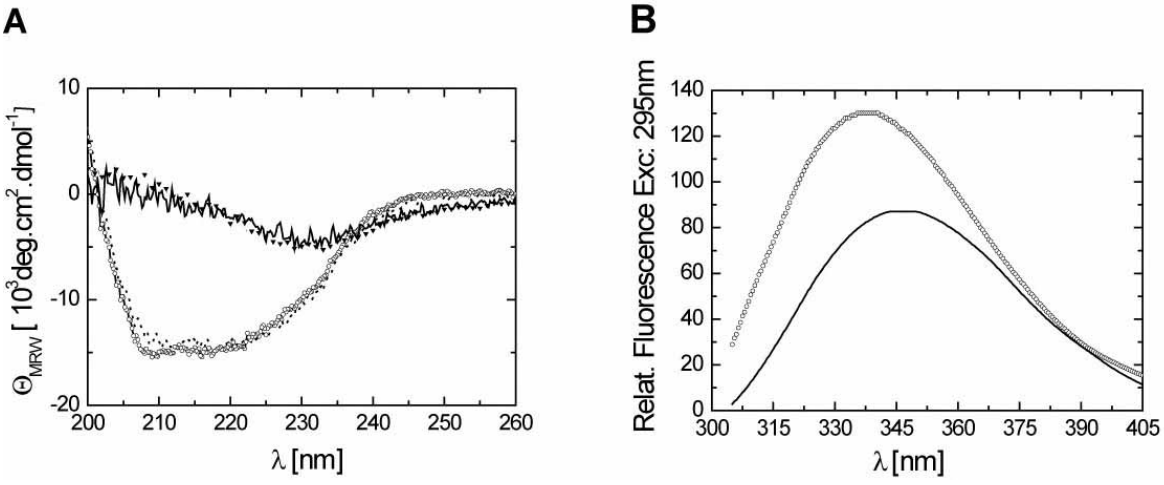

Figure 4-8: Ure2p stability in solvent

A) Far-UV CD spectra of Ure2p under different concentrations of TFE. (-o-) 0%, (--) 10%,(▼) 20%(—) 30% in v/v. B) Fluorescence spectra of Ure2p (-o-) 0% and (—) 30% T= 20 ˚C, Ure2p concentration: 15 μM. Buffer: 50 mM NaP, 0.2 M NaCl pH 7.5

Figure 4-8A shows CD spectra of Ure2p in presence of different TFE concentrations. Differences between the spectra recorded without and with 10% of TFE are not strong, showing a slight increase in the region of 230 nm for 10% of TFE. This suggests a native-like structure in presence of low concentration of solvent. This increase at 230 nm could mean that is a partial stabilization of the unfolded n-terminal domain. Increasing the TFE content to 20% induces an overall breakdown of the native tertiary structure resulting in a spectrum change that is stable at 30%TFE (4.2 M). The CD spectrum shows a disruption from α-helical and a stabilization of an aggregated state-like containing high content of β-sheet structure. This breakdown of structure is confirmed by the florescence spectrum measured at 30%TFE (Figure 4-8B). There is a red shift of the emission maximum from 337 to 347 nm accompanied by a decrease of the emission intensity indicating one exposure of the buried Trp to a more polar environment in presence of TFE-water then in native conditions (water). Thus TFE make weaker local interactions resulting in the formation of a β-sheet conformation. This means that TFE changes the conformation of Ure2p.

4.9 Temperature stability of dimeric Ure2p

In order to know the stability of the dimeric Ure2p under elevated temperature, denaturation experiments were performed analyzing the secondary structure stability over a range of temperature (section 2.7.1)

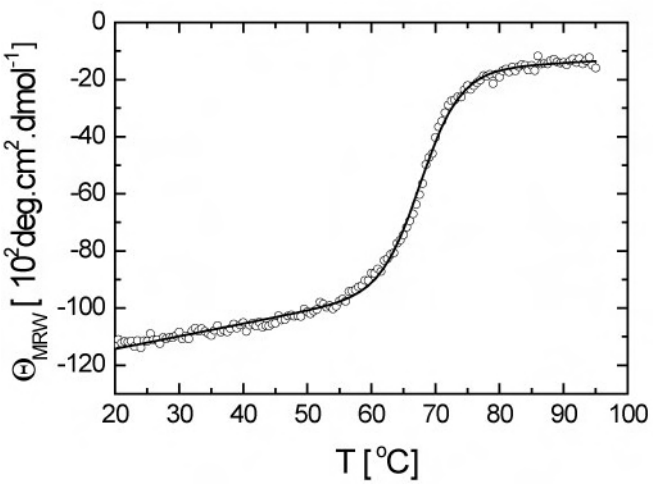

Figure 4-9 : Thermal denaturation of dimeric Ure2p
CD signal at 222 nm. Buffer: 50 mM NaP/Tris, 0.15 M NaCl pH 7.5

A single sigmoidal transition was observed for the thermal denaturation of Ure2p in Figure 4-9. The experiment was monitored following the CD signal at 222 nm (far-UV) which is the minimum in the far-UV CD spectrum for an α-helix. Figure 4-9 shows a single, co-operative transition with an apparent t_m of 68 $\pm$ 0.1°C (the mid-temperature of the transition). The ΔG value calculated by fitting the curve (section 2.8.4) to a 2 state transition was 312.1 $\pm$ 9 kJ/mol. These values of ΔG imply in a high value of enthalpy and in an irreversibility of the unfolding. As thermal denaturation was not reversible, this means that the data were qualitative. The protein is unsuitable for calorimetric studies due to the irreversibility formation of aggregates.

4.10 Equilibrium denaturation studies using fluorescence probes

An unfolding transition can show the populated states of a protein upon unfolding and is very useful for characterizing the environment of the indole side chain of Trp and the environment of Tyr as a function of denaturant concentration. The Tyr and Trp emission spectral changes associated with the denaturation of the C-terminal domain of Ure2p are shown in Figure 4-5 and Figure 4-6. The change of intrinsic fluorescence intensity of Ure2p was monitored at 327 nm. The Intrinsic fluorescence values were plotted versus

concentration of GdmCl. The effect of the environmental conditions on the stability of the protein was determined by fitting the unfolding curves to exponential equations (section 2.9.2). To compare different curves, they were normalized in respect to the fraction of folded protein.

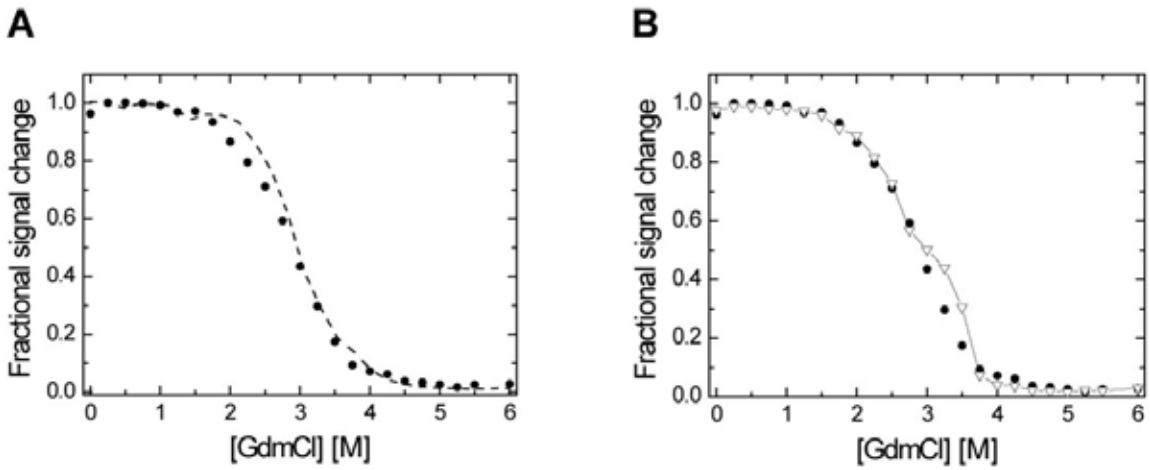

Figure 4-10 Equilibrium denaturation using Tris buffer

A) pH Effect on Equilibrium denaturation of Ure2p in 50 mM Tris 150 mM NaCl pH 7.5 (●) and pH 8.5 (---) protein concentration : 5 μM. B) Concentration effect on equilibrium denaturation of Ure2p in 50 mM Tris buffer pH 7.5 150 mM NaCl, T=20 ˚C, concentration (●) 5 μM and (-∇-) 35 μM.

The equilibrium denaturation data of Ure2p in Tris buffer show only one unfolding transition (Figure 4-10A). The chemical unfolding is a reversible process (data not shown) with some loss of protein by aggregation. This same behavior has been show by Perret for Ure2p unfolding (Perrett et al., 1999). Analysis of denaturation curves (Figure3.10A) was performed according to a two-state transition. The two unfolding curves are super-imposable with a transition between 1.5 and 4.0 M GdmCl, with a midpoint for unfolding of 2.9 M GdmCl (Table 4-1).

Table 4-1: Thermodynamic stability of Ure2p using Tris buffer and different pH.

Data were fitted to a two-state equation and $\Delta G(H_2O)$ was calculated. $[GdmCl]_{1/2}$, is the concentration of denaturant at which equal proportions of folded and unfolded protein are present and m the slope of the transition (section 2.9.2)

pH	[Ure2p]/ μM	$[GdmCl]_{1/2}$ /M	m/kJ.mol^{-1}.M^{-1}	$\Delta G(H_2O)$ /kJ/mol
7.5	5	2.86	6.2±0.2	17.8±0.9
8.5	5	2.98	6.8±0.4	20.3± 1.2

No pronounced change in ΔG is observed and both curves (Figure 4-10A) can be fitted by a two state mechanism very well (Table 4-1). This means that the unfolding process goes from native to the unfolded state without any detectable stable specie in between (all native or none), following the path $N \Leftrightarrow U$ of a two-state transition with an overall breakdown of the tertiary structure. Since Ure2p is a dimeric protein, one would expect that one of the species (native or unfolded) would present a change in fluorescence during analysis. To have a more detailed view, an unfolding transition was done looking for a concentration effect on it. At concentrations lower than 10 μM it is possible to fit the data to a two state model (Figure 4-10B). At higher concentration (e.g. 35 μM), a switch from two-state unfolding to one three-state unfolding mechanism was observed. All the data were fitted to a three-state model and to a two-state model, whatever was appropriate, and the suitability was observed by eye. The first transition is between 1.5–2.5 M GdmCl, and has a mid-point around 2.4 M and the second transition is between 2.7–3.7 M GdmCl and has a mid-point around 3.0 M (Table 4-2). This data shows that the position of the two transitions does not change too much with protein concentration and it is likely that a second transition starts while the first transition still is not finished. Despite the apparent visual increase of the second transition with concentration, the midpoint according with the fitting of the transition is not affected. The fitting shows a slight increase of ΔG (Table 4-2) with protein concentration. One hypothesis is that the effect of the protein concentration is not easily detectable because of the superposition of the two transitions. This indicates that the process is cooperative and the formation of the intermediate and unfolding is almost a simultaneous process. One additional standard

laboratory buffer was tested; in this case, it was NaP. NaP is very commonly used due to the low extinction coefficient in the far-UV region. In addition, it was used ANS as a probe. Due to the spectral blue shift companied by enhanced fluorescence intensity demonstrates by ANS experiment is expected that the environment of the ANS binding site is hydrophobic. This means that the binding of the ANS to a protein would be in a hydrophobic site. The change of the binding means the exposition of the hydrophobic site or hydrophobic surface area. The unfolding transitions were measured in presence of ANS fluorescence (section 2.5.4).

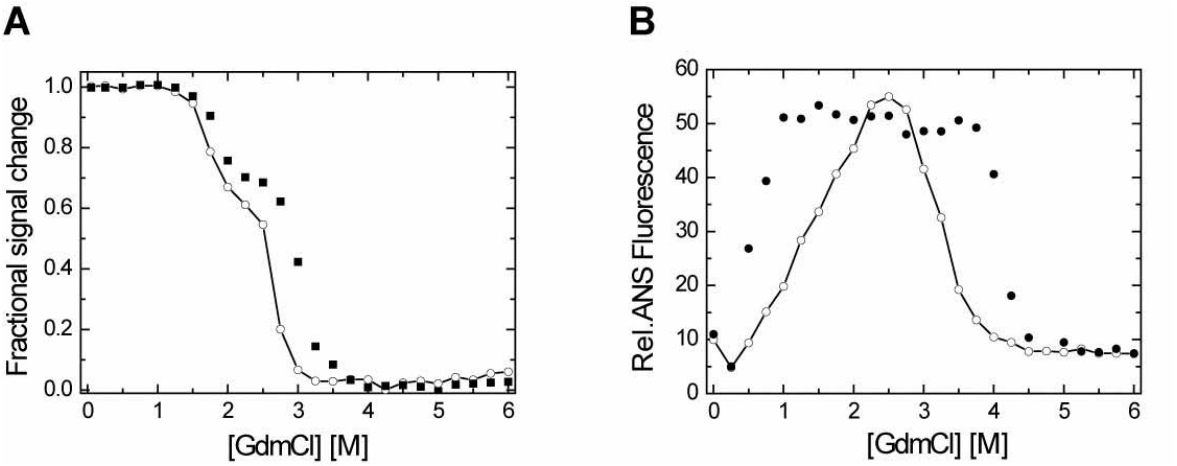

Figure 4-11: Comparison of equilibrium denaturation of Ure2p

A) Effect of pH on Equilibrium denaturation of Ure2p in phosphate buffer pH 7.5 (-○-) and pH 8.5 (■). B) Equilibrium denaturation of Ure2p monitored by ANS fluorescence in Tris (●) and phosphate (-○-). There is no change over protein concentration. Concentration was 5 μM and T= 20 ˚C. Buffers used: 50 mM NaP, 0.15 M NaCl pH 7.5 (or 8.5) and 50 mM Tris 150 mM NaCl pH 7.5.

As shown in Figure 4-11A the Ure2p curve in phosphate buffer shows two unfolding transitions at both pH values measured, while Tris shows only one transition at this condition (Figure 4-10A). The data were fitted to a three-state model (Table 4-2). Analyzing the fitted data it is possible to see a slight difference in the first transition (1-2.0 M).This shows a slight effect on the native state with the increase of the pH. The second transition is not super imposable at the two pH values measured. The mid-values of the transition and ΔG show an increase with pH. The reason for this pH effect could be protonation of charged amino acids. Analyzing the fitted data (Table 4-2) it is possible to see a clear difference between the two buffer systems comparing the first transition (1-2.5 M). At all the conditions measured in NaP buffer the unfolding occurs in

two transitions. Despite that the values of ΔG are higher in NaP buffer, the mid-points of transition are lower in the first and second transition. This shows that Tris buffer has some effect on the stability compared to NaP buffer.

Table 4-2: Thermodynamic stability of Ure2p at different conditions fitted by a three-state equation.

Subscribed a indicates the first transition (N-I) and b the second transition (I-D). $\Delta G_U(H_2O)$ is the overall free energy change for complete unfolding and dissociation, B means the buffer system where the transitions were done. Thermodynamic parameters were calculated according to Pace at all(Pace et al., 1996; Buchner and Kiefhaber, 2004) (section 2.9.2) by fitting the unfolding curves with equations for a two state (Table 4-1) and a three state transition.

Buffer	pH	[U] μM	[GdmCl] $_{1/2,a}$ / M	[GdmCl] $_{1/2,b}$ / M	m_a/ kJ. $mol^{-1}.M^{-1}$	m_b/ kJ. $mol^{-1}.M^{-1}$	$\Delta G_a(H_2O)$ $kJ.mol^{-1}$	$\Delta G_b(H_2O)$ $/kJ.mol^{-1}$	$\Delta G_U(H_2O$ $/kJ.mol^{-1}$
Tris	7.5	5	2.4	3.06	4.2 ± 0.3	9.4 ± 0.4	10.3±1.2	28.9±1.2	39.2±1.2
Tris	7.5	35	2.5	2.95	8.0 ±0.7	10.8±2.0	20,1±1.7	31.8±5.9	51.6±5
Tris	8.5	5	2.55	2.93	4.2±1.1	7.8±3.3	10.9± 3.1	23.0±1.1	33.9± 2.2
NaP	7.5	5	1.75	2.66	16.6±3.8	24.6±3.1	29.1±6.8	65,4±8.7	104±9.3
NaP	8.5	5	1.88	3.02	16.8±4.0	15.7±1.6	31.6±6.7	47.5±5.6	84.3±9.5

The mid-point of the first transition fitted according to a three-state mechanism is slightly lower than that fitted with a two state mechanism, although the values of m and ΔG are higher. The NaP buffer allows the detection of the pH effect on the first transition. As demonstrated in Figure 4-11B the unfolding transition in NaP shows a peak near the mid-point of the GdmCl transition around 2.5 M GdmCl. Results may indicate the maximum of the exposure of hydrophobic surface of the intermediate species during unfolding and indicating a intermediate species. The intermediate species is not stable at GdmCl concentration over 3.5 M. The unfolding transition in Tris buffer shows a plateau starting at 1 M until 4 M GdmCl. This shows that the exposition of hydrophobic surface starts earlier in Tris then in NaP. This indicates a superposition of the first and second transition (Figure 4-13). This assumption hints to the possibility of the existence of species from different transitions at

the same time. It could be the coexistence of partially folded intermediate with folded and unfolded species. Hence, a possibility would be that the species that persists until 4 M would be a dimeric intermediate once that the monomeric unfolded intermediate does not bind ANS above 4 M (shown by Perret (Zhu et al., 2003a)). The folded dimeric protein in aqueous environment is expected not to bind ANS to a significant amount, but still has a residual binding to ANS as seen at 0 M GdmCl.

4.11 Equilibrium denaturation studies using secondary structure analysis

The changes occurring at different structural levels during chemical unfolding processes were monitored by far UV CD spectroscopy and compared with fluorescence spectroscopy results. CD spectra were recorded under different GdmCl concentrations.

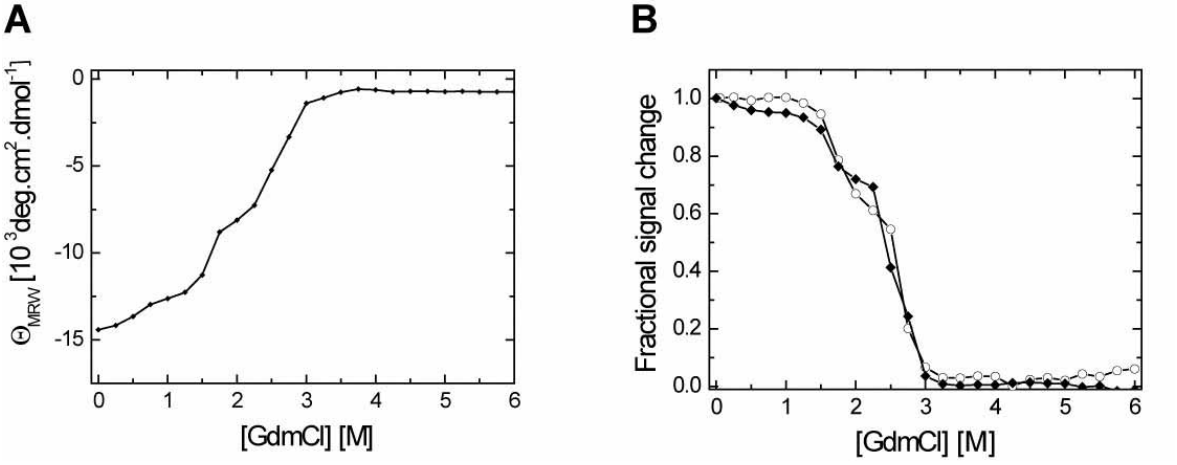

Figure 4-12: Equilibrium denaturation studies using secondary structure analysis

A) Unfolding transition of dimeric Ure2p monitored at 222nm. B) Normalization of the CD data monitored at 222nm (-♦-) and comparison with denaturation transition of dimeric Ure2p followed by fluorescence spectroscopy (-○-). Buffer: 50mM NaP, 150 mM NaCl pH 7.5 and 5 μM, T= 20 ˚C.

Table 4-3: Thermodynamic stability of Ure2p by monitored by intrinsic fluorescence spectroscopy and Circular Dichroism.

Data were fitted by a three-state equation (section 2.9.2).

Technique	$[GdmCl]_{1/2,a}$ $_{3st}$ /M	$[GdmCl]_{1/2,b}$ $_{3st}$ /M	m_a/ kJ. $mol^{-1}.M^{-1}$	m_b/ kJ. $mol^{-1}.M^{-1}$	$\Delta G_a(H_2O)$ kJ/mol	$\Delta G_b(H_2O)$ kJ/mol	$\Delta G_U(H_2O)$ kJ/mol
Intrinsic Fluorescence	1.75	2.66	16.6±3.8	24.6±3.1	29.1±6.8	65,4±8.7	104±9.3
CD	1.67	2.53	18.0±1.2	13.2±2.8	30.2±2.8	33.2±8.9	63.4±6.3

The far-UV CD signal shows a decrease in intensity with increase in GdmCl concentration under 2 M (Figure 4-12A). Above 3 M GdmCl the CD signal remains constant consistent with an unstructured polypeptide chain. The signals from far-UV CD spectra were fitted according to a three state model (Table 4-3) and found to be very similar in shape with intrinsic fluorescence when plotted as a fraction of folded protein (Figure 4-12B). CD spectroscopy shows that the major unfolding transition occurs between 1.5 and 2.5 M GdmCl, and after 3 M there is only unfolded species. Comparison of the signals of intrinsic fluorescence and far-UV CD data shows coincident transitions, indicating that secondary and tertiary structures are lost concomitantly. This confirms the ANS binding data showing that there is a dimeric species around 2.5 M GdmCl. Figure 4-12A shows that the intermediate species has a lower α-helical content then the native species.

4.12

4.13 Partial discussion

Ure2p was successfully purified under non-denaturing conditions to homogeneity. It is a soluble dimeric protein as shown by SDS-PAGE and SEC-HPLC. The protein is in a folded state and looses its secondary and tertiary structure under different conditions, like pH, organic solvent and GdmCl as denaturant (as shown by CD and Fluorescence spectroscopy). Near physiological conditions showed to be the best conditions to work on folding

studies. In the case of Ure2p, this structural globularity is showed by the crystal structure of the C-terminal domain (Umland et al., 2001) and by the preliminary AFM experiments using the C-terminal domain of Ure2p (Jiang et al., 2004). The Trp and Tyr in the globular C-terminal domain permit unfolding studies using GdmCl and different conditions. Analyzing the unfolding transition, it is possible to see a difference between ΔG values calculated for thermal and chemical unfolding using a two state model. This may be because the thermal unfolding of Ure2p is irreversible and chemical unfolding is a reversible process (Perrett et al., 1999). Of course, there is always the possibility that intermediates are present in unfolding by denaturants (Tris and NaP) buffer and not in thermal unfolding (NaP buffer). There is no rigorous way of confirming a real two-state thermal unfolding mechanism (Pace in Protein Folding Handbook (Buchner and Kiefhaber, 2004).

The chemical unfolding transition performed in Tris can be fitted to a two state model and in NaP transitions can be fitted to a three state model. This may happen because Tris stabilize the dimeric species and the first and second transition has a superimposition. The data obtained in NaP buffer using intrinsic fluorescence, ANS fluorescence and CD are coincident and suggest a dimeric intermediate species during unfolding. There is an exposition of buried groups to the solvent above 3 M, confirming the presence of intermediate species during unfolding of Ure2p. The intrinsic fluorescence data and the ANS data done using Tris buffer do not show this intermediate clearly but suggest exposition of the buried groups. One possibility is that this intermediate is invisible using these techniques with Tris buffer due to the merging of the two transitions. The data between NaP and Tris buffers present some coincident result: 1) the dimeric species, is stable up to 1.5 M denaturant and at 4 M GdmCl the protein is completely unfolded, 2) there is a total exposition of the intrinsic fluorescent probes to the solvent and 3) there is an effect of the pH on the first transition and a effect of concentration at the second transition. During the realization of this thesis three papers under the co-authorship of Sarah Perret were published studying the unfolding of Ure2p in Tris (Zhou et al., 2001) (Zhu et al., 2003a) and NaP buffer (Zhu et al., 2003b). In Tris buffer, Perret proposed a two state model(Zhou et al., 2001) and for NaP, it is a three state model(Zhu et al., 2003b).In addition to my work, Perret has shown that

the denaturation of Ure2p is multiphasic with first unfolding and then dimer dissociation using SAXS. Her results confirm the hypothesis that Ure2p unfolds via a dimeric intermediate in NaP. The mechanism proposed by Perret would be $N_2 \Leftrightarrow I_2 \Leftrightarrow 2U$, confirming the results proposed here. Results indicate that there is a superposition of transitions in Tris buffer.

These results would indicate the three state mechanisms:

$$N_2 \Leftrightarrow I_2 \Leftrightarrow 2U$$

Having two transitions, where the first transition represents the unfolding of the dimeric species and the second transition is the monomerization of the dimeric intermediate and completely unfolding of Ure2p (Figure 4-13). The Intermediate I, would be stable dimeric species which is already partially unfolded (less α-helical contend then the native species)

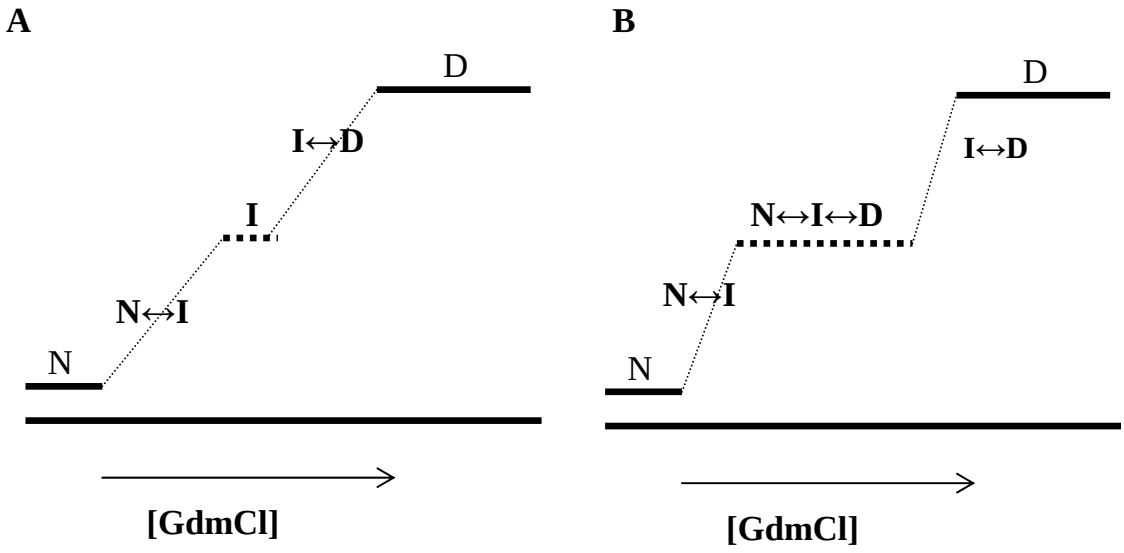

Figure 4-13: Diagram highlighting the differences between Ure2p in A) phosphate and B) Tris

This two-state model (also proposed by Perret for Tris buffer) may be due to the stabilization of the dimeric species in contact with Tris molecule and this would cover up the intermediate species during the transition. Other possibility in Tris presence could be some subunit interactions that contribute to the stability of the intermediate and this would not happen in phosphate buffer. According with the results described here, it is expectable that Ure2p follows three-state equilibrium with native, unfolded and partially folded intermediates coexist. The analysis of the Table 4-1 and Table 4-2, it is possible to see that

the two state model underestimates the value of $\Delta G_U(H_2O)$. This shows that the three state model better describes the equilibrium unfolding transition from Ure2p as has been showed, too, by Perret(Zhu et al., 2003b).

5 Characterization of the self-assembly behavior of Ure2p

5.1 Self-assembly monitored by biophysical assays

5.1.1 Analyses of aggregates by electron microscopy

Ure2p forms filaments *in vitro* (Schlumpberger et al., 2000). These filaments grow spontaneously in solutions without any addition of 'seeds' within a few hours, dependent on concentrations and temperature (Zhu et al., 2003b). To characterize these filaments, TEM and SEM were performed according to section 2.6.2 and 2.6.1, respectively.

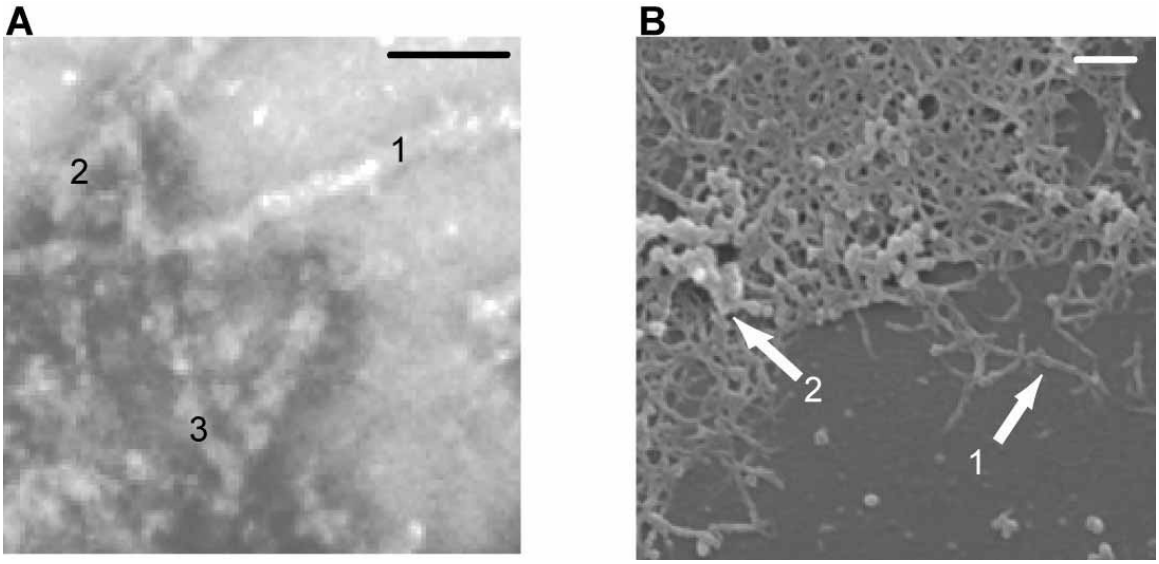

Figure 5-1: Electron microscopy of Ure2p fibrillation products.
A) TEM of negatively stained samples from Ure2p fibrils. Dimensions: (1) 28 nm, (2) 24 nm and (3) 18 nm. Scale bar: 90 nm. B) SEM from Ure2p fibrils, (1) fibrils and (2) amorphous aggregates. Scale bar: 1 μm. Measurements of fibrils polymerized in Tris buffer, pH 7.5, 15°C.

Figure 5-1 shows the electron micrograph of Ure2p fibrils formed *in vitro*. There is a variation in the filaments thickness (range 18-28 nm width, Figure 5-1A), with a strong variation of length (between 30 nm to a few micrometers, Figure

5-1B). The SEM image shows fibrils deposit over each other like in a net. During fibrillation, there is formation of amorphous aggregates, i.e. species without a regular structure, as a minor side product (2). These filaments are similar to the filaments on the yeast cells as published by Wickner (Speransky et al., 2001) where is described the Ure2p prion phenotype [URE3] found *in vivo* and in vitro (Taylor et al., 1999). Fibrils displaying average widths of 21.5, 25, and 28 nm could be distinguished by TEM. These numbers are similar to those shown by Prusiner (Schlumpberger et al., 2000) *in vitro* (average 22 nm and range of 17-28 nm). This slight difference may be due to experimental differences in the staining method used for TEM and individual measurements. These fibrils are similar to fibrils reported already for PrP(DeArmond et al., 1985) and Sup35(Glover et al., 1997).

5.1.2 Microscopic analyses of aggregates by AFM

AFM provides quantitative, three-dimensional and morphological information unavailable via electron microscopy. Fibrils were polymerized in solution, after 72 hours of the assembly process, the filaments solution were adsorbed to a piece of mica, left drying overnight and imaged by AFM (section 2.6.3).

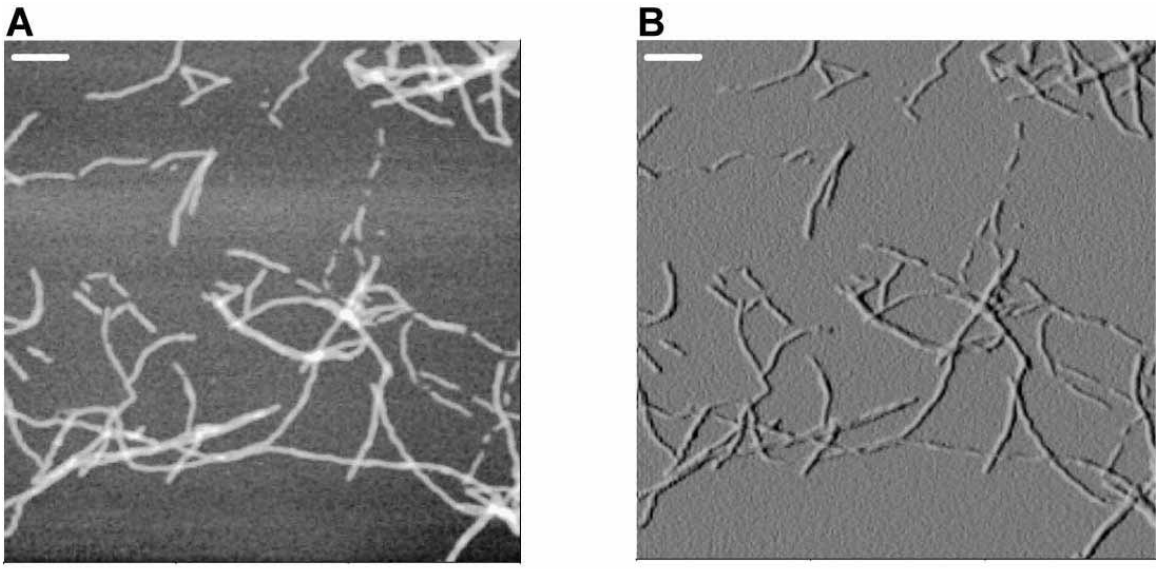

Figure 5-2: TM-AFM images of fibrillar aggregates from Ure2p.
A) Height image where the lightest color represents a height of 40 nm. B) Amplitude image. Both figures A and B are measured on 512 points, speed 1 Hz with same dimension at room temperature. The scale bar (white, upper left) represents 300 nm.

Figure 5-2 shows AFM images of fibrils of different length, adsorbed to mica, present at same time during fibrillation. The affinity of Ure2p toward the lightly anionic surface of mica is undoubtedly driven by positively charged amino acids like Lys, His and Arg located in the hydrophilic part of the C-terminal domain. From the height image (Figure 5-2A), it is possible to calculate the different height and width of the fibrils. The height (h), the length and the width of fibrils were extracted from data using the Nanoscope Software (section 2.1). The width was measured at the average half maximal height, h_{max} using Tapping mode (section 2.6.3). The amplitude image was used on this thesis to display some morphological characteristics and three-dimensional features.

5.1.3 ThT binding assay

The ability of the purified Ure2p to form fibrils was verified using the ThT assay, AFM and EM concomitantly. As shown before for amyloid protein, the kinetics of amyloid fibril formation is characterized by a significant lag phase in ThT binding (LeVine, III, 1993) (section 2.5.5).

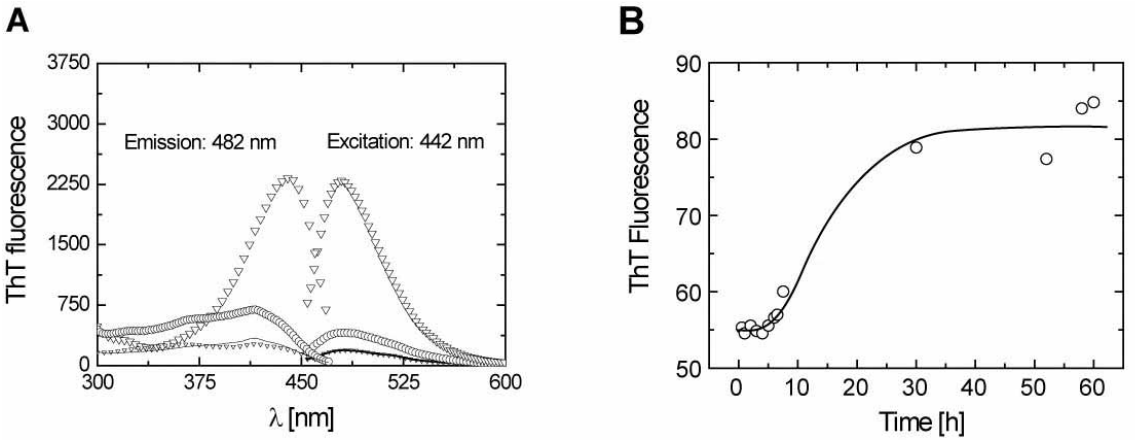

Figure 5-3: ThT assay establishment
A) Different conditions were tested in order to see the fluorescence emission of ThT. (-∇-) ThT buffer, (—) lysozyme, (o) Ure2p dimer and (∇) Ure2p fibrils. B) Time course of fibrillation followed by ThT fluorescence assay at 60 μM Ure2p in 50 mM Tris/HCl pH 7.5, 15°C.

Figure 5-3A shows the excitation and emission spectra of the ThT-buffer in the absence or presence of protein. Free ThT fluoresces weakly at 438 nm when excited at 350 nm(-∇-). ThT does not bind to monomeric or dimeric species of

Ure2p(o) or another β-sheet protein like lysozyme(—). ThT does not disassemble already formed oligomeric species and fibrils (data not shown). Both soluble and fibrillar forms of Ure2p were analyzed for ThT binding (section 2.5.5) and compared. In the presence of fibrils, a strong ThT fluorescence emission is observed at 490 nm upon excitation at 442 nm (LeVine, III, 1993). The emission correlates directly with the concentration of fibrils as was already demonstrated for several amyloid fibrils (LeVine, III, 1997). Figure 5-3B shows a fibrillation kinetic of dimeric Ure2p. The kinetics of fibril formation is characterized by a significant lag phase in ThT binding (first 5 hours). The lag phase is caused by a slow formation of nuclei that does not bind ThT (Figure 5-4A). The lag phase has been cited as a an indication of a nucleation polymerization mechanism – initial have been postulated for β-amyloid (Harper and Lansbury, Jr., 1997)(section 1.6.3). The increase of the fluorescence in the ThT kinetics is reflected by the appearance of elongated species and mature fibrils (Figure 5-3B). The duration of this lag phase had been already shown to be dependent on both the concentration of Ure2p and on the temperature (Zhu et al., 2003b). However, even at 4°C, short fibrils are formed within the first hours of the reaction (not shown). Therefore, processes such as concentrating or dialysis of Ure2p samples cannot be carried out without the concomitant formation of fibrillation products, some of which may be too small to be removed by centrifugation.

5.2 Fibrillation pathway of Ure2p

To understand the fibrillation pathway of Ure2p, ThT binding assay (Figure 5-3B) was carried out at different conditions and followed by AFM and TEM.

5.2.1 Time course of fibril formation in an unseeded reaction

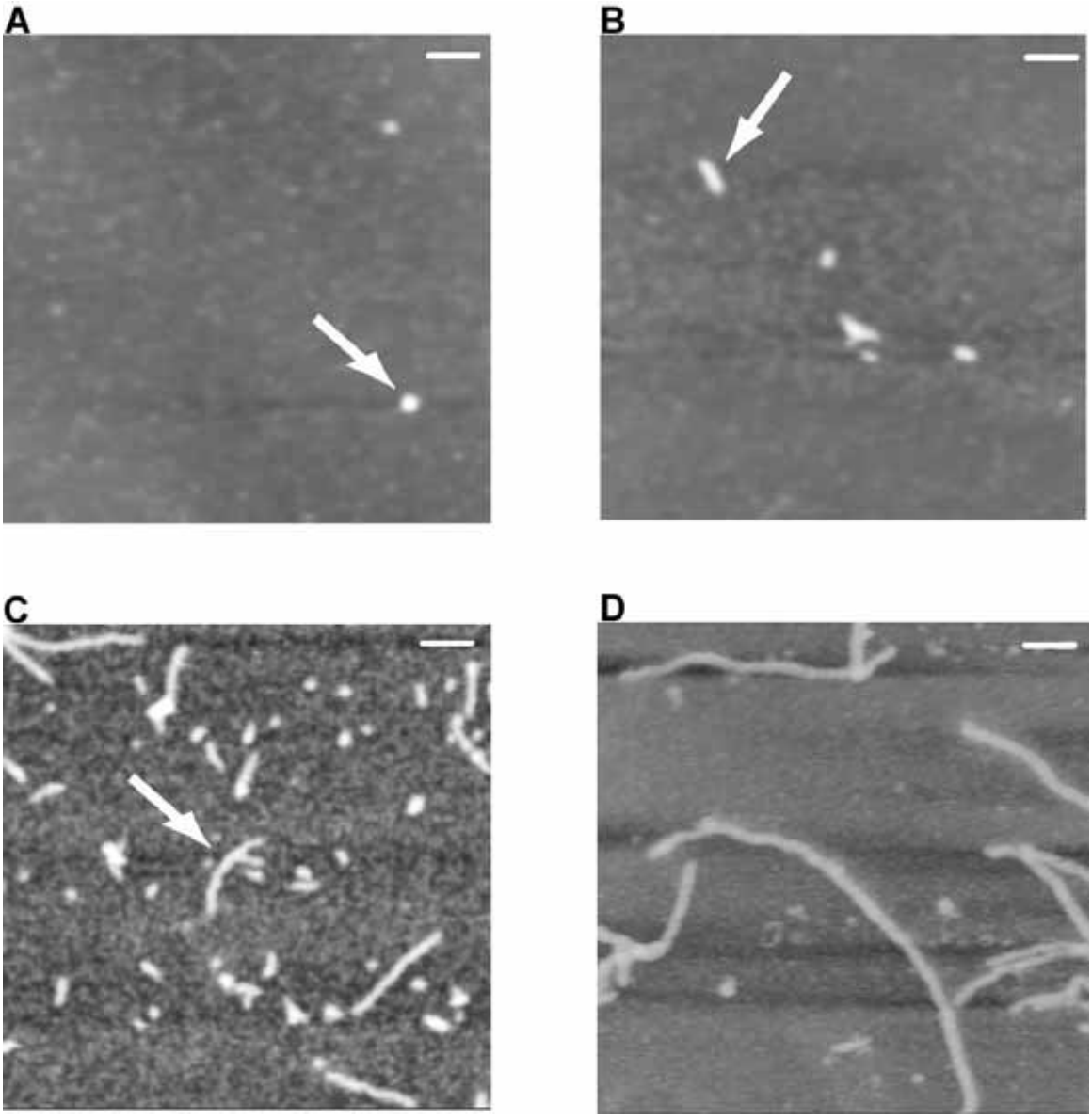

Figure 5-4: Fibril formation in an unseeded reaction.
Fibrils were grown under standard conditions (60 µM Ure2p, 50 mM Tris/HCl pH 7.5, 15°C) without agitation. Samples were taken after 2 h (A), 4 h (B), 8 h (C) and 24 h (D), deposited on mica, and analyzed by height image TM-AFM. The full range of the gray scale corresponds to a height of 30 nm. The scale bars represent 200 nm.

Figure 5-4 shows the fibrillation pathway of Ure2p. In early stages of the fibrillation process, it was possible to visualize distinct small species of globular (arrow, Figure 5-4A) and ellipsoidal shape (arrow, Figure 5-4B) respectively. These species were soluble. Their number increased early in the fibrillation reaction and decreased at later stages. The globular-shaped particles had heights of 3-10 nm, but particles found at later time points of the reaction were

up to 20 nm. Some of these spherical species have a smaller height than others, indicating an increase of height over time (data not shown). The ellipsoidal species had the same height as the globular species, and the cross-sections of both species were very similar to those of the fibrils. The next step in the process of Ure2p aggregation is the appearance of first fibrillar species called *protofibrils* (arrow, Figure 5-4C). Thus, the globular and ellipsoidal species may represent precursors of the protofibril species. With time, the population of longer protofibrils and fibrils increases while the shortest protofibrils decreased in number. Hence, the fibrils are elongating. After ~30 h, the ThT fluorescence of the samples reached a plateau (Figure 5-3B). The presence of fibrils at this time is evident from the AFM images (Figure 5-4D). This shows that fibril growth occurs spontaneously already at low ionic strength. The fibril dimensions ranging from 3.5-4 nm to 12 nm as determined by AFM were smaller than those determined by TEM (Figure 5-1A). While protofibrils were abundant in the middle section of the kinetics (10-20 hours, Figure 5-3B), mature fibrils are the main population at later time points but a small fraction (less then 5%) of relatively long fibrils could be seen even at the early elongation stage (10 h of incubation). Heights and widths of amorphous aggregates (> 100 nm, Figure 5-1B) were larger than those of fibrils and could reach macroscopic sizes (data not shown). These aggregates presumably represent dead-end products in the reaction pathway. The morphologies and the dimensions of fibrils were rather heterogeneous even within the same sample. In the final point measured a substantial quantity of fibrils are short then 1 μm. This may indicate that the process is not finished yet. These results show that the fibrillation of Ure2p is a multistep fibrillation pathway and may indicate the presence of a rate-limiting species on the pathway. Multi-step pathway have been already described for Ure2p (Jiang et al., 2004), Aβ(Harper and Lansbury, Jr., 1997; Harper et al., 1997; Harper et al., 1999) and for Transthyretin as reviewed by Kelly(Kelly, 1998).

5.2.2 Time course of fibril formation in a seeded reaction

Aggregation of PrP (and TSE) are characterized by a seeding effect (Prusiner, 1982), comparable to crystallization (Jarrett and Lansbury, Jr., 1993) (section

1.6.3). The seeding represents the addition of pre-formed fibrils bypassing the rate-limiting step in the fibril formation that is the nucleation (Jarrett and Lansbury, Jr., 1993) (Harper and Lansbury, Jr., 1997). To analyze this effect on Ure2p, seeds were prepared by sonication from already formed mature fibrils according to section 2.8.5. The seeded and non-seeded-reaction were monitored by the ThT assay and TEM.

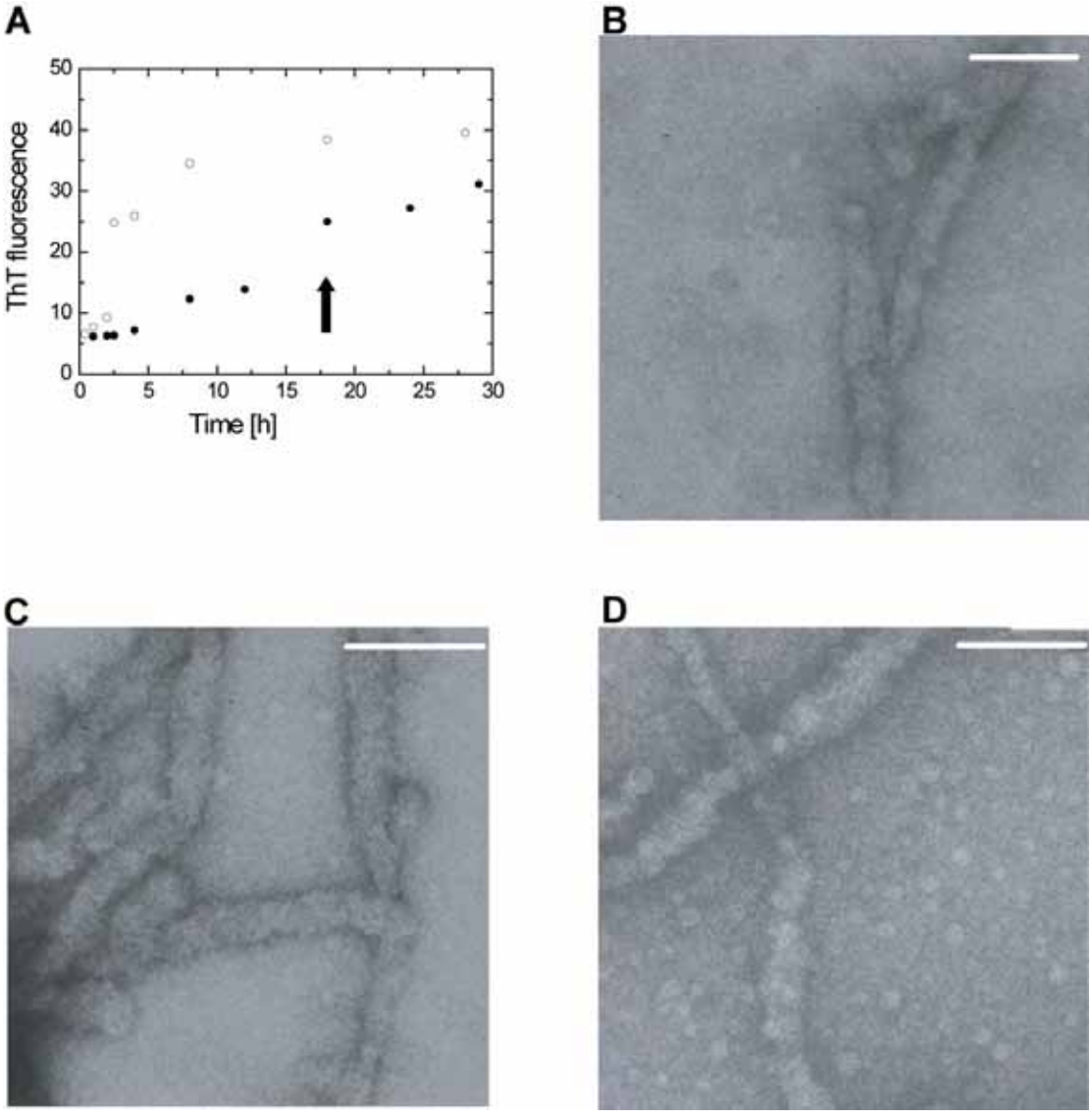

Figure 5-5: Aggregation of Ure2p by seeding.

A) ThT binding assay of a (o) seeded reaction and non-seeded reaction (●) ratio seeds/Ure2p: 1:1000. B) TEM showing the seeds. C) TEM showing fibrils originating from a seeded reaction. D) Non-seeded reaction at same time point of the kinetic. Scale bar: 90 nm. The arrow indicates the time when samples were taken.

Monitoring the polymerization by ThT binding assay (Figure 5-3A and Figure 5-5A) it shows the seeding effect on the kinetics of fibril formation. There is an

increase in the ThT fluorescence abruptly in the seeded sample while the non-seeded sample shows a lag phase. The seeding changes the kinetic form a sigmoidal curve to a first-order kinetic. This means that upon addition of preformed Ure2p fibers to the soluble form of the proteins there is no lag phase anymore. The TEM results shows that adding seeds (Figure 5-5B) to an Ure2p solution, result in a certain homogeneity of the fibril formation (Figure 5-5C) while the non-seeded reaction presents fibrils, protofibrils and some small particles (Figure 5-5D) indicating that the nucleation process is happening. The average width of the fibrils did not change significantly with time (data not shown), suggesting that growth occurs primarily, by addition of the Ure2p to the ends of the seeds. Melki (Fay et al., 2003) has showed this, too. These results suggest that the template mechanism (Griffith, 1967; Lansbury, 1994) (section 1.6.3) could explain part of the process of Ure2p fibrillation.

5.3 The morphological aspects of fibrillated species

Ure2p fibrils present a rich-morphological distribution during self-assembly. To identify these differences, it was analyzed height, length and diameter of fibrils. It was analyzed the three-dimensional structure displayed by TM-AFM and width, measured by TEM. Using the height and the average width along the length of the fibril it is possible to identify polymorphism in different kind of fibrils that would looks equal in SEM and TEM. When measuring the width with AFM, an overestimation of the width of the fibrils has to be considered due to the broadening effect of tip(Wetzel, 1999).

5.3.1 Protofibrils

According to Harper (Harper et al., 1997) “protofibrils are elongated oligomers that give origin to the fibrils”. Teplow (Walsh et al., 1997) uses this definition for precursor of fibrils with less then 200 nm length. The term protofibrils are used in general to define precursors of the fibril, acting like a template for fibril formation. There is not a homogeneous definition on the literature, some authors call protofibrils as “pre-protofilaments” (Deechongkit et al., 2005). The

definition of protofibril used here is based on height and length. Protofibrils here defined are elongated globular species that have already the height of a fibril although they have a short length. The morphology of protofibrils defines the morphology of the mature fibrils. This analysis was done by height image TM-AFM.

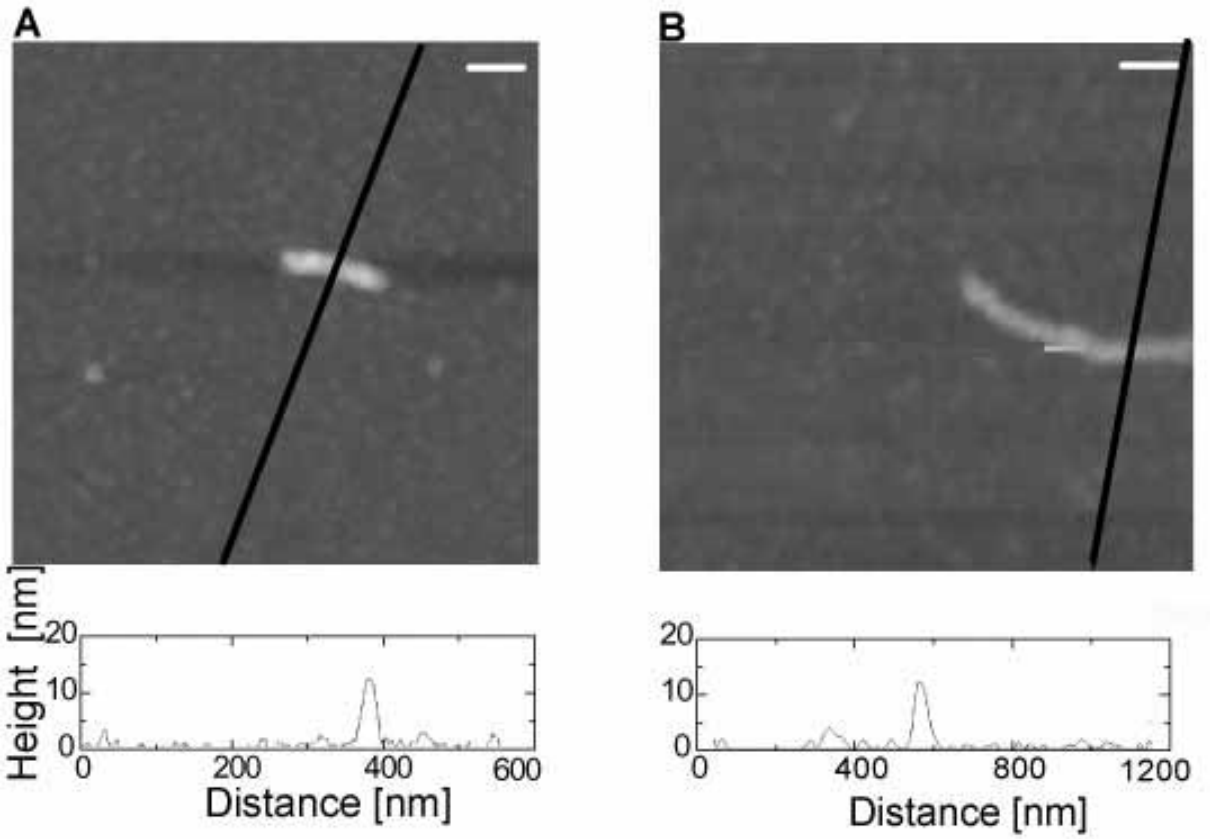

Figure 5-6 : TM-AFM of protofibrils

A) TM-AFM of protofibril. Scale bar: 60 nm. B) Fibril with similar characteristics to the protofibril. Scale bar: 100 nm. The black line represents the cross-section displayed under the figure.

Protofibrils could be seen in different points of the ThT kinetics of medium to high concentrated solutions (Figure 5-4C). Since the individual protofibrils are not indistinguishable from fully assembled fibrils in height, they could be classified as protofibrils due to small lenght (Figure 5-6AB). The morphology can be smooth or rough (not shown). Protofibrils were found to be at least 10 nm long, but could grow up to several µm becoming a mature fibril (Figure 5-6B). Protofibrils are compact like the mature fibrils and resemble templates

that can generate a mature fibril, having the same height as the bigger rounded species seen in early stages of fibrillation. The height of the protofibrils could be due to the several oligomers associated laterally or just formed with this dimension. It is possible that the protofibrils define the different self-assembly ways and morphology, acting like a template (section 1.6.3).

5.3.2 Protofilaments

The term protofilaments has a broaden use in papers from theoretical biophysics to structural and biological areas (Deechongkit et al., 2005; Jimenez et al., 2002; Chiti et al., 1999; Serpell et al., 2000). Protofilaments are between the protofibril and mature fibril and are the result of the polymerization of the protein and the building block for fibril formation (Blake et al., 1996). It is the most elementary fibrillar feature on the composition of mature fibrils. TM-AFM was used to identify the thickness of the Ure2p protofilaments using height image.

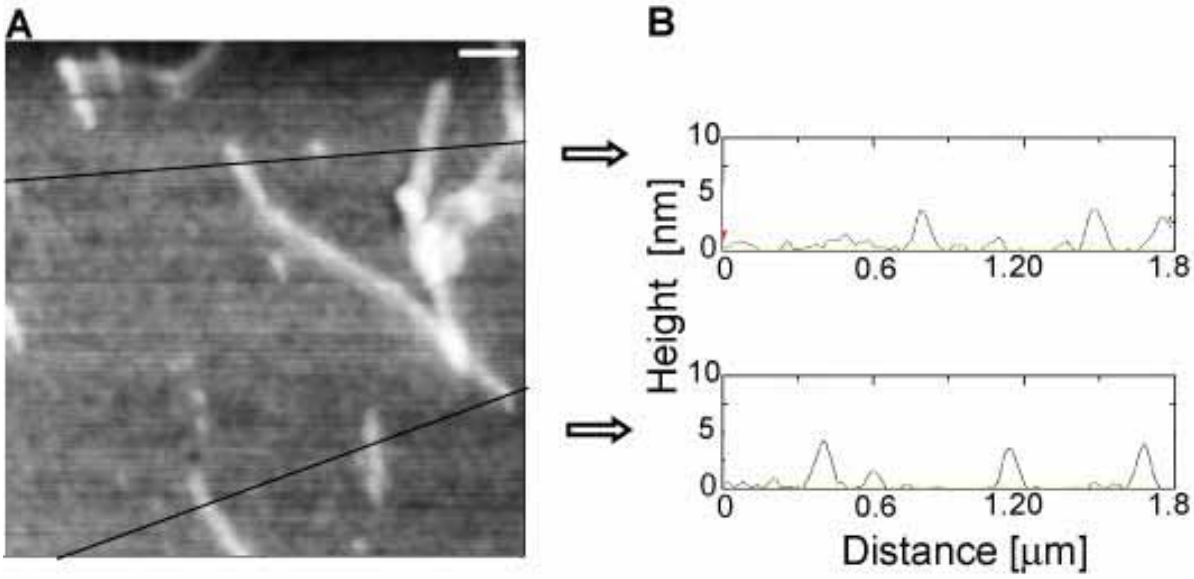

Figure 5-7: TM-AFM of Ure2p protofilaments.
A) Height image, the full range of the gray scale corresponds to a height of 20 nm. The scale bar is 200 nm. B) Cross-section of the image representing the black line. 10 µM Ure2p, 50 mM Tris/HCl pH 7.5, 15°C, without agitation

Figure 5-7 shows the image of Ure2p protofilaments. In this thesis, protofilaments are straight, single filaments in which no sub-filaments could be resolved by either AFM or TEM. The height of several protofilaments measured

ranged from 3.5 to 5 nm. Some sections of the filament above were observed with a periodicity of 60 nm. The appearance of isolated protofilaments depends of the concentration of Ure2p. Filaments were seen in very low concentrated solutions (section 5.1) and were absent in high concentrated solutions. The measurement of lateral dimensions of filaments can be performed by AFM although it should keep in mind that AFM tip can contribute to an overestimation of lateral feature size(Wetzel, 1999). Filaments above showed a 66 nm width. Errors can be included due to the dimension of the image that is in μm.

5.3.3 Mature fibrils

The mature fibrils are long, flexible and can display a number of different morphological types, sometimes in the same fibril. To analyze the morphology of the fibrils, it was used TM-AFM.

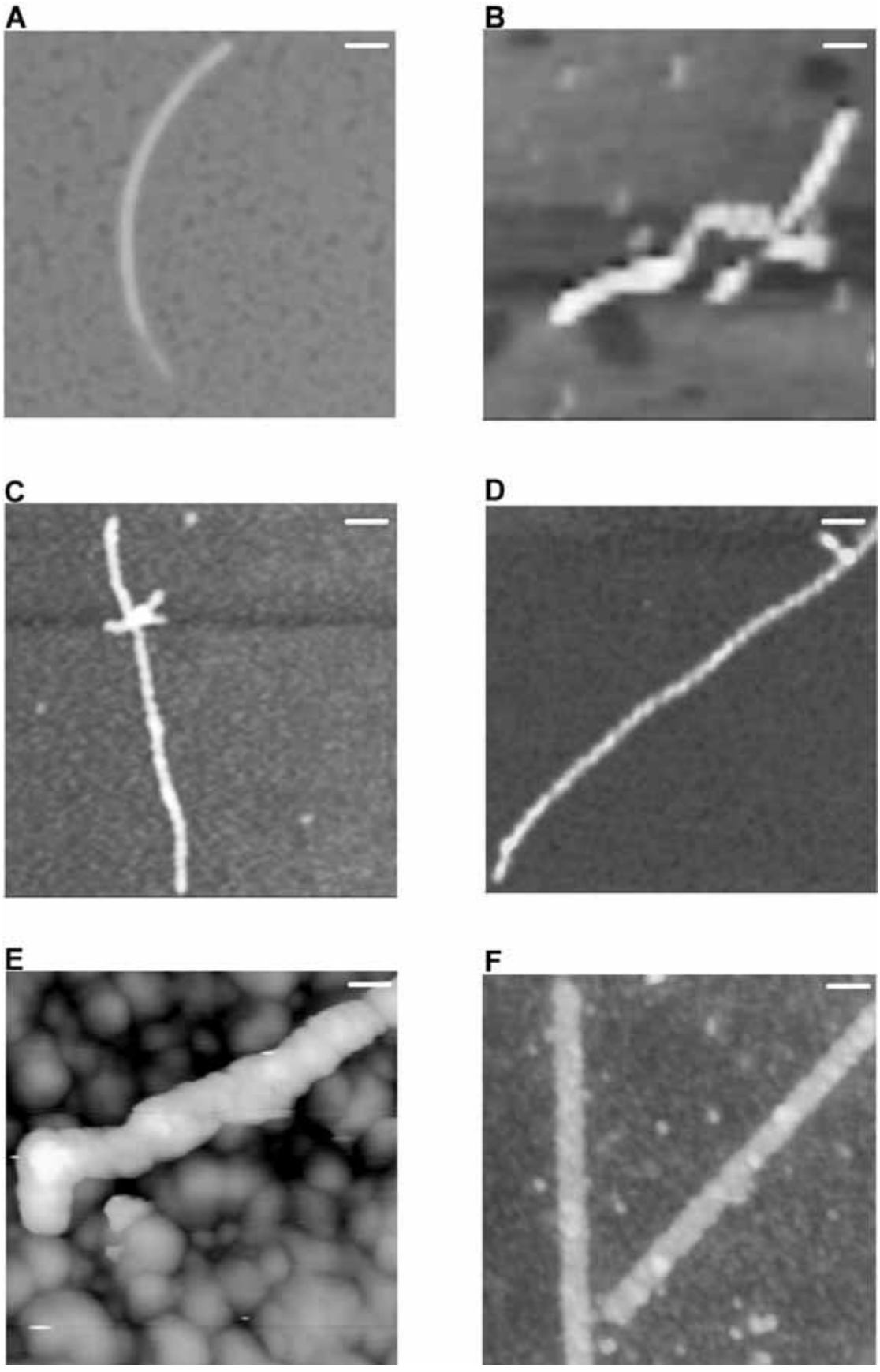

Figure 5-8: TM-AFM showing morphology of Ure2p fibrils at different conditions

A) Smooth fibrils B) A protofilament like a ribbon but twisting around itself C) Nodular fibril possibly resulting from the aggregation of small globular species D) The

protofilaments are twisted around each other like a left hand helices and was obtained with addition of 200 mM NaCl. E) Detail of a fibril morphology showing a rough surface in the fibril and a right hand twisting at same time. F) Microfiber from Ure2p showing more then 10 μm length and around 0.5 μm width. It was produced by freezing already existent fibrils in solution. Scale bar: C, D, F: 200 nm: A, B: 100 nm and E: 30 nm.

Different types of fibril occur upon Ure2p self-assembly. A cylinder form (Figure 5-8A) and twisted-ribbon morphology (Figure 5-8B) could be seen in samples. The later one is named by same authors as a super coiling morphology (Jimenez et al., 2002). Figure 5-6C shows a nodular fibril apparently composed of globular species, resembling linear associations of oligomers from different sizes as their diameter varied strongly along the fibril axis. This may indicate that globular species can associate to form fibrils, too. Figure 5-6D shows twisting fibrils. This can be due to two filaments twisting around each other with a width that varies between 6 and 10 nm and rarely some fibrils around 20 nm could be seen. Figure 5-6E shows a topographical image of an Ure2p fibril, where it is possible to visualize some segments. Figure 5-6F shows a microfibril produced by freezing fibrillated solution of Ure2p. It was identified difference of diameter, despite the same height, on the fibril self-assembled samples (data not shown). The differences in morphology possible are related to differences in the molecular structure of the involved protofilaments, as shown recently for $A\beta_{1-40}$(Petkova et al., 2005). This result shows that higher-order fibrillar assemblies are then, formed either by elongation of nuclei, or by the association of preformed protofilaments or a combination of both. The height image shown for Ure2p has been described by other amyloid fibrils like Aβ and α-synuclein (Rochet and Lansbury, Jr., 2000) and morphologies has already been described to Aβ(Blackley et al., 1999) using AFM. This results show that fibril formation by Ure2p is polymorphic.

5.3.4 Hierarchical formation of mature fibrils

Hierarchical formation of fibrils has been shown in a serie of human diseases(Goldsbury et al., 1997; Ross et al., 1998; Blake et al., 1996; Serpell et al., 2000). To analyze this process in Ure2p fibrils, it was used TM-AFM.

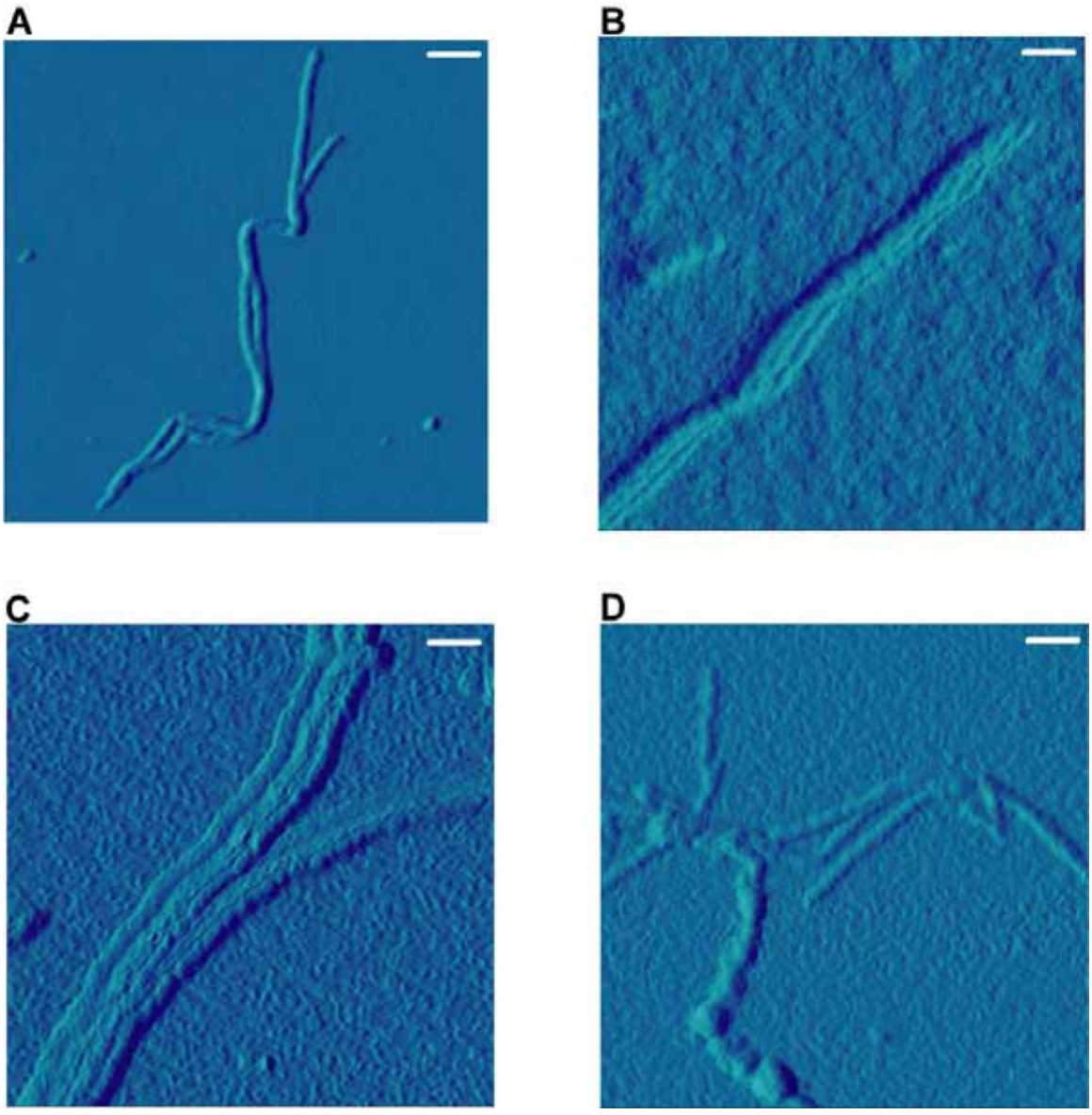

Figure 5-9: Hierarchical assembly of Ure2p fibrils

A) Individual protofilaments are twisted and then twisted again with each other forming a mature fibril. Every protofilament has a minimal measurement of 5 nm height. B) Individual protofilaments are interacting by parallel arrangement. C) Different composition of several protofilaments and fibrils forming a hierarchical structure resembling a hollow tube. D) Two mature fibrils with different kind of morphology assembled to each other. Scale bar: A, D: 200 nm and B and C: 100 nm.

Figure 5-9 shows the hierarchical formation of structures on the assembly pathway of Ure2p. Figure 5-9A shows two protofibrils of 5 nm height that twist around itself and around each other, thus generating an 8 nm fibril. The height of the fibril is less then the sum of the heights of the two adjacent protofibrils, indicating that it is not an artifact caused by superposition of two fibrils (Ionescu-Zanetti et al., 1999). Figure 5-9B shows a fibril formed from different protofilaments that are associated laterally with a small twist around the fibril.

Probably, this was generated during deposition on the mica. Analyzing the cross-section, there are some discrete steps of 4 nm. Presumably, are formed by lateral association of several protofilaments. In other cases, we observed a sudden drop in height to ~60% of the initial value when moving along the long fibril axis (data not shown). Both sections had a considerable length, ruling out that two protofibrils simply cross each other. The lateral association of protofibrils with differing length best explains this type of fibril. Figure 5-9C shows five protofilament forming a fiber and then separating in two types of fibrils, one with three filaments and another with 2 filaments. Figure 5-9D shows a composition of two mature fibrils with different kind of morphology assembled to each other forming tangles (net of fibrils). This happens after several days of fibrillation and could be seen in all samples analyzed (after long time of reaction). Under all conditions tested, this assembly behavior could be seen and suggests that fibril formation is a hierarchical process, in which Ure2p first polymerizes into protofibrils, which can later associate to mature fibrils. This would explain why the heights of most mature fibrils are multiples of 3.5-5 nm. The smallest fibril had width of ~3.5 nm. The Ure2p mature fibrils can exist as an assembly of different numbers of protofilaments in several manners. These fibrils either form by the lateral association of two, three, four or more elementary protofilaments. Other polymorphic variations are fibrils that twist around itself forming a higher order structure. The number of elementary protofilaments making up the major fibrillar species was different according to the growth conditions (will be discussed at section 5.3).

5.4 Solubility of fibrillated species

5.4.1 Stability of mature fibrils

To analyse the stability of mature fibrils we use left fibrils to drying, overnight under SDS and analyse by AFM and TEM.

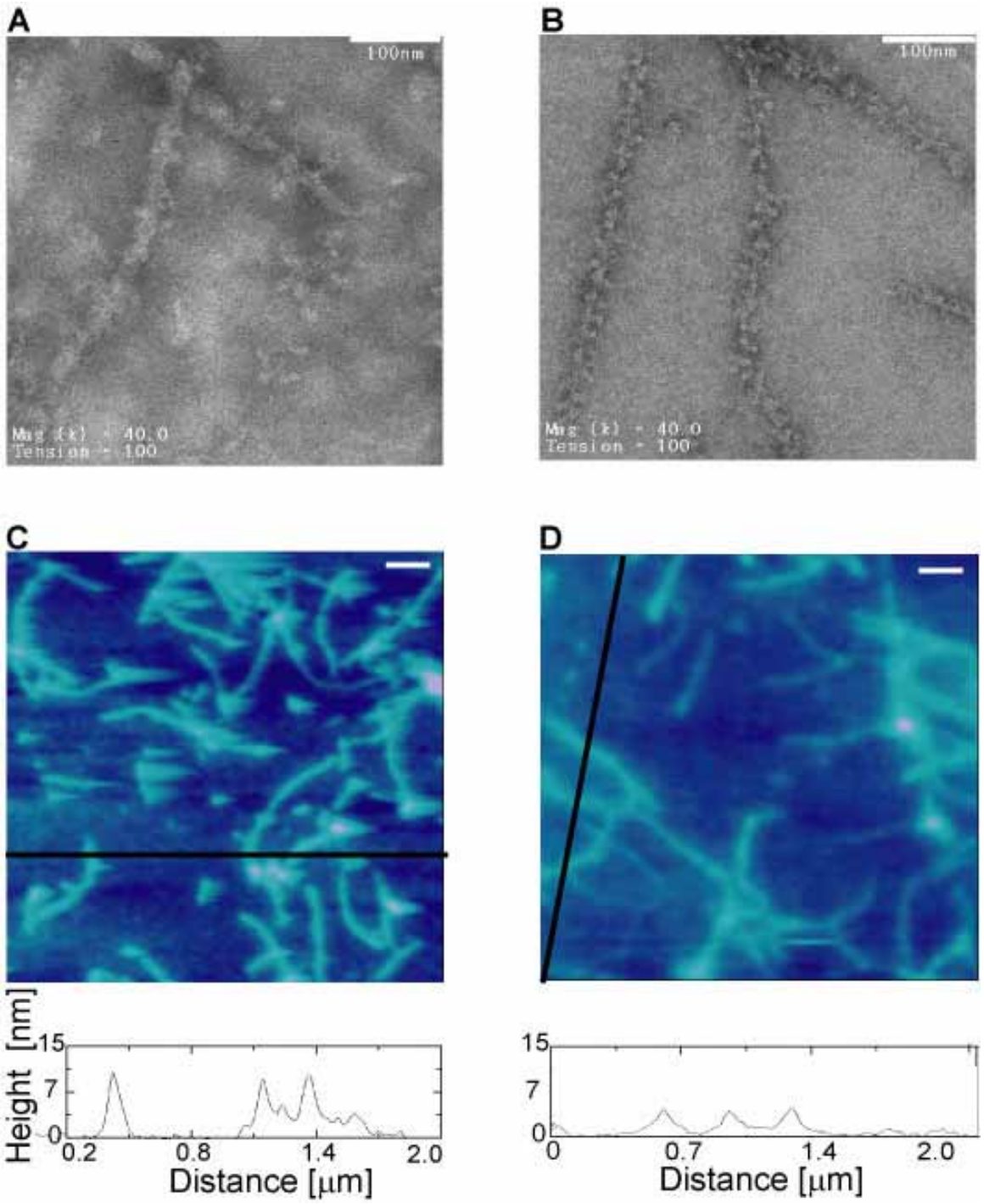

Figure 5-10: Stability of Ure2p fibrils in SDS and after drying

Ure2p fibrils were formed under standard conditions. Negative stained TEM of: (A) Ure2p fibrils in fibrillating solution (native conditions). (B) Ure2p fibril after overnight incubation in 1% SDS. TEM Scale bar: 100 nm. TM-AFM height image from Ure2p fibrils (C) in fibrillating solution deposited in mica and (D) dried in a dessecator for 2 days. AFM Scale bar: 200 nm.

Figure 5-10A shows a TEM of Ure2p fibril under native conditions and overnight under SDS solution (Figure 5-10B). This figure shows that Ure2p fibrils present a stable core under SDS with some globular species hanging out

of the core. Diameter measurements done by TEM, shows that the core presents a average of 4 nm width and when measured together with the globular part, display around 10 nm. This globular part likely represents the C-terminal domain that may not be involved in the fibrilization. Figure 5-10CD shows AFM of fibrils before and after drying. Again, the fibril differed from that observed under native conditions.There is a decrease in the height average of the fibrils after drying. These results show that fibrillar core of Ure2p has a remarkable stability against SDS and drying but the C-terminal may unfold.

5.4.2 Analysis of soluble and insoluble species during fibrillation process

Ure2p was defrosted and incubated at 15°C to initiate fibrillation. Solution was centrifugated (section 2.8.3) at every value on the time axis to separate between soluble and insoluble species (Figure 5-11A).

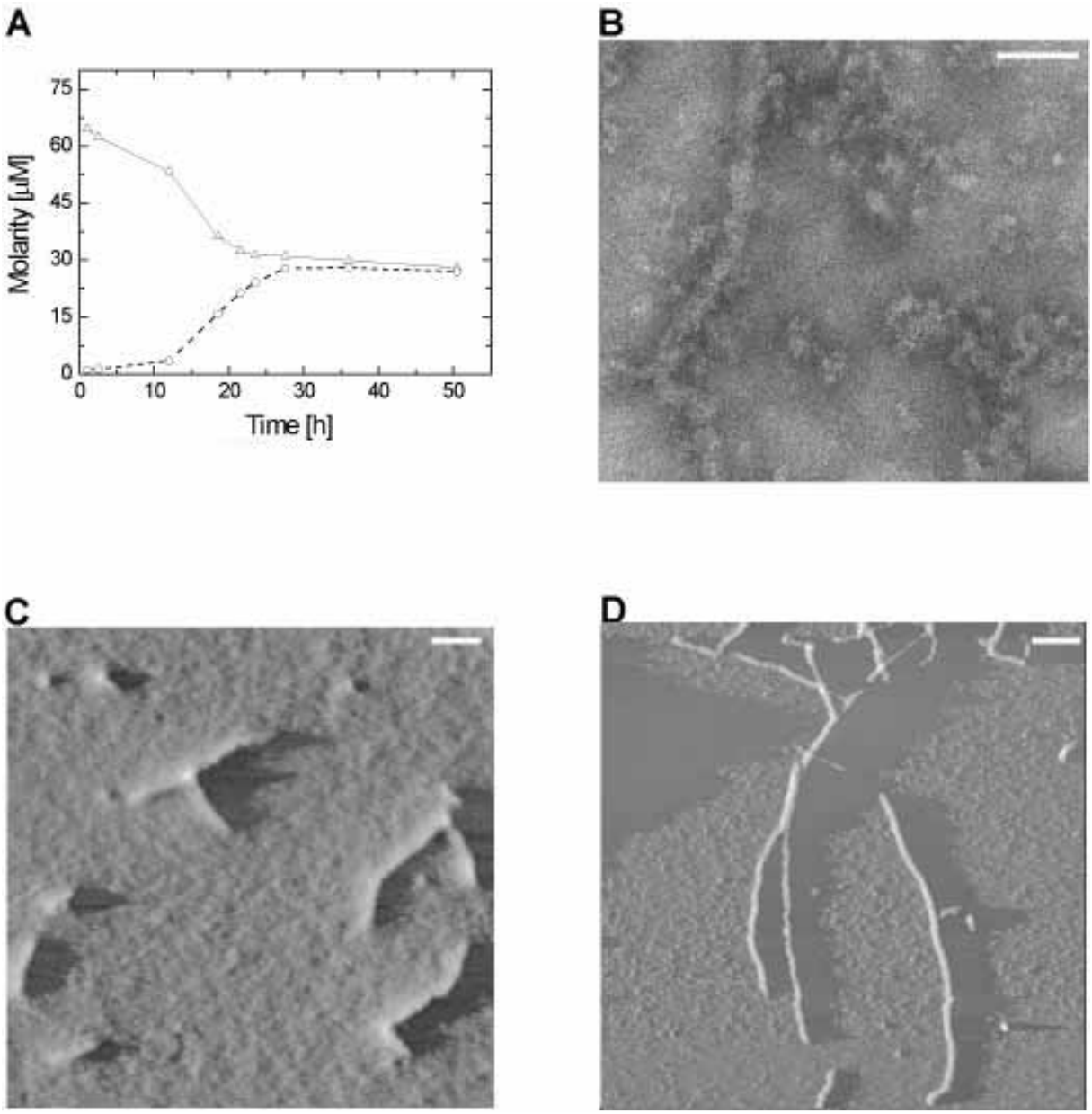

Figure 5-11: Sedimentation profile during self-association of Ure2p.
Sedimentation analysis of fibrillating Ure2p showing the decrease of the Ure2p concentration in the supernatant (Δ) and its increase in the pellet (○) during fibril formation; analysis by absorbance measurements. B) Negative stained TEM of fibrillating solution before sedimentation (16 hours). C) AFM from supernatant after sedimentation and D) AFM of resolubilized pellet. The experiment was carried at 15 C, 50mM Tris pH 7.5. TEM scale bar: 100 nm; AFM scale bar : 200 nm.

There is no difference in tertiary structure (fluorescence) between soluble and insoluble species (data not shown) as showed by dimer and fibrils (Figure 5-13A).The fibrillation solution before centrifugation was controlled by TEM (Figure 5-11B) and the supernatant (Figure 5-11C) and pellet (Figure 5-11D) was analyzed by AFM. Figure 5-11B shows the TEM image of a sample (t = 16 h) consisting of both fibrils and globular oligomeric species. Figure 5-11C

shows different species present in the supernatant like monomers, dimer, bigger oligomers and protofibrils. In the insoluble part there are mature fibrils and possible aggregates (Figure 5-11D). Analyzing Figure 5-11A, it is possible to see that the concentration of the solution does not change much upon centrifugation in the first 10 hours. Only little pelletable material was observed during this time. Subsequently, the amount of pellet increased until it reached a plateau after 30 h. This behavior is in good agreement with the results of the ThT binding assay. At the apparent end point of fibril formation, ~50% of Ure2p was still soluble. This fraction consisted of the globular/ellipsoidal species, protofibrils and dimeric Ure2p. As showed in Figure 5-11C, the protofibrils present in the solution are approximately 7 nm height and 100-400 nm in length.

5.4.3 Stability of soluble and insoluble species

Most amyloids were found to display an increased stability, e.g. against denaturants, when compared to the native protein. Under 5 M GdmCl, dimeric Ure2p dissociates into unfolded monomers (Zhu et al., 2003a). In order to characterize the stability of the Ure2p fibrils in GdmCl, Ure2p fibrillation was done at 15°C and the pellet fraction of the sedimentation assay (Figure 5-11A) was incubated in 5 M GdmCl overnight.

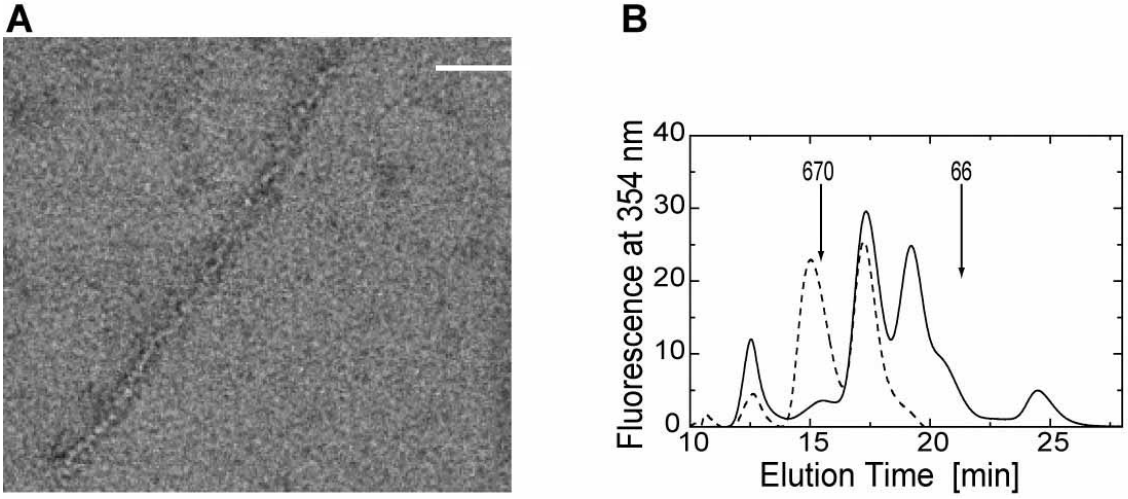

Figure 5-12: Identification of GdmCl-resistant Ure2p species

Ure2p fibrils were formed under standard conditions. (A) TEM of Ure2p fibrils after overnight incubation in 5 M GdmCl. (B) Fibrillated Ure2p was separated into soluble fraction and pellet by low-speed centrifugation. After incubation in 5 M GdmCl for 8

hours, the soluble (—) and insoluble (---) fraction was analyzed for the presence of GdmCl-resistant oligomers by size-exclusion chromatography (column: TosoHaas TSKG3000SW). The buffer was 50 mM Na_2HPO_4/NaH_2PO_4, 150 mM NaCl, 5 M GdmCl, pH 7.5, with a flow rate 0.4 ml/min. The arrows indicate the elution times of unfolded thyroglobulin (670 kDa) and BSA (66 kDa).Scale bar: 100 nm.

After 8 h in 5 M GdmCl, we could still observe fibrils in these samples by TEM (Figure 5-12A). This shows that fibrillar Ure2p has a remarkable stability against denaturation. However, the fibril morphology differed from that observed under native conditions (as seen in figure Figure 5-10). This is likely due to the GdmCl-induced unfolding of the C-terminal domain, whose stability is not increased by fibril formation (Figure 5-13). In a next step, was investigated whether GdmCl-resistant intermediates, i.e. potential precursors of protofibrils, could be observed early during fibrillation. To this end, supernatant and pellet (Figure 5-11) of a fibrillated sample were incubated for 8 h in 5 M GdmCl. Samples were subsequently analyzed on a size-exclusion chromatography (SEC) column equilibrated with buffer containing 5 M GdmCl (Figure 5-12B). The column was chosen such that a size range of 50-1000 kDa could be resolved. The appearance of distinct peaks suggests that the samples do not consist of molecules with an arbitrary number of Ure2p units but rather of a set of discrete oligomers. As expected, the distribution of species in the supernatant is centered at a lower molecular weight compared to the pellet fraction. The peaks in the two samples are coinciding, indicating that they contain the same set of species albeit in different relative populations.

5.5 Characterization of insoluble species

5.5.1 Spectroscopic analysis of Ure2p fibrils

To analyze the structural changes of Ure2p as consequence of fibril formation it was employed fluorescence spectroscopy (section 2.5.3). According with figure 3.1, all Tyr and Trp are in the C-terminal domain and the first position of the Trp is 179. Due to this localization, fluorescence is a specific structural probe for the C-terminal domain of Ure2p (as showed in section 3.6). The CD signal shows changes of the full length of Ure2p as already shown in figure 3.5 and

3.8. Using CD spectroscopy, the secondary structure of centrifuged Ure2p fibrils was analyzed in relation to the dimeric state.

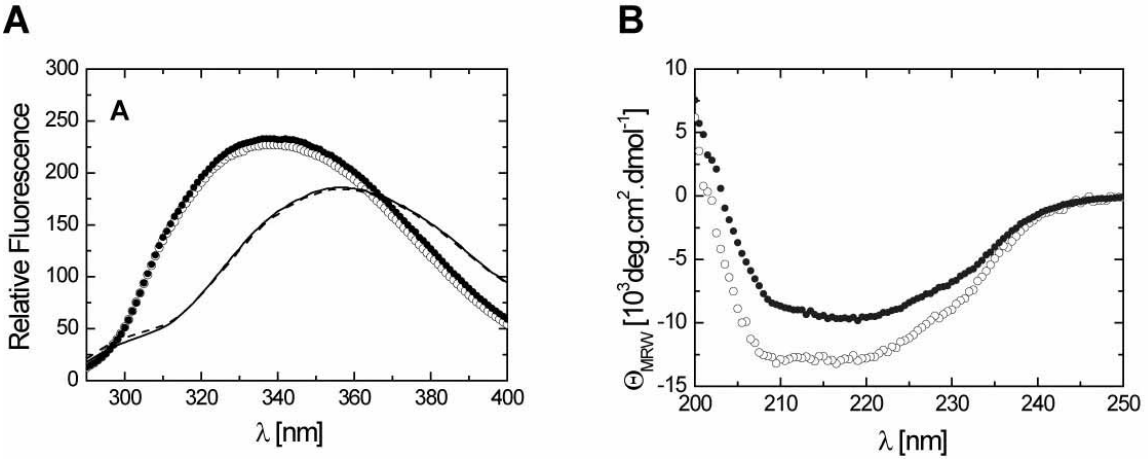

Figure 5-13 : Structure characterization of mature fibrils.
A) Intrinsic fluorescence of dimeric Ure2p in 0 M (○) and 5 M GdmCl (---), and of Ure2p fibrils in 0 M (●) and 5 M GdmCl (—). The protein concentration was 5 µM. Buffer: 50 mM Tris pH 7.5 0.2 M NaCl. B) far-UV circular dichroism spectra of dimeric Ure2p (○) and fibrillar Ure2p (●).Spectra were corrected for contributions from the buffer. Buffer: NaP/Tris 0.2 M NaCl pH 7.5 with 5 mM Tris pH 7.5

Under all conditions studied, the fluorescence spectra of fibrillated and dimeric Ure2p were found to be virtually identical (Figure 5-13A). Consequently, we were unable to detect any changes in the intrinsic fluorescence of Ure2p during the time course of fibrillation. This indicates that the C-terminal domain, which contains all of the 6 Trp and 11 Tyr residues present in Ure2p, has a similar structure in all species that are significantly populated during the fibrillation process. In particular, its structure within the fibrils should be similar to the structure it adopts in dimeric Ure2p. Furthermore, we could not detect any difference in intrinsic fluorescence between denatured dimers and denatured fibrils above 5 M GdmCl. The spectra do not show any difference due to quenching of the Trp by any neighbor amino acid in the dimeric and in the fibrillar structure. This would means that the structure after Trp 179 is not changed. Analyzing the Figure 5-13B and as showed in the figure 3.5, the dimeric protein shown a α-helical content. In the spectrum of fibrillar Ure2p, the overall intensity was reduced and the minimum at 208 nm was less distinct. Importantly, the zero-crossing was shifted from 202 nm to 203.5 nm upon fibril formation, and the signal intensity below 203 nm increased. Both observations rule out that the decreased intensity of the fibril spectrum between 205 and 230

nm is due to an erroneously lower protein concentration. Deconvolution of the CD spectra indicates that upon fibril formation, the β-sheet content in Ure2p increases by 25-30 residues. Analyzing the crystal structure of the C-terminal domain of Ure2p (Thual et al., 2001; Umland et al., 2001), it is difficult to imagine that the visualized structural change of this magnitude could occur in the C-terminal domain without an accompanying change in fluorescence. Therefore, the differences in the CD spectra are presumably caused by a change in the secondary structure of the N-terminal domain. Our results indicates that only a small number of amino acids change from helices to β-sheet, similar to what has been suggested for Sup35 (Balbirnie et al., 2001) and PrP(Gasset et al., 1992).

5.6 Characterization of early species in the fibril formation process

5.6.1 Early soluble species in the Ure2p fibrillation pathway

To analyze the globular species, high concentrated solutions of Ure2p (112μM) were left to fibrillate. The separation between soluble and insoluble species was done by centrifugation.

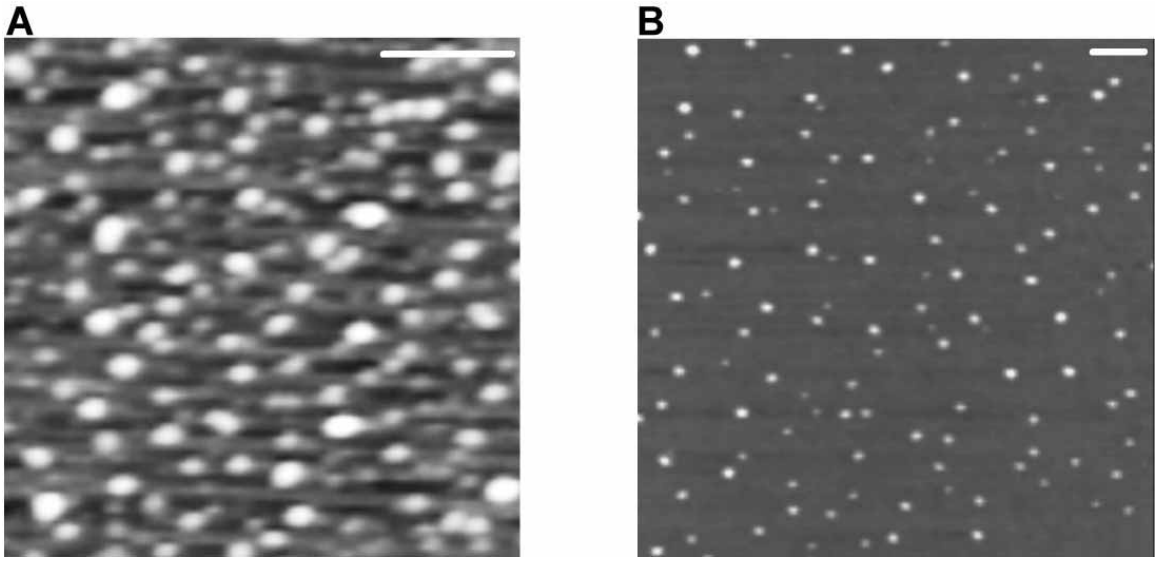

Figure 5-14: Globular species seen at early fibrillation time.

AFM height image after 4 hours of fibrillation deposited on: A) mica B) sapphire; scale bar: 200 nm, 50 mM Tris, pH 7.5, 15 ˚C.

Figure 5-14 shows the AFM from the globular species seen during the fibrillation pathway of Ure2p. On these images, it is possible to observe distinct small globular species that differed in radius. Figure 5-14 shows small and bigger oligomer on the Ure2p fibrillation pathway deposited on mica (A) and sapphire (B). These early oligomers and globular species are attached to subtract by charged (mica) and hydrophobic interactions (sapphire). These images indicate those charged and hydrophobic amino acids are part of the surface from the globular species. These images indicate, too, that the presence of multiple species and heterogeneity in the molecular mass during early fibrillation time and that aggregation happens with maintenance of the solubility. Mature fibrils bind to hydrophobic and hydrophilic substracts (data not shown), indicating the polar,charged and non-polar aminoacids are part of the Ure2p fibril surface in similar manner. To distinguish between the different species and analyze them, a series of microscopic and spectroscopic techniques were applied.

5.6.2 Molecular masses of early species

To dissect the pathway of Ure2p fibrillation, the different globular species found during the kinetics of fibril formation were analyzed by AFM by Perret (Jiang et al., 2004).According with this publication, the monomer would have 1.3 nm and the dimer would have 2.5 nm of height. In our approach, we used two dimensions, height and width, rather than just height to determine the size of the protein particles (section 2.8.4).

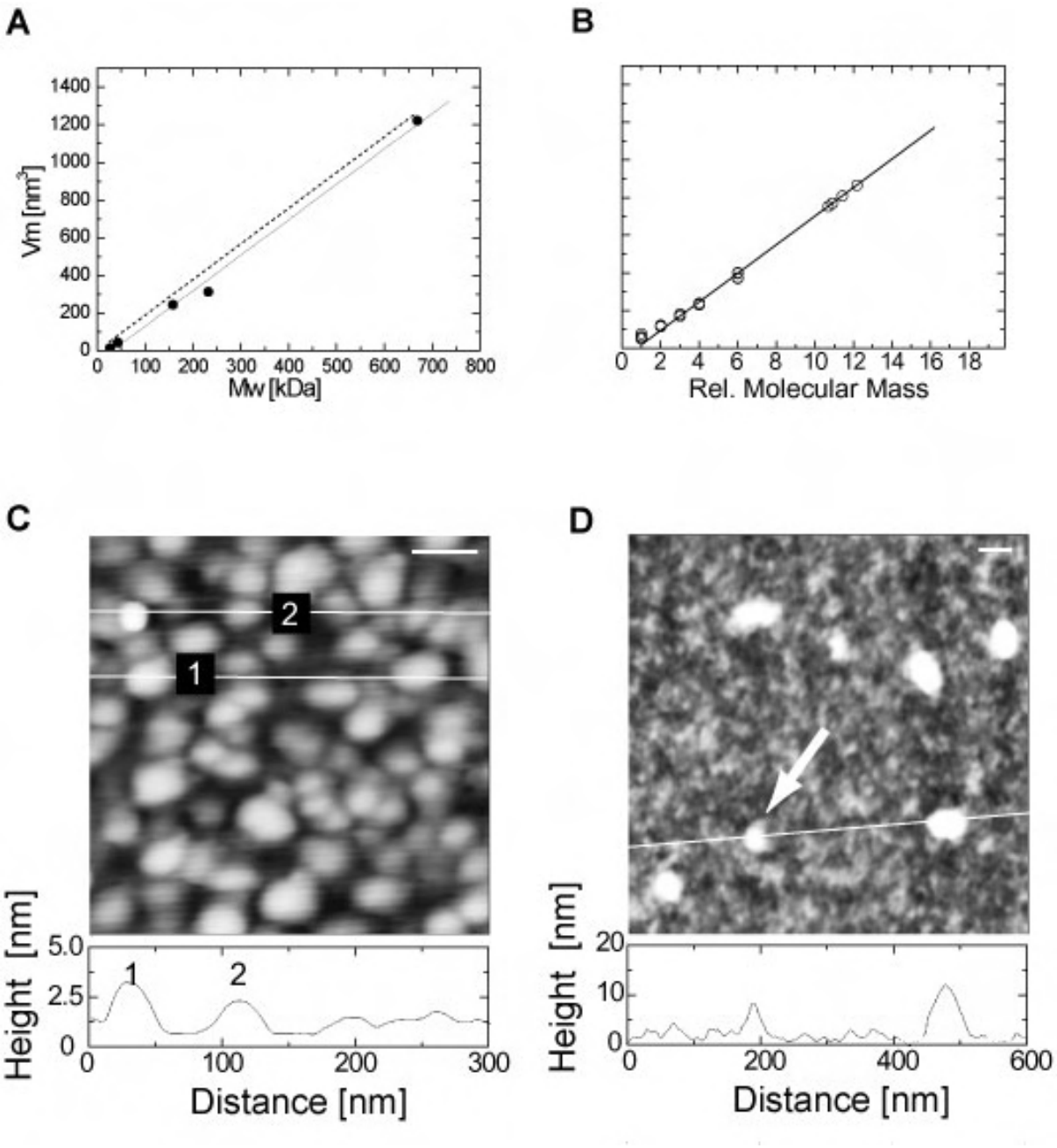

Figure 5-15: Size determination of small Ure2p species observed early during fibrillation.

A) Correlation between theoretical (---) and experimental molecular volume (●), as determined by TM-AFM in air for a set of standard proteins. The latter values were used to obtain a calibration curve (—). B) Experimental molecular volume of Ure2p in different oligomeric states. The line represents the calibration curve shown in panel (A). The molecular mass of the particles is normalized with respect to the molecular mass of the Ure2p monomer. C) AFM image of small oligomeric Ure2p species found in samples taken from the early lag phase of fibrillation. The white lines correspond to the (simplified) section analyses displayed on the bottom of the panel. According to their dimensions, species 1 is a hexamer, whereas species 2 is a tetramer. D) Globular particles of the late lag phase. The left particle (arrow) shown in the section analysis presumably is a 12mer. The globular particle on the right is too large for quantitative analysis. The full range of the gray scale in (C, D) corresponds to a height of 30 nm and the white scale bar is 30 nm.

First, a calibration curve was established using proteins of known molecular mass, in agreement with previous studies (Schneider et al., 1998; Valle et al., 2002). The molecular volume V_m of the reference proteins, as measured by AFM, correlated nicely with the molecular volumes V_c calculated from the molecular mass (Figure 5-15A). Next, it was determined the volumes of the Ure2p monomer and dimer by analyzing samples prepared from a series of dilutions. At a concentration of 0.1 μM, where Ure2p was shown to be predominantly monomeric, most particles had a height *h* of 1.3±0.3 nm and a radius *r* of 8.5±1.5 nm. This is in agreement with measurements by Perret and co-workers (Jiang et al., 2004). At 5 μM Ure2p, it was found that most molecules had dimensions between $h \approx 1.3$ nm, $r = 15$ nm and $h \approx 2.3$ nm, $r = 10$ nm (Figure 5-15B). According to the calibration curve, all these dimensions correspond to a molecular mass of 93 kDa, suggesting that these molecules represent different orientations of the Ure2p dimer on the mica. We also detected low molecular weight oligomers such as trimers, tetramers and hexamers. When samples from the lag phase of the ThT kinetics (Figure 5-3B) were analyzed by AFM, both tetrameric and hexameric species were present at very early time points. Based on our calibration, the dimensions of the hexamer are $h = 3.3\pm0.3$ nm, $r = 18\pm4$ nm (Figure 5-15C). In contrast, the globular/ellipsoidal species of the late lag phase (Figure 5-3B and Figure 5-14) are considerably larger and thus do not represent tetramers or hexamers. Figure 5-15D shows a molecule which corresponds to a 12mer ($h = 4.5$-5 nm). The globular particle to the right has a height of 11 nm, and is too large for analysis because the calibration curve is not reliable above 700 kDa.

5.6.3 Characterization of oligomeric species

To characterize these oligomeric species in detail, we subjected fibrillating samples of Ure2p to size-exclusion chromatography under native conditions. Prior to separation, longer fibrils, amorphous aggregates, and Ure2p dimers had been removed from the sample by filtration.

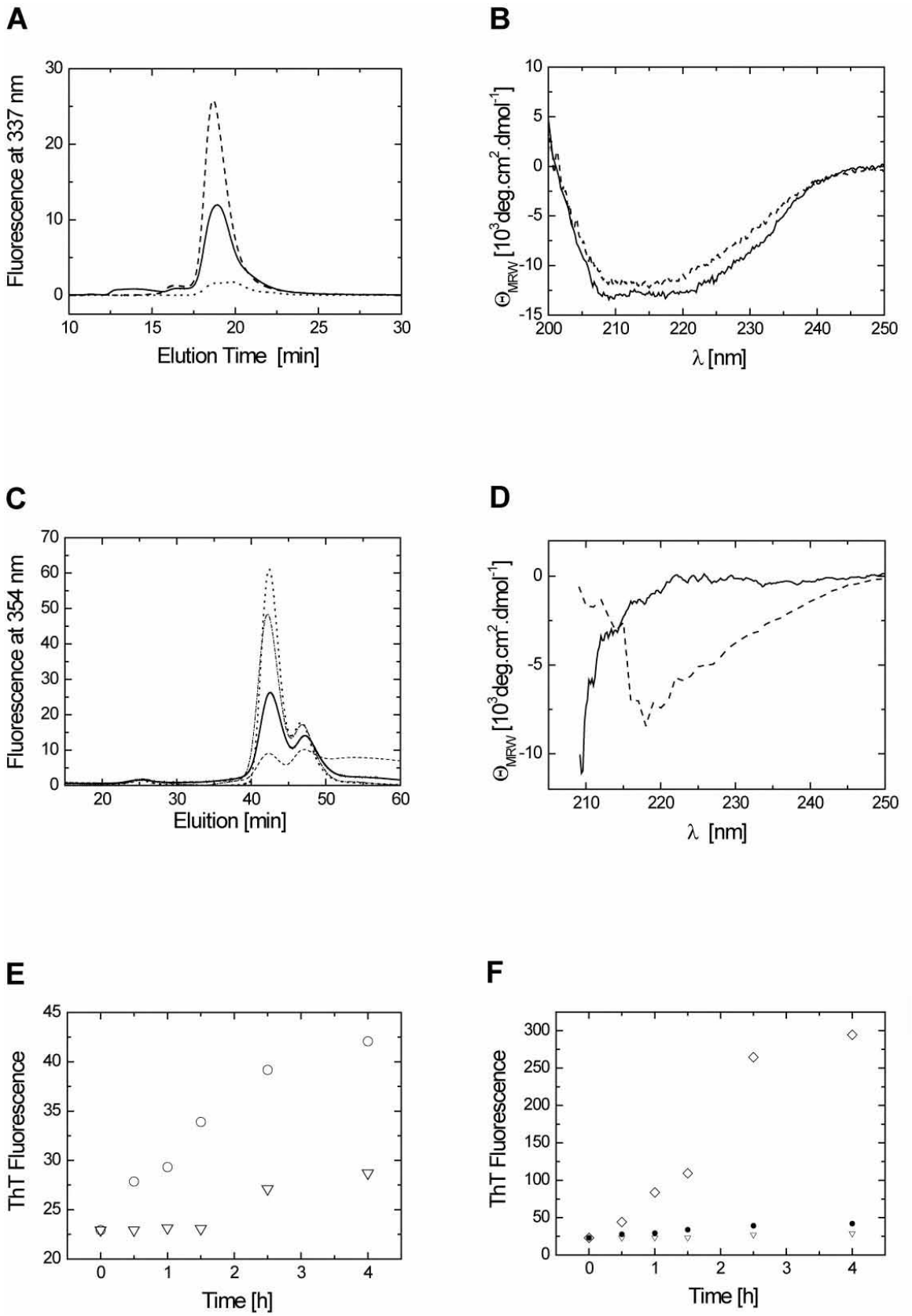

Figure 5-16: Characterization of small soluble Ure2p oligomers.

Aliquots were withdrawn from a fibrillation reaction under standard conditions. Large particles were eliminated by centrifugation, and the soluble species were depleted of dimeric Ure2p by filtration. A) SEC-HPLC analysis of aliquots taken after 3, (---) 24 (—) and 48 h (····) on a TosoHaas TSKG3000SW column. B) The peak eluting at ~18 min

was collected and characterized by far-UV CD spectroscopy (---) in 50 mM Na_2HPO_4/NaH_2PO_4 pH 7.5, 150 mM NaCl. For comparison, a spectrum of native dimeric Ure2p is included (—). C) Aliquots of a fibrillating sample of Ure2p were taken after 4 (---), 8 (—), 12 (····), 16 h (·-·) of fibrillation and separated by SEC-HPLC (Superose 6 HR 10/30) under denaturing conditions using 50 mM Na_2HPO_4/NaH_2PO_4, 150 mM NaCl, 5 M GdmCl, pH 7.5 as the mobile phase. The arrows indicate the elution times of unfolded thyroglobulin (670 kDa) and BSA (66 kDa) D) The peak eluting at 42 min was collected and characterized by far-UV CD spectroscopy (---). For comparison, a spectrum of dimeric Ure2p in the same buffer is included (—). E) Small oligomeric species can seed the fibrillation of Ure2p. Dimeric Ure2p (30 μM) was incubated in 50 mM Tris/HCl, 150 mM NaCl, pH 7.5, at 15°C. To one sample, ~0.3 μM Ure2p from the 150 kDa fraction of the SEC analysis shown in (A) was added (○), while a second reaction was carried out without addition of seeds (▽). Fibril formation in both samples was monitored by the change in ThT fluorescence. Data were corrected for the background signal from the seeds. F) The same as E, but compared with seeding using fibrils (◊).

The elution profiles of samples fibrillated for 3-48 h are shown in Figure 5-16A. The dominating species elutes at a molecular mass of ~150 kDa according to our calibration standard. They may thus represent a mixture of tetramers and hexamers. The corresponding peak was collected and analyzed by CD spectroscopy (Figure 5-16B). The signal intensity in the far-UV CD was slightly reduced compared to dimeric Ure2p, but in relation to mature fibrils (Figure 5-13B), the extent of conversion is relatively small. Either this peak contains a mixture of converted and non-converted molecules, or complete conversion only takes place in larger species such as fibrils. To eliminate the contribution of non-converted species, we carried out a similar analysis under denaturing conditions (Figure 5-16CD). It was possible to detect several (stable) oligomeric species. The smallest species, which corresponds to a broad peak around 55 min, likely represents unfolded monomers that dissociate from larger species during SEC analysis, as the elution time of unfolded Ure2p was much larger (71 min). These molecules became rapidly depleted upon further fibrillation, indicating the formation of more stable species. Based on the standard curve, the peak at 46 min was assigned to tetrameric Ure2p. While the concentration of this species increased only slightly over time, a larger species at 42 min, presumably the hexamer, showed a strong increase in population during the lag phase. Intriguingly, we found that the concentration of this species decreased after 12 h, indicating that it may represent an intermediate in the formation of an even larger species. Again, we collected the species eluting around 42 min and analyzed its secondary structure (Figure 5-16D). Here, the

increase in the content of β-structure is apparent, demonstrating that this stable oligomer has already undergone conversion to the prion conformation. Likely, these molecules are also present in the native samples (Figure 5-16AB), but are difficult to detect due to the large background from non-converted species and the strong CD signal of the large C-terminal domain. We also tested whether the small oligomeric species observed in SEC analysis (Figure 5-16A) are able to 'seed' Ure2p fibrillation. To this end, we collected the protein eluting in the 150 kDa fraction, and added it to a solution of dimeric Ure2p (ratio of seeds vs. dimer ~1:100). As shown in Figure 5-16E, fibril formation in this sample, as monitored by ThT binding, was significantly faster than in a reference sample to which no oligomers had been added. However, seeding with these oligomers was less efficient than seeding with an equal amount of fibrillated Ure2p. Likely, only some of the molecules in the 150 kDa fraction are converted and can act as seeds, in agreement without our conclusions from the CD spectra.

5.7 Partial Discussion

Yeast prions and mammalian prions share a lot of features with amyloids in relation to conversion to β-sheet structure and fibrillation, and consequently they were suggested as models for amyloid fibrillation (Lindquist et al., 2001). As suggested by Wickner (Wickner, 1994) Ure2p protein is a yeast prion. Later, it was shown that Ure2p fibrils bind the fluorescent dye Thioflavin T (ThT) and display an increased resistance against proteases (Zhu et al., 2003b; Komar et al., 1997).

Using AFM and other biophysical techniques, it was possible in this work to identify Ure2p fibrillation species (Figure 5-4). As also shown by Melki (Bousset et al., 2002) and Perret (Jiang et al., 2004), Ure2p has a similar pattern of fibrillation as other amyloids. AFM, TEM and spectroscopic characterization suggest that Ure2p follows a multistep self-assembly pathway. The formation of globular species, whose concentration decreases over time (AFM and TEM) during the lag phase of the ThT assay and, the appearance of fibrils in the solution (AFM and TEM) with a concomitant increase in the ThT fluorescence

signal are hallmarks of the nucleation polymerization model for self-assembly of proteins.

Ure2p fibrillation can be accelerated by seeding (fig 4.5 and 4.17), as shown previously for PrP and other amyloid proteins(Prusiner, 1982; Kaneko et al., 1995). This indicates that in vitro, Ure2p displays a protein-only mechanism of "inheritance", in agreement with the current model on the [URE3] and [PSI] phenotypes (Glover et al., 1997; Ter Avanesyan and Kushnirov, 1999). One of the open questions was whether Ure2p can be classified as an amyloid protein (Speransky et al., 2001; Baxa et al., 2003) or if Ure2p assembles like other biological polymers (actin and microtubules) without any significant change of structure (Bousset et al., 2002; Bousset et al., 2004). To answer this question, the Ure2p pathway was dissected and characterized in terms of species and structure. Species present during the fibrillation process were isolated and characterized using analytical techniques (Figure 5-8, Figure 5-9 and Figure 5-11). A spectroscopic analysis of the mature fibrils shows a difference in secondary structure between the fibrillated protein and dimeric Ure2p. Likely, this is due to a short stretch of amino acids which change from α-helix to β-sheet upon fibrillation. At the same time, we were unable to identify any differences in Trp fluorescence between the two states. Since all 6 Trp residues of Ure2p are located in the region comprising residues 179-354, this part of the protein must adopt a very similar structure in both dimers and fibrils. Therefore, the structural changes observed in far UV CD spectra must occur in the N-terminal region. This is in agreement with findings by Baxa *et al*., who showed that several cleavage sites for proteases in the N-terminal domain become inaccessible in fibrils (Baxa et al., 2003). It was demonstrated previously (Baxa et al., 2002) that the N-terminal domain of Ure2p can induce the fibrillation of other proteins when attached to their N-terminus. The fusion proteins retained their biological activity in the fibrillar state showing that the structure of the C-terminally located protein is not changed. These observations support the notion that the C-terminal domain of Ure2p is dispensable for fibril formation. Although the C-terminal domain becomes unfolded upon incubation with 5 M GdmCl and 1%SDS in both fibrillar and dimeric Ure2p, we still could observe fibrils under these conditions (Figure 5-12, Figure 5-10). This confirms that the N-terminal domain is entirely responsible for fibril formation. However, it is

possible that the C-terminal domain is involved in the formation of higher order structures such as the mature fibrils we observed with AFM. Intriguingly, we were unable to detect higher order fibrils in the presence of 5 M GdmCl, i.e. under conditions where the C-terminal domain is completely unfolded.

Another aspect of this study was the analysis of processes that lead to the formation of protofibrils. Using a range of analytical techniques, including CD spectroscopy, Trp fluorescence, AFM, and SEC-HPLC, some of the soluble intermediates present in the Ure2p fibrillation pathway were characterized. In contrast to previous studies (Jiang et al., 2004) both height and diameter were used to calculate particle sizes from AFM images. Also, it was ensured that fibrillation was non-seeded by filtering the Ure2p solution immediately before starting the reaction (while the starting solution of other groups already contained some seeds) (Jiang et al., 2004).

The results of this study showed that small globular species are formed during the lag phase of the fibrillation kinetics before any fibrils could be detected by ThT binding and AFM (Figure 5-3 and Figure 5-4). The dimensions of some of these particles (3-4 nm) closely match the diameter of protofibrils suggesting that represent precursors (Figure 5-4, Figure 5-6 and Figure 5-14). Based on our AFM calibration curve (Figure 5-15), we conclude that these molecules are tetramers or hexamers of Ure2p. The same small oligomers were detected when samples of “lag phase Ure2p” were analyzed by SEC (Figure 5-15). According to the elution profiles, these species represent less than 5% of the fraction of the soluble Ure2p in this stage of the fibrillation process. The important and novel finding is that during the lag phase, some Ure2p molecules already adopt a converted conformation. They share three properties with fibrillar Ure2p that distinguish them from the dimeric state: (i) an increased content of β-structure, (ii) resistance against denaturation by 5 M GdmCl, and (iii) the capability to ‘seed’ fibril formation of dimeric Ure2p. These molecules may also explain the existence of a soluble variant of the [*URE3*] prion phenotype (Fernandez-Bellot et al., 2002).

Presumably, the oligomers that were observed in SEC analysis originate from two sources. Some have formed during the association and conversion of dimeric Ure2p, i.e. they represent intermediates of the fibrillation process, while

others represent fragments of larger converted species that were disrupted during analysis. The pellet fraction of the sedimentation assay consisted predominantly of fibrils as judged by AFM. However, when the same pellet was analyzed by SEC under denaturing conditions (Figure 5-16) it contained also small oligomers indicating that some of the fibrillar structures must have dissociated during analysis. On the other hand, fibrils seem to be remarkable stable structures, as judged by their resistance to strong denaturants and proteases. These contradictory observations could be explained by the existence of “fibrils” that do not contain a continuous β-sheet core, but rather represent linear associations of small oligomers (Figure 5-8C). Accordingly, the forces that connect these linear assemblies can be destroyed by GdmCl, and the (converted) building blocks of these molecules appear in SEC analysis. These molecules cannot be simple aggregates because of their β-sheet content. Real fibrils are more stable and survive the GdmCl treatment as shown by TEM. The fact that these species can seed Ure2p solutions implies that globular species are not end-product of an independent assembly mechanism, but are rather part of a pathway to the end product. The existence of these species just indicates that the kinetics have not finished yet.

Another aspect analyzed in this work is the polymorphism found in the Ure2p fibrillation pathway. Polymorphism has been identified for a number of amyloid fibrils under different conditions (Ionescu-Zanetti et al., 1999; Goldsbury et al., 1997) (Harper et al., 1997). Ure2p forms polymorphic structures (Figure 5-8 and Figure 5-9) that can assemble in parallel, twisted or nodular ways similar to amyloid fibrils.

The variation of morphology among mature fibrils of Ure2p, likely based on differences in protofilament assembly (Figure 5-7 and Figure 5-9), has also been described for Aβ (Blake et al., 1996; Serpell, 2000b) and insulin (Jimenez et al., 2002). Since the domain texture of the mature Ure2p fibril is very similar to that of a protofibril (Figure 5-6), the observation of the fibrils supports the theory that mature fibrils are formed through the association of protofibrils, early species and monomers as is in this theses described.

Different values of protofibril diameters were obtained by AFM/TEM measurements. This could be explained by the different numbers of molecules

forming the protofilament. Excluding the seeding, once that the fibril dimensions follow the template characteristic (Figure 5-4), there are some possibilities to explain this difference of cross-section of the fibrils: The diameter is related to 1) the number of protofilaments associated to form the mature fibril (Figure 5-9); 2) the size of the nucleus that generates the protofibril (Figure 5-14).

This means, it is more likely that each of these fibrillar types arises from a common nucleation core, which diverges in structure early on during growth, leading to parallel pathways in vitro. It is possible that this parallel pathway may have a different biological function in vivo.

The presence of polymorphic species and their potentially varying growth mechanisms represents an additional level of complexity on the formation of the fibril.

Twisted fibrils (Figure 5-8A) may form as a mechanism to decrease the hydrophobic forces. This would lead to the idea that the dimer hydrophobic surface would be responsible for the fibril-fibril interaction. Nodular fibrils (Figure 5-8C) have no regularly spaced compared to twisted fibrils that present a very regular repetition. It is not clear if nodular fibrils correspond to a sequential stage of globular attachment in a single linear aggregation process due to diffusion problems (Figure 5-17) or if they represent different structures formed through distinct coexisting parallel pathways. The formation of ribbons (fig 4.8B), it is already described by polyQ(Chen et al., 2002) and may be the result of cylindrical fibrils (Figure 5-8 and Figure 5-10A) attached in parallel. The flattening of the ribbons could be due to the water expulsion and attraction of amino acids of different charges. Only twisting fibrils have been reported for Ure2p (Jiang et al., 2004). This may be due to the conditions used (agitation, high ionic strength). In this study agitation was not used because this can cause fibril breaking, as reported by Weissmann for Sup35 (Collins et al., 2004). The fibrillation pathway of ure2p here analyzed is summarized in Figure 5-17.

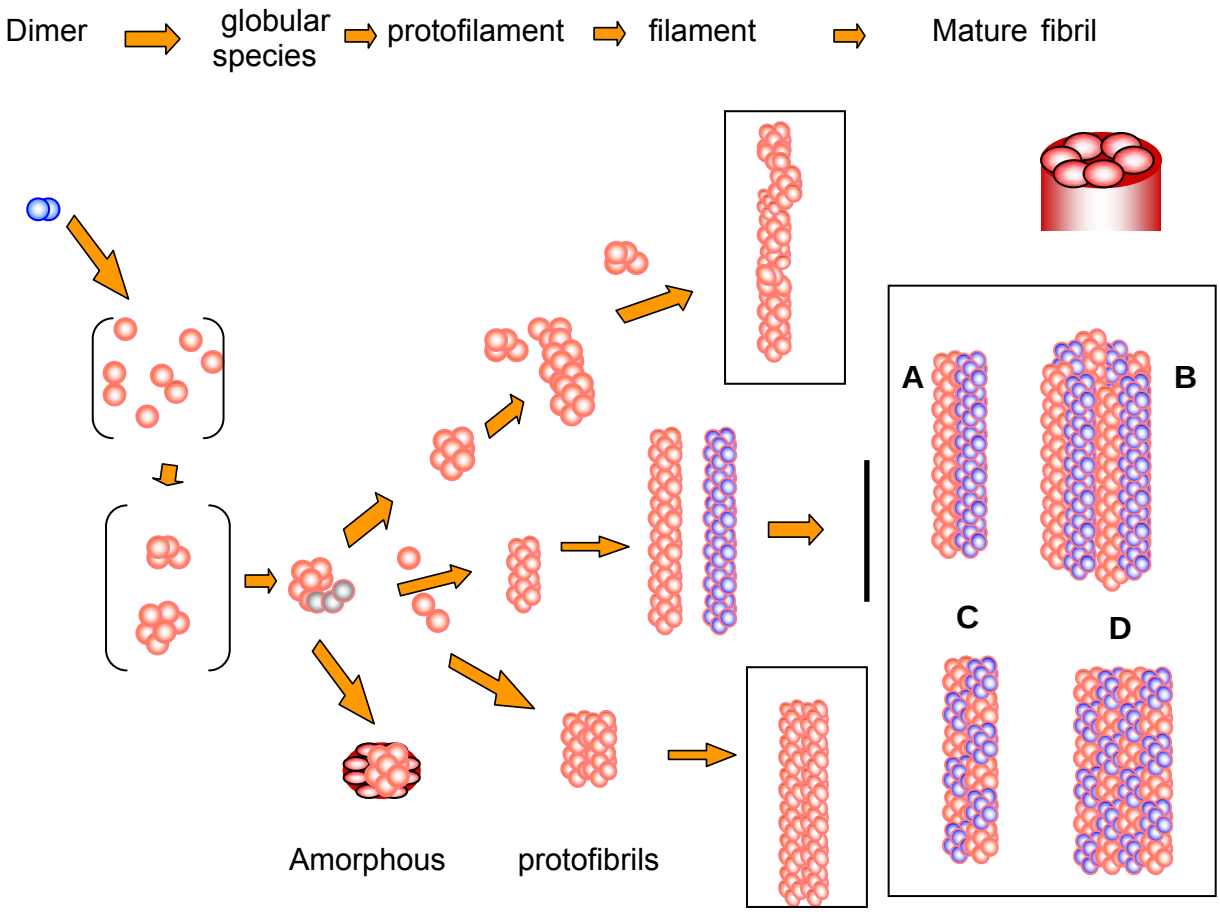

Figure 5-17: scheme for ure2p fibrillation pathway.

The fibrillations pathway start with the dimer (in blue), a nucleus that grows some globular species. The globular species start to elongate and form protofilaments or associate to form a polymorphic set of fibrils. These globular species can generates mature fibrils, by oligomers association (upper pathway), filaments and then to hierarchical assembly (middle pathway), generate protofibrils that acts like a seed (lower pathway). Other possibility would be that some of this globular species can be in the pathway for amorphous aggregates. Fibril A and B shows some parallel assembly like ribbon (A) and like a hollow tube (B). Fibril C and D represent twisted fibrils where D represents some more complex structure like tangles.

The formation of polymorphic fibrils with the same thickness as the amyloids is not a special case of Ure2p.This behaviour seems to be driven by enviromental e structural features but not the specific sequence of a protein.

6 Searching for optimal conditions for fibrillation

To better understand the molecular events that lead to the assembly of Ure2p into protein fibrils, an attempt was made to identify the conditions that are favorable for Ure2p fibrillation.

6.1 Effect of Ure2p solution concentration on fibrillation

In order to analyze the effect of Ure2p concentration on fibrils morphology and hierarchy, solutions containing different protein concentrations were let to fibrillate on a plastic tube. Aliquots were added to mica and analyzed by AFM.

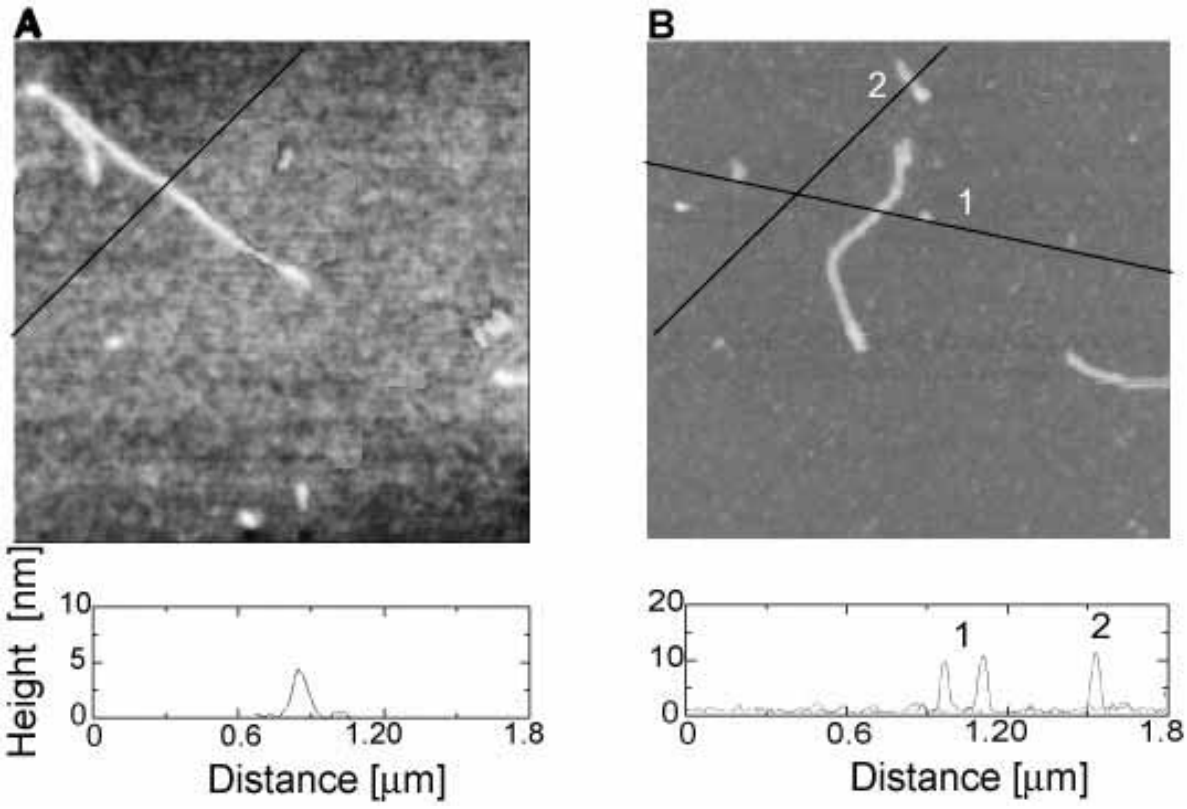

Figure 6-1: Effect of the Ure2p concentration on fibril dimensions.
A) 10 µM Ure2p B) 85 µM Ure2p, the black lines represent the cross-section of the height images displayed below. Fibrillation conditions: 50 mM Tris/HCl pH 7.5, 15°C, without agitation.

Figure 6-1shows the effect of Ure2p concentration on fibril height and diameter. Figure 6-1A display a protofilament with a minimum height of 3 nm as shown previously in Section 4.4. An increase in the concentration of Ure2p leads to an increase in the protofibril (Figure 6-1B) size and consequently in the fibril height and diameter (species 2, Figure 6-1B). The effects of Ure2p concentration on the kinetics of Ure2p fibrillation have been discussed previously by Perret(Zhu et al., 2003b) showing that there is an increase of fibril quantity with increase of ure2p concentration but no reference has been made to the increase of fibril diameter. This might be due to diffusion effects in the solution, leading to formation of smaller nuclei.

6.2 Effects of buffer and pH on fibrillation

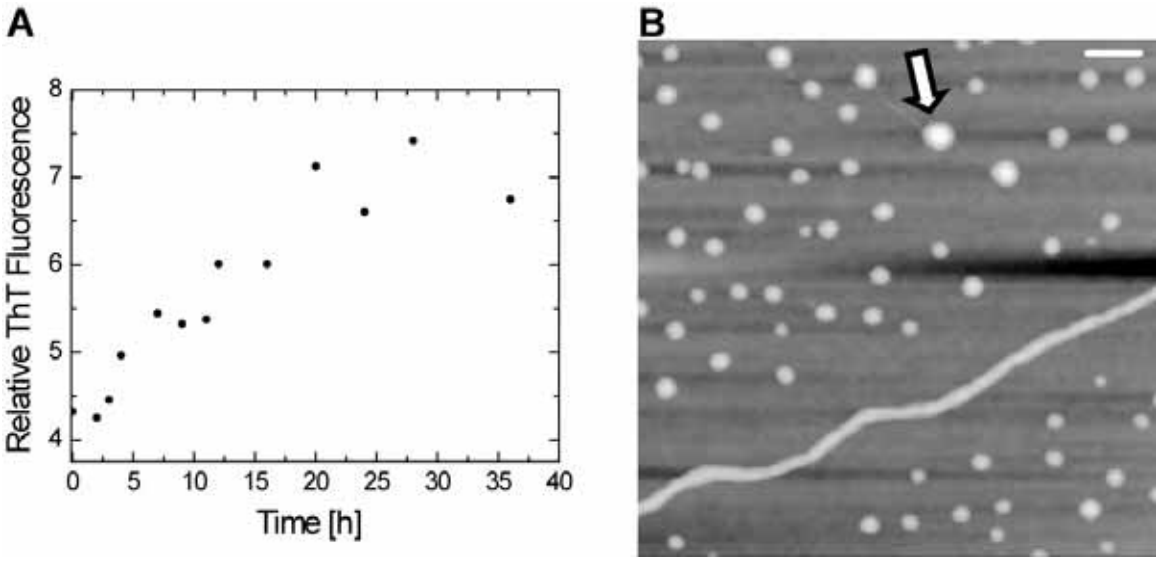

Figure 6-2: Ure2p fibrillation in NaP buffer.
A) ThT assay of Ure2p in 50 mM NaP buffer. B) Height image from Ure2p fibrils at 50 mM NaP pH 7.5. The full range of the gray scale corresponds to a height of 30 nm. The scale bars represent 250 nm. Time: 12 hours. Concentration: 85 μM. T= 15°C.

The height image in Figure 6-2 shows some globular species and fibrils formed in NaP buffer. The fibril formation of Ure2p in NaP buffer follows the same pathway as in Tris buffer with a lag phase and an elongation phase in ThT binding assay (Figure 6-2A). The Table 6-1 shows a reduction of the lag phase in NaP buffer compared to Tris buffer. Figure 5-3B inferring an increase in the nucleation and elongation rate in NaP buffer.

Table 6-1: Dependence of the rate of fibril formation buffer type in unseeded reaction.

Buffer	k_{app} (elongation) [h^{-1}]	Lag phase [h]	Nucleation rate [h^{-1}]
NaP	0.24	1.6	0.63
Tris	0.21	2.8	0.36

Analysis by AFM shows the existence of the same globular species (B) and ellipsoidal species, protofibrils, protofilaments and mature fibrils (data not shown). The fibril heights measured are centered around 8-11 nm. It could be seen globular species with a high variety of height values, between the dimer and the fibril height values. Globular species with higher height values than the fibril could be seen, too (arrow, Figure 6-2B) dispersed between dispersed between different species in solution. These big globular species were classified as potential amorphous aggregates based on the fact that no fibril with these diameters or higher ones could be identified in solution, but some amorphous species with higher values than the fibrils could be identified. On this way, it is possible to say that these species are precursor of amorphous aggregates. These results lead to the suggestion that in phosphate buffer fibril formation generate more “dead end’ species (Ripaud et al., 2003)(arrow in Figure 6-2B). Analysis by TEM shows no difference in morphology of the fibrils between buffer NaP and Tris. Although the behavior of Ure2p in NaP buffer is similar to Tris and the fibrillation pathway are the same, the results above show a difference in fibril quality. This may be explained by the GdmCl transition (as shown in section 3.10). The presence of particles bigger than the diameter of the fibrils can indicate that globular species are precursor of the amorphous aggregates too. The effects of buffer on Ure2p fibrillation have been discussed previously by Perret (Zhu et al., 2003b) using ThT assay. The results showing that Ure2p fibrillates in NaP buffer and Tris, with a difference in lag phase but no values were discussed. Considering the fibril quality showed in NaP Buffer, further studies were done using Tris Buffer.

To understand pH effects on fibril formation, Ure2p was let to fibrillate at different pH and analyzed by AFM.

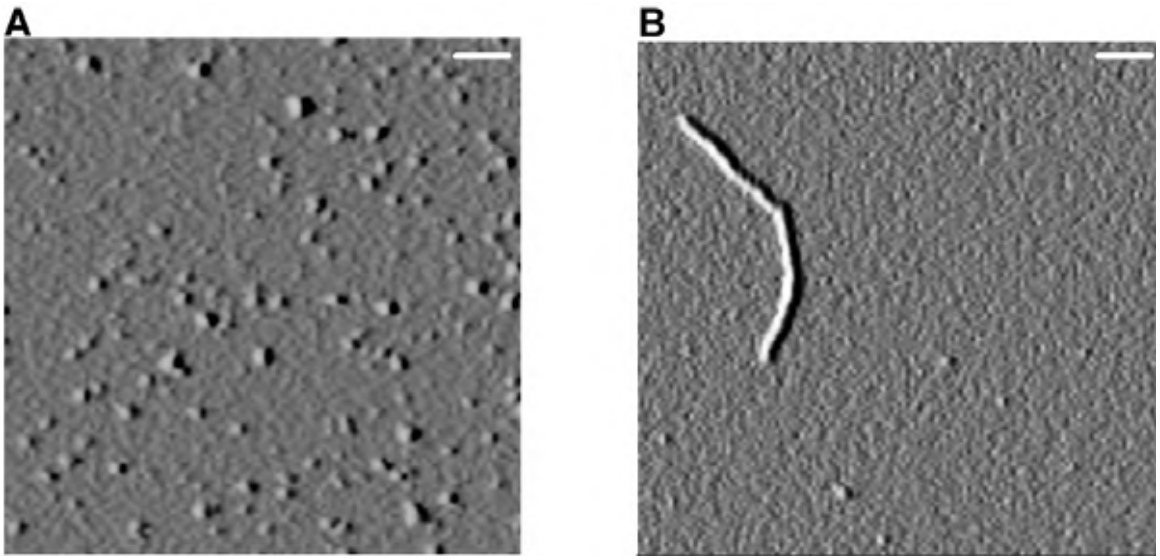

Figure 6-3: pH effect on Ure2p fibrillation.
Buffer: 50 mM Tris. A) pH 6.5 B) pH 8.0; scale bar: 200 nm concentration: 60 µM, T= 15 C. Time: 24 hours.

Incubation in low pH (< 6) and near the isoeletrical point of Ure2p leads to aggregation with the formation of amorphous rather than fibrillar aggregates. Solutions of Ure2p between 6 and 7 lead to the precipitation of the protein (Figure 6-3A). These results are independent of the incubation time and temperature. Fibrils are formed only between pH 7.2 and 8.7 (Figure 6-3B). These fibrils show no difference in height and diameter [identical concentration, buffer and temperature] in these pH ranges. Adding globular species formed at pH 7.5 to the Ure2p solution at pH 5, 6.5 or pH 10 does not lead to the formation of fibrils (data not shown). These results indicate that neutral pH is required for the formation of fibrils and that elongation does not happen at extreme pH values. Perret (Zhu et al., 2003b) showed that the pH between 7.5 and 8.5 has little influence on the fibrillation rate of ure2p under non seeded reaction.

6.3 Salt effects on fibrillation

6.3.1 Effects of NaCl concentration on Ure2p fibril formation

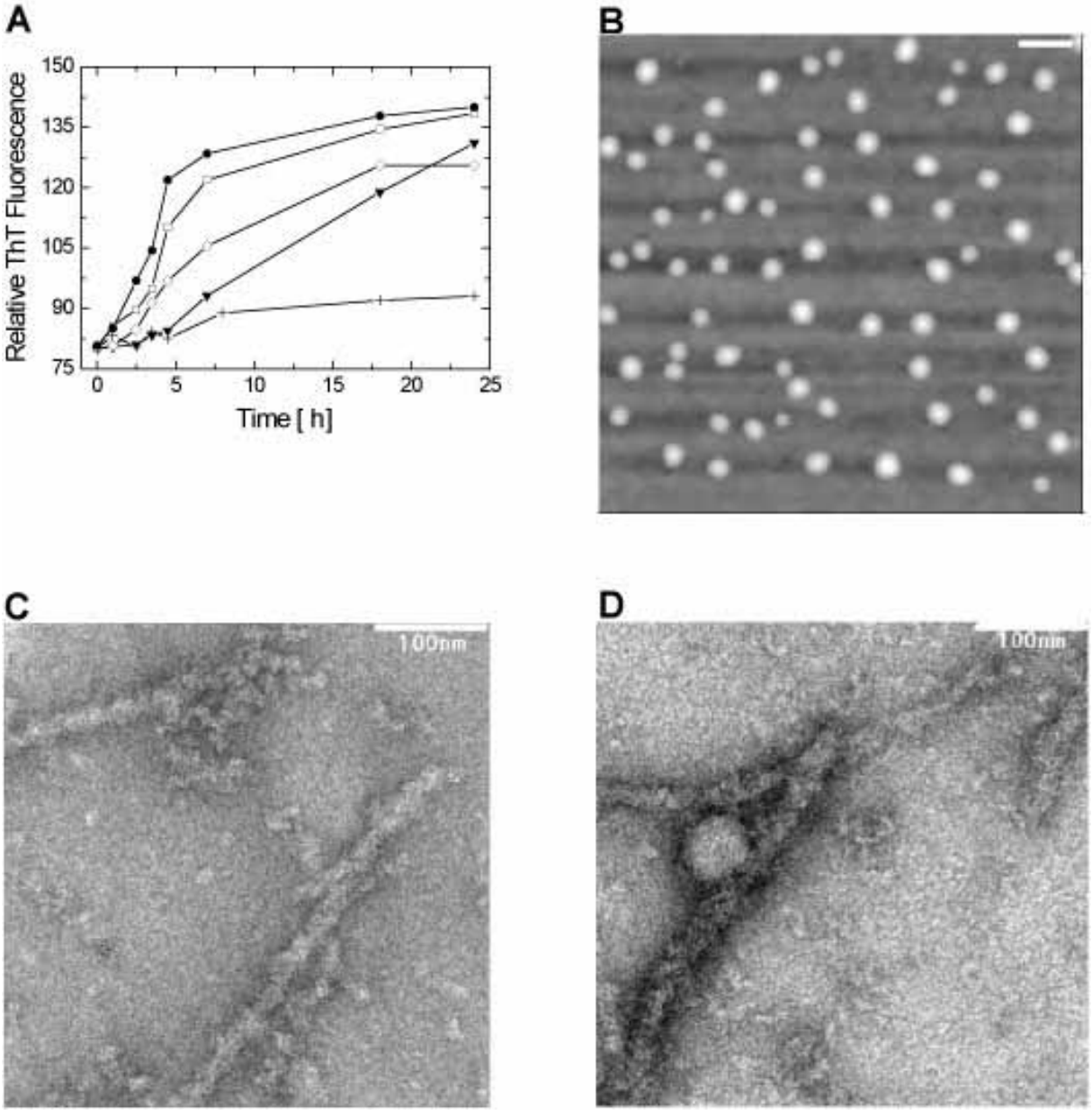

Figure 6-4: Effects of NaCl concentration on fibril growth at 15 °C.

A) Fibril growth monitored by ThT fluorescence as a function of time in 50 mM Tris pH 7.5 alone (-▼-) and in buffer containing 75 mM (-◊-), 150 mM (-□-), 200 mM (-●-) and 500 mM (-+-) NaCl.B) Globular species present during lag phase at 200 mM NaCl. C) TEM of Ure2p fibril formed 200 mM after 18 hour of fibrillation. D) TEM of Ure2p fibrils formed at 500 mM after 18 hour of fibrillation. All scale bars represent 100 nm.

Figure 6-4 shows the effect of the NaCl concentration on Ure2p fibrillation. Figure 6-4A shows the time course of Ure2p fibrillation at different

concentrations of NaCl monitored by ThT assay. There is not a dramatic change in the shape of the sigmoidal curve with the addition of NaCl. The intensity of ThT fluorescence increases with time at all NaCl concentration. At 0 M NaCl concentration, there is a lag phase of 2.7 hours. After 3 hours, the ThT fluorescence increases slowly showing that the elongation of the oligomeric species started. The lag phase of 2.7 hours at 0 M NaCl decreased to 1.4 hour for 75 mM NaCl, and almost vanished in 150 and 200 mM NaCl (Table 6-2). The ThT fluorescence intensity of the sample is considered proportional to the extent of amyloid fibril-bound ThT (LeVine, III, 1997).The Table 6-2 shows a considerable reduction of the lag phase with increasing NaCl concentration inferring an increase in the nucleation and elongation rate. Further increase in the concentration of NaCl beyond 200 mM, however, led to a decrease in the fibril growth (Figure 6-4A) as shown by the ThT fluorescence and an increase in the number of amorphous aggregates in the lag phase. Figure 6-4B shows globular species species present during fibrillation under salt conditions. There is no large variation in fibril width below 200 mM NaCl. Figure 6-4C shows fibril at 18 hours at 200 mM NaCl.

Table 6-2: Dependence of the rate of fibril formation on salt concentration

[NaCl]	k_{app} (elongation) [h^{-1}]	Lag phase [h]	Nucleation rate[h^{-1}]
0	0.21459	2.77	0.36
10	0.27778	2.28	0.43
75	0.38462	1.44	0.69
150	0.52632	0.68	1.47
200	0.625	0.53	1.88

This shows that the extent and the rate of fibril growth depend on the salt concentration, with a maximum being reached at 200 mM NaCl. Figure 6-4CD display fibrils formed at a different NaCl concentration (200 and 500 mM, respectivaly). Figure 6-4D shows some mature fibrils, protofilaments and some amorphous aggregates. The only difference in fibril morphology related to range of salt concentration was in relation to the fibril width. Monitoring the width by TEM (data not shown), it was verified that an increasing on the salt

concentration in the solution up to physiological values did not lead to a significant increase in the average width of the fibrils. Although the numbers of experiments carried out is not enough for quantitative statistics, it appears that with an increasing salt concentration the distribution of fibril width became broader due to the increase of the standard deviation with increasing salt concentration. This may be due to an increase in association of protofilaments due to hierarchical assembly. Most of the species visualized at 500 mM were amorphous aggregates. The effect of salt on protein solubility has been reviewed by Curtis (Curtis et al., 1998) with a salting-in region at low salt concentrations and a salting-out region for high ionic-strength solutions. Following this classification, the region under 200 mM, can be described as favorable for the interaction between the salt ions and the protein charged residues, increasing the solubility of protein. Above 200 mM NaCl (salting-out region) the charged residues are neutralized. These results show that the kinetics of fibril formation is influenced by the salt concentration of the solution. Far-UV CD and fluorescence spectroscopy showed no difference in the shape and in the intensity of the spectra between the Ure2p dimeric solutions independently of NaCl concentration (data not shown). In order to analyze this hierarchical behavior, samples were measured by AFM.

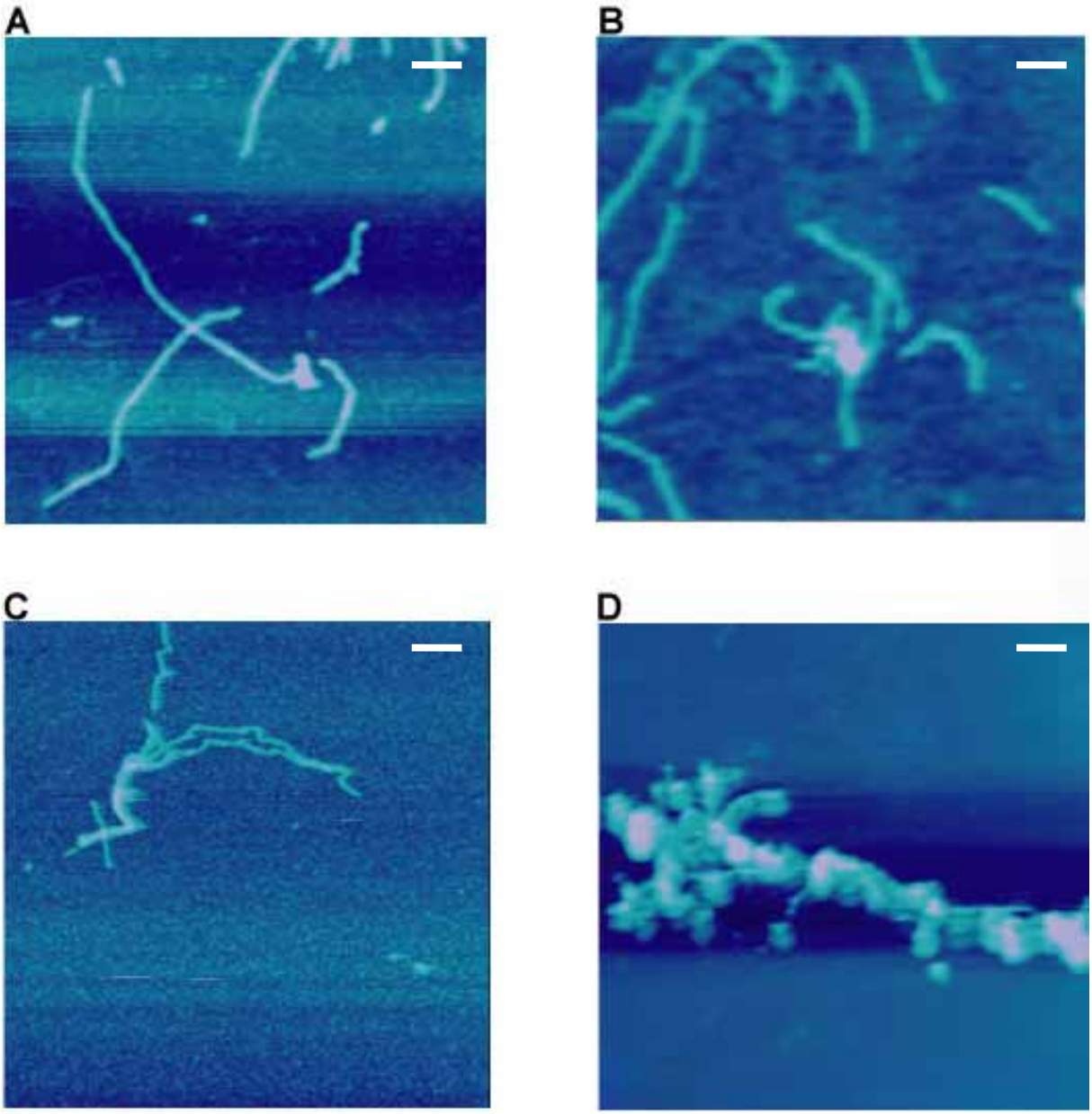

Figure 6-5: Effect of different salt concentration on Ure2p fibril growth.
TM-AFM height image of fibrils, growth in 50 mM Tris pH 7.5 and different salt concentrations A) 0 M NaCl B) 150 mM NaCl, C) 500 mM NaCl and D) 1 M NaCl. The scale bars represent 250 nm.

By monitoring the effects of salt concentration by AFM using mica as substrate, one can see an increase in mature Ure2p fibril density as the ThT curve approaches the plateau in the sample containing 200 mM NaCl. In the samples containing no salt there are still small fibrils (data not shown). As expected, at all salt concentrations there is an increase in the number of small particles in the lag phase with time and a decrease of these particles during the increase of the ThT curve (data not shown). Monitoring the morphology of the mature

fibrils, it is possible to see some differences in relation to morphological and hierarchical behavior. Fibrils grown in low NaCl concentration are smoother than fibrils grown under physiological conditions, which tend to be more homogeneously twisted (Figure 6-5A and B). The increasing of the NaCl concentration above 200 mM increases the oligomeric species sizes and consequently the fibril cross section, showing some association of 3 or 4 protofilaments together (Figure 6-5C) while the presence of some thin protofilaments appear to increase in solution (data not shown). This results in an increase of the height distribution of the fibrils in solution. At higher concentration of NaCl (1 M), the sample was basically composed of amorphous aggregates, aggregates containing fibril and very thin fibrils. The high speed of fibrillation at high salt concentrations can lead to the formation of anisotropic species like shown in Figure 6-5D. This shows that an optimal concentration is required for fibrillation and organization of the system. Perret and co-workers (Jiang et al., 2004) analyzed the Ure2p fibrillation using 150 mM NaCl and observed that twisted fibrils.

6.3.2 Effect of different anions on fibrillation

To understand the role of different anions, two other salts were chosen, composed of different anions but the same countercation, Na^+. A cosmotropic salt (Na_2SO_4), and a chaotropic salt (NaI) were compared to NaCl which is a weak cosmotropic salt. Ure2p was let to fibrillate for 18 hours in these different salt solutions and the corresponding ThT signals were compared.

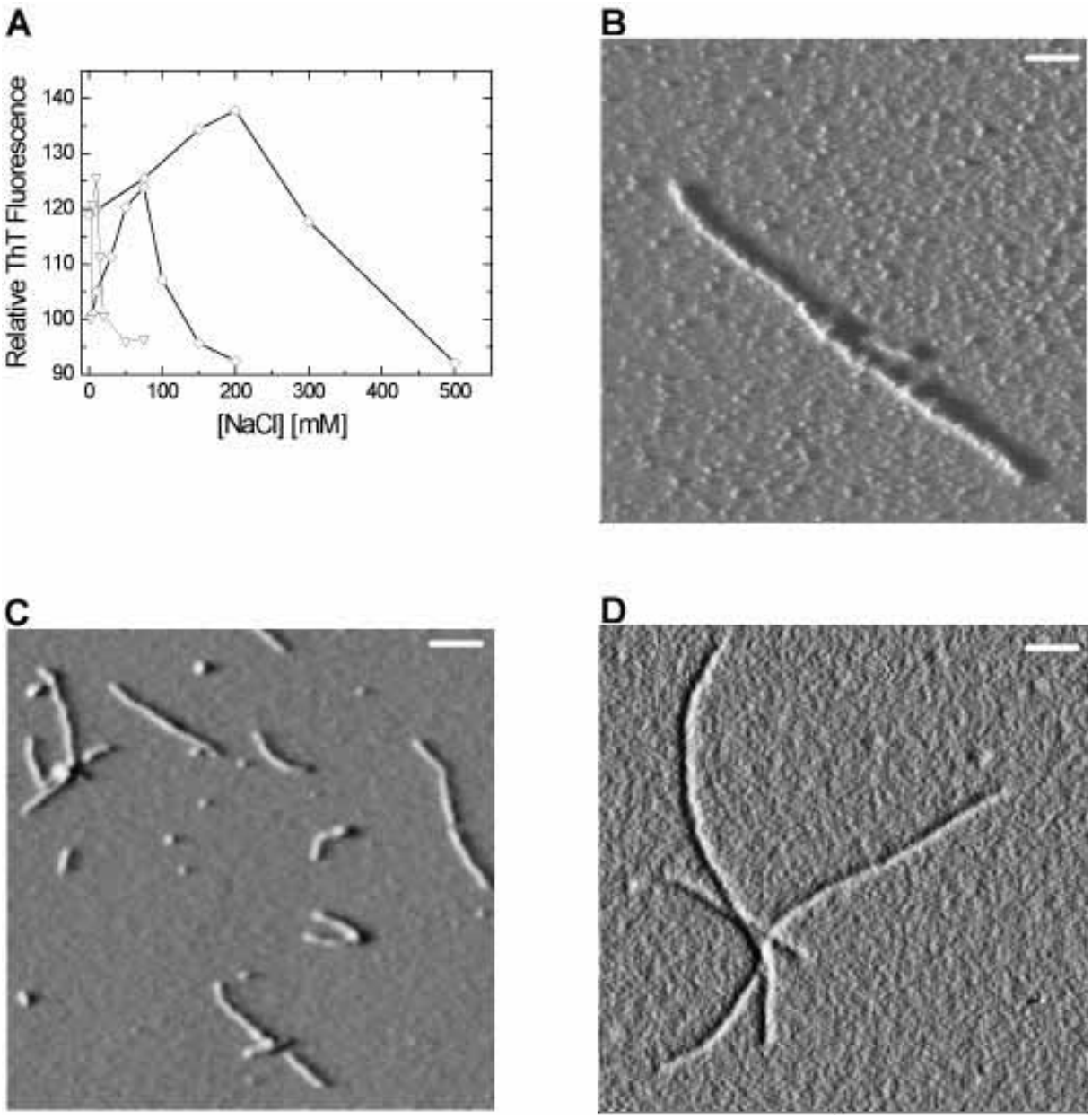

Figure 6-6: Effects of the anion on the Ure2p fibril growth after 18 hours at 15 ˚C.
A) ThT Fluorescence intensity of the samples at 482 nm, NaCl (-◊-), NaI (-□-) and Na_2SO_4 (-∇-). B, C and D) Amplitude AFM images of fibrils formed in the presence of different salts at 15 ˚C, 65 μM Ure2p, 50 mM Tris/HCl pH 7.5, without agitation. B) Fibril formed in the presence of 10 mM Na_2SO_4, scale bar: 100 nm C) Fibril formed at 50 mM NaI. Scale bar: 200 nm and D) fibril formed at 200 mM NaCl. Scale bar: 200 nm.

Figure 6-6 shows the effect of different anions on Ure2p fibril growth. These salts have similar behavior to NaCl, showing an optimum concentration and thereafter a decrease in ThT fluorescence with increasing salt concentration. According to the ThT fluorescence, the optimum concentration of NaI and Na_2SO_4 is 75 mM and 10 mM, respectively. The presence of fibrils was confirmed by AFM (Figure 6-6BC and D). The ThT graph shows that the

interaction of the anions to Ure2p follows the electro-selective series SO_4^{2-} > I^- > Cl^- (Baldwin, 1996). Divalent ions interact stronger with the protein than monovalent ions. Between the two monovalent anions I and Cl, the size of the anion is important (showing a deviation of the Hofmeister series). This deviation is due to a stronger interaction of the iodide with the protein than with the water, while Cl has a higher attraction to the water (Curtis et al., 1998). All three salts show this salting out effect on the protein and inhibiting the fibril growth of the fibril above the optimum concentration. These three salts promote the fibrillation of Ure2p with nucleation and oligomeric species as previously shown in 50 mM Tris (data not shown). The fibrils formed in different salt solutions show no difference in the fluorescence (in the intrinsic fluorescence of the Trp). The fibrillar state shows no difference from that of the native state in fluorescence. Microscopy shows that despite some difference in the fibril length, there is no clear difference in the morphology between the fibrils formed in different salts. Analysis by AFM shows that NaI and Na_2SO_4 do not have any effect on the diameter of fibrils. Na_2SO_4 and NaI display fibrils around 8-10 nm with some twisting, which may indicate that a constant hierarchical behavior is a property of the protein at the optimum salt concentration independently of the type of anion used. TEM data in NaI and Na_2SO_4 are in agreement with AFM results (data not shown).

6.3.3 Effect of different cations on fibrillation

Cations minimize the electrostatic repulsion between negatively charged amino acids. In order to see if cations have any effect on Ure2p fibril formation, solutions were incubated in KCl and then compared to solutions containing both KCl and $MgCl_2$. KCl and $MgCl_2$ are frequently used to mimic cellular conditions.

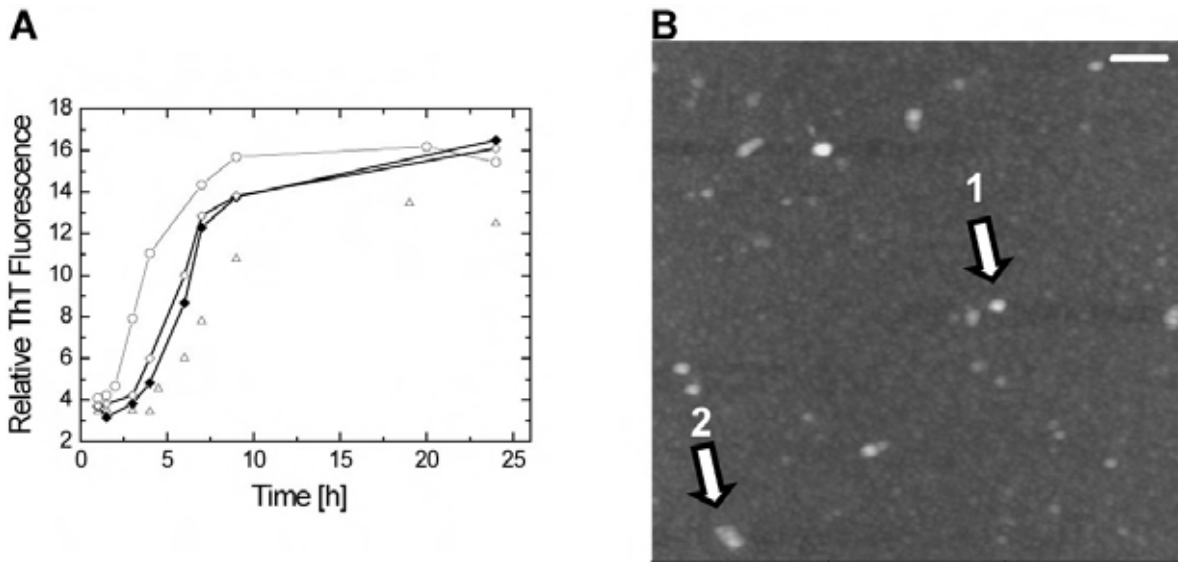

Figure 6-7: Effect of different cations on Ure2p fibrillation

A) ThT binding assay Ure2p in 5 mM KCl(△), 5 mM $MgCl_2$ (-◊-), 100 mM KCl (-●-) and 100 mM KCl, 5 mM $MgCl_2$ (-○-). B) AFM from aggregates generated by incubation for 4 hours in 100 mM KCl, 5 mM $MgCl_2$.

Figure 6-7 shows the effect of different cation on Ure2p fibril growth. The ThT curve (Figure 6-7A) in the presence of other cations then sodium has a sigmoidal characteristic, with an initial lag phase, and a subsequent growth phase like observed for NaCl. Addition of 100 mM KCl increases the fibrillation rate and decreases the lag phase. These results infer that KCl affects the nucleation and elongation in a similar way as NaCl, shortening the lag phase (Table 6-3). Adding a small concentration of $MgCl_2$ alone increases the shortening of the lag phase compared to KCl or Tris alone. The addition of 5 mM of $MgCl_2$ to a solution with KCl decreases more abruptly the lag phase. This means that Magnesium results in an effect on the ure2p fibrillation stronger than potassium. Analyses of the AFM images show no differences between KCl and NaCl in relation to fibril morphology and fibril height (data not shown). The fibrillation pathway using KCl and Mg has no difference to KCl. On Figure 6-7B is displayed an image taken from a sample already in the elongation phase, indicating some globular species (1) and protofibrils (2). The probable reason for the effect of KCl is the same as NaCl, where Mg would have a stronger interaction to the protein then potassium and sodium. This infers that the divalent cations interact stronger with the protein than monovalent cations.

Table 6-3: Dependence of the rate of fibril formation on temperature - unseeded reaction.

Salt	k_{app} (elongation) [h^{-1}]	Lag phase [h]	Nucleation rate [h^{-1}]
Tris	0.255	4.76	0.21
Tris/KCl	0.27	3.63	0.28
Tris/MgCl	0.34	3	0.34
Tris/KCl/MgCl	0.56	1.33	0.75

Despite the differences in kinetics, the cations and anions do not change the height average of the fibrils.

6.4 Temperature effects on fibrillation

6.4.1 Effects of freezing on fibrillation

To investigate the effects of freezing on Ure2p, three different freezing procedures were tested. Solutions of dimeric Ure2p and fibrils were frozen at -5°C, -20°C and with liquid nitrogen (-180°C). The freezing in liquid nitrogen is almost instantaneous, while at the other temperatures the protein solution freezes more slowly.

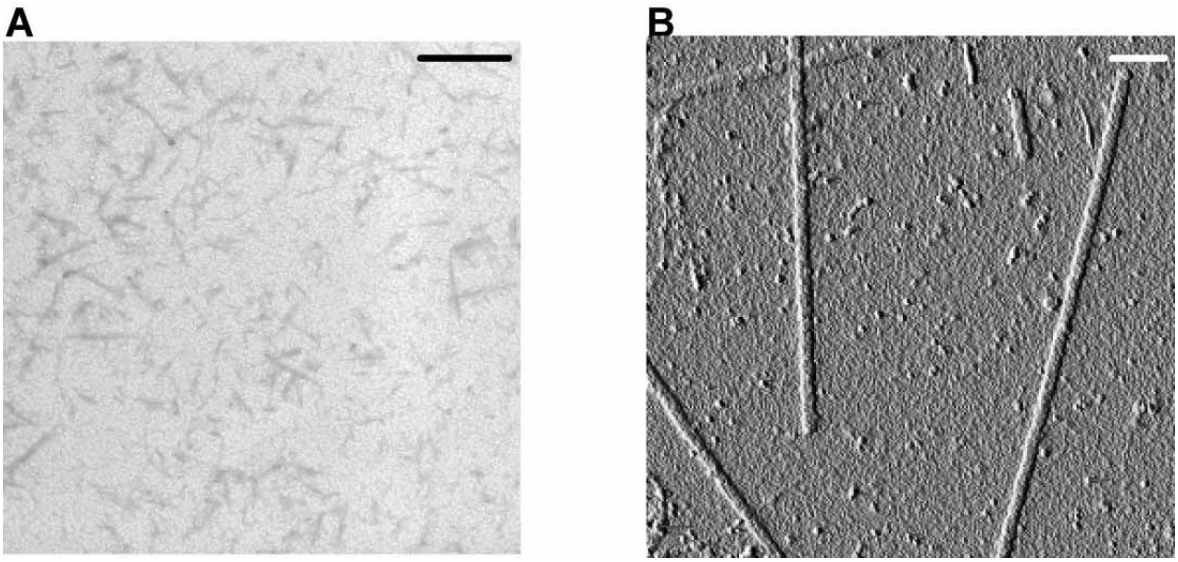

Figure 6-8: Effects of freezing on the Ure2p protein.
A) TE micrograph of a freshly thawed solution of Ure2p. This sample was frozen in liquid nitrogen after gel filtration and left to thaw at 4°C for 10 min. B) TM-AFM amplitude images of Ure2p fibrils frozen at -20° C and thawed slowly. Fibril dimension are 160 nm height and more then 10 μm. scale bar: 1 μm.

Figure 6-8 shows the formation of aggregates in thawed solutions of dimeric and fibrillated Ure2p. These results suggest that Ure2p aggregates during freezing at the tested temperatures, even when using liquid nitrogen (Figure 6-8A). The reason for this behavior is the process of freeze-concentration. Especially when freezing occurs slowly, parts of the solution consist of ice crystals. The protein becomes concentrated in the remaining liquid which facilitates aggregation. A similar effect could be observed for fibrils grown at 15°C, which were subsequently frozen at –20°C (Figure 6-8B). This procedure changes the morphology and the dimensions of the fibrils. Moreover, an Ure2p particle aggregates together with the fibrils. This result shows that the best way to store the fibrils while maintaining their characteristics is to freeze them in a very dilute solution using liquid nitrogen. It has already been shown for poly-Q (Chen et al., 2002) that solutions can aggregate upon freezing and thawing.

6.4.2 Effects of temperature on the fibril secondary structure

In order to determine how temperature affects the fibrillation process, solutions of dimeric Ure2p were incubated at different temperatures. The following methods were applied to monitor fibrillation: (i) the ThT assay was used to

record the kinetics of fibril growth (section 2.5.5). (ii) TEM and AFM were used to determine the dimensions of the fibrillar species as well as their morphology (section 2.6). (iii) CD spectroscopy was used to monitor changes in secondary structure (section 2.5.6). X-ray fiber diffraction was used to analyze the internal structure of the fibril. The temperatures used were 4, 7, 10, 15, 20, 25, 30, 37, 42, 48 and 60°C. Both seeded and non-seeded reactions were analyzed. Seeding was performed by addition of pre-formed fibrils (section 2.8.5) grown at the same temperature and salt conditions.

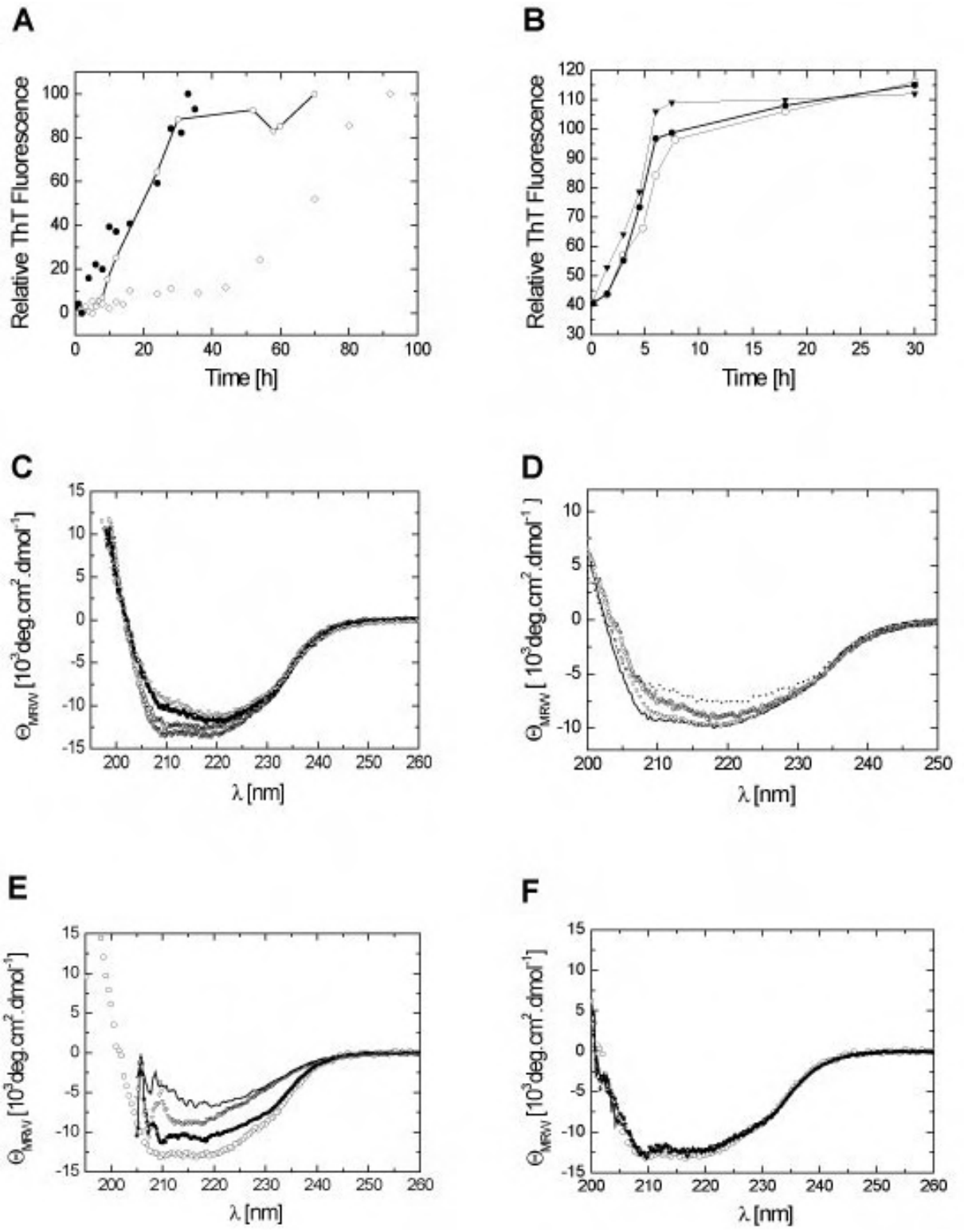

Figure 6-9: Effects of temperature on the fibrillation of Ure2p.

Dimeric Ure2p (50 µM) was incubated in 20 mM Tris/HCl, 20 mM NaP, pH 7.5. A) ThT binding assay of a non-seeded reaction at (◊) 4°C, (-o-) 15°C, (●) 37°C. B) ThT binding assay of a seeded reaction (o) 4°C, (-●-) 15°C, (-▼-) 37°C. The ratio seeds/Ure2p was 1:500. C) Far-UV CD spectra of the non-seeded fibril solution kinetic. (▽) dimer incubated for 5 min at 37°C, (o) 1 h, (-□-) 18 h, (-▽-) 24 h. D) far-UV CD spectra of the non-seeded mature fibril solution after sedimentation and resuspension (▬) 4°C, (▽) 15°C, (o) 30°C, (····) 37°C. E) Far-UV CD spectra of the non-seeded fibril solution

kinetic incubated at 42°C, 25 µM. (o) dimer incubated for 10 min at 20°C, (-□-)1 h at 42°C, (▽) 14 h at 42°C, (—)18 h at 42°C. F) Far-UV CD spectra of the non-seeded fibril solution kinetic incubated at 42°C, 10 µM. (□) dimer incubated for 10 min at 42°C, (-+-)1 h at 42°C, (—)18 h at 42°C.

The ThT kinetics demonstrates that the length of the lag phase decreases with increasing temperature in unseeded reactions (Figure 6-9A and Table 6-4). When the incubation was done at 37°C, fibrillation starts almost immediately, while at 15°C there is still a lag phase. At 4°C the lag phase apparently is longer, but there is a slow and steady increase of the ThT signal for some time (Figure 6-9A). During this lag phase in 4°C, some small fibrils still can be seen with AFM and TEM (data not shown) but it is not enough to produce a significant change in fluorescence.

Table 6-4: Dependence of the rate of fibril formation on temperature in unseeded reaction.

Temp [°C]	k_{app} (elongation) [h^{-1}]	Lag phase [h]	Nucleation rate [h^{-1}]
4	0.06173	22.4	0.04464
15	0.18622	6.52	0.15337
37	0.20534	0.58	1.72414

Seeding effectively eliminates the lag phase at all temperatures studied, inducing a rapid growth of fibrils from the moment of addition of seeds (Figure 6-9B and Table 6-5). There is a small difference between the seeded reaction at 37°C and the seeded reaction at 7°C and 15°C. A difference in the fluorescence signal (around 10% of the signal) indicating a larger number of fibrils after 8 hours at 37°C than at 15°C was obtained. The Far-UV CD kinetics demonstrates a increasing loss of ellipticity at 208 nm with incubation overtime at 37°C(Figure 6-9C) This result is reprodutible for lower temperatures. The content of secondary structure of the fibrillated protein was estimated by deconvolution of the data using the CDNN software. CDNN deconvolution shows that a major conformational change from α-helix to β-sheet is happening. Figure 6-9D shows the CD spectrum of fibrils formed at different temperatures in non-seeded reactions. Fibrils solutions were spin down when the ThT curve showed a plateau. There is an increasing loss of ellipticity at 208

nm with increasing temperature, too. CDNN deconvolution shows that a conformational change is happening.This could represent a conformational change, e.g. from α-helix to β-sheet due to the increase of temperature. According to CDNN, there is a small decrease of the α-helix and an increase of the β-sheet and random coil content. Incubation of Ure2p at 42°C in high concentrations lead to a high decrease of the α-helix and on increase of the β-sheet and random coil content overtimeas (Figure 6-9E) as showed by CDNN (data not shown). When the Ure2p solutions were incubated at higher temperature then 42°C and high concentration, AFM shows that they contain a larger number of amorphous aggregates (data not shown). The incubation of Ure2p at 42°C at very low concentrations (to avoid polymerization) for 24 h leads to an almost no change in the helices content (Figure 6-9F) as verified by CDNN (data not shown). The incubation of Ure2p at temperatures above 42°C at very low concentrations leads to the unfolding of Ure2p (data not shown). It is possible that there is a competition between unfolding and fibrillation when the temperature is increased. The course of aggregation was followed by AFM at all temperatures (data not shown). The aggregation pathway of Ure2p at 15°C by AFM, which was described before (Section 4), is reproduced for temperatures from 4°C to 37°C.The presence of intermediate species were verified and compared with section 4. The results showed that intermediate species discussed in Section 4 constitute a regular species in the pathway of Ure2p fibrillation independente of temperature.

Table 6-5: Dependence of the rate of fibril formation on temperature in seeded reaction.

Temp [°C]	**k_{app} (elongation) [h^{-1}]**
4	0.54
15	0.73
37	0.85

6.4.3 Effects of temperature on the morphology

In order to see if differences in the incubation temperature had effects on the morphology of fibrils, solutions of Ure2p in the stationary phase were analyzed by TEM.

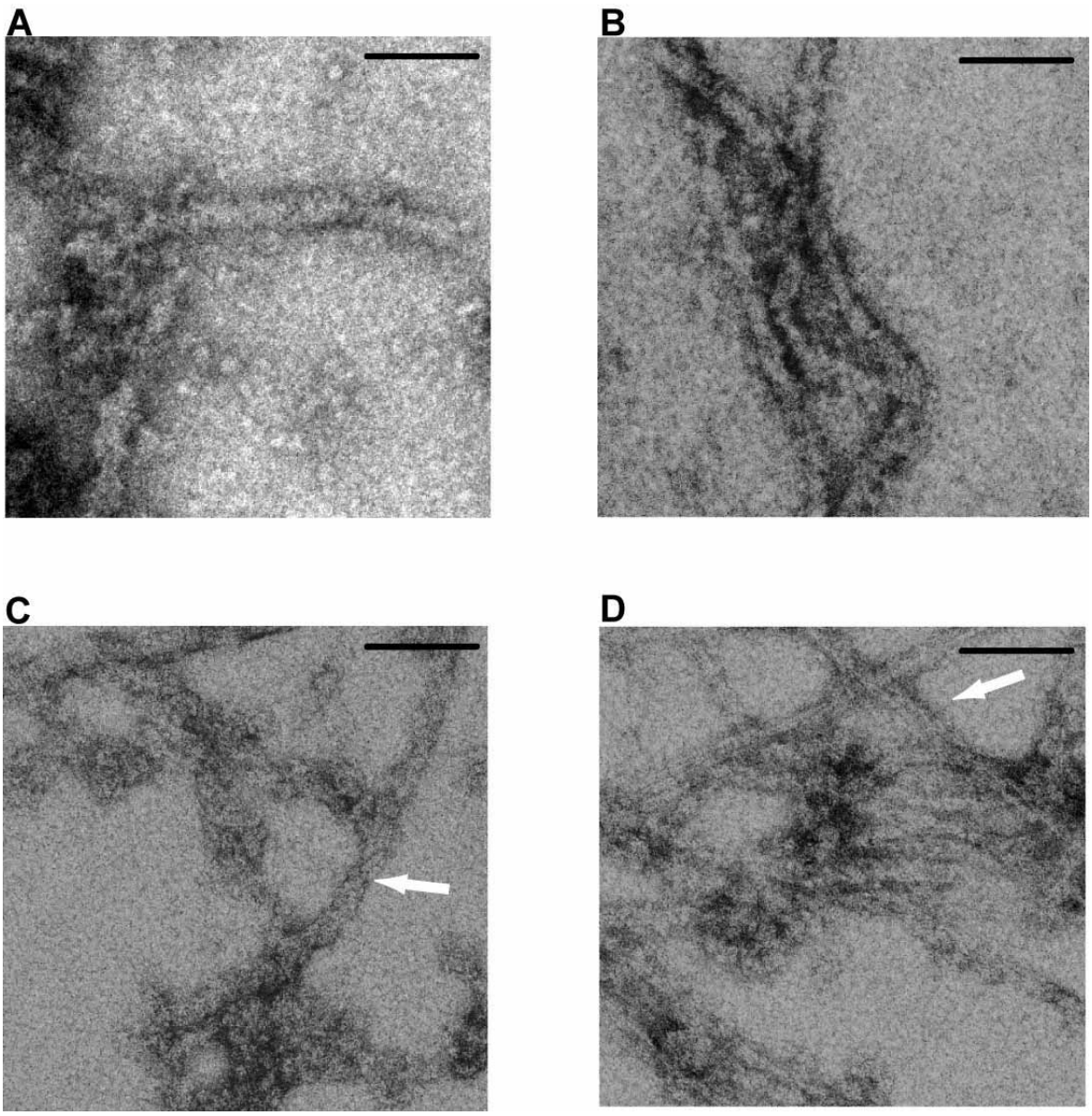

Figure 6-10: Temperature effects on fibril morphology – TEM analysis.
Negatively stained TE micrograph showing fibrils grown at different temperatures in a non-seeded reaction. A) 7°C B) 15°C C) 30°C D) 37°C Scale bar: 90 nm. The arrow indicates the described morphology (see text). Samples were fibrillated at 20 mM Tris/20 mM NaP 0.2 M NaCl pH 7.5

Figure 6-10 illustrates the effect of temperature on the morphology of fibrils. Figure 6-10A shows a fibril grown at 7°C with a compact morphology, but also

twisted fibrils were found at this temperature. The twisting becomes more clear and accentuated in Figure 6-10B and Figure 6-11C. Figure 6-11C shows protofilaments twisting around them. The arrow points to a region of smaller width due to the twist of the fibril. Figure 6-10D does not show a clear twisting but rather a parallel association of fibrils, leading to a clear change in the morphology of the fibrils at 30 °C and 37°C.

In order to verify if Ure2p display a cross-beta pattern and if this is affected by morphology, AFM and x-ray fiber diffraction were performed on fibrils at different temperatures.

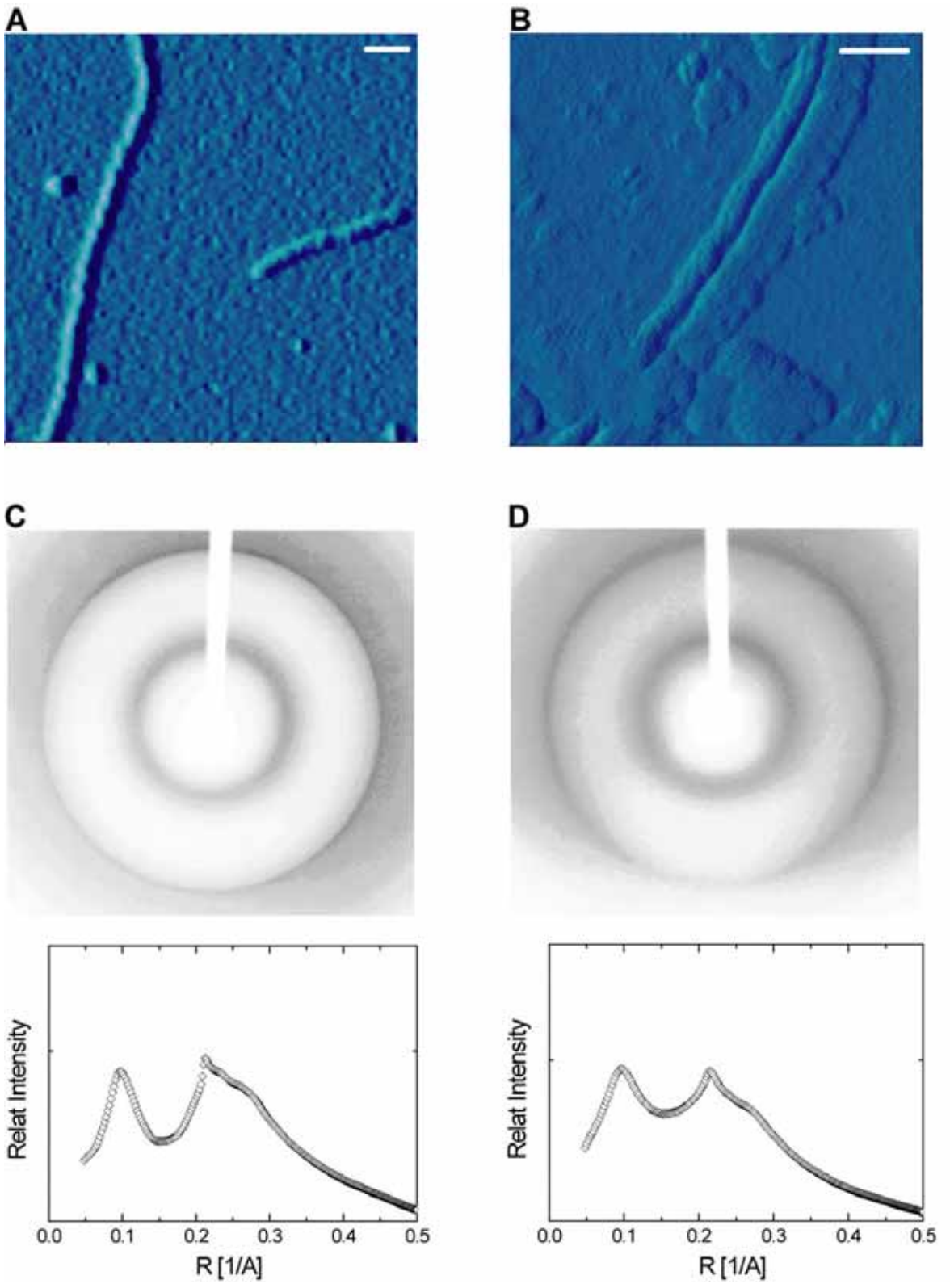

Figure 6-11 Analysis of the effect of temperature on fibrils

A) TM-AFM of a fibrillated solution at 30 °C. Scale bar: 200 nm B) TM-AFM fibril of solution fibrillated at 37 °C. Scale bar: 100 nm. X-ray diffraction patterns of fibrils grown (above) and averaged intensity of the reflections (under) at C) 30°C and D) 37 °C. Samples were fibrillated in 20 mM Tris/20 mM NaP pH 7.5 0.2 M NaCl.

Figure 6-11 shows AFM images of fibrils grown at different temperatures as well as the corresponding fiber diffraction images. Figure 6-11A, shows two fibrils of 8 nm which associate in a twisted manner (30°C). At 37°C (Figure 6-11BC, fibrils assemble in parallel and form a ribbon-like structure, similar to the one in Figure 6-10D.Despite this different assembly there is no difference in the height average between different temperatures (data not shown). Analyzing this data together with data obtained at 15 °C (section 4) and 4°C, one can conclude that temperature rather than ionic strength determines whether the fiber morphology is twisted or parallel. The analysis of the AFM data also indicates a decrease of the fibril height with temperature (data not shown). In order to verify that the fibrils contain cross-beta structure, X-ray fiber diffraction was carried out. Figure 6-11C shows the X-ray diffraction pattern of fibrils grown at 30°C. The diffraction pattern is characterized by intense reflections at 4.7 Å and broader reflections at around 10 Å. These results indicate a β-sheet conformation, in which the hydrogen bond distance is at 4.7 Å and the intersheet distance is 10 Å. This same pattern is displayed by fibrils grown at 37°C (Figure 6-11D), which have a parallel assembly morphology (Figure 6-10D and Figure 6-11B). The same patterns are seen for fibrils assembled at 15°C (data not shown) and at 4°C, as shown by Baxa (Baxa et al., 2005). This indicates that Ure2p fibrils have a cross-beta character similar to amyloids (Blake et al., 1996; Blake and Serpell, 1996) and Sup35 (Serio et al., 2000). The absence of meridional and equatorial difference patterns in these samples is due to the only partial alignment of the fibrils. Ure2p fibrils align very poorly, and an electron diffraction of single fibrils would be required to differentiate between these morphologies. Based on these results, it is likely that despite their differing appearance and assembly, Ure2p fibrils grown at different temperatures contain a common protofilament as showed for lysozyme (Jimenez et al., 2002). The differences in morphology are possible related to differences in the molecular structure of the involved protofilaments, as shown recently for $A\beta_{1\text{-}40}$ (Petkova et al., 2005) although this could not be shown here with these techniques.

6.5 Partial Discussion

The influence of pH, concentration, and buffer on Ure2p fibrillation has already been studied by Perret (Zhu et al., 2003b; Jiang et al., 2004). In all publications, 150 mM NaCl (or KCl) were used. According to the results presented here and those of Perret (Zhu et al., 2003b), Ure2p forms highly organized fibrils as shown by AFM and TEM. It also displays a certain insensitivity in the lag phase to change in protein concentration compared with other proteins that follow the nucleation polymerization model (Zhu et al., 2003b). Such an insensitivity has already been described for Sup35p (Serio et al., 2000) and other prion proteins. The kinetics obtained using ThT does not reflect the multistep pathway that is characteristic of Ure2p (section 4 and 5, fig 5.1, 5.2 and 5.4). It cannot show too, some processes like the association of protofilaments to higher hierarchical species or the effect of the concentration on the dimensions of the fibrils (that can be seen by AFM and TEM). One of the reasons could be that ThT only binds to certain elongated species. Thus, ThT kinetics was used mainly to determine the length of the lag phase. As the lag phase is caused by the slow formation of the nuclei and small oligomeric species, an increase of ionic strength likely increases the population of these species during the lag phase. A number of recent observations have been published about the role of electrostatic interactions and salts in the folding and conformational conversions of amyloid proteins, e.g. the increase in salt concentration lead to the increase of oligomerization in the cases of PrP(Apetri and Surewicz, 2003) and microglobulin(Raman et al., 2005). The increase of fibril formation and an optimum may indicate that the system arrives at an equilibrium directed to the oligomerization, allowing the formation of very organized structures. Perret and co-workers(Jiang et al., 2004) analyzed the Ure2p fibrillation using 150 mM NaCl and observed that twisted fibrils appear later in the stationary phase, suggesting that twisting is a result of the association of mature fibrils. In these experiments, this kind of fibrils was present since the beginning of the exponential growth of the curve and the twisted fibrils could be seen in all different lengths. The twisting was rather a result of the salt concentration and not of the long time fibrillation. The ThT fluorescence at the maximum is different for each salt. This is because of the characteristics of each of them:

Na_2SO_4 is a cosmotropic salt and can stabilize the native state of the protein more than the other salts, slowing down the fibril formation in relation to NaCl which is a weaker cosmotrope (Baldwin, 1996; Timasheff, 1998) NaI is a chaotropic salt and the I ion can interact with the peptide group and thereby possibly weakening some intermolecular interactions, thus slowing down the fibrillation process. The results here show that independent of the type of salt, Ure2p fibrillation is a multi-step process, which includes more than one intermediate during fibril formation. The formation of highly organized structures requires regular inter-molecular interactions involving some specific regions of the polypeptide chain. This may be driven by a kinetic and a thermodynamic process. Therefore, varying the environmental conditions like temperature and salt concentration can give valuable information about the forces that are involved in fibril formation and association. The dependence of the fibrillation process on salt concentration and changes in pH shows that the charge distribution on the protein influences the propensity of fibril formation (Section 5.2 and 5.3). Higher salt concentrations result in a screening of electrostatic repulsion and in a stronger tendency to make intra- and inter-molecular interactions. The lag phase is affected by the ionic strength of the solution and decreases with increasing salt concentration (Figure 6-1). This effect has been shown already for PrP by Surewicz (Apetri and Surewicz, 2003). According to CD and fluorescence experiments (not shown), salt has no effect on the secondary and tertiary structure of the protein. The results here represent an optimal salt concentration (different for each salt, Figure 6-6A and Figure 6-9) for efficient fibril growth. A similar result has been published for microglobulin (Raman et al., 2005) at low pH. One explanation for this effect would be that at lower ionic strength, the electrostatic repulsive forces are larger and the rates of aggregation processes become significantly slower. This would mean that thermodynamics rather than kinetics govern the system allowing well-organized structures to form. The kinetic effect of salt on fibril formation is shown by the rapid aggregation upon increasing salt concentrations (Figure 6-4A and Figure 6-6). When the aggregation is fast enough to restrict the mobility of the polypeptide chain, amorphous or poorly organized structures can form such as those observed here at high ionic strengths (Figure 6-5, Figure 6-6 and Figure 6-12). While the NTD has relatively little charged residues, both aggregation

and fibrillation are likely influenced by the C-terminal domain. It is difficult to conceive that Ure2p molecules aggregate or fibrillate via their NTD when the C-terminal domain carries a high net charge. Moreover, high salt concentrations will affect the hydration of the protein, because salt ions and the protein will compete for water molecules. Under these conditions, the polar residues may have a high tendency to engage in intermolecular hydrogen bonds by forming aggregates or fibrils. This change in kinetics goes to have an influence on fibril morphology, the twisting and the increase of filament assembly. Since the interactions observed between protofilaments are stronger at high salt concentration, it appears that electrostatic effects are particularly significant for protofilament assembly and variation in morphology. This effect can be the result of two factors: a) It can be linked to a neutralization of charges making it possible to form contacts that were previously unfavorable b) Another effect of salt is the dehydration of the protein surface. This would also increase the strength of hydrophobic interactions. With the neutralization of repulsive forces and the increase of exposed hydrophobic surfaces, it would be easier for the protein to associate. Hence, electrostatic forces are involved in the hierarchical assembly of Ure2p and the elimination of electrostatic repulsion can increase the amorphous aggregation. The data reported here about the ionic strength show that not only does it influence the rate of aggregation and the distribution of amorphous and fibrillar material, but it also affects the morphology adopted by the mature fibrils.

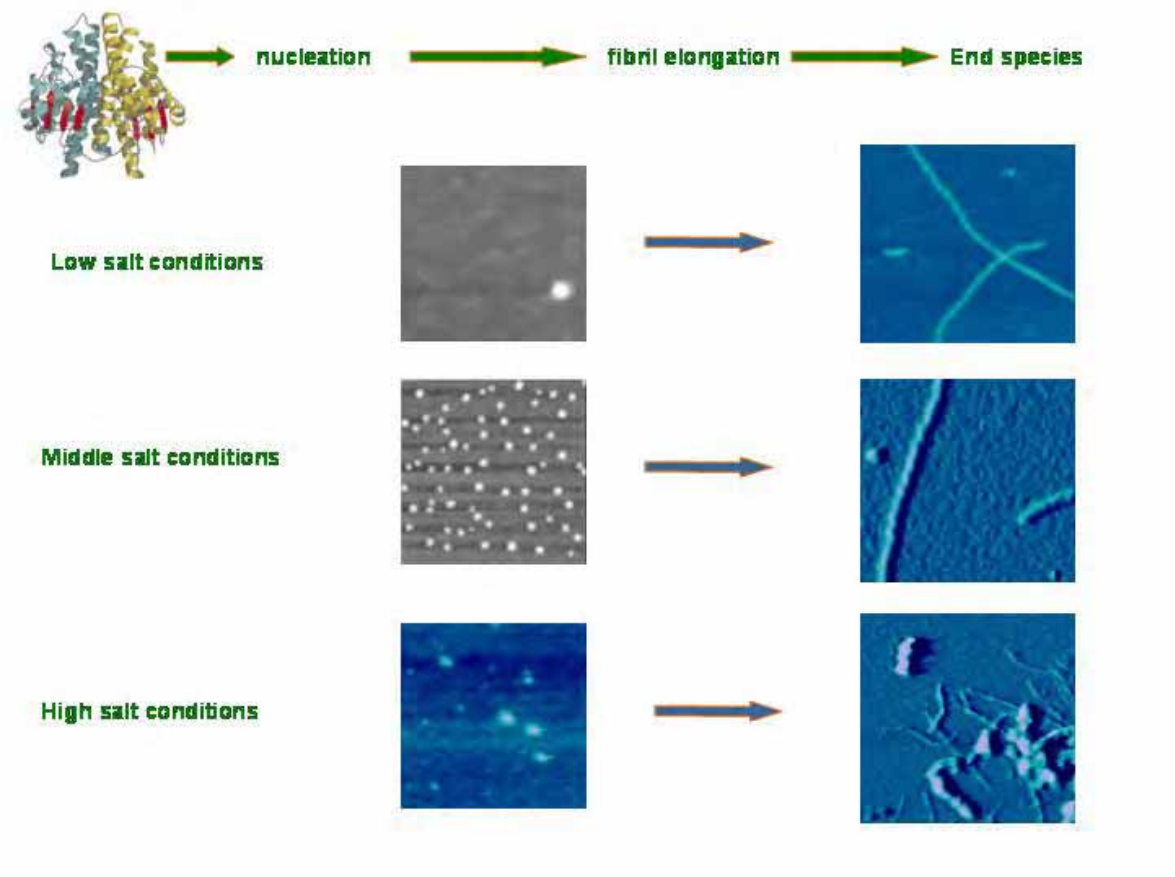

Figure 6-12: Scheme summarizing the effects of the salt concentration on fibril formation.
The figure shows AFM images obtained at different salt concentrations.

Fibrillation of Ure2p is a spontaneous process that could be observed at all temperatures studied. The basic pathway of Ure2p fibrillation is apparently temperature-independent: globular species form early, which subsequently transform into protofibrillar species and then into fibrils. Temperature, however, had a marked influence on the kinetics of fibrillation. According to the ThT data, the lag phase becomes shorter when the temperature increases (Figure 6-9AB). Heat increases the conformational mobility of the polypeptide chain, which in turn could accelerate conformational changes required for fibril formation (Figure 6-9CD). Also, there was an effect of temperature on fibril morphology. At low temperature, the population was dominated by twisted fibrils. Above 30°C, an increasing amount of parallel fibrils could be observed (Figure 6-10 and Figure 6-11). Above 40°C, analysis becomes more complicated because the C-terminal domain starts to unfold (Figure 6-9EF), which may have a major impact on the balance between fibrillation and non-specific aggregation. These results show that, at least in the case of the full-

length protein, a certain stability of the C-terminal domain is necessary in order to produce fibrils. The formation of aggregates at elevated temperature also precluded the evaluation of thermal unfolding transitions, making difficult obtain any valuable results. The results obtained in the region where the C-terminal domain is stable, shows that changing conditions (ionic strength or temperature) can accelerate both fibrillation and amorphous aggregates, although to a different extent. It is not clear yet, whether the separation between the pathway of non-specific aggregation and the fibrillar pathway is in an early event. Probably, the increase of aggregation is a result of non-specific interactions due to the hydrophobic dimer interface of the C-terminal domain. Perret and co-workers (Jiang et al., 2004) have done some screens concerning temperature but there was no clear-cut result. This may be because their samples were seeded (as shown in their discussion). In this case, their results would agree with the results for seeded solutions presented here. The twisting of the protofilaments generated by fibril association here shown is explained by Serpell (Serpell, 2000b). She showed that in order to pack protofilaments with a consistent interface they must twist, resulting too in the twisting of the β-strands.

7 The N-terminal domain of Ure2p

7.1 Structure prediction of Ure2p N-terminal domain

The N-terminal domain (1-94) of Ure2p (NTD) has an unusual amino acid composition, consisting of 36% Asn, 10%Gln, 11% of Ser, 5% Gly and 5%Thr. As shown in Figure 7-1, the Jigsaw algorithm predicts that more than 50% of amino acids adopt a random coil conformation. This may be due to the high content of Asn (Figure 1-7). The Asn-rich tract extends to residue 89 and it defines the prion forming domain of Ure2p.This unstructured region showed in Figure 7-1, may be responsible for the protease-sensitive of the N-terminal domain (Perrett et al., 1999) (Thual et al., 2001) (Pierce et al., 2005).

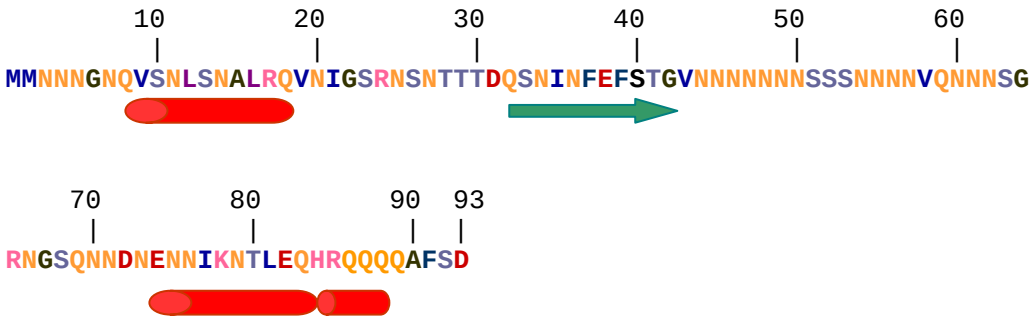

Figure 7-1: Secondary structure prediction of the N-terminal of Ure2p by Jigsaw. Helices are represented by cylinders and strands by arrows. Hydrophobic amino acids are represented with a dark color and hydrophilic/polar are represented with light colors.

The sequence contains 11 charged amino acids, of which 6 are negatively charged and 5 are positively charged. The NTD has a theoretical pI of 5.62 and a mass of 10471.73 Da. In the His-tag version, H6, the theoretical pI is 6.63 and the molecular mass was 11294.58 Da as can be calculated (Apweiler et al., 2004; Gasteiger et al., 2003). From the first 10 amino acids, 5 are polar as the majority of the amino acids between 43-63 sequence residues. These regions are believed to be a key in the oligomerization due to the high content of Asn. Deletion of the amino acids 15-29 has been shown that do not affect

the oligomerization (Zhu et al., 2003b), although this region can form fibrils alone (Baxa et al., 2005). Scrambling the amino acid composition of NTD still results in prions formation in vitro (Edskes and Wickner, 2002). This shows that the unusual amino acid composition of the NTD is responsible for the fibrillation.

7.2 Recombinant NTD-Ure2p purification

Plasmids NT-pET28 containing the N-terminal fragment 1-94, donated by Stefan Walter were transformed into *E. coli* BL21 (DE3) cells. The expression of the Ure2p fragment was carried out at 37°C for 10 hours (section 2.4.7). The NTD was found soluble in the supernatant fractions when bacterial cell extracts were clarified by centrifugation. The protein was purified under non-denaturing conditions and monitored by Coomassie blue staining. The protein was purified in two steps using a nickel-NTA Superflow column and a SEC chromatography. After elution from the SEC column, the protein was immediately frozen in liquid nitrogen and stored at -80 °C.

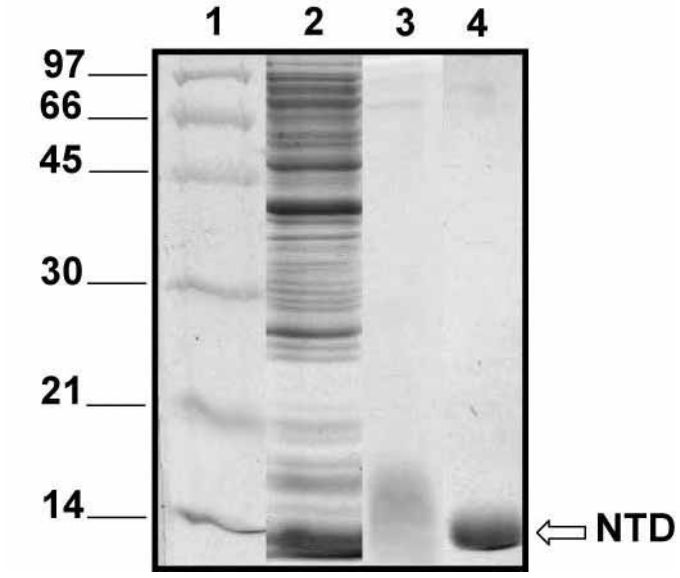

Figure 7-2: 15% SDS-PAGE staining summarizing the purification of the N-terminal domain purification

1) Molecular weight standard 2) Bacterial extract after expression of the NTD-His-tag after 10 hours of induction 3) Elution from the Ni-NTA column 4) Elution from SEC (Superdex 75pg)

Figure 7-2 shows that the N-terminal domain has a decreased electrophoretic mobility, running with a slight difference from the mobility of proteins of the same size protein from the marker. It can run as a double band in lower concentrations in the in the SDS-PAGE. This abnormal migration and staining behavior of Ure2p NTD in SDS-PAGE was already described by Prusiner (Schlumpberger et al., 2000) and Wickner (Baxa et al., 2003)._NTD-Ure2p presents a very weak coomassie blue staining due to the high number of polar amino acids. Samples were subjected to Mass spectrometry (data not shown), indicating a peak with an average molecular mass of 11,376 kDa. The his-tag could not be removed due the fact that the N-terminal domain has a cleavage by thrombin (Zhu et al., 2003b). Moreover, some studies indicate that the His-tag has no effect on the structural and functional properties of a self-assembly protein (Chang et al., 1999). The purification of the N-terminal domain from Ure2p has already been described in the literature. However in these cases, the purification was done using NTD fusions with enzymes (Schlumpberger et al., 2000) (Baxa et al., 2002) or under denaturing conditions (Baxa et al., 2003). This is the first time that NTD-Ure2p was purified in the soluble native state.

7.3 Concentration determination

NTD shows no UV absorbance signal between 240 and 400 nm due to absence of Tyr and Trp (Figure 7-3).The absorbance measurements were done at 205 nm. This region permits the determination of protein concentration without knowing the individual absorbance coefficients of the proteins (section 2.5.1). The concentration determination on the region of 205 nm is extremely sensible to salt conditions, pH variation and others impurities. The extinction coefficient was assayed in different buffer conditions and pH. Average value of $\varepsilon_{205}^{1\ mg/ml}$ 27.35 was determined (section 2.5.1). Due to the variability of the extinction coefficient at 205 nm, it was calculated in different conditions of the measurements.

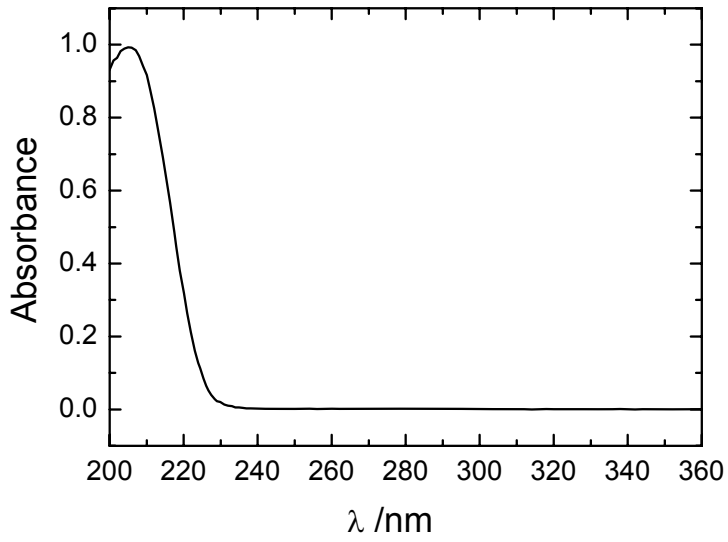

Figure 7-3: Concentration determination of NTD by UV absorbance.
The buffer used was 25 mM NaP pH 7.5, 20 mM NaCl. Cuvette path length: 0.1 cm.

The second method used was the Bradford assay using bovine serum albumin and Ure2p as references (data not shown). The Bradford assay has advantage over other staining methods and it is over 10 times more sensitive than the Lowry method. The only problem with the Bradford assay is that there is non-linearity between the absorbance of the Coomassie dye–protein complex and the concentration of protein. These characteristics restrict a reliable measurement of the concentration to certain regions of the graph. The concentration of NTD (in 50 mM Tris pH 7.5 200 mM NaCl) measured with Bradford assay was 0.68 mg/ml. The experimental error of the concentration measured at 205 nm in relation to Bradford method could reach up to 7% of variation. This may be related to the poor coomassie binding to the N-terminal domain.

7.4 Ure2p NTD fragment structure

In order to analyze the folding state of the purified NTD, a secondary structure analysis was carried out by CD spectroscopy (section 2.5.6). After the analysis of the folded state of NTD, it was tested if the NTD can change its conformation. Short polypeptides usually adopt a mainly unordered structure in

aqueous solution. The addition of some organic solvent (in particular TFE) mimics the environment in the interior of a protein molecule and often results in the helices (Del Vecchio et al., 2003). The NTD was diluted into different concentrations of TFE. Far UV CD spectra were recorded in the presence of TFE up to 50% v/v (0 to 7M TFE).

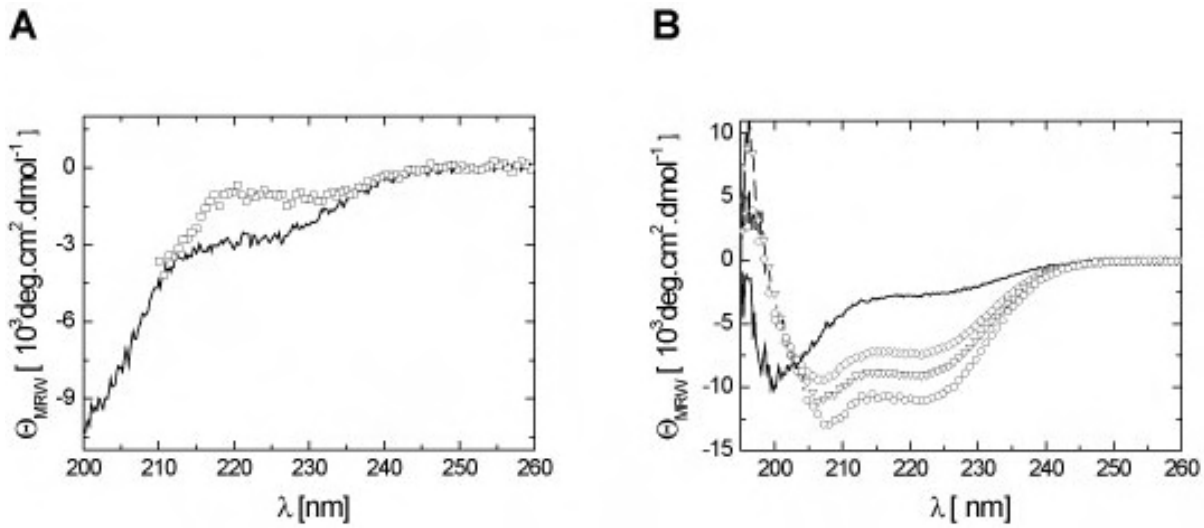

Figure 7-4: Secondary structure of the recombinant native N-terminal domain of Ure2p in different conditions.

A) Far-UV spectra of native NTD-Ure2p (-○-) and in 6 M GdmCl (—). Averaged spectra of 10 records for each sample are shown. Buffer NaP/Tris 200 mM NaCl pH 7.5, for native conditions and NaP/Tris 200 mM NaCl pH 7.5 6 M GdmCl for final concentration in denatured conditions. B) Far UV-CD of NTD until 50% v v^{-1} (7 M TFE). (—) 0 %, (-∇-) 25 % (3.5 M), (-○-) 30% (4.2 M) and (◊) 50 % (7 M) of TFE in NaP buffer, T=20 ºC. Pathlength: 0.1 cm.

Figure 7-4A shows CD spectra of the purified NTD in native and unfolding conditions (6 M GdmCl). The purified NTD under native conditions shows a minimum around 200 nm, with no significant ellipticity at >220 nm. These are characteristic of a non-structured protein although the spectrum is not similar to the protein under 6 M GdmCl. The deconvolution of the CD spectra for the native protein using CDNN shows a high content of random coil (55.5%) and a small content of α-helices (23.2%) and β-sheet (21.3%). This indicated that the secondary structure predicted from CDNN matches very good with the prediction of Jigsaw shown in Figure 7-1.The Figure 7-4B shows the far-UV CD spectra of the NTD between 0 and 50% (7 M). The graphic clearly shows that TFE modifies the structure due to an abrupt change of the spectrum, inducing non-native helical structure. Increasing the percentage of TFE in the solution

increases the content of secondary structure, i.e., the intensity of the helical band at 208 and 222 nm. This happens because the TFE stabilizes local interactions in partially folded peptides specially helices structure. This behavior of NTD clears differs from the full length Ure2p (figure 3.10) where at 25% (3.5 M) the spectrum changes to an aggregated state-like containing high content of β-sheet structure. This happens in the full length protein because it is folded and TFE weakens the hydrophobic interactions that stabilize folded states (Del Vecchio et al., 2003).

7.5 Self-assembly from NTD Ure2p

As reported previously the unfolded N-terminal domain has the capacity to self-aggregate (Schlumpberger et al., 2000) (Baxa et al., 2003). To verify this behavior, samples were let to fibrillate at 15 ˚C in 50 mM Tris, 0.2 M NaCl pH 7.5. The fibrillation pathway was followed by ThT (section 2.5.5), samples were analyzed by TEM and TM-AFM (section 2.6).

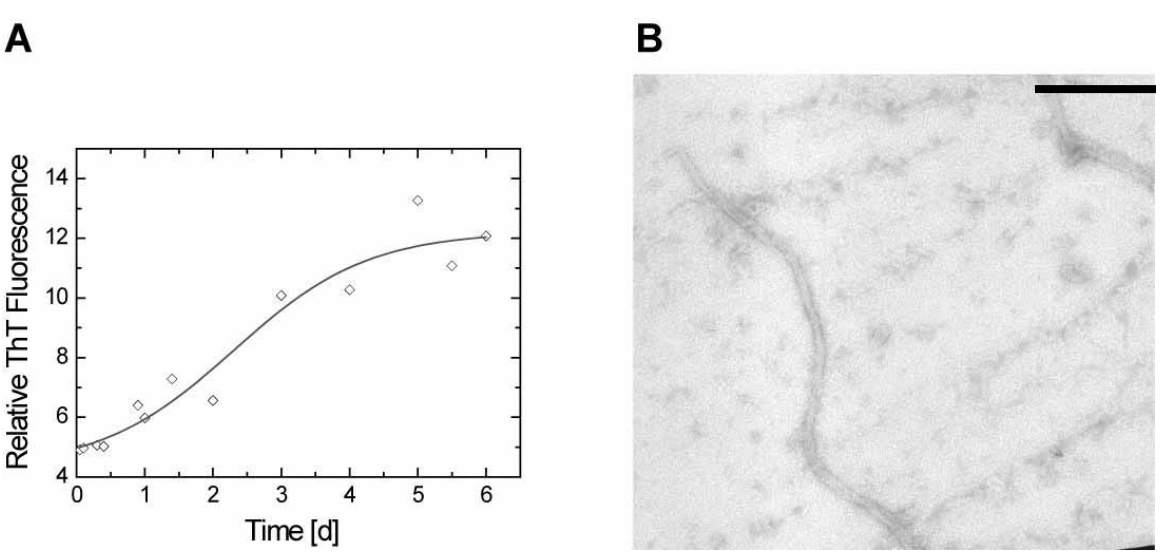

Figure 7-5: Self-assembly of NTD-Ure2p in TBS buffer.
A) ThT assay of Ure2p in Tris Buffer; B) TE micrograph of negatively stained sample after one week; Scale bar: 20 nm.

Figure 7-5 shows the ThT binding assay and a micrograph showing fibrils after 4 days of polymerization. The fibril formation of NTD follows the profile of the full length protein with a lag phase and an elongation phase in the ThT binding assay. Despite this similarity the time course is in days while for the full length it

is in hours. This could be the result of a very poor ThT binding in the N-terminal domain or a slower fibrillation rate. Measurements by TEM show a width of the fibrils around 20 nm due to the staining of the fibrils by Uranyl acetate. As shown before for amyloid protein (LeVine, III, 1993) and Ure2p (Jiang et al., 2004) (Bousset et al., 2003), the kinetics of fibril formation is characterized by a significant lag phase in ThT binding to NTD.

7.6 Fibril formation from Ure2p NTD fragment

The fibrillation pathway of the purified protein was analyzed using the ThT assay (Figure 7-5 and section 2.5.5) and AFM concomitantly (section 2.6).

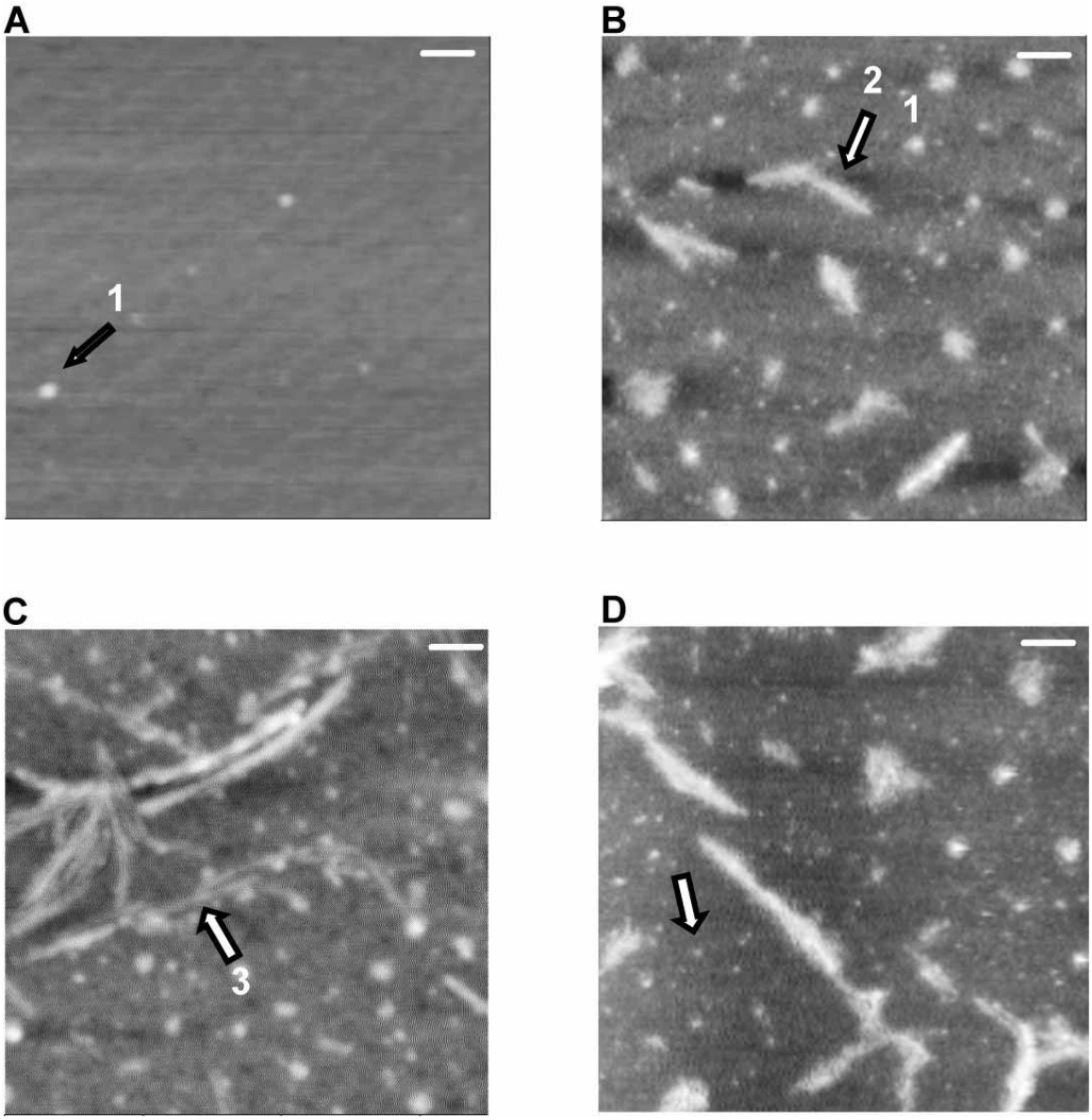

Figure 7-6: Fibrillation pathway of the NTD of Ure2p.

TM-AFM height images of fibril formation of soluble NTD at 55 μM under TBS buffer pH 7.5, T= 15 ˚C. Aliquots were added to mica, dried overnight. Scale bar is 200 nm. A) 1 day. B) 2 days. C) 3 days. D) 4 days. Species: 1- globular species, 2- protofilament, 3- thin protofilament like sheets

Figure 7-6 shows AFM images of dried samples prepared from a NTD polymerization kinetics in TBS. Spherical units of varying dimensions are observed following the initiation of fibrillation, suggesting a lag phase as already seen in the ThT Kinetics (Figure 7-5A). In the first 24 hours, only globular species (Figure 7-6A) could be detected. The height obtained from AFM shows values ranging from 1.0 to 2.0 nm for nucleation species. The presence of very thin fibrillar-form was observed after 2 days of reaction concomitantly with globular species (arrow 1). These globular species present in the images A and B, together with the ThT curve indicate that the fibril formation by NTD is a spontaneous nucleation process. Images B, C and D, show elongated pre-fibrillar species and fibrils. The pre-fibrillar species in image B and C has an average height of 2-4 nm (indicated with arrow 2).These different species found during the kinetics of fibril formation were analyzed by AFM in relation to height. Figure 7-6 B, C and D shows that during the fibrillation pathway globular, pre-fibrillar species and fibrils coexisted. The average height of fibrils after one week remained in the range of 4-8 nm. The height of spherical species matches with the height of ellipsoidal species and pre-fibrillar species. The globular and ellipsoidal species may thus represent precursors of the fibrillar species. The shape and size of globular aggregates forming during the NTD fibrillation pathway, resembled that of globular and protofibrillar species from Ure2p full-length kinetics (Jiang et al., 2004) and (figures 3.5 and 3.6), although the height and width are smaller for NTD species because of the lack of the C-terminal domain. There is a length variation between all the fibrils. Longer protofilaments were characterized by a clearly periodic substructure, with around 23 nm intervals. The mature fibrils measured after 2 weeks were around 4-10 nm in height and approximately 20 nm in width. Measurements by TEM show a width increase to 25 nm due to the staining of the fibrils by Uranyl acetate. One interesting observation was that no amorphous aggregates were found. All protein seems to be converted to fibrils.

7.7 Secondary structure of fibrils of the NTD fragment

To verify is there was any conformational conversion during fibrilization, soluble and unsoluble species were analysed.

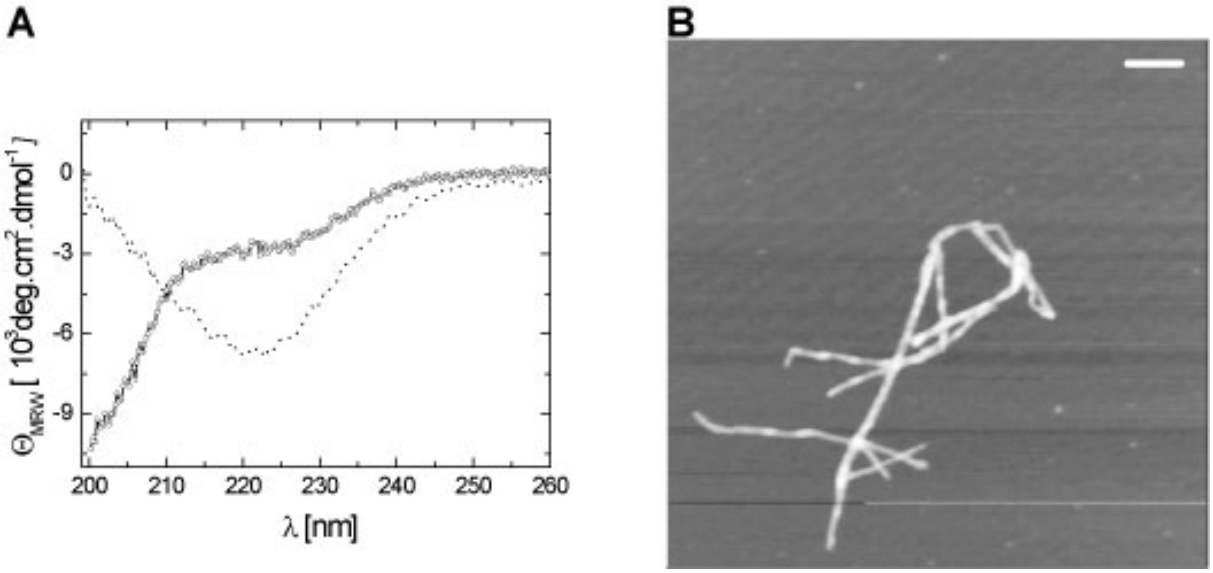

Figure 7-7: Fibril secondary structure from NTD fragment
A) Far-UV CD from NTD-Ure2p (----) and polymerized NTD fibrils (o); B) The NTD Solution was incubated at 30 ºC for fibrillation in 50 mM Tris pH 7.5, 0.2 M NaCl, scale: 100 nm.

Freshly thawed solutions of NTD in PBS showed a CD spectrum with a minimum at around 200 nm (Figure 7-4), characteristic of a protein with a high content of random coil. Upon incubation at 30 °C, for 1 week, the minimum around 200 nm disappeared and it was replaced by a characteristic β-sheet spectrum with minimum around 220 nm (Figure 7-7). The deconvolution of the spectra by CDNN is given in the Table 7-1.

Table 7-1: Deconvolution of the CD spectra from NTD fibrils.

Secondary structure	Monomer*	Fibril
α-helices	23	13%
β-sheet and turns	21%	50%
Random coil	56%	37%
Total	100%	100%

Table 7-1 shows the secondary structure content of the monomer and fibrils according with CDNN deconvolution. The fibrillation of the NTD leads to an increase of β-sheet content and a decrease in the α-helices and random coil content. This high content of β-sheet was shown by Prusiner (Schlumpberger et al., 2000) using FTIR for the N-terminal fibrils secondary structure. In this case, fibrils were polymerized with the fusion protein and then the N-terminal fibril was cleaved off and separated form the fusion protein.

7.8 Fibril formation of the N-terminal domain at different conditions

7.8.1 Fibril formation at different pH values

To verify if NTD-Ure2p form fibrils at same pH of full length protein, NTD-Ure2p was let to fibrillate at different pH and analyzed by AFM.

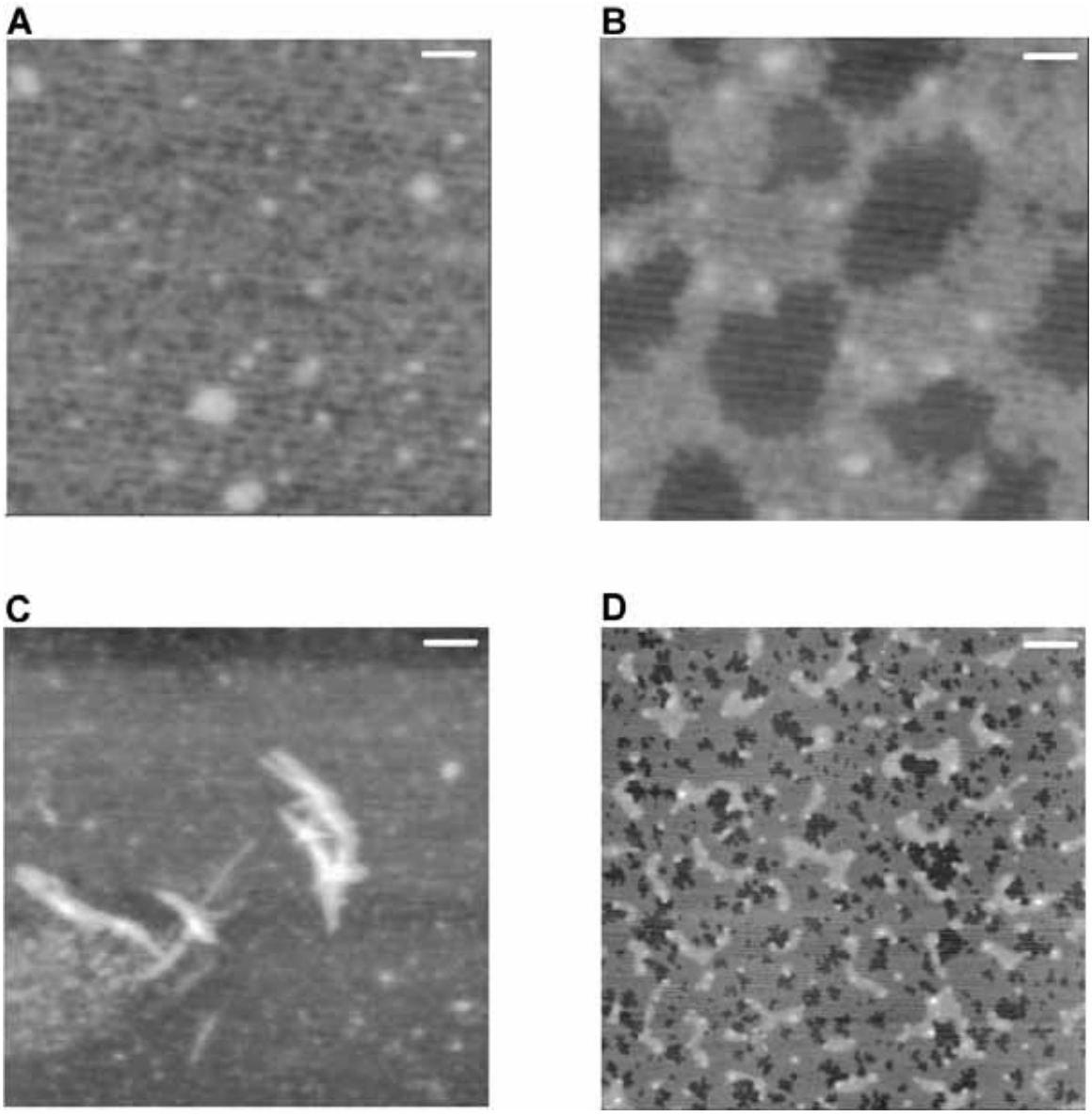

Figure 7-8: pH effect on NTD fibrillation

NTD solution was incubated at different pH in acetate or NaP, 200 mM NaCl, T= 20 ºC, the dimensions and the scale is variable for each image. A) pH 5 at 20 mM Acetate buffered saline solution, scale bar: 75 nm, height gray scale: 10 nm. B) pH 6.5 at 20 mM PBS buffer, scale bar : 75 nm, height gray scale:10 nm C) pH 7.5 at 20 mM PBS buffer, scale bar : 200 nm, height gray scale: 30 nm and D) pH 9.0 at 20 mM PBS buffer, scale bar : 100 nm, height gray scale:10 nm

Figure 7-8 shows the result of NTD solution left to polymerize in different pH. Images A, B and D show amorphous globular species and soluble protein present in the solution but no pre-fibrillar or mature fibrils were seen under these conditions (even after 1 month -data not shown). Only image C shows a small spherical species, pre-fibrillar species and mature fibrils. This shows that that fibril formation and elongation is a pH dependent process and that neutral pH is required for the formation of fibrils. These results agree with the results of

Ure2p full length. This means that protonation of some amino acids like His can have some effect in repulsion and avoid fibrillation, requiring a neutral environment. To analyze this, the pH of a fibrillating solution at pH 7.5 in early stage of fibrillation was changed to lower pH (6.5). There was no increase in the length of fibrils and the number of longer fibrils over time in comparison with fibrils of another sample formed in pH 7.5 (data not shown). It is possible to conclude that a balance of charges is required for the fibrillar formation of the NTD and for its elongation. This implies that different charges may be involved in the fibril elongation. Moreover the incubation of NTD solution in the presence of different concentration of TFE (as shown in Figure 7-4B) and arginine completely abolishes the fibrillation of the Ure2p NTD domain (data not shown)

7.8.2 NTD fibrils form at different temperatures in a hierarchical manner

In order to see if differences in the incubation temperature had effects on the morphology of NTD fibrils, solutions of NTD-Ure2p in the stationary phase at different temperatures were analyzed by AFM .

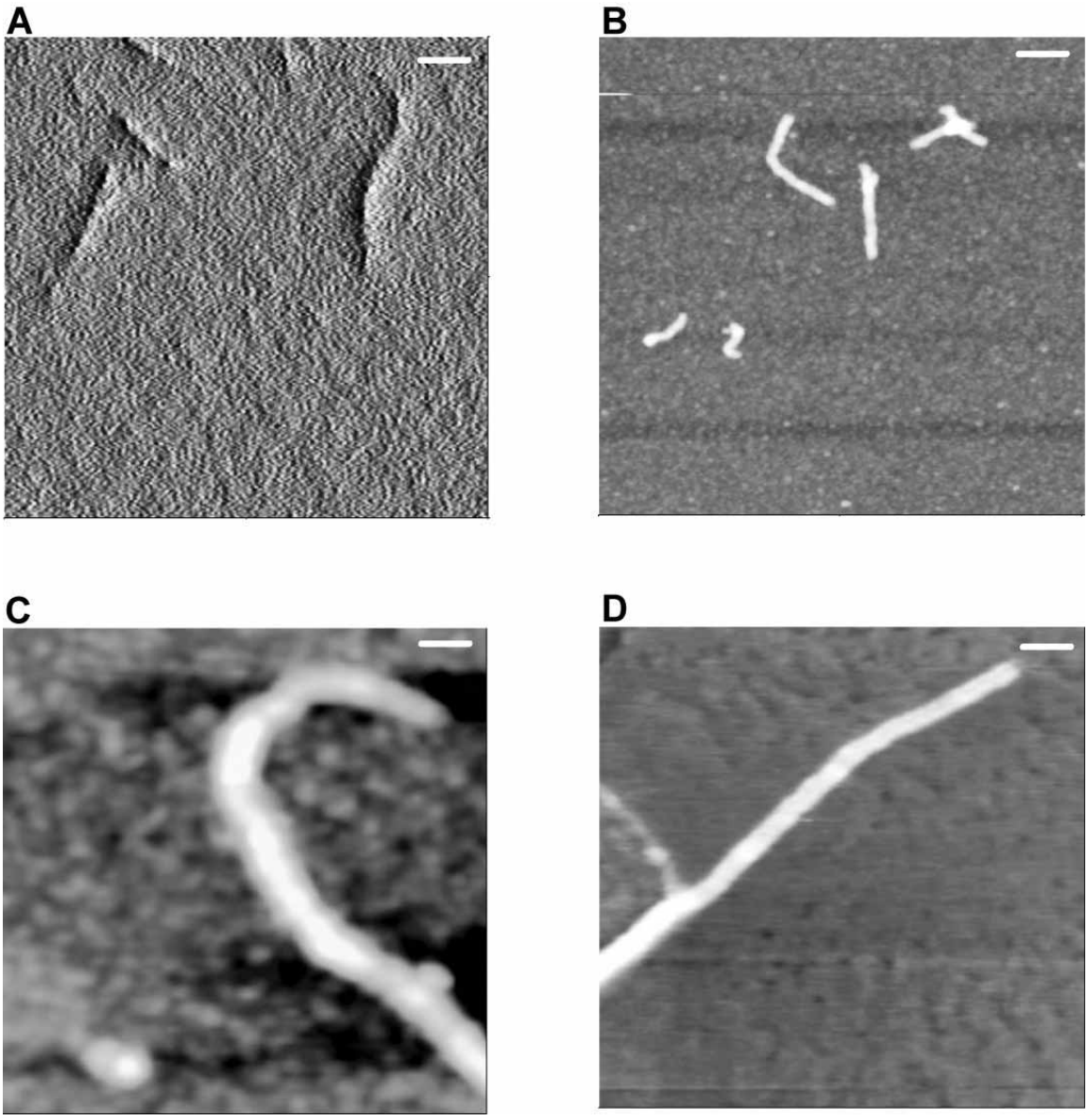

Figure 7-9: NTD solution fibrillated at different temperatures.

AFM images, time = 1 week and NTD concentration: 55 μM. A) T = 4 ºC (in amplitude); b) T = 15 ºC, gray scale 40 nm; C) T = 37ºC, gray scale is 15 nm and D) T = 45ºC, gray scale 40 nm. Scale bar is 200 nm for A, B and D: 100 nm, C: 50 nm.

Figure 7-9 shows fibrils formed at different temperatures. Analysis of the cross-section of the height images shows a increase of the height average of the fibril from around 3 nm (4 ºC) to 8-10 nm height (15, 37, 45 ºC, Figure 7-9BCD and 30 ºC, Figure 7-7B). In none of these conditions amorphous aggregates could be observed. At all temperatures, protofibrils elongate and become less numerous over time, suggesting ongoing association. Figures C and D show fibrils that are the result of an intertwined association (C) and parallel association (D). With this result it is possible to conclude that NTD form fibrils in a hierarchical manner. Although hierarchical behavior could be seen in NTD

fibrils, it could not be observed a morphological behavior like in the Ure2p full length protein. Higher temperature produces a higher height average, but the repeating units are around 25 nm (AFM data not shown).

7.9 A comparasion between NTD and full length fibril

In order to verify that if the NTD fibrils contain cross-beta structure, X-ray fiber diffraction was carried out. The pattern was compared with Ure2p fulllenght fibrils.

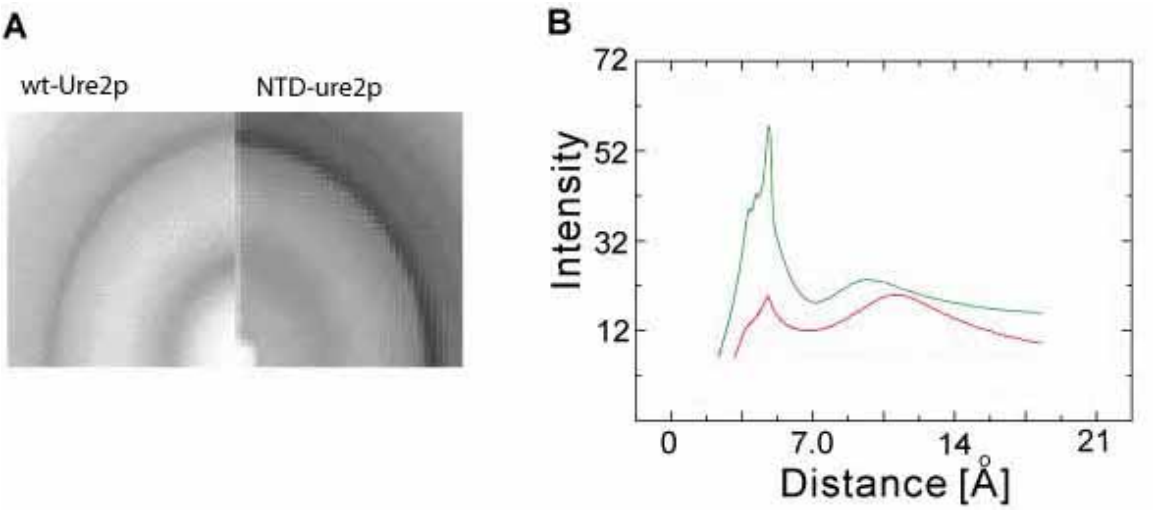

Figure 7-10: Comparison between full length Ure2p and NTD domain fibril diffraction pattern.

X-ray diffraction patterns of fibrils grown (A) and (B) averaged intensity of the reflections of Ure2p full length (red) and NT domain fibrils (green). Samples were fibrillated in 20 mM Tris/20 mM NaP pH 7.5 0.2 M NaCl at 37 °C.

Figure 6.10 shows the X-ray diffraction pattern of fibrils grown at 37°C. The diffraction pattern of Ure2p full length is characterized by intense reflections peak at 4.7 Å and broader reflections peak at around 10 Å (as showed in Figure 6-11). The diffraction pattern of the N-terminal domain is characterized by sharp reflections peak at 4.7 Å and difuse reflections peak at around 10 Å. These results indicate a β-sheet conformation for the full length protein and the C-terminal mutant.Figure 6-10B shows the average reflections of the both fibril type. The N-terminal display a difference of intensity on the 4.7 Å that is responsible for the hydrogen bond distance. Another difference is a average peak at around 9 Å responsible for the the intersheet distance. This difference

may happen due to the easier packing from the N-terminal domain because it is a smaller molecule. The presence of the C-terminal domain would increase the intersheet distances. These results are similar to the prion protein results obtained using x-ray fiber diffraction. On this way, these experiments indicate that similar to the full length protein, the N-terminal domain fibrils has a cross-beta character similar to amyloids (Blake et al., 1996; Blake and Serpell, 1996) and Sup35 (Serio et al., 2000). Based on these results, it is likely that despite their differing appearance and assembly, Ure2p fibrils grown at different temperatures contain a common protofilament as showed for lysozyme (Jimenez et al., 2002).

7.10 Partial Discussion

Full-length Ure2p and the N-terminal domain, NTD, show a number of similarities in these analyses. In the case of the full-length protein, both its conformation and fibrillation appear to be dependent on the physical environment (sections 2 and 4). As already has been shown, the N-terminal domain of Ure2p is responsible for fibrillation (Taylor et al., 1999; Speransky et al., 2001; Baxa et al., 2004). It is largely unfolded in solution (section 6) and displays the typical behavior of an intrinsically unfolded protein (see section 1.4). The NTD adopts a β-sheet conformation upon fibril formation (section 6) (Baxa et al., 2005), similar to the NM-Sup35p(Serio et al., 2000). The CD spectra obtained for the fibrillated NTD (section 6) agree very well with the CD spectra of the 'unfolded' nuclei in GdmCl (section 4 and 6). This indicates that the NTD is responsible for the β-sheet formation in the full-length protein, while the structure of the C-terminal domain is not altered in the fibril (stability and intrinsic fluorescence data - section 4). These results agree with data from Melki(Bousset et al., 2002) who showed that the C-terminal domain binds glutathione with similar affinities in dimeric and in fibrillar Ure2p.

Another similarity is that both full-length Ure2p and the N-terminal domain do not form fibrils in organic solvents. In a helix-promoting solvent such as TFE, the N-terminal domain adopts a helical conformation, whereas full-length Ure2p aggregates (section 3 and 6). In both cases, TFE induces a non-native

conformation that blocks the fibril formation. This probably happens because the polypeptide backbone, which is essential for fibril formation, becomes inaccessible. It is possible that some backbone non-local interactions are important for fibril formation, and TFE hides regions responsible for that. The behavior of Ure2p in TFE is different from that of some globular proteins like AcP(Chiti et al., 1999; Monti et al., 2004). In the case of ACP, TFE enhances the exposition of the amyloidogenic sequence of the protein, and stimulates fibril formation. Another possibility would be that the addition of TFE reduces the flexibility of the backbone in the N-terminal region, which may be important for fibril formation. This is in agreement with data from Wickner (Pierce et al., 2005), who concluded based on NMR studies of Ure2p that a large number of asparagine and glutamine residues are flexible in the full-length protein.

According to results from ThT assays, the polymerization of the NTD is a two-step process (nucleation and elongation), in which a nucleation event is the rate-limiting step (as shown by the existence of a lag phase - section 6). The current model in the literature that can kinetically express the fibrillation of the NTD is the NCC mechanism proposed by Lindquist for Sup35p (Serio et al., 2000) (section 1.5). ThT results show that nucleation for the isolated N-terminal domain occurs more slowly than for full-length Ure2p. There are possible several reasons:

a) The isolated N-terminal domain in ‘native’ buffer makes some ‘inhibitory’ interactions, which do not occur in the presence of the C-terminal domain. Baxa (Baxa et al., 2005; Pierce et al., 2005) suggested that the fibrillation process of the N-terminal domain purified under denaturing conditions starts immediately after removal of the denaturant by dilution in native buffer. Although it is difficult to compare these data with the ones presented here because the conditions were different, it suggests that these ‘inhibitory’ interactions are broken in GdmCl and once they are broken the fibrillation starts. One candidate region for making native interactions with the C-terminal and for non-native interaction within the N-terminal could be residues 71-94. Wickner showed that the mutant △71-95 of the full length protein has an increased ability to form the [URE3] phenotype compared with the wt-type protein (Pierce et al., 2005).

The issue of interaction between the C-terminal domain and the N-terminal domain has been investigated in a number of studies, but so far there is only evidence *in vivo* from Wickner's (Maddelein and Wickner, 1999) and Cullin's groups (Fernandez-Bellot et al., 1999). According with Wickner (Maddelein and Wickner, 1999), the C-terminal domain has some "inhibitory" segments which can decrease the probability of yeast cells to acquire [URE3]. Once these promoting regions are deleted, the fibrillation occurs more rapidly at its 'intrinsic' rate. Cullin suggested that there are interactions between the N-terminal part and the C-terminal part (Fernandez-Bellot et al., 1999) after analyzing some mutants *in vivo*. Later on, using NMR, Wickner could not clearly confirm this interactions *in vitro* using other mutants(Pierce et al., 2005) although he said that the interaction could be the only explanation for the enhancement of the prion forming ability in the studied mutants (*in vivo and in vitro*).

One suggestion why it was not possible to detect this interaction *in vitro* is the buffer conditions. All *in vitro* experiments were done at high salt concentration. The results of this thesis show that full-length Ure2p has an enhanced tendency to fibrillate in presence of increased salt concentration. Probably, the C-terminal domain and N-terminal domain interact via charge-charge interactions, which are screened in high buffer and the NTD is free to fibrillate. This would agree with the fact the region 65-94 is a highly charged region. In this scenario, people would fail to observe this interaction in their experiments.

8 Discussion

8.1 A structural model for Ure2p

Knowledge of the fibril structure is essential for understanding the molecular mechanism of amyloid formation and to show a conformational conversion upon fibril formation. A number of fibrils has been shown by X-ray fiber diffraction to have cross beta structure, e.g. Sup35p (Serio et al., 2000), amyloid peptides (de la Paz and Serrano, 2004), microglobulin (Ivanova et al., 2004), Sup35p peptide (Diaz-Avalos et al., 2003) and Aβ peptide (Serpell, 2000b; Serpell, 2000a).

The results of fiber diffraction from dried fibrils obtained in this work show a structural β-core, or so-called cross-β structure, irrespective of the morphology of the fibrils and of the temperature at which they were grown. There is a average reflection peak at 4.7 Å, representing the β-strand distance, and an average reflection peak around 10 Å, coming from the pleated β-sheet, respectively. This is reproductible for Ure2p fulllenght and N-terminal domain fibrils. A comparison between the crystal structure (section 1.7) of the dimeric protein and the interpretation of the x-ray patterns (section 5) shows that the fibril presents a cross-beta structure while the crystal structure shows not sign of cross-β-stacking. This result (X-ray fiber diffraction, section 5) together with the CD spectra of the NTD fibrils (section 6) and the CD spectra of the fibrillation intermediate of the full-length protein (section 4) clearly demonstrates that a conformational change occurs upon fibrillation.

The x-ray diffraction pattern is characteristic of a cross-β-structure, implying that the β-sheet lie approximately perpendicular to the fibril axis. The results here obtained do not permit to imply whatever the β-strands are parallel, antiparallel or mixed. The degree of twisting doesn't permit to conclude it, too.

The inter-strand and inter-sheet distances averages peak (4.7 and around 10.0 Å, respectively) for Ure2p fibrils are in agreement with results from the Steven

group for Ure2p fibrils at 4°C (Baxa et al., 2005). Since these reflections are not changing with the temperature, the only discussion possible is that temperature may lead to increasing the number of amino acids incorporated in the β-sheet due to the unfolding of the C-terminal domain (section 5). This conclusion is supported by the analysis NTD fibrils formed at different temperatures (section 6). There is no change in morphology due upon temperature variation in the N-terminal fibrils. There is only an increase in the number of protofilaments assembled.

Melki reported X-ray fiber diffraction of Ure2p filaments and shows that he could not observe the reflection at 4.7 Å(Bousset et al., 2002). This problem also appeared in the experiments shown when fibrils were 'contaminated' with amorphous aggregates that influence in the alignment of the fibrils. One explanation for the reason that he could not see would be not enough alignment or too much amorphous aggregates together with fibrillar species(Baxa et al., 2005).

Baxa suggested a pleated sheet model in a shape of a serpentine (Kajava et al., 2004; Kajava et al., 2005) (Figure 1.8B). This model does not consider that fibrillar Ure2p may be a water-filled nanotube (result from section 4), as suggested by Perutz for Sup35p (Perutz et al., 1994) (Perutz et al., 2002a) Although the model of Baxa (Kajava et al., 2004) is very nicely presented and is based on a cross-β structure (Baxa et al., 2005), its assumption that Ure2p fibrils are solid tubes is based on the dimensions calculated by TEM. These dimensions do not consider a staining enlargement and does not agree with the AFM data obtained until now (section 4, 5 and 6). Other problems is that the data from Baxa were acquired using dried fibrils in air, and this could lead to a shrinking of the nanotube generating a stacking of the β-sheet.

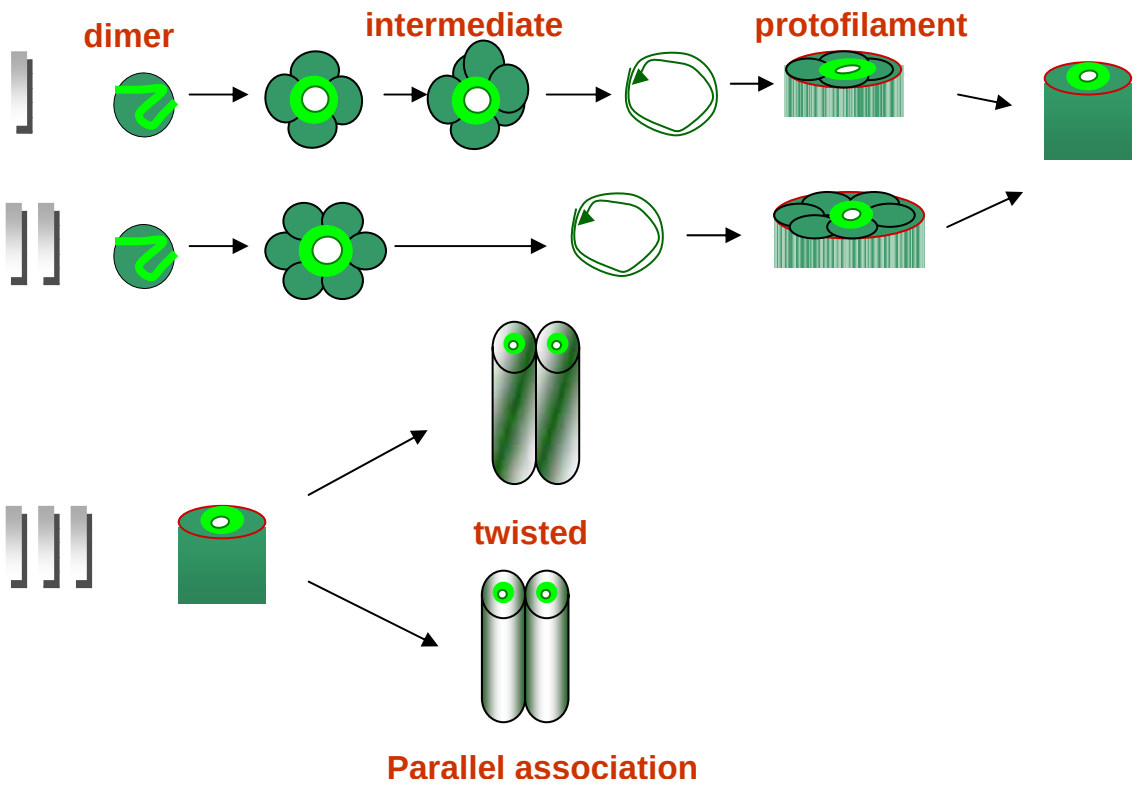

Figure 8-1: scheme for ure2p fibrillation pathway considering the conformational conversion to intermediate species (detailed scheme from figure 4.16).
The fibrillations pathway start with the dimer (in green) with the C-terminal domain marked in dark green and the N-terminal domain marked in light green. From the dimeric specie, an intermediate specie is formed with the C-terminal domain remaining outside. The intermediate specie can be composed of 4 monomers and increase to 6 monomers (pathway I) or start with 6 monomers (pathway II). A alternative pathway composed of pathway I and II at the same time is also considered. The globular species start to elongate in a circular form where the N-terminal is inside of the fibril generating the pathway (III). The assembly by twisting or to parallel assembly can be influenced by a combination of diverse factors like the orientation of the β-sheets and hydrophobic region (dark green) of the C-terminal domain (pathway III).

Figure 8-1 shows a scheme based on figure 4.16 where the conformational conversion is incorporated to the model presented and the main species are showed. The fibrilization start from a dimeric species generating a intermediate species composed of 4 monomers (pathway I) or 6 monomers (pathway II). The elongation happens with the addition of ure2p in an organized way where the C-terminal remains outside and the fibrilized N-terminal domain is buried inside.The assembly procedes in a beta helix way (Figure 1.5B). The high polarity of the C-terminal domain suggests that can be a water filled nanotube. Small protofilaments and longer protofilaments can assembly in parallel or twisted manner according with the orientation of β-sheets and hydrophobic region (dark green) of the C-terminal domain (pathway III).

The morphology data obtained in this thesis support a model similar to the model proposed by Pedersen (Li et al., 1999; Blake et al., 1996) for amyloids, in which the pleated sheet would form the core of the amyloid although this model would not be satisfying for Ure2p fibrils data obtained here. A more satisfying model due to the X-ray fiber diffraction data would be that the pleated sheet would stack in helices forming a β-helices model as already suggested by Perutz(Perutz et al., 2002b; Perutz et al., 2002a) and Lindquist for Sup35(Krishnan and Lindquist, 2005) and Prusiner(Wille et al., 2002) for PrP. This may be confirmed in future experiments and simulations and assembled in a beta helix form (Kishimoto et al., 2004; Krishnan and Lindquist, 2005).

The data obtained in this work are in good agreement with data for polyQ, Sup35, PrP, and beta amyloid. Despite that some details are particular for every protein, in general Ure2p can be considered as a good model for amyloid proteins because it shares a large number of features with them. The Yeast prion denomination fits very well due to the similarities to PrP.

8.2 Final Considerations about the conformational conversion of the N-terminal domain from ure2p.

Analyzing the results about Ure2p it is possible to say that the first step here uncovered is the nuclei, or one of the smallest specie detectable on the pathway. As shown by kinetic data, this is a slow process, a kind of unlikely event. This probably only happens when the chains comes correctly in the right conformation avoiding repulsive interactions. Only at this point is possible that nucleation can happen. Once this process happens, then fibril can grow more rapidly by additions of chains successively, without stop. Since that fibrils are more stable then the dimer, this means that the fibril formation is a kinetically process going to the lowest state of energy.

This fibrillation pathway makes it possible to do an analogy to the protein folding pathway where there is a specific sequence of events that has to happen during the folding process. To the other hand, our knowledge about fibrillation of the unfolded N-terminal of ure2p (and the full length) might profit

with the nucleation-condensation picture envisaged by Fersht (section 1.3.2) (Fersht, 2000). His picture of folding is that a certain set of amino acids must be ordered in a specific way (this would be the nucleus formation or lag phase), and after that the rest of the protein chain can rapidly condense into the native structure (this would be the elongation process or the seeding process).

According with Fersht (Daggett and Fersht, 2003), the “nucleation” event would happens when a small number of amino acids comes together to form a critical core that drives the formation of the final structure. This could be here applied too and it would suggest transitional specie where the conformation happens. Considering the data here shown it is not possible to infer where is positioned this transitional species - before the smallest species detected or after that.Some recent breakthrough in science like single molecule experiments (Rief et al., 1997) (Cecconi et al., 2005) may give contributions to this problem.

This data shows that ure2p fibrilizates in a folding/misfolding pathway.On this way, folding and misfolding of Ure2p can be use in a “profitable” way by the yeast. The unffolding of Ure2p and sequent Misfolding to oligomeric and stable species may help to keep the infectious inheritance of yeast, in a way that the phenotype can be passed to the daughter cells without being destroyed by the normal cell quality control.

9 Conclusion

The growing numbers of severe diseases has been attributed to cellular protein aggregation, has increased in the literature in the last 10 years, and between these are very known diseases like Alzheimer's disease, Chorea-Huntington, and Amyotrophic Lateral Sclerosis. To develop medicaments it is necessary to understand the mechanism of folding and misfolding that generate these diseases. In this thesis, the dimeric wild-type protein and an N-terminal domain mutant were purified and characterized in relation to structure and stability. Results showed that Ure2p, the protein responsible for the [*URE3*] prion phenotype of *Saccharomyces cerevisiae,* shares many features with mammalian prions, poly-glutamine related disorders and many other misfolding diseases. On this point, Ure2p protein has become a good model to study amyloid diseases. The results here suggest that the N-terminal domain of Ure2p is essential for prion formations. Polymerization kinetics of wild-type protein and mutant were investigated under varying conditions e.g. salt concentration, salt type, temperature, pH and buffer, and the resulting fibrillar states were characterized. Fibrillation of Ure2p is a spontaneous process that could be observed at all conditions here studied. The increase of the salt concentration and temperature increases fibrillation. This shows that kinetics plays a strong role upon fibrillation. Moreover, the mechanism of fibril formation was studied by isolating soluble oligomeric species (nuclei) and characterizing them with respect to size and structure. The conversion of Ure2p into a structure with a higher content of β-sheets was demonstrated for both fibrillation intermediates and mature fibrils. These results support the crucial role of the N-terminal domain for conformational conversion and fibril formation, while the structure of the C-terminal domain is very similar in dimeric and fibrillar Ure2p. The results here obtained shows that ure2p fibrilizates in a folding/Misfolding pathway similar to Misfolding diseases. On this way, folding and Misfolding of Ure2p can be use in as a model system for studying protein Misfolding diseases.

10 Bibliography

Reference List

Albanese,V. and Frydman,J. (2002). Where chaperones and nascent polypeptides meet

3. Nat. Struct. Biol. *9*, 716-718.

Anfinsen,C.B. (1973). Principles that govern the folding of protein chains

2. Science *181*, 223-230.

Apetri,A.C. and Surewicz,W.K. (2003). Atypical effect of salts on the thermodynamic stability of human prion protein

1. J. Biol. Chem. *278*, 22187-22192.

Apweiler,R., Bairoch,A., Wu,C.H., Barker,W.C., Boeckmann,B., Ferro,S., Gasteiger,E., Huang,H., Lopez,R., Magrane,M., Martin,M.J., Natale,D.A., O'Donovan,C., Redaschi,N., and Yeh,L.S. (2004). UniProt: the Universal Protein knowledgebase

1. Nucleic Acids Res. *32*, D115-D119.

Bai,M., Zhou,J.M., and Perrett,S. (2004). The yeast prion protein Ure2 shows glutathione peroxidase activity in both native and fibrillar forms

1. J. Biol. Chem. *279*, 50025-50030.

Bailey,J.E., Beaven,G.H., Chignell,D.A., and Gratzer,W.B. (1968). An analysis of perturbations in the ultraviolet absorption spectra of proteins and model compounds

3. Eur. J. Biochem. *7*, 8-14.

Balbirnie,M., Grothe,R., and Eisenberg,D.S. (2001). An amyloid-forming peptide from the yeast prion Sup35 reveals a dehydrated beta-sheet structure for amyloid

2. Proc. Natl. Acad. Sci. U. S. A *98*, 2375-2380.

Baldwin,R.L. (1996). How Hofmeister ion interactions affect protein stability

1. Biophys. J. *71*, 2056-2063.

Balguerie,A., Dos,R.S., Ritter,C., Chaignepain,S., Coulary-Salin,B., Forge,V., Bathany,K., Lascu,I., Schmitter,J.M., Riek,R., and Saupe,S.J. (2003). Domain organization and structure-function relationship of the HET-s prion protein of Podospora anserina

2. EMBO J. *22*, 2071-2081.

Baneyx,F. (1999). Recombinant protein expression in Escherichia coli

5. Curr. Opin. Biotechnol. *10*, 411-421.

Baskakov,I. and Bolen,D.W. (1998). Forcing thermodynamically unfolded proteins to fold

7. J. Biol. Chem. *273*, 4831-4834.

Baxa,U., Cheng,N., Winkler,D.C., Chiu,T.K., Davies,D.R., Sharma,D., Inouye,H., Kirschner,D.A., Wickner,R.B., and Steven,A.C. (2005). Filaments of the Ure2p prion protein have a cross-beta core structure

1. J. Struct. Biol. *150*, 170-179.

Baxa,U., Ross,P.D., Wickner,R.B., and Steven,A.C. (2004). The N-terminal prion domain of Ure2p converts from an unfolded to a thermally resistant conformation upon filament formation

5. J. Mol. Biol. *339*, 259-264.

Baxa,U., Speransky,V., Steven,A.C., and Wickner,R.B. (2002). Mechanism of inactivation on prion conversion of the Saccharomyces cerevisiae Ure2 protein. Proc. Natl. Acad. Sci. U. S. A *99*, 5253-5260.

Baxa,U., Taylor,K.L., Wall,J.S., Simon,M.N., Cheng,N., Wickner,R.B., and Steven,A.C. (2003). Architecture of Ure2p prion filaments: the N-terminal domains form a central core fiber. J. Biol. Chem. *278*, 43717-43727.

Beck,T. and Hall,M.N. (1999). The TOR signalling pathway controls nuclear localization of nutrient-regulated transcription factors. Nature *402*, 689-692.

Beissinger,M. and Buchner,J. (1998). How chaperones fold proteins

2. Biol. Chem. *379*, 245-259.

Bennett,M.J., Choe,S., and Eisenberg,D. (1994). Domain swapping: entangling alliances between proteins

13. Proc. Natl. Acad. Sci. U. S. A *91*, 3127-3131.

Bennett,M.J. and Eisenberg,D. (2004). The evolving role of 3D domain swapping in proteins

1. Structure. (Camb.) *12*, 1339-1341.

Bennett,M.J., Schlunegger,M.P., and Eisenberg,D. (1995). 3D domain swapping: a mechanism for oligomer assembly

11. Protein Sci. *4*, 2455-2468.

Benzinger,T.L., Gregory,D.M., Burkoth,T.S., Miller-Auer,H., Lynn,D.G., Botto,R.E., and Meredith,S.C. (2000). Two-dimensional structure of beta-amyloid(10-35) fibrils

1. Biochemistry *39*, 3491-3499.

Blackley,H.K., Patel,N., Davies,M.C., Roberts,C.J., Tendler,S.J., Wilkinson,M.J., and Williams,P.M. (1999). Morphological development of beta(1-40) amyloid fibrils

2. Exp. Neurol. *158*, 437-443.

Blake,C. and Serpell,L. (1996). Synchrotron X-ray studies suggest that the core of the transthyretin amyloid fibril is a continuous beta-sheet helix

1. Structure. *4*, 989-998.

Blake,C.C., Serpell,L.C., Sunde,M., Sandgren,O., and Lundgren,E. (1996). A molecular model of the amyloid fibril

15. Ciba Found. Symp. *199*, 6-15.

Blinder,D., Coschigano,P.W., and Magasanik,B. (1996). Interaction of the GATA factor Gln3p with the nitrogen regulator Ure2p in Saccharomyces cerevisiae. J. Bacteriol. *178*, 4734-4736.

Blondelle,S.E., Forood,B., Houghten,R.A., and Perez-Paya,E. (1997). Polyalanine-based peptides as models for self-associated beta-pleated-sheet complexes

1. Biochemistry *36*, 8393-8400.

Boehm, G. *CDNN: CD Spectra Deconvolution*, Version 2.1. 1997.

Ref Type: Computer Program

Bolton,D.C., McKinley,M.P., and Prusiner,S.B. (1982). Identification of a protein that purifies with the scrapie prion. Science *218*, 1309-1311.

Bossy-Wetzel,E., Schwarzenbacher,R., and Lipton,S.A. (2004). Molecular pathways to neurodegeneration

1. Nat. Med. *10 Suppl*, S2-S9.

Bousset,L., Briki,F., Doucet,J., and Melki,R. (2003). The native-like conformation of Ure2p in fibrils assembled under physiologically relevant conditions switches to an amyloid-like conformation upon heat-treatment of the fibrils. J. Struct. Biol. *141*, 132-142.

Bousset,L., Redeker,V., Decottignies,P., Dubois,S., Le Marechal,P., and Melki,R. (2004). Structural Characterization of the Fibrillar Form of the Yeast Saccharomyces cerevisiae Prion Ure2p. Biochemistry *43*, 5022-5032.

Bousset,L., Thomson,N.H., Radford,S.E., and Melki,R. (2002). The yeast prion Ure2p retains its native alpha-helical conformation upon assembly into protein fibrils in vitro. EMBO J. *21*, 2903-2911.

Bradford,M.M. (1976). Rapid and Sensitive Method for Quantitation of Microgram Quantities of Protein Utilizing Principle of Protein-Dye Binding. Analytical Biochemistry *72*, 248-254.

Brandts,J.F. and Kaplan,L.J. (1973). Derivative sspectroscopy applied to tyrosyl chromophores. Studies on ribonuclease, lima bean inhibitors, insulin, and pancreatic trypsin inhibitor. Biochemistry *12*, 2011-2024.

Bross,P. and Gregerson,N. (2003). Protein Misfolding and Disease.

Bryngelson,J.D., Onuchic,J.N., Socci,N.D., and Wolynes,P.G. (1995). Funnels, pathways, and the energy landscape of protein folding: a synthesis

1. Proteins *21*, 167-195.

Buchner,J. and Kiefhaber,T. (2004). Protein folding Handbook.

Burnette,W.N. (1981). "Western blotting": electrophoretic transfer of proteins from sodium dodecyl sulfate--polyacrylamide gels to unmodified nitrocellulose and radiographic detection with antibody and radioiodinated protein A. Anal. Biochem. *112*, 195-203.

Burns,C.S., Aronoff-Spencer,E., Dunham,C.M., Lario,P., Avdievich,N.I., Antholine,W.E., Olmstead,M.M., Vrielink,A., Gerfen,G.J., Peisach,J., Scott,W.G., and Millhauser,G.L. (2002). Molecular features of the copper binding sites in the octarepeat domain of the prion protein

1. Biochemistry *41*, 3991-4001.

Castilla,J., Saa,P., Hetz,C., and Soto,C. (2005). In vitro generation of infectious scrapie prions

1. Cell *121*, 195-206.

Caughey,B., Kocisko,D.A., Raymond,G.J., and Lansbury,P.T., Jr. (1995). Aggregates of scrapie-associated prion protein induce the cell-free conversion of protease-sensitive prion protein to the protease-resistant state

1. Chem. Biol. *2*, 807-817.

Cecconi,C., Shank,E.A., Bustamante,C., and Marqusee,S. (2005). Direct observation of the three-state folding of a single protein molecule

1. Science *309*, 2057-2060.

Chang,M., Bolton,J.L., and Blond,S.Y. (1999). Expression and purification of hexahistidine-tagged human glutathione S-transferase P1-1 in Escherichia coli

1. Protein Expr. Purif. *17*, 443-448.

Chen,S., Ferrone,F.A., and Wetzel,R. (2002). Huntington's disease age-of-onset linked to polyglutamine aggregation nucleation

1. Proc. Natl. Acad. Sci. U. S. A *99*, 11884-11889.

Chernoff,Y.O., Derkach,I.L., and Inge-Vechtomov,S.G. (1993). Multicopy SUP35 gene induces de-novo appearance of psi-like factors in the yeast Saccharomyces cerevisiae. Curr. Genet. *24*, 268-270.

Chiti,F., Webster,P., Taddei,N., Clark,A., Stefani,M., Ramponi,G., and Dobson,C.M. (1999). Designing conditions for in vitro formation of amyloid protofilaments and fibrils

1. Proc. Natl. Acad. Sci. U. S. A *96*, 3590-3594.

Collins,S.R., Douglass,A., Vale,R.D., and Weissman,J.S. (2004). Mechanism of prion propagation: amyloid growth occurs by monomer addition

3. PLoS. Biol. *2*, e321.

Colon,W. and Kelly,J.W. (1992). Partial denaturation of transthyretin is sufficient for amyloid fibril formation in vitro

1. Biochemistry *31*, 8654-8660.

Colon,W., Lai,Z., McCutchen,S.L., Miroy,G.J., Strang,C., and Kelly,J.W. (1996). FAP mutations destabilize transthyretin facilitating conformational changes required for amyloid formation

7. Ciba Found. Symp. *199*, 228-238.

Coschigano,P.W. and Magasanik,B. (1991). The URE2 gene product of Saccharomyces cerevisiae plays an important role in the cellular response to the

nitrogen source and has homology to glutathione s-transferases. Mol. Cell Biol. *11*, 822-832.

Cox,B.S., Tuite,M.F., and McLaughlin,C.S. (1988). The psi factor of yeast: a problem in inheritance

14. Yeast *4*, 159-178.

Curtis,R.A., Prausnitz,J.M., and Blanch,H.W. (1998). Protein-protein and protein-salt interactions in aqueous protein solutions containing concentrated electrolytes

5. Biotechnol. Bioeng. *57*, 11-21.

Daggett,V. and Fersht,A.R. (2003). Is there a unifying mechanism for protein folding?

6. Trends Biochem. Sci. *28*, 18-25.

Damaschun,G., Damaschun,H., Gast,K., and Zirwer,D. (1999). Proteins can adopt totally different folded conformations

1. J. Mol. Biol. *291*, 715-725.

DAVIS,B.J. (1964). DISC ELECTROPHORESIS. II. METHOD AND APPLICATION TO HUMAN SERUM PROTEINS. Ann. N. Y. Acad. Sci. *121*, 404-427.

de la Paz,M.L. and Serrano,L. (2004). Sequence determinants of amyloid fibril formation

2. Proc. Natl. Acad. Sci. U. S. A *101*, 87-92.

DeArmond,S.J., McKinley,M.P., Barry,R.A., Braunfeld,M.B., McColloch,J.R., and Prusiner,S.B. (1985). Identification of prion amyloid filaments in scrapie-infected brain. Cell *41*, 221-235.

Deechongkit,S., Powers,E.T., You,S.L., and Kelly,J.W. (2005). Controlling the morphology of cross beta-sheet assemblies by rational design

1. J. Am. Chem. Soc. *127*, 8562-8570.

Del Vecchio,P., Graziano,G., Granata,V., Barone,G., Mandrich,L., Rossi,M., and Manco,G. (2003). Effect of trifluoroethanol on the conformational stability of a hyperthermophilic esterase: a CD study

1. Biophys. Chem. *104*, 407-415.

Diaz-Avalos,R., Long,C., Fontano,E., Balbirnie,M., Grothe,R., Eisenberg,D., and Caspar,D.L. (2003). Cross-beta order and diversity in nanocrystals of an amyloid-forming peptide

1. J. Mol. Biol. *330*, 1165-1175.

Dill,K.A. and Chan,H.S. (1997). From Levinthal to pathways to funnels

1. Nat. Struct. Biol. *4*, 10-19.

Dinner,A.R., Sali,A., Smith,L.J., Dobson,C.M., and Karplus,M. (2000). Understanding protein folding via free-energy surfaces from theory and experiment

7. Trends Biochem. Sci. *25*, 331-339.

Dobson,C.M. (2001). The structural basis of protein folding and its links with human disease

7. Philos. Trans. R. Soc. Lond B Biol. Sci. *356*, 133-145.

Dobson,C.M. (2003). Protein folding and misfolding

1. Nature *426*, 884-890.

Dobson,C.M. (2004a). Experimental investigation of protein folding and misfolding

1. Methods *34*, 4-14.

Dobson,C.M. (2004b). Principles of protein folding, misfolding and aggregation

3. Semin. Cell Dev. Biol. *15*, 3-16.

Doonan,S. (1996a). Protein purification protocols. General strategies

13. Methods Mol. Biol. *59*, 1-16.

Doonan,S. (1996b). Bulk Purification by Fractional Precipitation. In Protein purification protocols, J.Walk, ed. (London: pp. 135-168.

Eaglestone,S.S., Ruddock,L.W., Cox,B.S., and Tuite,M.F. (2000). Guanidine hydrochloride blocks a critical step in the propagation of the prion-like determinant [PSI(+)] of Saccharomyces cerevisiae

8. Proc. Natl. Acad. Sci. U. S. A *97*, 240-244.

Eanes,E.D. and Glenner,G.G. (1968). X-ray diffraction studies on amyloid filaments

1. J. Histochem. Cytochem. *16*, 673-677.

Edskes,H.K., Gray,V.T., and Wickner,R.B. (1999). The [URE3] prion is an aggregated form of Ure2p that can be cured by overexpression of Ure2p fragments. Proc. Natl. Acad. Sci. U. S. A *96*, 1498-1503.

Edskes,H.K. and Wickner,R.B. (2002). Conservation of a portion of the S. cerevisiae Ure2p prion domain that interacts with the full-length protein. Proc. Natl. Acad. Sci. U. S. A *99 Suppl 4*, 16384-16391.

Edskes,H.K. and Wickner,R.B. (2004). Transmissible spongiform encephalopathies: prion proof in progress

1. Nature *430*, 977-979.

Eisenberg,D., Schwarz,E., Komaromy,M., and Wall,R. (1984). Analysis of membrane and surface protein sequences with the hydrophobic moment plot

1. J. Mol. Biol. *179*, 125-142.

Ekiel,I. and Abrahamson,M. (1996). Folding-related dimerization of human cystatin C

2. J. Biol. Chem. *271*, 1314-1321.

Elam,J.S., Taylor,A.B., Strange,R., Antonyuk,S., Doucette,P.A., Rodriguez,J.A., Hasnain,S.S., Hayward,L.J., Valentine,J.S., Yeates,T.O., and Hart,P.J. (2003). Amyloid-like filaments and water-filled nanotubes formed by SOD1 mutant proteins linked to familial ALS

2. Nat. Struct. Biol. *10*, 461-467.

Englander,S.W. (2000). Protein folding intermediates and pathways studied by hydrogen exchange

1. Annu. Rev. Biophys. Biomol. Struct. *29*, 213-238.

Fairbanks,G., Steck,T.L., and Wallach,D.F. (1971). Electrophoretic analysis of the major polypeptides of the human erythrocyte membrane. Biochemistry *10*, 2606-2617.

Fay,N., Inoue,Y., Bousset,L., Taguchi,H., and Melki,R. (2003). Assembly of the yeast prion Ure2p into protein fibrils. Thermodynamic and kinetic characterization. J. Biol. Chem. *278*, 30199-30205.

Fernandez-Bellot,E., Guillemet,E., Baudin-Baillieu,A., Gaumer,S., Komar,A.A., and Cullin,C. (1999). Characterization of the interaction domains of Ure2p, a prion-like protein of yeast. Biochem. J. *338 (Pt 2)*, 403-407.

Fernandez-Bellot,E., Guillemet,E., and Cullin,C. (2000). The yeast prion [URE3] can be greatly induced by a functional mutated URE2 allele. EMBO J. *19*, 3215-3222.

Fersht,A.R. (1995). Optimization of rates of protein folding: the nucleation-condensation mechanism and its implications

12. Proc. Natl. Acad. Sci. U. S. A *92*, 10869-10873.

Fersht,A.R. (2000). Transition-state structure as a unifying basis in protein-folding mechanisms: contact order, chain topology, stability, and the extended nucleus mechanism

2. Proc. Natl. Acad. Sci. U. S. A *97*, 1525-1529.

Fersht,A.R. and Daggett,V. (2002). Protein folding and unfolding at atomic resolution

1. Cell *108*, 573-582.

Frankel,A.D. and Kim,P.S. (1991). Modular structure of transcription factors: implications for gene regulation

4. Cell *65*, 717-719.

Frydman,J. and Hartl,F.U. (1996). Principles of chaperone-assisted protein folding: differences between in vitro and in vivo mechanisms

10. Science *272*, 1497-1502.

Garcia,d.l.T. (2001). Hydration from hydrodynamics. General considerations and applications of bead modelling to globular proteins

3. Biophys. Chem. *93*, 159-170.

Gasset,M., Baldwin,M.A., Lloyd,D.H., Gabriel,J.M., Holtzman,D.M., Cohen,F., Fletterick,R., and Prusiner,S.B. (1992). Predicted alpha-helical regions of the prion protein when synthesized as peptides form amyloid

2. Proc. Natl. Acad. Sci. U. S. A *89*, 10940-10944.

Gasteiger,E., Gattiker,A., Hoogland,C., Ivanyi,I., Appel,R.D., and Bairoch,A. (2003). ExPASy: The proteomics server for in-depth protein knowledge and analysis

2. Nucleic Acids Res. *31*, 3784-3788.

Gershoni,J.M. and Palade,G.E. (1983). Protein blotting: principles and applications. Anal. Biochem. *131*, 1-15.

Gill,S.C. and von Hippel,P.H. (1989). Calculation of protein extinction coefficients from amino acid sequence data

1. Anal. Biochem. *182*, 319-326.

Glover,J.R., Kowal,A.S., Schirmer,E.C., Patino,M.M., Liu,J.J., and Lindquist,S. (1997). Self-seeded fibers formed by Sup35, the protein determinant of [PSI+], a heritable prion-like factor of S. cerevisiae

2. Cell *89*, 811-819.

Goldfarb,L.G. and Brown,P. (1995). The transmissible spongiform encephalopathies

4. Annu. Rev. Med. *46*, 57-65.

Goldsbury,C.S., Cooper,G.J., Goldie,K.N., Muller,S.A., Saafi,E.L., Gruijters,W.T., Misur,M.P., Engel,A., Aebi,U., and Kistler,J. (1997). Polymorphic fibrillar assembly of human amylin

9. J. Struct. Biol. *119*, 17-27.

Griffith,J.S. (1967). Self-replication and scrapie. Nature *215*, 1043-1044.

Hamada,D. and Dobson,C.M. (2002). A kinetic study of beta-lactoglobulin amyloid fibril formation promoted by urea

1. Protein Sci. *11*, 2417-2426.

Hanahan,D. (1983). Studies on transformation of Escherichia coli with plasmids

130. J. Mol. Biol. *166*, 557-580.

Hardesty,B. and Kramer,G. (2001). Folding of a nascent peptide on the ribosome

5. Prog. Nucleic Acid Res. Mol. Biol. *66*, 41-66.

Harjes,P. and Wanker,E.E. (2003). The hunt for huntingtin function: interaction partners tell many different stories

1. Trends Biochem. Sci. *28*, 425-433.

Harper,J.D. and Lansbury,P.T., Jr. (1997). Models of amyloid seeding in Alzheimer's disease and scrapie: mechanistic truths and physiological consequences of the time-dependent solubility of amyloid proteins

5. Annu. Rev. Biochem. *66*, 385-407.

Harper,J.D., Wong,S.S., Lieber,C.M., and Lansbury,P.T. (1997). Observation of metastable Abeta amyloid protofibrils by atomic force microscopy

1. Chem. Biol. *4*, 119-125.

Harper,J.D., Wong,S.S., Lieber,C.M., and Lansbury,P.T. (1999). Assembly of A beta amyloid protofibrils: An in vitro model for a possible early event in Alzheimer's disease. Biochemistry *38*, 8972-8980.

Hartl,F.U. and Hayer-Hartl,M. (2002). Molecular chaperones in the cytosol: from nascent chain to folded protein

3. Science *295*, 1852-1858.

He,M., Wilde,A., and Kaderbhai,M.A. (1990). A simple single-step procedure for small-scale preparation of Escherichia coli plasmids

2. Nucleic Acids Res. *18*, 1660.

Heukeshoven,J. and Dernick,R. (1988). Improved silver staining procedure for fast staining in PhastSystem Development Unit. I. Staining of sodium dodecyl sulfate gels

2. Electrophoresis *9*, 28-32.

Hofrichter,J., Ross,P.D., and Eaton,W.A. (1974). Kinetics and mechanism of deoxyhemoglobin S gelation: a new approach to understanding sickle cell disease

1. Proc. Natl. Acad. Sci. U. S. A *71*, 4864-4868.

Hornby,J.A., Luo,J.K., Stevens,J.M., Wallace,L.A., Kaplan,W., Armstrong,R.N., and Dirr,H.W. (2000). Equilibrium folding of dimeric class mu glutathione transferases involves a stable monomeric intermediate

1. Biochemistry *39*, 12336-12344.

Ikai,A. (1996). STM and AFM of bio/organic molecules and structures. Surf. Sci. Rep *26*, 261-332.

Ionescu-Zanetti,C., Khurana,R., Gillespie,J.R., Petrick,J.S., Trabachino,L.C., Minert,L.J., Carter,S.A., and Fink,A.L. (1999). Monitoring the assembly of Ig light-chain amyloid fibrils by atomic force microscopy. Proc. Natl. Acad. Sci. U. S. A *96*, 13175-13179.

Ivanova,M.I., Sawaya,M.R., Gingery,M., Attinger,A., and Eisenberg,D. (2004). An amyloid-forming segment of beta2-microglobulin suggests a molecular model for the fibril

1. Proc. Natl. Acad. Sci. U. S. A *101*, 10584-10589.

Jackson,S.E. (1998). How do small single-domain proteins fold?

1. Fold. Des *3*, R81-R91.

Jaenicke,R. and Seckler,R. (1997). Protein misassembly in vitro

1. Adv. Protein Chem. *50*, 1-59.

James,T.L., Liu,H., Ulyanov,N.B., Farr-Jones,S., Zhang,H., Donne,D.G., Kaneko,K., Groth,D., Mehlhorn,I., Prusiner,S.B., and Cohen,F.E. (1997). Solution structure of a 142-residue recombinant prion protein corresponding to the infectious fragment of the scrapie isoform

1. Proc. Natl. Acad. Sci. U. S. A *94*, 10086-10091.

Janowski,R., Kozak,M., Jankowska,E., Grzonka,Z., Grubb,A., Abrahamson,M., and Jaskolski,M. (2001). Human cystatin C, an amyloidogenic protein, dimerizes through three-dimensional domain swapping

1. Nat. Struct. Biol. *8*, 316-320.

Jarrett,J.T. and Lansbury,P.T., Jr. (1993). Seeding "one-dimensional crystallization" of amyloid: a pathogenic mechanism in Alzheimer's disease and scrapie?

1. Cell *73*, 1055-1058.

Jenkins,J. and Pickersgill,R. (2001). The architecture of parallel beta-helices and related folds

1. Prog. Biophys. Mol. Biol. *77*, 111-175.

Jiang,Y., Li,H., Zhu,L., Zhou,J.M., and Perrett,S. (2004). Amyloid nucleation and hierarchical assembly of Ure2p fibrils. Role of asparagine/glutamine repeat and nonrepeat regions of the prion domains. J. Biol. Chem. *279*, 3361-3369.

Jimenez,J.L., Nettleton,E.J., Bouchard,M., Robinson,C.V., Dobson,C.M., and Saibil,H.R. (2002). The protofilament structure of insulin amyloid fibrils

1. Proc. Natl. Acad. Sci. U. S. A *99*, 9196-9201.

Jones,S. and Thornton,J.M. (1995). Protein-protein interactions: a review of protein dimer structures

1. Prog. Biophys. Mol. Biol. *63*, 31-65.

Kajava,A.V., Aebi,U., and Steven,A.C. (2005). The parallel superpleated beta-structure as a model for amyloid fibrils of human amylin

1. J. Mol. Biol. *348*, 247-252.

Kajava,A.V., Baxa,U., Wickner,R.B., and Steven,A.C. (2004). A model for Ure2p prion filaments and other amyloids: the parallel superpleated beta-structure

4. Proc. Natl. Acad. Sci. U. S. A *101*, 7885-7890.

Kaneko,K., Peretz,D., Pan,K.M., Blochberger,T.C., Wille,H., Gabizon,R., Griffith,O.H., Cohen,F.E., Baldwin,M.A., and Prusiner,S.B. (1995). Prion protein (PrP) synthetic peptides induce cellular PrP to acquire properties of the scrapie isoform

1. Proc. Natl. Acad. Sci. U. S. A *92*, 11160-11164.

Karplus,M. and Weaver,D.L. (1994). Protein folding dynamics: the diffusion-collision model and experimental data

1. Protein Sci. *3*, 650-668.

Kayed,R., Head,E., Thompson,J.L., McIntire,T.M., Milton,S.C., Cotman,C.W., and Glabe,C.G. (2003). Common structure of soluble amyloid oligomers implies common mechanism of pathogenesis

3. Science *300*, 486-489.

Kelly,J.W. (1998). The alternative conformations of amyloidogenic proteins and their multi-step assembly pathways

4. Curr. Opin. Struct. Biol. *8*, 101-106.

King,C.Y., Tittmann,P., Gross,H., Gebert,R., Aebi,M., and Wuthrich,K. (1997). Prion-inducing domain 2-114 of yeast Sup35 protein transforms in vitro into amyloid-like filaments

1. Proc. Natl. Acad. Sci. U. S. A *94*, 6618-6622.

Kishimoto,A., Hasegawa,K., Suzuki,H., Taguchi,H., Namba,K., and Yoshida,M. (2004). beta-Helix is a likely core structure of yeast prion Sup35 amyloid fibers

1. Biochem. Biophys. Res. Commun. *315*, 739-745.

Knaus,K.J., Morillas,M., Swietnicki,W., Malone,M., Surewicz,W.K., and Yee,V.C. (2001). Crystal structure of the human prion protein reveals a mechanism for oligomerization

6. Nat. Struct. Biol. *8*, 770-774.

Kocisko,D.A., Come,J.H., Priola,S.A., Chesebro,B., Raymond,G.J., Lansbury,P.T., and Caughey,B. (1994). Cell-free formation of protease-resistant prion protein

2. Nature *370*, 471-474.

Komar,A.A., Guillemet,E., Reiss,C., and Cullin,C. (1998). Enhanced expression of the yeast Ure2 protein in Escherichia coli: the effect of synonymous codon substitutions at a selected place in the gene. Biol. Chem. *379*, 1295-1300.

Komar,A.A., Lesnik,T., Cullin,C., Guillemet,E., Ehrlich,R., and Reiss,C. (1997). Differential resistance to proteinase K digestion of the yeast prion-like (Ure2p) protein synthesized in vitro in wheat germ extract and rabbit reticulocyte lysate cell-free translation systems. FEBS Lett. *415*, 6-10.

Komar,A.A., Melki,R., and Cullin,C. (1999). The [URE3] yeast prion: from genetics to biochemistry. Biochemistry (Mosc.) *64*, 1401-1407.

Koo,E.H., Lansbury,P.T., Jr., and Kelly,J.W. (1999). Amyloid diseases: abnormal protein aggregation in neurodegeneration

2. Proc. Natl. Acad. Sci. U. S. A *96*, 9989-9990.

Krishnan,R. and Lindquist,S.L. (2005). Structural insights into a yeast prion illuminate nucleation and strain diversity

1. Nature *435*, 765-772.

Lacroute,F. (1971). Non-Mendelian mutation allowing ureidosuccinic acid uptake in yeast

1. J. Bacteriol. *106*, 519-522.

Ladurner,A.G., Itzhaki,L.S., and Fersht,A.R. (1997). Strain in the folding nucleus of chymotrypsin inhibitor 2

6. Fold. Des *2*, 363-368.

Laemmli,U.K. (1970). Cleavage of structural proteins during the assembly of the head of bacteriophage T4. Nature *227*, 680-685.

Lansbury,P.T. (1994). Mechanism of scrapie replication

1. Science *265*, 1510.

Legname,G., Baskakov,I.V., Nguyen,H.O., Riesner,D., Cohen,F.E., DeArmond,S.J., and Prusiner,S.B. (2004). Synthetic mammalian prions

1. Science *305*, 673-676.

LeVine,H., III (1993). Thioflavine T interaction with synthetic Alzheimer's disease beta-amyloid peptides: detection of amyloid aggregation in solution

1. Protein Sci. *2*, 404-410.

LeVine,H., III (1997). Stopped-flow kinetics reveal multiple phases of thioflavin T binding to Alzheimer beta (1-40) amyloid fibrils

1. Arch. Biochem. Biophys. *342*, 306-316.

Li,L., Darden,T.A., Bartolotti,L., Kominos,D., and Pedersen,L.G. (1999). An atomic model for the pleated beta-sheet structure of Abeta amyloid protofilaments

1. Biophys. J. *76*, 2871-2878.

Lichtenthaler,S.F., Beher,D., Grimm,H.S., Wang,R., Shearman,M.S., Masters,C.L., and Beyreuther,K. (2002). The intramembrane cleavage site of the amyloid precursor protein depends on the length of its transmembrane domain

2. Proc. Natl. Acad. Sci. U. S. A *99*, 1365-1370.

Lindquist,S., Krobitsch,S., Li,L., and Sondheimer,N. (2001). Investigating protein conformation-based inheritance and disease in yeast. Philos. Trans. R. Soc. Lond B Biol. Sci. *356*, 169-176.

Liu,Y. and Eisenberg,D. (2002). 3D domain swapping: as domains continue to swap

4. Protein Sci. *11*, 1285-1299.

Liu,Y., Gotte,G., Libonati,M., and Eisenberg,D. (2001). A domain-swapped RNase A dimer with implications for amyloid formation

7. Nat. Struct. Biol. *8*, 211-214.

Liu,Y., Gotte,G., Libonati,M., and Eisenberg,D. (2002). Structures of the two 3D domain-swapped RNase A trimers

5. Protein Sci. *11*, 371-380.

Lomakin,A., Chung,D.S., Benedek,G.B., Kirschner,D.A., and Teplow,D.B. (1996). On the nucleation and growth of amyloid beta-protein fibrils: detection of nuclei and quantitation of rate constants

1. Proc. Natl. Acad. Sci. U. S. A *93*, 1125-1129.

Maddelein,M.L. and Wickner,R.B. (1999). Two prion-inducing regions of Ure2p are nonoverlapping. Mol. Cell Biol. *19*, 4516-4524.

Makrides,S.C. (1996). Strategies for achieving high-level expression of genes in Escherichia coli

2. Microbiol. Rev. *60*, 512-538.

Marianayagam,N.J., Sunde,M., and Matthews,J.M. (2004). The power of two: protein dimerization in biology

1. Trends Biochem. Sci. *29*, 618-625.

Masino,L. and Pastore,A. (2002). Glutamine repeats: structural hypotheses and neurodegeneration

1. Biochem. Soc. Trans. *30*, 548-551.

Masison,D.C., Maddelein,M.L., and Wickner,R.B. (1997). The prion model for [URE3] of yeast: spontaneous generation and requirements for propagation. Proc. Natl. Acad. Sci. U. S. A *94*, 12503-12508.

Masison,D.C. and Wickner,R.B. (1995). Prion-inducing domain of yeast Ure2p and protease resistance of Ure2p in prion-containing cells. Science *270*, 93-95.

Matulis,D., Baumann,C.G., Bloomfield,V.A., and Lovrien,R.E. (1999). 1-anilino-8-naphthalene sulfonate as a protein conformational tightening agent

1. Biopolymers *49*, 451-458.

Maxwell,K.L., Wildes,D., Zarrine-Afsar,A., Los Rios,M.A., Brown,A.G., Friel,C.T., Hedberg,L., Horng,J.C., Bona,D., Miller,E.J., Vallee-Belisle,A., Main,E.R., Bemporad,F., Qiu,L., Teilum,K., Vu,N.D., Edwards,A.M., Ruczinski,I., Poulsen,F.M., Kragelund,B.B., Michnick,S.W., Chiti,F., Bai,Y., Hagen,S.J., Serrano,L., Oliveberg,M., Raleigh,D.P., Wittung-Stafshede,P., Radford,S.E., Jackson,S.E., Sosnick,T.R., Marqusee,S., Davidson,A.R., and Plaxco,K.W. (2005). Protein folding: defining a "standard" set of experimental conditions and a preliminary kinetic data set of two-state proteins

1. Protein Sci. *14*, 602-616.

Michelitsch,M.D. and Weissman,J.S. (2000). A census of glutamine/asparagine-rich regions: implications for their conserved function and the prediction of novel prions

1. Proc. Natl. Acad. Sci. U. S. A *97*, 11910-11915.

Monti,M., Garolla di Bard,B.L., Calloni,G., Chiti,F., Amoresano,A., Ramponi,G., and Pucci,P. (2004). The regions of the sequence most exposed to the solvent within the amyloidogenic state of a protein initiate the aggregation process

1. J. Mol. Biol. *336*, 253-262.

Mouillet-Richard,S., Ermonval,M., Chebassier,C., Laplanche,J.L., Lehmann,S., Launay,J.M., and Kellermann,O. (2000). Signal transduction through prion protein

2. Science *289*, 1925-1928.

Naiki,H. and Nakakuki,K. (1996). First-order kinetic model of Alzheimer's beta-amyloid fibril extension in vitro

1. Lab Invest *74*, 374-383.

Nazabal,A., Dos,R.S., Bonneu,M., Saupe,S.J., and Schmitter,J.M. (2003). Conformational transition occurring upon amyloid aggregation of the HET-s prion protein of Podospora anserina analyzed by hydrogen/deuterium exchange and mass spectrometry

1. Biochemistry *42*, 8852-8861.

Ness,F., Ferreira,P., Cox,B.S., and Tuite,M.F. (2002). Guanidine hydrochloride inhibits the generation of prion "seeds" but not prion protein aggregation in yeast

99. Mol. Cell Biol. *22*, 5593-5605.

Nguyen,J., Baldwin,M.A., Cohen,F.E., and Prusiner,S.B. (1995a). Prion protein peptides induce alpha-helix to beta-sheet conformational transitions

8. Biochemistry *34*, 4186-4192.

Nguyen,J.T., Inouye,H., Baldwin,M.A., Fletterick,R.J., Cohen,F.E., Prusiner,S.B., and Kirschner,D.A. (1995b). X-ray diffraction of scrapie prion rods and PrP peptides

11. J. Mol. Biol. *252*, 412-422.

Nielsen,L., Khurana,R., Coats,A., Frokjaer,S., Brange,J., Vyas,S., Uversky,V.N., and Fink,A.L. (2001). Effect of environmental factors on the kinetics of insulin fibril formation: elucidation of the molecular mechanism

1. Biochemistry *40*, 6036-6046.

Ogihara,N.L., Ghirlanda,G., Bryson,J.W., Gingery,M., DeGrado,W.F., and Eisenberg,D. (2001). Design of three-dimensional domain-swapped dimers and fibrous oligomers

8. Proc. Natl. Acad. Sci. U. S. A *98*, 1404-1409.

Onuchic,J.N. and Wolynes,P.G. (2004). Theory of protein folding

8. Curr. Opin. Struct. Biol. *14*, 70-75.

ORNSTEIN,L. (1964). DISC ELECTROPHORESIS. I. BACKGROUND AND THEORY. Ann. N. Y. Acad. Sci. *121*, 321-349.

Pace,C.N., Shirley,B.A., McNutt,M., and Gajiwala,K. (1996). Forces contributing to the conformational stability of proteins

3. FASEB J. *10*, 75-83.

Pace,C.N., Vajdos,F., Fee,L., Grimsley,G., and Gray,T. (1995). How to measure and predict the molar absorption coefficient of a protein

5. Protein Sci. *4*, 2411-2423.

Pan,K.M., Baldwin,M., Nguyen,J., Gasset,M., Serban,A., Groth,D., Mehlhorn,I., Huang,Z., Fletterick,R.J., Cohen,F.E., and . (1993). Conversion of alpha-helices into beta-sheets features in the formation of the scrapie prion proteins

1. Proc. Natl. Acad. Sci. U. S. A *90*, 10962-10966.

Patino,M.M., Liu,J.J., Glover,J.R., and Lindquist,S. (1996). Support for the prion hypothesis for inheritance of a phenotypic trait in yeast. Science *273*, 622-626.

Paushkin,S.V., Kushnirov,V.V., Smirnov,V.N., and Ter Avanesyan,M.D. (1997). In vitro propagation of the prion-like state of yeast Sup35 protein

1. Science *277*, 381-383.

Pelton,J.T. and McLean,L.R. (2000). Spectroscopic methods for analysis of protein secondary structure

8. Anal. Biochem. *277*, 167-176.

Perrett,S., Freeman,S.J., Butler,P.J., and Fersht,A.R. (1999). Equilibrium folding properties of the yeast prion protein determinant Ure2

88. J. Mol. Biol. *290*, 331-345.

Perutz,M.F. (1995). Polar zippers: their role in human disease

1. Pharm. Acta Helv. *69*, 213-224.

Perutz,M.F. (1996). Glutamine repeats and inherited neurodegenerative diseases: molecular aspects

2. Curr. Opin. Struct. Biol. *6*, 848-858.

Perutz,M.F., Finch,J.T., Berriman,J., and Lesk,A. (2002a). Amyloid fibers are water-filled nanotubes

2. Proc. Natl. Acad. Sci. U. S. A *99*, 5591-5595.

Perutz,M.F., Johnson,T., Suzuki,M., and Finch,J.T. (1994). Glutamine repeats as polar zippers: their possible role in inherited neurodegenerative diseases

4. Proc. Natl. Acad. Sci. U. S. A *91*, 5355-5358.

Perutz,M.F., Pope,B.J., Owen,D., Wanker,E.E., and Scherzinger,E. (2002b). Aggregation of proteins with expanded glutamine and alanine repeats of the glutamine-rich and asparagine-rich domains of Sup35 and of the amyloid beta-peptide of amyloid plaques

117. Proc. Natl. Acad. Sci. U. S. A *99*, 5596-5600.

Petkova,A.T., Leapman,R.D., Guo,Z., Yau,W.M., Mattson,M.P., and Tycko,R. (2005). Self-propagating, molecular-level polymorphism in Alzheimer's beta-amyloid fibrils

2. Science *307*, 262-265.

Pierce,M.M., Baxa,U., Steven,A.C., Bax,A., and Wickner,R.B. (2005). Is the prion domain of soluble Ure2p unstructured?

2. Biochemistry *44*, 321-328.

Plakoutsi,G., Taddei,N., Stefani,M., and Chiti,F. (2004). Aggregation of the Acylphosphatase from Sulfolobus solfataricus: the folded and partially unfolded states can both be precursors for amyloid formation

3. J. Biol. Chem. *279*, 14111-14119.

Porath,J., Carlsson,J., Olsson,I., and Belfrage,G. (1975). Metal chelate affinity chromatography, a new approach to protein fractionation

150. Nature *258*, 598-599.

Premzl,M., Gready,J.E., Jermiin,L.S., Simonic,T., and Marshall Graves,J.A. (2004). Evolution of Vertebrate Genes Related to Prion and Shadoo Proteins--Clues from Comparative Genomic Analysis. Mol. Biol. Evol. *21*, 2210-2231.

Premzl,M., Sangiorgio,L., Strumbo,B., Marshall Graves,J.A., Simonic,T., and Gready,J.E. (2003). Shadoo, a new protein highly conserved from fish to mammals and with similarity to prion protein. Gene *314*, 89-102.

Prusiner,S.B. (1982). Novel proteinaceous infectious particles cause scrapie. Science *216*, 136-144.

Ptitsyn,O.B. (1995a). Molten globule and protein folding

19. Adv. Protein Chem. *47*, 83-229.

Ptitsyn,O.B. (1995b). Structures of folding intermediates

4. Curr. Opin. Struct. Biol. *5*, 74-78.

Ptitsyn,O.B. and Rashin,A.A. (1973). [Self-organization of the myoglobin molecule]

2. Dokl. Akad. Nauk SSSR *213*, 473-475.

Qu,Y., Bolen,C.L., and Bolen,D.W. (1998). Osmolyte-driven contraction of a random coil protein

2. Proc. Natl. Acad. Sci. U. S. A *95*, 9268-9273.

Quiagen (1998). The QIAexpressionist: A handbook for high-level expreeeion and purification of 6xHis-tagged proteins. (Hilden: Quiagen).

Raman,B., Chatani,E., Kihara,M., Ban,T., Sakai,M., Hasegawa,K., Naiki,H., Rao,C., and Goto,Y. (2005). Critical balance of electrostatic and hydrophobic interactions is required for beta 2-microglobulin amyloid fibril growth and stability

1. Biochemistry *44*, 1288-1299.

Rief,M., Gautel,M., Oesterhelt,F., Fernandez,J.M., and Gaub,H.E. (1997). Reversible unfolding of individual titin immunoglobulin domains by AFM

3. Science *276*, 1109-1112.

Riek,R., Hornemann,S., Wider,G., Billeter,M., Glockshuber,R., and Wuthrich,K. (1996). NMR structure of the mouse prion protein domain PrP(121-321)

133. Nature *382*, 180-182.

Ripaud,L., Maillet,L., and Cullin,C. (2003). The mechanisms of [URE3] prion elimination demonstrate that large aggregates of Ure2p are dead-end products

126. EMBO J. *22*, 5251-5259.

Rochet,J.C. and Lansbury,P.T., Jr. (2000). Amyloid fibrillogenesis: themes and variations

1. Curr. Opin. Struct. Biol. *10*, 60-68.

Ross,C.A., Margolis,R.L., Becher,M.W., Wood,J.D., Engelender,S., Cooper,J.K., and Sharp,A.H. (1998). Pathogenesis of neurodegenerative diseases associated with expanded glutamine repeats: new answers, new questions

2. Prog. Brain Res. *117*, 397-419.

Ross,C.A. and Poirier,M.A. (2004). Protein aggregation and neurodegenerative disease

2. Nat. Med. *10 Suppl*, S10-S17.

Ross,C.A., Wood,J.D., Schilling,G., Peters,M.F., Nucifora,F.C., Jr., Cooper,J.K., Sharp,A.H., Margolis,R.L., and Borchelt,D.R. (1999). Polyglutamine pathogenesis

1. Philos. Trans. R. Soc. Lond B Biol. Sci. *354*, 1005-1011.

Ross,E.D., Baxa,U., and Wickner,R.B. (2004). Scrambled prion domains form prions and amyloid

1. Mol. Cell Biol. *24*, 7206-7213.

Rumbley,J., Hoang,L., Mayne,L., and Englander,S.W. (2001). An amino acid code for protein folding

4. Proc. Natl. Acad. Sci. U. S. A *98*, 105-112.

Saborio,G.P., Permanne,B., and Soto,C. (2001). Sensitive detection of pathological prion protein by cyclic amplification of protein misfolding

1. Nature *411*, 810-813.

Sambrook,J. and Russell,D. (2001). Molecular Cloning: A Laboratory Manual. (Cold Spring Harbour, NY: Cold Spring Harbour Laboratory Press).

Santos,N.C. and Castanho,M.A. (2004). An overview of the biophysical applications of atomic force microscopy

1. Biophys. Chem. *107*, 133-149.

Scheibel,T., Bloom,J., and Lindquist,S.L. (2004). The elongation of yeast prion fibers involves separable steps of association and conversion

2. Proc. Natl. Acad. Sci. U. S. A *101*, 2287-2292.

Scherzinger,E., Lurz,R., Turmaine,M., Mangiarini,L., Hollenbach,B., Hasenbank,R., Bates,G.P., Davies,S.W., Lehrach,H., and Wanker,E.E. (1997). Huntingtin-encoded polyglutamine expansions form amyloid-like protein aggregates in vitro and in vivo

1. Cell *90*, 549-558.

Schlumpberger,M., Wille,H., Baldwin,M.A., Butler,D.A., Herskowitz,I., and Prusiner,S.B. (2000). The prion domain of yeast Ure2p induces autocatalytic formation of amyloid fibers by a recombinant fusion protein

31. Protein Sci. *9*, 440-451.

Schlunegger,M.P., Bennett,M.J., and Eisenberg,D. (1997). Oligomer formation by 3D domain swapping: a model for protein assembly and misassembly

10. Adv. Protein Chem. *50*, 61-122.

Schmid,F.X. (1989). Spectral methods of characterizing protein conformation and conformational changes. In Protein Structure, a Practical Approach, T.E.Creighton, ed. (Oxford: Oxford University Press), pp. 251-285.

Schmid,F.X. (1998). Spectral methods of characterizing protein conformation and conformational changes. In Molecular Chaperones in the Life Cycle of Proteins, A.L.Fink and Y.Goto, eds. (New York: Marcel Dekker Inc.).

Schneider,S.W., Larmer,J., Henderson,R.M., and Oberleithner,H. (1998). Molecular weights of individual proteins correlate with molecular volumes measured by atomic force microscopy. Pflugers Arch. *435*, 362-367.

Schubert,U., Anton,L.C., Gibbs,J., Norbury,C.C., Yewdell,J.W., and Bennink,J.R. (2000). Rapid degradation of a large fraction of newly synthesized proteins by proteasomes

4. Nature *404*, 770-774.

Schymkowitz,J.W., Rousseau,F., and Serrano,L. (2002). Surfing on protein folding energy landscapes

5. Proc. Natl. Acad. Sci. U. S. A *99*, 15846-15848.

Scopes,R.K. (1974). Measurement of protein by spectrophotometry at 205 nm

4. Anal. Biochem. *59*, 277-282.

Selkoe,D. and Kopan,R. (2003). Notch and Presenilin: regulated intramembrane proteolysis links development and degeneration

1. Annu. Rev. Neurosci. *26*, 565-597.

Selkoe,D.J., Yamazaki,T., Citron,M., Podlisny,M.B., Koo,E.H., Teplow,D.B., and Haass,C. (1996). The role of APP processing and trafficking pathways in the formation of amyloid beta-protein

4. Ann. N. Y. Acad. Sci. *777*, 57-64.

Serio,T.R., Cashikar,A.G., Kowal,A.S., Sawicki,G.J., Moslehi,J.J., Serpell,L., Arnsdorf,M.F., and Lindquist,S.L. (2000). Nucleated conformational conversion and the replication of conformational information by a prion determinant

110. Science *289*, 1317-1321.

Serpell,L.C. (2000b). Alzheimer's amyloid fibrils: structure and assembly

4. Biochim. Biophys. Acta *1502*, 16-30.

Serpell,L.C. (2000a). Alzheimer's amyloid fibrils: structure and assembly

4. Biochim. Biophys. Acta *1502*, 16-30.

Serpell,L.C., Sunde,M., Benson,M.D., Tennent,G.A., Pepys,M.B., and Fraser,P.E. (2000). The protofilament substructure of amyloid fibrils

3. J. Mol. Biol. *300*, 1033-1039.

Shakhnovich,E., Abkevich,V., and Ptitsyn,O. (1996). Conserved residues and the mechanism of protein folding

5. Nature *379*, 96-98.

Sikorski,P. and Atkins,E. (2005). New model for crystalline polyglutamine assemblies and their connection with amyloid fibrils

1. Biomacromolecules. *6*, 425-432.

Snyder,S.W., Ladror,U.S., Wade,W.S., Wang,G.T., Barrett,L.W., Matayoshi,E.D., Huffaker,H.J., Krafft,G.A., and Holzman,T.F. (1994). Amyloid-beta aggregation: selective inhibition of aggregation in mixtures of amyloid with different chain lengths

1. Biophys. J. *67*, 1216-1228.

Sondheimer,N. and Lindquist,S. (2000). Rnq1: an epigenetic modifier of protein function in yeast

1. Mol. Cell *5*, 163-172.

Speransky,V.V., Taylor,K.L., Edskes,H.K., Wickner,R.B., and Steven,A.C. (2001). Prion filament networks in [URE3] cells of Saccharomyces cerevisiae

15. J. Cell Biol. *153*, 1327-1336.

Sunde,M. and Blake,C. (1997). The structure of amyloid fibrils by electron microscopy and X-ray diffraction

2. Adv. Protein Chem. *50*, 123-159.

Switzer,R.C., III, Merril,C.R., and Shifrin,S. (1979). A highly sensitive silver stain for detecting proteins and peptides in polyacrylamide gels

1. Anal. Biochem. *98*, 231-237.

Taylor,K.L., Cheng,N., Williams,R.W., Steven,A.C., and Wickner,R.B. (1999). Prion domain initiation of amyloid formation in vitro from native Ure2p

48. Science *283*, 1339-1343.

Ter Avanesyan,M.D. and Kushnirov,V.V. (1999). Prions: infectious proteins with genetic properties

37. Biochemistry (Mosc.) *64*, 1382-1390.

Ter Avanesyan,M.D., Kushnirov,V.V., Dagkesamanskaya,A.R., Didichenko,S.A., Chernoff,Y.O., Inge-Vechtomov,S.G., and Smirnov,V.N. (1993). Deletion analysis of the SUP35 gene of the yeast Saccharomyces cerevisiae reveals two non-overlapping functional regions in the encoded protein

1. Mol. Microbiol. *7*, 683-692.

Thual,C., Bousset,L., Komar,A.A., Walter,S., Buchner,J., Cullin,C., and Melki,R. (2001). Stability, folding, dimerization, and assembly properties of the yeast prion Ure2p

19. Biochemistry *40*, 1764-1773.

Thual,C., Komar,A.A., Bousset,L., Fernandez-Bellot,E., Cullin,C., and Melki,R. (1999). Structural characterization of Saccharomyces cerevisiae prion-like protein Ure2

47. J. Biol. Chem. *274*, 13666-13674.

Timasheff,S.N. (1998). Control of protein stability and reactions by weakly interacting cosolvents: the simplicity of the complicated

1. Adv. Protein Chem. *51*, 355-432.

Tompa,P. (2002). Intrinsically unstructured proteins

1. Trends Biochem. Sci. *27*, 527-533.

Torok,M., Milton,S., Kayed,R., Wu,P., McIntire,T., Glabe,C.G., and Langen,R. (2002). Structural and dynamic features of Alzheimer's Abeta peptide in amyloid fibrils studied by site-directed spin labeling

1. J. Biol. Chem. *277*, 40810-40815.

Towbin,H., Staehelin,T., and Gordon,J. (1979). Electrophoretic transfer of proteins from polyacrylamide gels to nitrocellulose sheets: procedure and some applications. Proc. Natl. Acad. Sci. U. S. A *76*, 4350-4354.

Tuite,M.F. (2000). Yeast prions and their prion-forming domain

34. Cell *100*, 289-292.

Turner,G.C. and Varshavsky,A. (2000). Detecting and measuring cotranslational protein degradation in vivo

1. Science *289*, 2117-2120.

Tycko,R. (2003). Insights into the amyloid folding problem from solid-state NMR

1. Biochemistry *42*, 3151-3159.

Umland,T.C., Taylor,K.L., Rhee,S., Wickner,R.B., and Davies,D.R. (2001). The crystal structure of the nitrogen regulation fragment of the yeast prion protein Ure2p

20. Proc. Natl. Acad. Sci. U. S. A *98*, 1459-1464.

Uptain,S.M. and Lindquist,S. (2002). Prions as protein-based genetic elements

116. Annu. Rev. Microbiol. *56*, 703-741.

Uversky,V.N., Li,J., and Fink,A.L. (2001). Evidence for a partially folded intermediate in alpha-synuclein fibril formation

7. J. Biol. Chem. *276*, 10737-10744.

Valle,F., DeRose,J.A., Dietler,G., Kawe,M., Pluckthun,A., and Semenza,G. (2002). AFM structural study of the molecular chaperone GroEL and its two-dimensional crystals: an ideal "living" calibration sample. Ultramicroscopy *93*, 83-89.

van den,B.B., Wain,R., Dobson,C.M., and Ellis,R.J. (2000). Macromolecular crowding perturbs protein refolding kinetics: implications for folding inside the cell

3. EMBO J. *19*, 3870-3875.

Van Holde,K.E., Johnson,W.C., and Ho,P.S. (1998). Principles of physical biochemistry. (New York: Prentice Hall).

Vendruscolo,M., Paci,E., Dobson,C.M., and Karplus,M. (2001). Three key residues form a critical contact network in a protein folding transition state

3. Nature *409*, 641-645.

Vendruscolo,M., Zurdo,J., MacPhee,C.E., and Dobson,C.M. (2003). Protein folding and misfolding: a paradigm of self-assembly and regulation in complex biological systems

10. Philos. Transact. A Math. Phys. Eng Sci. *361*, 1205-1222.

Voges,D., Zwickl,P., and Baumeister,W. (1999). The 26S proteasome: a molecular machine designed for controlled proteolysis

1. Annu. Rev. Biochem. *68*, 1015-1068.

Walsh,D.M., Lomakin,A., Benedek,G.B., Condron,M.M., and Teplow,D.B. (1997). Amyloid beta-protein fibrillogenesis. Detection of a protofibrillar intermediate

1. J. Biol. Chem. *272*, 22364-22372.

Walter,S. and Buchner,J. (2002). Molecular chaperones--cellular machines for protein folding

5. Angew. Chem. Int. Ed Engl. *41*, 1098-1113.

Walter,S., Hubner,B., Hahn,U., and Schmid,F.X. (1995). Destabilization of a protein helix by electrostatic interactions

1. J. Mol. Biol. *252*, 133-143.

Weissmann,C. (1994). The prion connection: now in yeast? Science *264*, 528-530.

Wetlaufer,D.B. (1973). Nucleation, rapid folding, and globular intrachain regions in proteins

1. Proc. Natl. Acad. Sci. U. S. A *70*, 697-701.

Wetzel,R. (1999). Amyloid, prions and other protein aggregates.

Wickner,R.B. (1994). [URE3] as an altered URE2 protein: evidence for a prion analog in Saccharomyces cerevisiae. Science *264*, 566-569.

Wickner,R.B., Masison,D.C., and Edskes,H.K. (1995). [PSI] and [URE3] as yeast prions. Yeast *11*, 1671-1685.

Wickner,R.B., Taylor,K.L., Edskes,H.K., Maddelein,M.L., Moriyama,H., and Roberts,B.T. (1999). Prions in Saccharomyces and Podospora spp.: protein-based inheritance

41. Microbiol. Mol. Biol. Rev. *63*, 844-861.

Wille,H., Michelitsch,M.D., Guenebaut,V., Supattapone,S., Serban,A., Cohen,F.E., Agard,D.A., and Prusiner,S.B. (2002). Structural studies of the scrapie prion protein by electron crystallography

1. Proc. Natl. Acad. Sci. U. S. A *99*, 3563-3568.

Wolynes,P.G., Onuchic,J.N., and Thirumalai,D. (1995). Navigating the folding routes

3. Science *267*, 1619-1620.

Woolley,A.T., Cheung,C.L., Hafner,J.H., and Lieber,C.M. (2000). Structural biology with carbon nanotube AFM probes

1. Chem. Biol. *7*, R193-R204.

Wright,P.E. and Dyson,H.J. (1999). Intrinsically unstructured proteins: re-assessing the protein structure-function paradigm

2. J. Mol. Biol. *293*, 321-331.

Xing,Y. and Higuchi,K. (2002). Amyloid fibril proteins

1. Mech. Ageing Dev. *123*, 1625-1636.

Zahn,R., Liu,A., Luhrs,T., Riek,R., von Schroetter,C., Lopez,G.F., Billeter,M., Calzolai,L., Wider,G., and Wuthrich,K. (2000). NMR solution structure of the human prion protein

17. Proc. Natl. Acad. Sci. U. S. A *97*, 145-150.

Zhou,J.M., Zhu,L., Balny,C., and Perrett,S. (2001). Pressure denaturation of the yeast prion protein Ure2

11. Biochem. Biophys. Res. Commun. *287*, 147-152.

Zhu,L., Kihara,H., Kojima,M., Zhou,J.M., and Perrett,S. (2003a). Small angle X-ray scattering study of the yeast prion Ure2p

84. Biochem. Biophys. Res. Commun. *311*, 525-532.

Zhu,L., Zhang,X.J., Wang,L.Y., Zhou,J.M., and Perrett,S. (2003b). Relationship between stability of folding intermediates and amyloid formation for the yeast prion Ure2p: a quantitative analysis of the effects of pH and buffer system

85. J. Mol. Biol. *328*, 235-254.

Zou,W.Q. and Gambetti,P. (2005). From microbes to prions the final proof of the prion hypothesis

1. Cell *121*, 155-157.

11 Acknowledgements

I would like to express my most grateful thanks to Prof. Dr. Johannes Buchner for giving me the great opportunity to be part of his group and for the financial of this work. I want to give too, many thanks for his trust on my scientific capability, for giving me freedom to develop the project, for his big patience along the thesis and remarkable diplomacy. Not only that, but his constant friendly way of interacting was a remarkable differential on my work and filled me with a deep respect to his person.

About Dr. Martins Halsbeck I would have to write a thesis to describe how helpful in the small things he was and about my admiration for his capacity to share himself in more then 10 task at same time. Despite his multiple responsibilities, he still could find some time for sharing his knowledge and to discuss problems. I want also, to thanks his patience on reading the thesis and valuable comments on how to improve it. Hasi, my deepest thanks for the encouragement, open ear and support given during my PhD work.

I would like to express my grateful thanks to Assistant-Professor Dr.Stefan Walter, for introducing me to biophysical techniques, having always an open ear, sharing the office, correct my English and for his valuable comments on how to improve this dissertation. Besides the scientific interaction, there were also many friendly moments shared with other people in the lab and in parties around Munich. After all, I want also to express here my respect for his teaching capabilities and wish him a lot of success in his scientific carrier.

To Assistant-Professor Dr. José Antonio Garrido and to Prof.Dr.Stutzamn group of the Physics Department I want to thanks for the very fruitful scientific interaction and collaborations. I wish to Ze' a lot of success in his scientific carrier. My thanks also to Claudio Miskys for introducing me to AFM techniques.

For Assistant-Professor Dr. Thomas Scheibel, Prof. Dr. Sevil Weinkauf, Prof. Dr. Bern Reif and their respective groups, for the friendly scientific interaction and material support.

My thanks to Prof. Dr. David Eisenberg for the hospitality in his group at University of California – Los Angeles and to Dr. Magdalena Ivanova for team work on performing the X-ray fiber diffraction experiments.

My thanks to Prof.Dr. Manfred Sippl and his group at CAGE, for introducing me to protein prediction area and for the hospitality in Salburg, Austria.

I want to show here my special thanks to Frau Susanne Hilber, who is an extremely efficient secretary. Thanks for the Technical Assistants, in special Bettina Richter, for the TEM images. My thanks, too, for Sebastian and Lin, for Intranet management.

My thanks also to the Buchner's group for the friendly environment, for sharing pizzas at late night, the ridding home after the last bus and for always read to help in one or another way. One special thanks for Marcus Mayer for introducing me to the lab work in the starting weeks in the group and for the PDI, necessary for the JBC publication.

"Friends are angels in our life". Thanks for my friends in Munich and worldwide, for helping me to recharge after some stressful period of time in the lab. In Special, for the "angel" Jan Stefan, for his friendship, great heart, patience and that despite the Atlantic Ocean between us, he could give emotional support during the writing of the thesis like he would be here in Munich. Thanks, from the deepest of my heart.

I want to thanks Marco for his undescribed support that goes beyond this work and his love.To my German family, Hans and Gertraud that adopt me like I would be their own daughter. To my Brazilian family that always supported me and for their love. For all people of my family for understanding when I could not spend time with them. To whom I want to dedicate this Title.

I want to thanks to all these people that looked out of their world and that did not leave themselves be lead by the cultural shock misunderstandings. A thanks to those people who where able to openly discussed about "German way of life" and culture without get my questions in a personal way. Those who permitted that I could learn a lot but never enough about this incredible rich culture. Anyway, a big thanks.

If you leave your home country is because you believe that you will succeed. For this, you must have a history on your life of succeed battles, learned from lost battles and not only that, but a strong backup from family and friends. To have great friends you must be as great as they are and value them. About my family I can say: Only who had love at home knows what love is and for their love I will be always thankfully. Their love was my big motivation.